DYNAMIC LOAD EFFECTS ON JOURNAL BEARINGS

by

James K. Patrick
B.Sc., A.R.C.S.T., A.M.I.Mech.E.

A THESIS

Submitted to the University of Glasgow

for the degree of

Doctor of Philosophy

May 1967.

ProQuest LLC.
789 East Eisenhower Parkway
P.O. Box 1346
Ann Arbor, MI 48106 – 1346

ACKNOWLEDGEMENTS

The programme of experimental research presented in this thesis was carried out in the Department of Civil and Mechanical Engineering of the Royal Technical College, Glasgow, and latterly in the Department of Mechanical Engineering of the University of Strathclyde.

The author wishes to express his appreciation of the laboratory facilities and the extensive instrumentation required for this type of experimental investigation, which were provided by Professor A.S.T. Thomson, D.Sc., Ph.D., A.R.C.S.T., M.I.C.E., M.I.Mech.E., F.R.S.E. and his gratitude to Dr. H.L. McBroom, B.Sc., Ph.D., A.R.C.S.T., A.M.I.Mech.E., for his interest throughout the project and for the helpful discussions which took place in the latter stages of the investigation.

CONTENTS

Page

CHAPTER THREE

Experimental Procedure

NOMENCLATURE

The following symbols have been used throughout the text. The definition of any symbol not listed will be found where it first appears in the text.

D: Journal Diameter, inches.

L: Bearing Length, inches

N': Journal Speed, revolutions per second

P: Unit Bearing Load: lb f./in^2

R: Radius of Bearing Bore: inches

S: Sommerfeld Variable: $\left(\frac{R}{c}\right)^2 \quad \frac{\mu \ N'}{P}$

S_M: Sommerfeld Variable: $\left(\frac{R}{c}\right)^2 \quad \frac{\mu \ N'}{P}$

where P is the maximum bearing load in a given cycle.

S_o: Sommerfeld Variable: $\left(\frac{c}{R}\right)^2 \quad \frac{P}{\mu \ \omega}$

C_n: Capacity Number: $S \left(\frac{L}{D}\right)^2$

U_o: Linear Velocity of Bearing Surface

U_1: Linear Velocity of Journal Surface

V_1: Radial Velocity of Journal Centre.

c: Radial Clearance:

e: Eccentricity, distance between Journal and bearing centres: inches.

f: Coefficient of Friction.

$f\left(\frac{R}{c}\right)$ Friction Variable

h: Oil Film Thickness: inches

q_n: Oil Flow Number: ratio $\frac{\text{Measured Flow}}{\text{Swept Volume}}$

t: Time: seconds

ε: Eccentricity Ratio $\frac{e}{c}$

μ: Oil Film Viscosity: Reyns

θ: Angle between a point on the bearing surface and a reference axis

σ: Load Speed Ratio = ω_p/ω

ϕ Load Phase Angle = $\omega_p t$

Φ Angle between the Line of Centres and the Load Line measured in the direction of rotation.

ω Angular Velocity of Journal: radians per second

ω_p: Frequency of Applied Dynamic Load: radians per second.

SUMMARY

This thesis presents the findings of an Experimental Investigation of the behaviour of the oil film in a journal bearing supporting Dynamic Loads.

The instrumentation developed for an existing loading frame is described and includes a balance piston capable of detecting tensile stresses in the oil film, and a lever system which measures journal centre displacement with commercially available displacement transducers.

The conversion of a crankshaft test rig into a Second Testing Machine is described. A feature of this second machine is the use of an Externally Pressurised Bearing as a 'frictionless support' for the test bearing housing. This construction enabled extremely sensitive bearing friction measurements to be recorded simultaneously with the co-ordinates of the journal centre within the clearance circle, and of the applied load.

The loading mechanism in both testing machines consisted of a Hydraulic Load Capsule pressurised from an eccentric driven ram pump. The diaphragm was bonded to the capsule body in the First Testing

Machine and was sealed by a series of piston rings to form a free piston arrangement in the Second Testing Machine.

Oil film pressures in bearings of 3 inches diameter and 3 inches long with diametral clearance of .0015 and .003 inches were surveyed in the First Testing; Machine for a range of Static and Dynamic Loads. The Dynamic Loads were of sinusoidal form with unit bearing loads up to 1650 lb f./in.^{2} and the ratio of the Load Frequency to the Journal Speed set at unity. Integration of the oil film pressures acting on the bearing surface, indicated pressure loads which were in good agreement with the applied loads.

The pressure surveys indicated that, under conditions of Static or Dynamic Loads, the load bearing film pressures were retained within an arc bounded by the axial supply grooves, and that the clearance space on the unloaded arc of the bearing was not full of oil but contained a large quantity of air released by the cavitation of the oil film.

The oil film over the unloaded arc of a Dynamically Loaded bearing consists of a trough of very low pressures prior to the area of constant sub-atmospheric pressures previously reported for dynamic loads. The oil film sustains tensile stresses in this trough during the period

of increasing load, and on eventual rupture air is released from solution and forms cavities in the oil. As the oil film does not rotate within the clearance space under Dynamic Loads, it cavitates and reforms within the same bearing arc. This process forms depressions in the profile of the developing film pressures as the entrapped air is dissolved.

Journal displacement measurements made in the First Testing Machine indicated that a certain degree of restraint was imposed on the test bearing housing by the loading mechanism. It was also noted that the bulk of the balance piston cylinder gave the test shaft a stiffness which varied with the plane of bending. These factors combined to make interpretation of the Dynamic Load Displacement measurements difficult without recourse to correction factors.

To avoid these problems in the Second Testing Machine no pressure transducer was included in the test shaft and the bearing was mounted so that the journal was simply supported in the plane of loading.

Static Load measurements were compared with published experimental results to evaluate the measuring techniques before their application to Dynamic Load Conditions.

Journal centre co-ordinates were measured in .003 inch diameter clearance bearings with a length to diameter ratio of 1, $\frac{2}{3}$ and $\frac{1}{2}$. The journal paths under Dynamic Loads of sinusoidal form had the simple elliptical shape predicted from theoretical considerations. The presence of two axial grooves in bearings subjected to this form of loading, holds the major axis of the elliptical path in a position close to the line of applied load, irrespective of the magnitude or speed ratio of that load.

The experimental techniques used, failed to detect a load frequency to journal speed ratio at which the oil film had zero load capacity. There is no doubt, that for a given dynamic load the bearing operates at its thinnest film at speed ratios of the order of 0.5. When the speed ratio is unity, a bearing has greater load carrying capacity under Dynamic Loads than under equivalent Static Loads.

The dynamic load carrying capacity of a journal bearing is largely dependent on pressures generated by the squeeze film associated with the movement of the journal centre within the clearance space. A bearing has the same load capacity under Dynamic and Static Loads at the instant of maximum eccentricity, when no squeeze film pressures are generated.

Coefficients of friction measured under Static Load Conditions were considerably lower in magnitude than had been expected from current theoretical treatises. This difference is due to the presence of large stable air bubbles in the unloaded arc of the bearing.

The cyclic variation of friction force in a bearing subjected to Dynamic Loads is considerably greater in magnitude than has been reported to date. The friction variation was found to be proportional to the load and inversely proportional to the speed ratio in the range $.33 \leq \sigma \leq 1.0$.

Thin film operation occurred within the range of Dynamic Loads examined in full length and half length bearings. In all cases examined the bearings operated with higher friction values under Dynamic Loads than under Static Loads.

A method of predicting the oil flow in axial grooved bearings has been formulated for Constant Load Conditions, and reasonable quantitative and qualitative agreement has been established between measured journal eccentricities and those predicted by an advanced computerised analysis.

CHAPTER I

1. An Introduction to the Dynamically Loaded Bearing.

Any type of load which is not exactly constant when applied to a Bearing can be classified as a Dynamic Load. While the bearings associated with any form of reciprocating machinery are typical examples of Dynamically Loaded Bearings, turbine installations subjected to an out of balance load can be similarly classified.

Dynamically Loaded Bearings present both analytical and experimental researchers with a complex set of interdependent variables governed by the need to balance the load applied to a bearing by developing sufficient pressure in the oil film occupying the clearance space between the journal and bearing bush to prevent the occurrence of metal to metal contact. Only in the last decade has the development of instrumentation and electronic computers provided the research tools necessary for the detailed investigation of bearings subjected to this type of load.

When this research programme was initiated in 1955, little guidance was available from experimental or theoretical researches to assist the designer in the proportioning of Dynamically Loaded

Bearings and numerous empirical rules based on operating experience gained in similar applications were used to provide adequate bearings for a given application. In fact reciprocating primemovers have passed into history, in several applications, before the development of a clear cut design procedure for their principal bearings.

The general equation governing the behaviour of a lubricant in the clearance space of a bearing can be derived from a consideration of the static equilibrium of an elementary cube of the lubricant within that space. Using the symbols of Fig. 1.1, the velocity of the fluid in the circumferential and axial directions can be shown

to be $$u = \frac{1}{2\mu} \frac{\partial p}{\partial x} y(y - h) + \frac{h - y}{h} \cdot U_o + \frac{y}{h} U_1$$

and $$w = \frac{1}{2\mu} \cdot \frac{\partial p}{\partial z} \cdot y(y - h)$$ respectively.

As the fluid is assumed incompressible, the volume of oil entering and leaving the elementary cube will be equal, giving rise to volume - continuity equation

$$\frac{\partial u}{\partial x} + \frac{\partial v}{\partial y} + \frac{\partial w}{\partial z} = 0$$

Integration of the volume continuity equation establishes;

$$\frac{1}{6\mu}\left[\frac{\partial}{\partial x}\left(h^3\frac{\partial p}{\partial x}\right)+\frac{\partial}{\partial z}\left(h^3\frac{\partial p}{\partial z}\right)\right]=(U_o-U_1)\frac{\partial h}{\partial x}+h.\frac{\partial (U_o+U_1)}{\partial x}+2V_1$$

This equation, which has been the basis of all hydrodynamic bearing analysis since its introduction by Reynolds[1] in 1886, could not be rigidly applied to finite bearings subjected to dynamic loads, until the advent of digital computers. Because of this analytical difficulty approximate solutions of the equation have been developed for statically loaded bearings and subsequently applied to the dynamically loaded condition.

An approximation typical of many was introduced by Sommerfeld[2] who in considering a bearing of infinite length reduced axial flow terms to zero. This approximation gives rise to a solution in which the oil film is a continuous function with positive and negative pressures of equal magnitude.

A more recent approximation suggested by Michell[3] and Cardullo[4] and developed by Ocvirk[5] is based on the fact that as the bearing length is reduced the circumferential pressure gradient becomes small compared to that of the axial pressure gradient, so that terms involving the circumferential pressure gradient ($\partial p/\partial x$) can be neglected. This solution also gives rise to a continuous pressure

function but in determining the load carrying capacity of such a bearing the negative film pressures are ignored.

An early approximate solution of Reynold's equation as applied to dynamically loaded bearings was presented by Swift[6] in 1937. Swift based his analysis on an infinite bearing working with a continuous isoviscous oil film in the clearance space. The pressure generated in the clearance space was built up from the superposition of pressure components due to the individual modes of journal movement.

The pressure loads Q, due to the rotation of the journal about its centre, and P_1 and P_2, due to the tangential and radial movement of the journal centre relative to the bearing centre, must balance the components F_1 and F_2 of the applied load, so that from Fig 1.2.

$$(Q - P_1) \sin \theta + P_2 \cos \theta = F_1$$
$$(Q - P_1) \cos \theta - P_2 \sin \theta = F_2$$

The solution of the Reynold's equation for each of the above modes of journal displacement evaluates, Q, P_1, and P_2, and results in the following relationship between the applied load and the bearing variables.

$$\left(\omega - 2\frac{d\theta}{dt}\right)\frac{\varepsilon}{(2+\varepsilon^2)\sqrt{1-\varepsilon^2}} \cdot \sin\theta + \frac{\frac{d\varepsilon}{dt}}{(1-\varepsilon^2)^{3/2}} \cdot \cos\theta = \frac{F_1 c^2}{12\pi\mu R^3}$$

$$\left(\omega - 2\frac{d\theta}{dt}\right)\frac{\varepsilon}{(2+\varepsilon^2)\sqrt{1-\varepsilon^2}} \cdot \cos\theta + \frac{\frac{d\varepsilon}{dt}}{(1-\varepsilon^2)^{3/2}} \cdot \sin\theta = \frac{F_2 c^2}{12\pi\mu R^3}$$

Swift solved these equations using the simple harmonic function $F_1 = F \sin\theta$, $F_2 = 0$, to represent an alternating load, as he could not readily solve the more useful function $F_1 = F \sin\omega t$ at that time.

Integrating the above equations yields the following relationship for these selected values of applied load.

$$8.\ \Delta_o \cdot \sin^2\theta = \frac{(1-\varepsilon^2)^{3/2}}{\varepsilon^2}\left\{\frac{\varepsilon(1+\varepsilon^2)}{(1-\varepsilon^2)^2} - \frac{1}{2}\log_e\frac{(1+\varepsilon)}{(1-\varepsilon)} + C\right\}$$

where $\Delta_o = \dfrac{F c^2}{12\pi\mu\omega R^3}$ and C is a constant of integration.

If ε_1, the value of ε when $\theta = 0$ is selected, this equation can be solved to give a family of polar curves passing through ε_2, the value of ε when $\theta = \frac{\pi}{2}$, which display distinct modes of procession as shown in Fig 1.3. When $\varepsilon_1 > \varepsilon_2$ the frequency of the alternating load ω_p is more than half the shaft speed ω and the journal centre follows an

elliptical path which in the limit coincides with the axis $\theta = 0$ between the limits $\pm \varepsilon_1$. When $\varepsilon_1 = \varepsilon_2$ the speed ratio $\omega_p/\omega = .5$ and the pressure load produced by the bearing is zero, while the major axis of the elliptical path swings through 90^o and gradually changes to a figure of eight configuration when $\varepsilon_1 < \varepsilon_2$ and the speed ratio is less than 0.5.

Subsequent to the work of Swift approximate solutions of the Reynold's Equation were made by assuming a definite journal path and determining the corresponding variation in applied load. These selected paths were elliptical in shape as analysed by Dick[7] and that of a journal moving along a straight line with sinusoidal motion as investigated by Frankel[8].

While these analyses were of interest, the analysis of Dynamically Loaded Bearings did not advance until 1947, when Burwell[9] presented a paper on the analysis of time dependent alternating loads applied to bearings of infinite length. Burwell solved the Reynold's Equation for both a sinusoidally alternating load and a square wave form of reciprocating load, using a standard step by step method of numerical integration. This method requires two integration constants to ensure that the journal path closes at the end of every load cycle. Burwell

determined these constants by a trial and error process, and from his solution of the Reynold's Equation was able to predict the maximum eccentricity and journal path for a given magnitude of Alternating Load.

On the application of a sinusoidally alternating load, the journal centre followed an elliptical path within the bearing clearance circle. The major axis of the path was in line with the plane of the applied load when the speed ratio $\sigma = \omega_p / \omega > 0.5$ and normal to the load plane when $\sigma < 0.5$. At $\sigma = 0.5$ the journal centre followed a circular path coincident with the clearance circle and at speed ratios below 0.25 the elliptical path was complicated by additional loops

A similar analysis for the square wave load form, indicated journal paths which were basically the same path along which Swift predicted a bearing would oscillate under conditions of constant load of fixed direction.

The general conclusion from Burwell's analysis was that for any form of alternating or rotating load, capacity increases with the load speed ratio from zero load capacity at $\sigma = 0.5$. At any given load frequency except $\sigma = 0.5$, the more peaked the load form

the greater the load carrying capacity of a given bearing with its journal operating within a given maximum value of eccentricity.

The first analysis of a Dynamically Loaded Bearing of Finite Length was published by Hahn[10] in 1957. This analysis transformed the Reynold's Equation into a linear differential equation which indicated in dimensionless terms the relationship between oil film pressure and the position and velocity of the journal centre. Hahn based his integration constants on an assumed pressure distribution in which the oil pressure was zero at the bearing ends and varied periodically in the circumferential direction with zero pressure at the points of maximum and minimum film thickness. The transformed equation was solved, for the case when the journal rotates when supporting a uniform load of constant direction and the case when the journal moves radially without rotation, by a finite difference technique using uniform axial grid steps and circumferential grid steps of $\frac{\pi}{9}$ when $\varepsilon \leq \cdot 4$ and $\frac{\pi}{8}$ when $\varepsilon \geq \cdot 6$

The general solution of the pressure distribution for a given eccentricity was established from a knowledge of the tangential and radial velocities of the journal centre, as they appear as multiplication factors of these separate solutions in the transformed differential

equation. The pressure load was determined from each pressure distribution by using Simpson's Integration Rule and neglecting negative film pressures in the process. The large number of cases investigated were summarised in the graphical representation of the length and angle of a polar load vector for all eccentricity ratios and a range of the ratio of radial to tangential components of journal velocities.

To calculate the journal path from a given applied load diagram, a system of non-linear differential equations was set up for the angular and radial components of the journal position and solved by a step by step integration technique. Any starting value of the variables may be assumed, as the solution is solved as an initial value problem and the true starting position for the solution will be apparent after the calculation for one load cycle has been completed. Journal centre paths predicted for a half length bearing supporting a Sinusoidally Varying Applied Load are shown on Fig 1.4 and 1.5 for a range of loads applied at constant speed ratio σ and for the same load applied with a range of speed ratios respectively.

The only approximate solution of the Dynamically Loaded bearing problem which used an extension of the short bearing theory, was

completed by Milne[11] in 1962. Milne used a step by step integration method in a series of programmes, designed for use in a small computer, which predicted the journal path for an arbitrary load cycle or vice versa, with or without a complete oil film in the clearance space. Qualitative agreement with early experimental work was established and it was concluded that while a bearing operating with a cavitated oil film was inherently stable the same bearing operating with a complete oil film was in a state of neutral equilibrium.

An important physical dimension of a hydro-dynamic bearing which the analyst finds difficult to include as a variable, is the extent of the oil film occupying the clearance space in the bearing. The majority of theoretical studies assume a continuous film and choose to ignore the resultant negative film pressures.

In 1963 Horsenell and McCallion[12] evaluated the effect of cavitation on analytical results by computing the performance of a central circumferentially grooved bearing with a land length to diameter ratio of .282. They solved the Reynold's Equation with a relaxation technique and established that under Dynamic Loads, oil film disruption provides a differential resistance to positive and negative radial velocities which reduces the maximum eccentricity reached during any given load cycle. At high eccentricity ratios,

the magnitude of the load determined from a continuous film concept gives a good approximation of the load determined from the cavitated condition in the particular bearing type investigated.

Similar methods of solution to those outlined above have been developed by Holland[13] and Eberhard and Lang[14], while Someya[15] solved the Reynold's Equation by establishing a double Fourier Series.

A programme developed by Lloyd (16) et al. for use in a large high speed computer, forms the most versatile analysis to date, and is capable of predicting the performance of main and big end bearings of Internal Combustion engines. The analysis recognises cavitation by selecting a disruption pressure and equating all lower pressures to the selected value. It solves the Reynold's Equation by a finite difference technique using a variable distance between the mesh points to predict journal centre locus, cumulative friction work, oil flow, the position and magnitude of the maximum film pressures, and the extent of the disrupted oil film for a given load cycle. This versatile programme has one minor and one major limitation at present. It can only handle a bearing with some form of circumferential groove and requires a constant value of oil film viscosity which is assumed to be representative of the range of values existing in the oil film.

There is no doubt that analytical investigations of Dynamically Loaded bearings have reached the stage where they give a clear indication to the designer of the effect of varying the physical parameters in a given bearing problem. Radermacher and Hahn[28] have shown this clearly in the application of computer programmes to Oil Engine problems where computerised bearing analysis give a clear indication of the optimum crankshaft balance weights required in a given engine.

Several experimental investigators have shown that the analyst cannot predict quantitatively the performance of a Dynamically Loaded Bearing, and assumptions which ignore the effect temperature and pressure on the lubricant viscosity, an accurate assessment of the extent of cavitation in the oil film, and the recognition of the distortion of the oil film by the oil supply grooves, are major problems which must be solved before an accurate quantitative design system for this important category of bearings is established.

In the field of experimental research, the endurance test was until recently a popular means of evaluating the performance of Dynamically Loaded bearings. In a historical review of fifteen testing machines, reported between 1932 and 1955, Hersey and Snapp[17]

indicate only five cases in which any attempt was made to evaluate oil film pressure or thickness under varying loads.

In 1937, Buske and Rolli[18] carried out pressure surveys in a bearing (2.953" Dia. x 1.772 in. long x 9.843 x 10^{-3} in rad. cl) subjected to Dynamic Loads up to a maximum value of 6.5 Tons f. The pressures in the oil film were measured by a series of balanced pressure pistons set at specific points in the test bearing. This investigation was primarily concerned in determining the maximum value of film pressure at any given survey point and did not indicate the development of the load bearing pressure film under dynamic loads.

With the intervention of the Second World War, no further experimental work was published until 1950, when Simons[19, 20] reported on a research programme in which considerable care was taken to avoid errors in physical measurements. The displacement of a 4 inch diameter journal running in a 2 inch long bearing with .004 inch diametral clearance was measured by a capacitance method and gave good qualitative agreement with the predictions of Burwell. Simons established experimentally that bearings operate at considerably reduced film thickness when the journal speed is twice the load frequency. He also concluded that the existance of the zero film thickness predicted

by analytical studies at this speed ratio was dependent on the absolute alignment of journal and bearing in the test rig.

This work was an important experimental contribution to the study of Dynamically Loaded Bearings but was limited in its application as the Maximum Unit Bearing Load of 62.5 p.s.i. was considerably lower than those used in practice.

An experimental investigation of the pressure variations in the oil film surrounding a 1.0 inch diameter journal, running with a .0106 inch diametral clearance in a 1.5 inch long bearing, submerged in an oil bath, was reported by McBroom[21] in 1953. This investigation indicated that the unloaded arc of a bearing was largely filled with air bubbles which accumulated in the oil film. Under Dynamic Load conditions these air bubbles rapidly filled the clearance space and reduced the bearing load capacity to zero. If the journal was stopped, the entrapped air escaped from the clearance space and the load capacity of the bearing was restored for a short period. This series of events indicated the absolute necessity of a pressurised oil supply system to maintain load capabilities in a Dynamically Loaded bearing.

In the same year Shawki and Freeman[22] published the results of an investigation into the effects of Sinusoidally Alternating Loads

of up to 233 lb f./in.^{2} on a 4 inch diameter journal running with a diametral clearance of .0064 inches in a bearing 6 inches long. These experimenters measured journal displacement with photo-electric pick-ups driven from ball races adjacent to the test journal, and made a first estimate of journal friction by recording the power supplied to the journal drive motor. This investigation agreed in general with Simons and indicated that the film thickness reached minimum and the friction maximum values at $\sigma = 0.5$. The investigators also indicated that variations in friction and journal eccentricity for a given speed ratio could be presented as a function of a load variable equivalent to the inverse of the Sommerfeld Number. Although the authors did not comment on the fact in their paper, their results gave the first experimental indication of the considerable load carrying capacity of the pressure generated in the oil film by the radial movement of the journal centre known as the squeeze film action.

During the period 1956-1962 no experimental work on Dynamically Loaded bearings was published. At this time the Engineering Institute of the Technische Hochschule at Karlsruhe, developed a large scale investigation of the Dynamically Loaded Bearing subsequent to

the work of Hahn[10]. These investigations bore fruit in the early sixties with publications by Carl[23] and Radermacher[24] in the experimental field and by Someya[15] and Motosh[25] in the analytical field.

Carl presented the results of an investigation of sinusoidally loaded bearings on a programme which was complementary to the analytical work of Hahn. The bearing testing machine used could apply loads of up to 2000 p.s.i. at frequencies from 0 to 2550 cycles per minute to a shaft 2.559 inches diameter running at speeds from 30 to 6000 r.p.m. in a bearing 1.299 inches long. Journal displacements were measured by capacitance probes and film pressures by a .078 inch diameter radial piston placed in the test journal and through a linkage on a piezo-electric crystal. The cyclic variations of the measured journal displacements agreed with the predictions of Hahn though the maximum value of eccentricity was less than that predicted by Hahn.

The pressure measurements indicated the growth and decay of the oil film pressures under dynamic loads, although in the opinion of this author the pressure transducer could not detect sub-atmospheric pressures in the bearing.

The following conclusions were drawn from this investigation:

a) Any bearing calculation which does not take into account the effects of pressure and temperature on viscosity, predicts excessive pressures in the oil film.

b) The radial movement of the journal centre in the clearance space is the predominant mode of pressure generation in a Dynamically Loaded Bearing.

Radermacher[24] was primarily concerned with the investigation of journal displacement under Dynamic Loads similar to those applied to the main bearings of an I.C. engine and with the comparison of these experimentally determined displacements with those predicted by computer programmes published by Someya[15] and Lang[14].

Initially a bearing testing machine was developed which could produce the required polar load diagrams on bearings 4.7244 inches diameter and 2.3622 inches long with maximum loads of up to 1400 p.s.i. at a speed of 1000 r.p.m. The required load was produced by Hydraulic Load Capsules arranged at 120 degree intervals around the test bearing housing and the journal displacements detected by capacitance gauges.

When a trapezoidal load variation was applied to the bearing it was found that increases of load beyond 700 p.s.i. produced little change in the maximum value of eccentricity ratio but did produce a narrowing of the elliptical journal path as the increasing load was balanced by increased squeeze film pressures.

Both methods of computation were qualitatively accurate and quantitatively the difference between the calculations was less than the difference between either calculation and the equivalent experimental measurement. The agreement between the experimental and analytical results was improved if steps were taken to increase the oil flow through the bearing, thereby producing conditions closer to the isoviscious solution of both analytical methods.

Radermacher carried out similar experimental and analytical comparisons based on the behaviour of a crankshaft journal in a main bearing of a single cylinder oil engine. This study also came to the conclusion that as the difference between analysis and experiment was predominant either method of analytical prediction was suitable for qualitative studies of Dynamically Loaded Bearings.

Cooke[26] reported a series of investigations on the main bearing of a single cylinder oil engine. Inductance transducers placed in

planes at both ends of the test bearing indicated the mean journal displacent for a range of speeds and oil grades when the engine was running under no load conditions.

The load required to produce a given journal path compared favourably with that indicated by Miller's analysis. It was concluded, however, that it was unreasonable to predict quantitatively minimum oil film thickness in an engine main bearing due to the complications of crankcase deflections, crankshaft bonding, and thermal distortion. The principal use of the analytical programme is in indicating the shape and magnitude of a journal path and the period of the load cycle coincident with the maximum eccentricity of the journal in the clearance space.

A recent development in which experimental rigs are designed to reproduce isoviscous conditions in an undistorted bearing as assumed by most analytical studies, is typified by an investigation reported by Middleton[27] et al. A rig was designed to suit a central circumferentially grooved bearing with a diameter of 3 inches and a land length of .846 inches. The journal ran at a speed of 70 r.p.m. with a diametral clearance of .0075 inches.

Good agreement was established between theoretical and experimental results for a variety of polar load diagrams with Unit Bearing Loads up to 18 p.s.i.

The experimental programme presented in this thesis includes the development of two bearing testing machines, which with their associated instrumentation were capable of measuring the pressure, thickness and friction, of the oil film in a 3 inch diameter bearing loaded cyclically with unit loads up to 1600 p.s.i. These investigations span the years 1955-1958, with an additional investigation in 1966, so that any experimental findings published since Shawki and Freemans' paper in 1955 are contemporaries of those presented from this programme.

In the light of the foregoing survey of experimental investigations, the findings presented in this thesis expand the work of Carl and Radermacher although in time they preceed their findings.

The pressure surveys reveal for the first time in a large bearing the cycle of events taking place in the unloaded arc of a full length journal bearing supporting a sinusoidally alternating load. The displacement measurements indicate the successive journal paths associated with a range of alternating loads, speed

ratios and bearing lengths. Cyclic variations of bearing friction and corresponding mean coefficients of friction are also presented.

Examples of the actual load variations applied experimentally to full and half length bearings have been processed by the computer programme of Lloyd[16] to establish a comparison of analytical and experimental journal paths and friction variations.

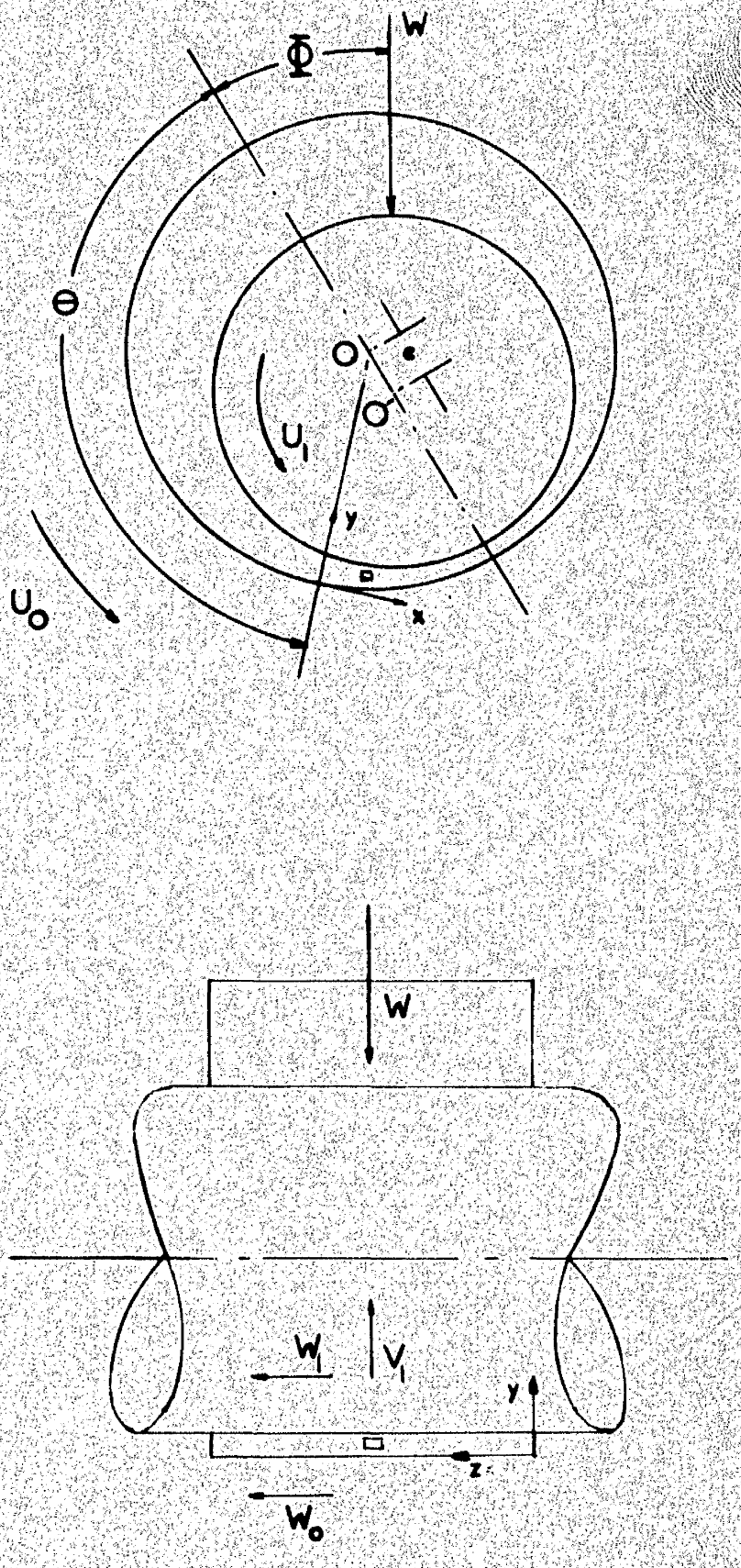

FIG 1-1

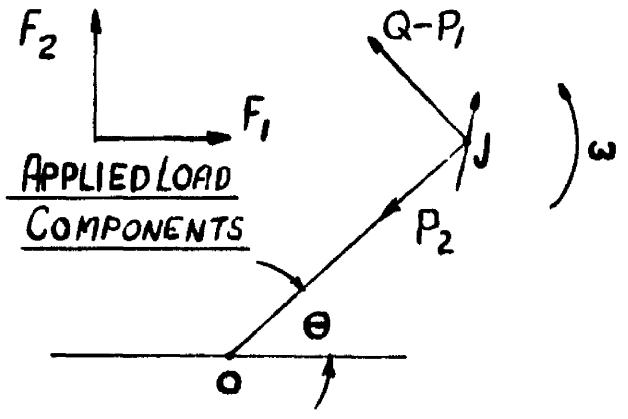

FIG: 1·2

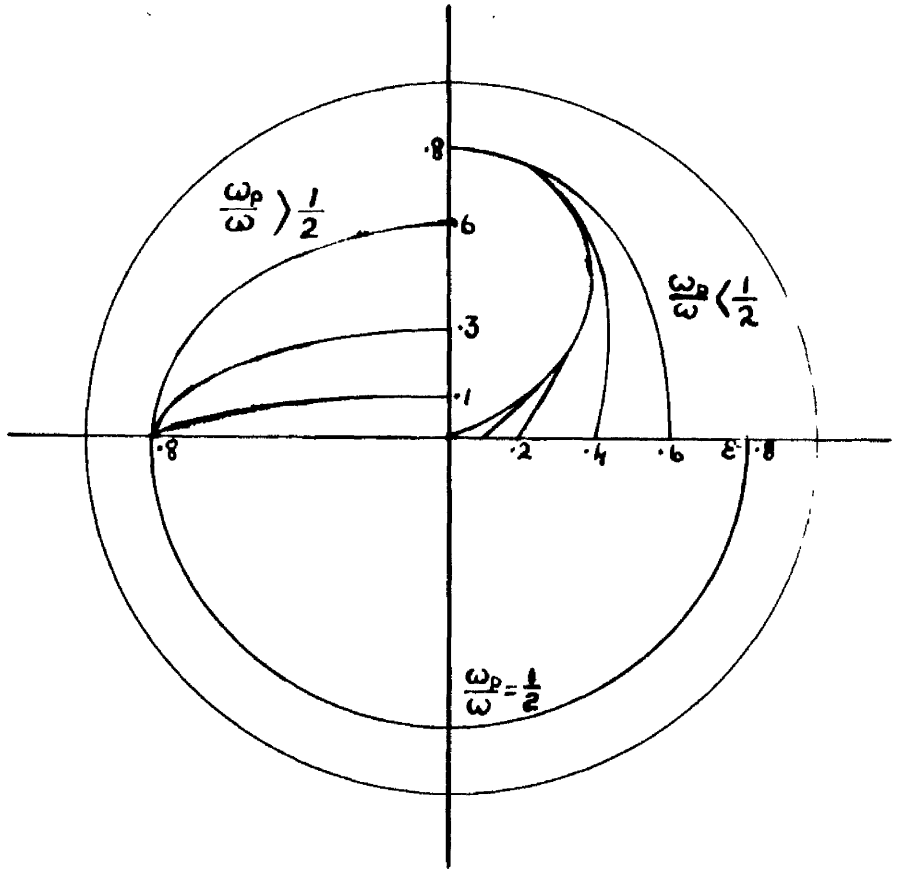

JOURNAL PATHS UNDER ALTERNATING LOADS
AFTER SWIFT

FIG: 1·3

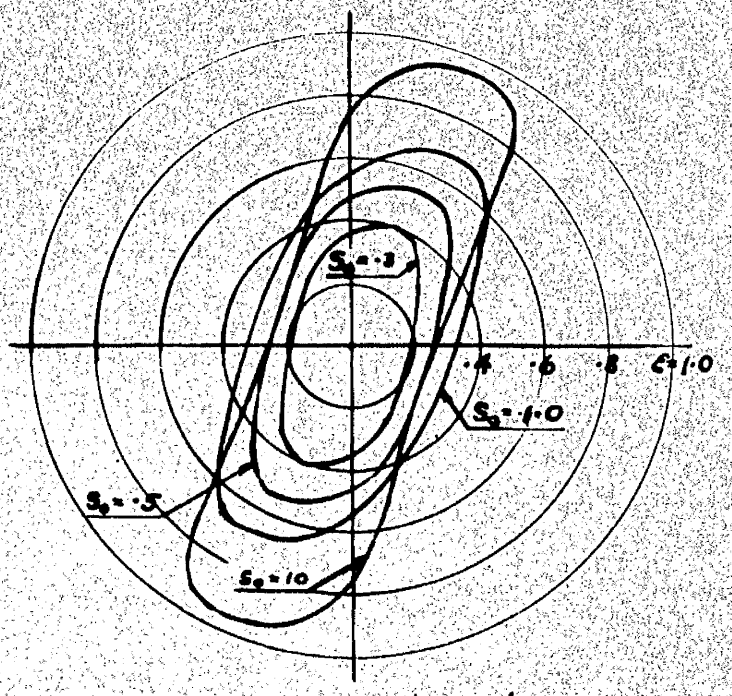

$\sigma = 1$ $L/D = 1/2$

FIG: 1·4

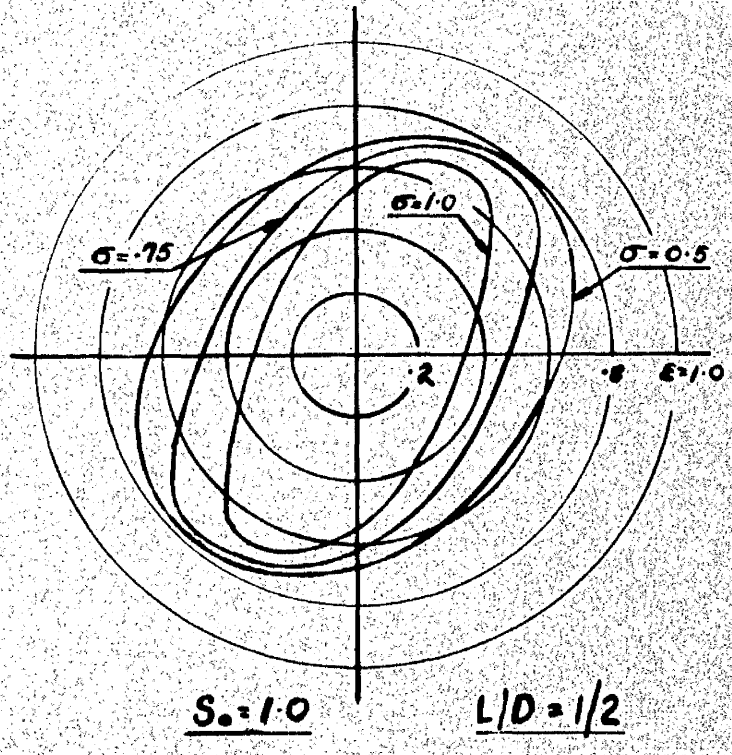

$S_0 = 1.0$ $L/D = 1/2$

CALCULATED JOURNAL CENTRE PATHS UNDER SINUSOIDAL LOADS OF CONSTANT DIRECTION AFTER HAHN

FIG: 1·5

CHAPTER II

2. Testing Machines and Associated Instrumentation.

2.1. Background.

The research programme detailed in this thesis is an early contribution to a large programme of research into the behaviour of an oil film when subjected to polar load diagrams similar to those existing in the main and big end bearings of a two-stroke marine oil engine.

When the author undertook the experimental investigations associated with this programme, the loading system and framework of a testing machine had been designed and constructed, but no instrumentation had been considered. A description of this first testing machine, and of subsequent modifications are detailed below.

Certain difficulties were experienced in measuring bearing friction in the First Testing Machine and a redundant crankshaft testing machine of suitable load capacity was adapted for use as a Second Testing Machine.

The initial instrumentation carried out by the author is described below, together with the improvements incorporated

in its application to the Second Testing Machine.

2.2. First Bearing Testing Machine.

The First Bearing Testing Machine shown diagrammatically in Fig. 2.1 is capable of applying Dynamic Loads of up to 10 tons f. to a variety of test bearings of 3 inch diameter and up to 3 inches in length. The shaft diameter was selected as a compromise between the physical limitation of size imposed by a laboratory and the need to minimise scale effect on the behaviour of the oil film. The load is applied by four Statimeter Capsules arranged in two perpindicular planes so that one or more of these load capsules can be phased to produce a variety of polar load diagrams and include: Sinusoidal Alternating, Unidirectional Pulsating, and Constant Loads.

The load capsule is essentially a steel piston, with an effective area of 50 sq. ins, bonded to the main capsule body by a flexible rubber joint. This construction can transmit loads of 20 tons f. with a safe working movement of $\pm$ 1/8 inch for static loads and $\pm$ 3½ inch for Dynamic Loads. The thrust from each capsule is transmitted to the Test Bearing Housing by a single 1 inch diameter

ball and 2 inch diameter connecting rod. Each load capsule forms a closed Hydraulic Circuit with separate Ram Pump Unit detailed in Fig. 2.2.

The closed Hydraulic Circuit incorporates a 10 cu.in. Greer Mercier Accumulator to introduce an elastic medium (air) to an otherwise inelastic hydraulic system. The Greer Mercier Hydro-Pneumatic Accumulator is basically a steel shell containing a neoprene bag which separates the air from the Hydraulic Fluid. A steel plug assembly with a spring actuated forged steel poppet valve retains the neoprene bag within the accumulator shell. A constrained volume of air follows the law PV^n = constant, and it is necessary to prime the Hydraulic System to a Base Pressure of at least 100 p.s.i.g. to approach linear load characteristics.

Four ram-pump-accumulator units are mounted on a sub-assembly and driven from a common camshaft by eccentrics phased at 90^o intervals, Fig. 2.3.

The cam faces are case-hardened and the camshaft is supported by 3 self-aligning roller bearings. The cam follower is a 2.5 in. diameter roller bearing mounted in an Mild Steel crosshead. The Cast Iron Crosshead guide has slots milled along

its length to restrain the follower from rotation relative to the cam, and is lapped to a running fit with its associated crosshead. The lower end of the crosshead has a reduced diameter and is threaded to take the ram of the pump. The case hardened mild steel ram is ground to size and lapped to the bore of the Cast Mechanite Pump Body to effect a Hydraulic Seal as no sealing rings are used in this design.

The Pump body has two ports along its length and is connected to the hydraulic system as shown in Fig. 2.1. The upper port is connected to the inlet manifold and is uncovered when the ram is at Top Dead Centre. This port ensures that pressure conditions are constant at the start of each pump stroke and allows a return flow of fluid as the load capsule is compressed by the movement of the Test Bearing Housing in reaction to the load applied by the opposing capsule.

The One Quart Greer Mercier Accumulator connected to the inlet manifold, serves a dual purpose, namely:- to eliminate Inlet Manifold Pressure fluctuations, when the ram pumps are operating, and to make up any small leakage losses from the closed system. During prolonged testing, the manifold pressure

can be restored to its datum value through a suitable valve arrangement attached to the hand priming pump.

The octagonal configuration of the Test Bearing Housing, provides suitable faces for connecting rod seatings and instrument mountings. The housing, 9 inches across the flats and 3 inches high, is bored to take a test bearing of 3½ inch outside diameter and provide an oil gallery with its associated oilways. The Test Bearing Housing is separated from a levelling plate by three 0.75 inch diameter steel balls. The steel balls have hardened steel seatings recessed into the upper surface of the levelling plate and the lower surface of the test housing Fig. 2.15.

The construction of the Testing Machine detailed above required two modifications not associated with subsequent measuring techniques. As constructed the end support frames were in a 'black' condition, and a few preliminary tests indicated the need of a reference plane for alignment purposes. A series of such planes was provided by removing the end support frames and machining their upper and lower surfaces true to the bore of the support bearing.

The friction from the single one inch diameter ball associated with each connecting rod proved excessive throughout the load range. This ball was replaced by a knife edge, 3.0 inches long, placed at the centre of curvature of the cylindrical thrust surface of the connecting-rod Fig. 2.4. Such an arrangement accommodated a small angle of Test Bearing Housing rotation and facilitated bearing friction measurements.

The lubrication system developed for the 1st Testing Machine is shown on Fig 2.14. The lubricating oil manifold is pressurised by an Imo pump delivering through a full flow felt type filter. All bearings on the testing machine are supplied from this manifold and pressure tappings taken to a central gauge board. The pressure tapping for the Test Bearing supply is taken immediately before a short length of flexible pipe which connects the Housing Oilways to the Manifold System.

2.3 Second Bearing Testing Machine.

The crankshaft testing machine which was modified to form the Second Testing Machine used a similar loading system to that described in § 2.2. The ram pumps were driven from adjustable throw eccentrics by brass eccentric straps and the pistons of the

load capsules were sealed to the capsule bodies by a series of piston rings and neoprene 'O' rings. Detailed modifications to this system were carried out including the addition of 10 cubic inch Greer Mercier Accumulators and a forced feed lubrication and cooling system for the eccentric straps.

Three basic considerations governed the design of the Second Testing Machine

These were;

1) That the test shaft should be supported by bearings which operate in planes normal to the deflected form of the test shaft.

2) That the main bearing by which the load was applied to the test shaft should be set up initially and remain undisturbed throughout an extensive programme of investigation, and

3) That the test journal should be of 3 inches diameter and the test bearings should be up to 3 inches long.

The layout shown in Fig 2.5 satisfies these conditions. The thrust from the load capsules is transferred by adjustable connecting rods to the Main Bearing Housing and thence by a self-aligning Roller Bearing to the test shaft. The clamping friction associated with the connecting rods is an advantage in this arrangement as the housing is not used for friction measurement.

The test shaft is supported by a self-aligning Ball Bearing and a Hydrodynamic Journal Bearing mounted in a housing incorporating a 'Frictionless' Support. This bearing housing is supported on Needle Roller Bearings set in a substantial U-frame bolted to the bed plate of the loading frame.

The 'Frictionless' Support.

The Hydrodynamic Test Bearing was initially supported by a Needle Roller Bearing with which it was hoped to measure friction torque by a sum and difference technique. The needle bearing proved unsatisfactory at high static loads, and was never used with Dynamic Loads.

The 'frictionless' support of the Test Housing was provided by a six pocket externally pressurised bearing. Bearings of this type are capable of supporting a range of Static or Dynamic Loads without rotation, and if held stationary, when the friction torque on the housing is being measured, will operate with zero friction.

The original design for a bearing of this type was completed by Raimondi and Boyd[29] for a four pocket bearing and later extended to cover the six pocket case by Cunningham[30]. In the

application of these design studies to this bearing, the choice of parameters was restricted by the need to fit the bearing into the space occupied by the original needle roller bearing.

Six pockets, .020 inches deep, are machined into the outer surface of the test housing hub, and six orifice type restrictors are set into a bush pressed into the frame of the housing Fig 2.6. This bush is machined from a centrifugally cast Cast Iron Pot, and has rectangular grooves cut on its outer surface to accommodate 'O' rings. The brass restrictors, Fig 2.7 which have an orifice bore of .008 inches, require a batch of at least 50 units, manufactured under closely controlled conditions, if six closely matched units are required. This expense was avoided by selecting 3 closely matched pairs from a batch of 24 units. Each pair was inserted in diametrically opposed pockets.

Operating experience with this bearing indicated that a) at clearances below .0015 ins this 5.5 inch diameter bearing failed at operating temperatures by differential expansion, and b) prolonged operation was possible only if an one micron filter was fitted in the high pressure oil line close to the restrictor oilways.

Oil is supplied to the Hydrodynamic and Externally Pressurised Bearing by separate systems which drain to a common dry sump, Fig 2.28. The drainage oil is raised to a header tank where it is maintained at a constant preset temperature by a thermostatically controlled electric heater.

2.4 Bearings .

The test bearings for both machines were machined from cored Phosphor Bronze castings and pressed into their respective Test Bearing Housings before final boring. The test bearings have a 3.5 inch outside dia, 3 inch nominal bore and two closed end diametrically opposed axial grooves. Each groove, of the form shown in Fig 2.22, is 0.25 inches broad with a length 0.25 inches less than that of the bearing, and is supplied with oil from a central hole connected to an annular groove cut in the bearing housing. Full length bearings were machined with diametral clearances of .0015 and .0034 inches for use in the First Testing Machine, and bearings with lengths of 3, 2, and 1½ inches Fig 2.22 and diametral clearance of .003 inches were manufactured for use in the Second Testing Machine.

Several auxiliary bearings were used on the First Testing Machine including the support bearings and split bush associated with the test shaft.

The support bearings comprised of white-metal lined mild-steel shells pressed into the cross members. Oil is supplied to the bearings from four holes equally spaced around the centre section of each bearing.

The split bush supplies oil to the balance piston via the test shaft oilways. This mild steel bush, 2.5 inch bore and 2 inches long, is white metal lined with a central oil supply groove and four outer grooves to accommodate Neoprene sealing rings.

2.5 Test Shafts.

The test shafts used in the First Testing Machine, were designed to accommodate a balanced pressure piston and to present a journal surface suitable for displacement measurements.

The original mild steel test shaft, shown in Fig 2.19 was 30 inches long by 3.0 inches diameter. Electrical connections from the balanced pressure piston were led along the oilways to a slip ring at the upper end of the test shaft.

Development of measuring techniques necessitated the use of the redesigned shaft shown on Fig 2.20. This shaft, 22 inches long by 3 inches diameter, was case hardened before being ground to a finished size with a surface finish of 4 micro-inches C.L.A. The oilways are supplied from a split bush at the lower end and electrical connections from the balance piston are taken to a slip-ring on the upper surface of the test shaft. Provision was also made at the upper surface for concentric mercury bath slip rings required for temperature measuring devices Fig 2.12.

The test shaft for the Second Testing Machine has no internal drillings, is 22 inches long, 3 inches diameter, and was case hardened before grinding to the finished size with a surface finish of 3.5 micro-inches C.L.A.

2.6 Balanced Pressure Piston

The pressures in the oil film are detected by means of a single balanced pressure piston developed from the original concept of Buske and Rolli[18]. The piston operates in a lapped radial hole in the test shaft, with its outer end flush with the surface of the journal. The measuring technique indicates the pressure at an instant in the load cycle determined by a normally open phasing switch

driven from the ram pump camshaft. The test shaft is driven from the same camshaft by a non-slip drive incorporating an indexing mechanism, so that the position of the balance piston in the bearing is known at the instant the phasing switch closes. The indexing mechanism Fig 2.9 enables the piston to survey the pressure at thirty six specific points in the bearing for any given phase in the load cycle. The point of balance is determined by means of an electrical circuit incorporating two switches and a headset. The switches are the normally open load phasing switch and a normally closed switch of which the balance piston is the moving element. Increasing the pressure applied to the inner end of the balanced pressure piston until the closing of the phasing switch can no longer be detected on the headset, establishes the point of balance and the oil film pressure at a specific survey point.

A spring force, opposing the pressure applied to the inner end of the piston, avoids the problems associated with using oil at sub-atmospheric pressure, and provides a means of detecting sub-zero pressures, i.e. tensile stresses, in the oil film.

The initial design of balanced pressure piston incorporated a tension spring and contact ring abutting on the piston shoulder as shown in Fig 2.10. This design of piston proved incapable of accurate pressure measurement as the ring contact lacked the necessary sensitivity and the spring assembly was difficult to adjust.

The final design of piston incorporates a compression spring as shown in Fig 2.11. This design features a complete piston assembly which can be adjusted to a suitable spring pressure and piston travel, before being positioned in the Test Shaft. The .065 in. diameter piston operates with a nominal backing pressure of 90 p.s.i.g. when recording atmospheric pressure. Fine adjustment to this pressure can be made by altering the initial compression of the spring. The piston travel, which is restricted by the electrical contact screw, is set at the minimum distance required for decisive switching.

The balanced pressure piston requires a supply of constant pressure oil, at any pressure in the range 50 - 4000 p.s.i.g. A pneumatic free piston oil pump has been chosen for this duty, as its delivery pressure, which is proportional to the easily varied air pressure, can be varied to give the required range of constant

pressure. The pump delivers through a throttle valve to a system which incorporates a 10 cu. in. accumulator to minimise fluctuations at the higher pressure, Fig 2.13. The oil is supplied via a flexible pipe and split bush to the lower end of the Test Shaft and thence by the oilways to the balance piston, Fig. 2.15. The static pressure applied to the balanced pressure piston is indicated on one of three gauges in the ranges 0-250, 0-1000, and 0-5000 p.s.i.g. The latter gauge is of sealed pressure tube construction.

Indexing Mechanism.

The sprocket wheel of the Indexing Mechanism, Fig. 2.9, is bolted to a 36 tooth escapement wheel and the assembly bored to take a brass bush. This assembly sits on a thrust race and is free to rotate on the drive shaft. Above the escapement wheel a drive plate is keyed to the shaft and slotted to take 2 spring loaded pawls which transmit the drive to the escapement wheel. A tripping plate, free to slide along the shaft, but driven by the driving plate feather, has 2 tripping levers positioned inside the slots which accommodate the pawls.

The indexing action of these tripping levers rotates the pawls and allows the escapement wheel to slip by half of a tooth pitch on the downward stroke and allows the pawl to engage the next tooth on the return stroke. Thus the position of the test shaft relative to the camshaft is altered by 10 degrees per indexing action.

2.7 Measurement of Journal Displacement.

The co-ordinates of the position of the journal centre within the bearing clearance space are determined by measuring linear displacement in two planes through the bearing axis. A lever system has been developed to transmit these journal movements to a Philips' Displacement Pick Up Unit. This system, shown on Fig 2.16, incorporates two sapphire needles which are held against the journal surface, at points beyond the end of the bearing, by light compression springs. The system automatically compensates for any misalignment of the journal and bearing, by measuring the displacement of the mid-point of the vertical lever connecting the horizontal levers which contact the journal surface. Two such lever systems are bolted to the Test Bearing Housing, with their measuring planes set at 90° to each other and at 45° to the load line.

Case hardened journals are required with this measuring system as the operating pressure on the sapphire needles causes rapid wear in a mild steel shaft.

The pick up units are supplied with calibrated leads and, in conjunction with a matched A.C.Bridge incorporating a Direct Reading centre zero Galvanometer, can measure displacements from 10^{-1} to 10^{+3} microns. No further instrumentation is required for constant load conditions as the galvanometer indicates the journal displacement. Dynamic load conditions require a simultaneous record of displacement in both reference planes for graphical tracing of the journal path. Considerable development resulted in a circuit shown diagrammatically on Fig. 2.17 which could operate a pen recorder without signal distortion by extraneous voltages. The modulated carrier frequency from the measuring bridge is fed into a High Gain A.C. amplifier and the output signal rectified i.e. the carrier frequency removed to earth. The modulation is fed into a Direct Coupled Amplifier of an Evershed and Vignoles Rapid Response Pen Recorder, giving a simultaneous record of displacement in both reference planes with a timing pulse derived from the load phasing switch referred to in § 2.6.

This displacement measuring system can display 2 microns of pick-up displacement on 1 inch of pen travel. The normal operating range of the equipment is, however, 20 microns per inch of pen travel.

The system as applied to the Second Testing Machine reflects experience gained with the above system and the considerable advances in instrument technology in the intervening period.

The basic difference in the two systems is that displacements are measured at one end of a self-aligning test bearing housing by a lever system which features a mechanical magnification by a factor of four, Fig 2.18. The wear problem, mentioned above, was not entirely solved by the use of a case-hardened shaft, and the sapphire needles have been replaced by Phosphor-Bronze Balls. The basic measuring transducer is still a Philips Displacement Pick-Up Unit but the means of recording the journal behaviour have been simplified. The pen recorder has been replaced by an Ultra-Violet Recorder which records simultaneously the journal displacement co-ordinates, applied load, friction and timing. Apart from the multichannel feature, the great advantage of the U-V recorder is

that the galvanometer of the A.C. Bridge can be replaced by a galvanometer in the recorder producing an adequate trace without further amplification.

An alternative display facility has been incorporated in the measuring system by modifying a Standard Oscilloscope to work as an x - y plotter. This displays the journal path either as a continuous trace or as a series of sixteen points representing a known value of load phase.

2.8 Friction Measurement.

A torque arm is bolted to the Test Bearing Housing of the First Testing Machine, and the thrust from the arm transmitted via a steel ball to a cantilever arm bolted to the lower support frame. The deflection of the cantilever is continuously measured by a Philips Displacement Pick-Up Unit, and provides a record of the variation of the friction force on the Test Bearing.

Friction Torque on the Test Bearing of the Second Testing Machine is measured by means of the frictionless support described in § 2.2. Torque Arms are bolted to the ends of the test housing hub supporting the hydrodynamic test bearing, and the torque balanced by a thrust transmitted to a dynamometer ring by knife

edges, Fig. 2.6. The load in the dynamometer ring is measured by silicon crystal strain gauges. The response of these gauges to small strains is sufficient to operate the galvanometer of a U-V recorder without amplification. Fig. 2.23.

2.9 Load Measurements.

Three systems are available for the measurement of Applied Load in the First Testing Machine.

The first system provides a spot check on the magnitude of the maximum applied load per cycle by means of a Dobbie-McInnes Peak Pressure Indicator connected to each load capsule.

The cyclic variations in load capsule pressure are recorded in the second system by C.A.V.-Ricardo Photoelectric Pressure Gauges. The output signals from gauges attached to opposing capsules are simultaneously recorded on the pen recorder detailed in § 2.7.

The measurement of strain in the connecting-rods of the loading system is the basis of the third system of recording Applied Load. Three, 200 ohm resistance, strain gauges are secured axially to each connecting-rod and with three similar temperature compensating

gauges form the two active arms of a bridge connected to the bridge circuit described in § 2.7. The strain variations in the connecting rods are simultaneously recorded and the nett load determined by graphical means.

A single differential pressure transducer is used to measure the load applied to the test shaft of the Second Testing Machine. This pressure transducer works on a variable inductance principle and is powered in this application by a Philips Direct Reading Bridge. The galvanometer of a U-V recorder replaces the direct reading galvanometer of the bridge, and provides a continuous record of the pressure differential between diametrially opposed load capsules.

2.10 Temperature Measurement

A survey of temperature sensitive elements (31-36) was carried out as a preliminary to measuring the oil film temperature in the First Testing Machine. This survey indicated that Thermistors operated with a shorter response time than thermocouples, and it was thought feasible to mount such a device in the Tufnol plug already mounted in the test shaft. Preliminary trials with thermistor elements were encouraging but more pressing problems

prevented further development of this technique, and the measurement of the temperature of leakage oil, flowing over the upper surface of the test housing, with a mercury bulb thermometer has to suffice.

In the Second Testing Machine the temperatures of the oil at the inlet to the supply groove and of the phosphor bronze in the central plane of the bearing in the vicinity of the minimum oil film is measured by Eureka-Nickel Chromium thermocouple junctions mounted on the end of stainless steel hypodermic tubes.

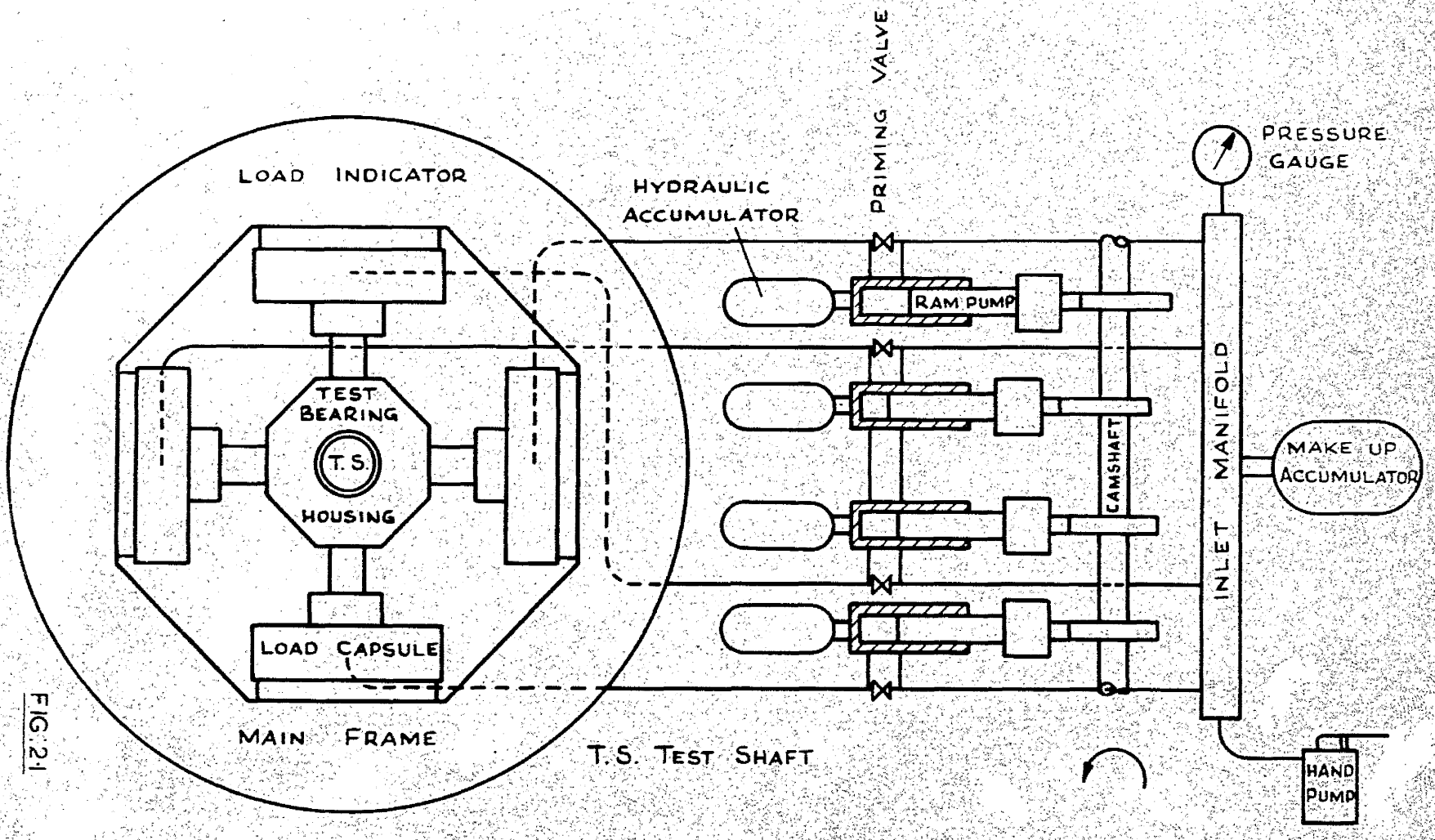
LOAD INDICATOR
HYDRAULIC ACCUMULATOR
PRIMING VALVE
PRESSURE GAUGE
RAM PUMP
TEST BEARING
T.S.
HOUSING
CAMSHAFT
INLET MANIFOLD
MAKE UP ACCUMULATOR
LOAD CAPSULE
HAND PUMP
MAIN FRAME
T.S. TEST SHAFT

FIG. 2.1

HYDRAULIC RAM PUMP

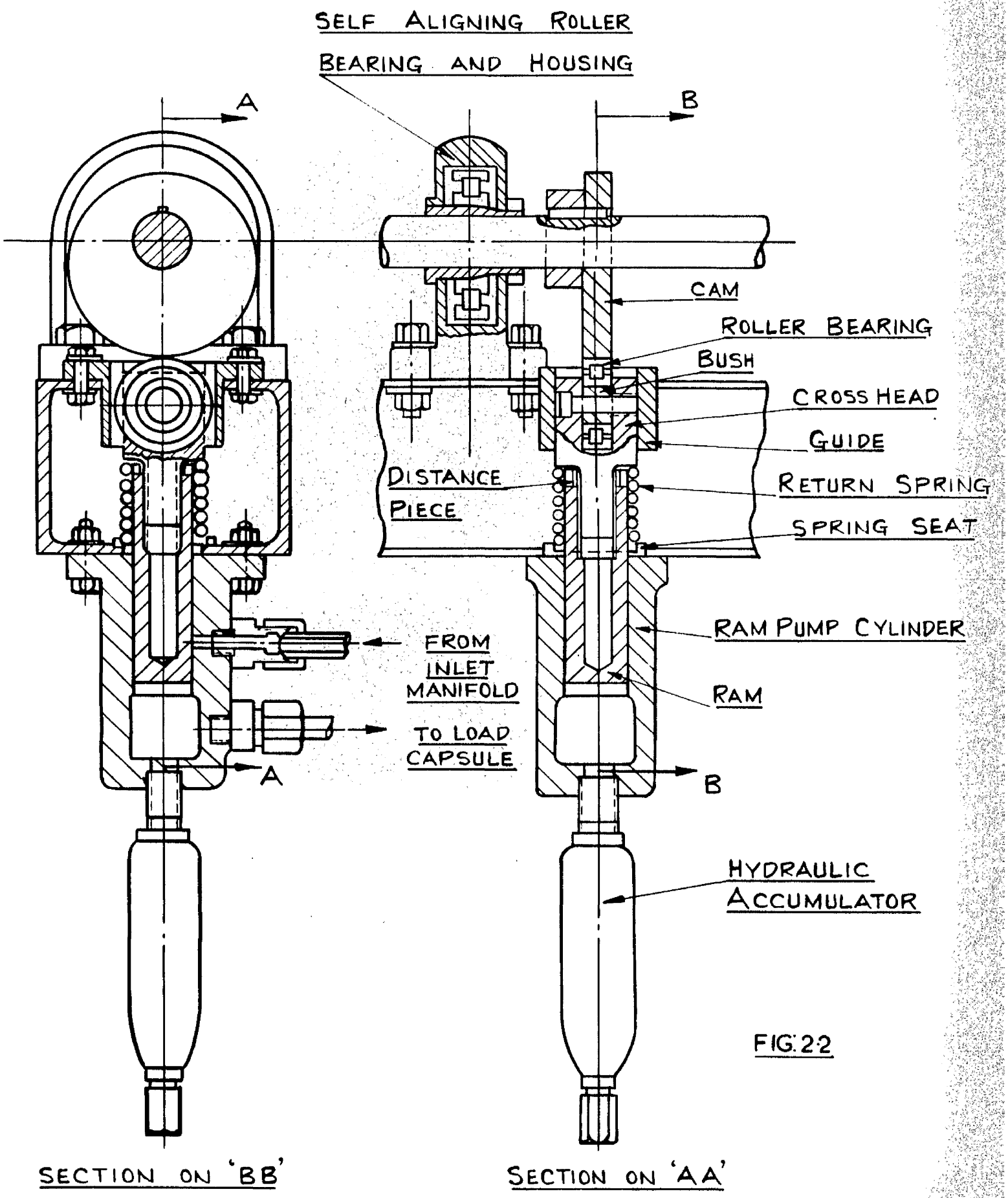

FIG. 2·2

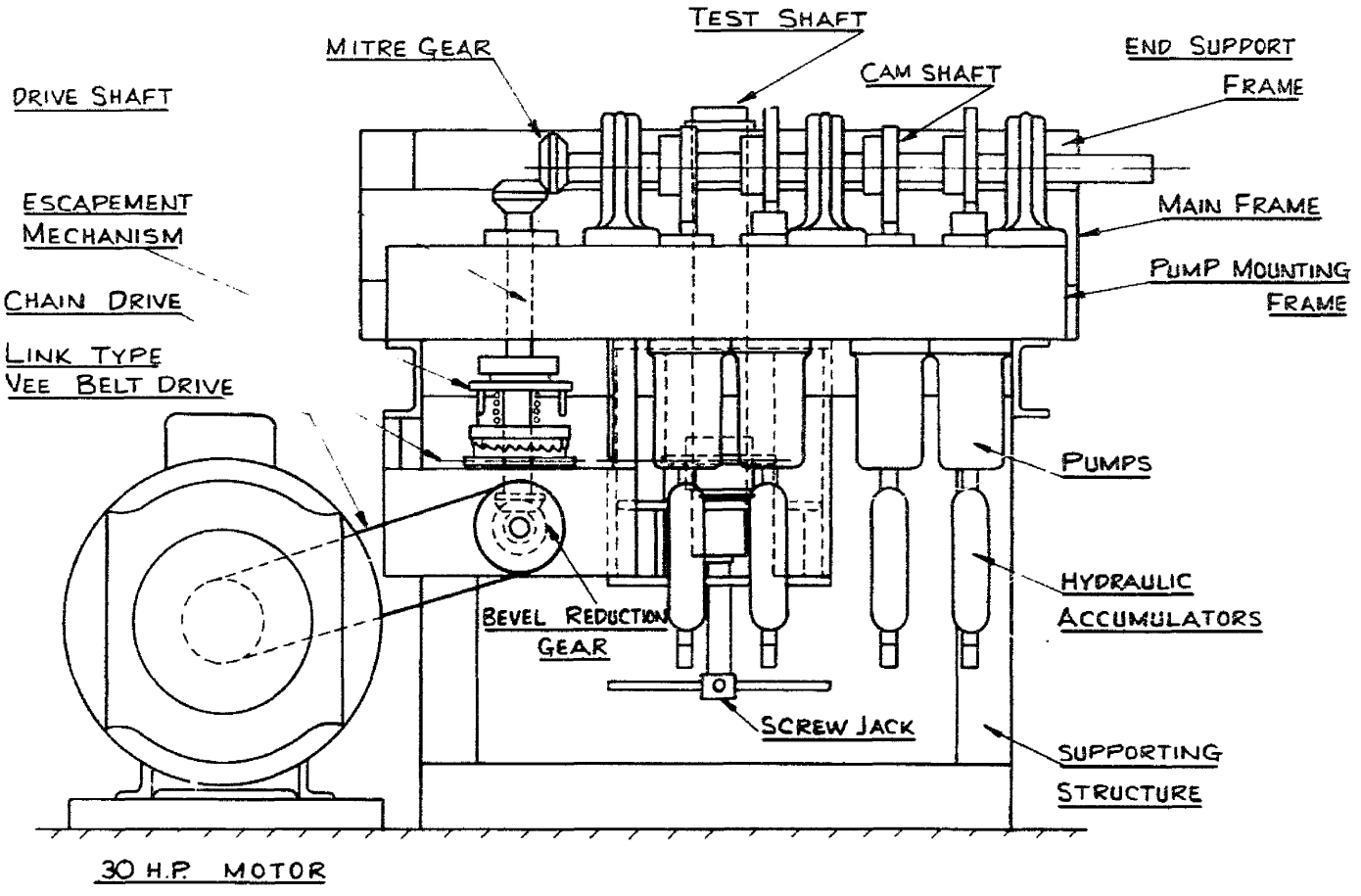

ARRANGEMENT OF DRIVES, SHAFTS AND RAM PUMPS

FIG. 2·3

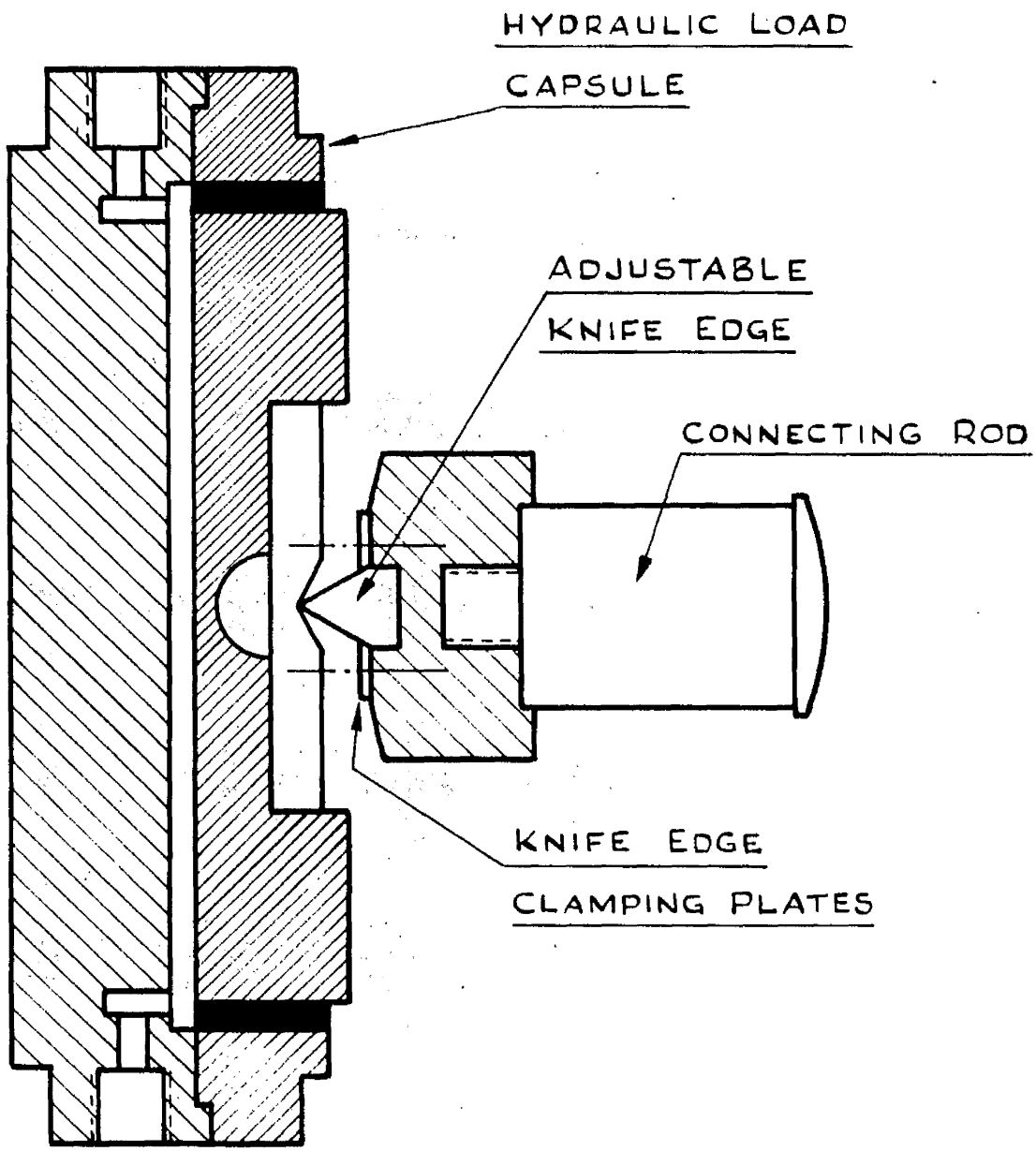

CONNECTING ROD AND KNIFE EDGE

FIG:2.4

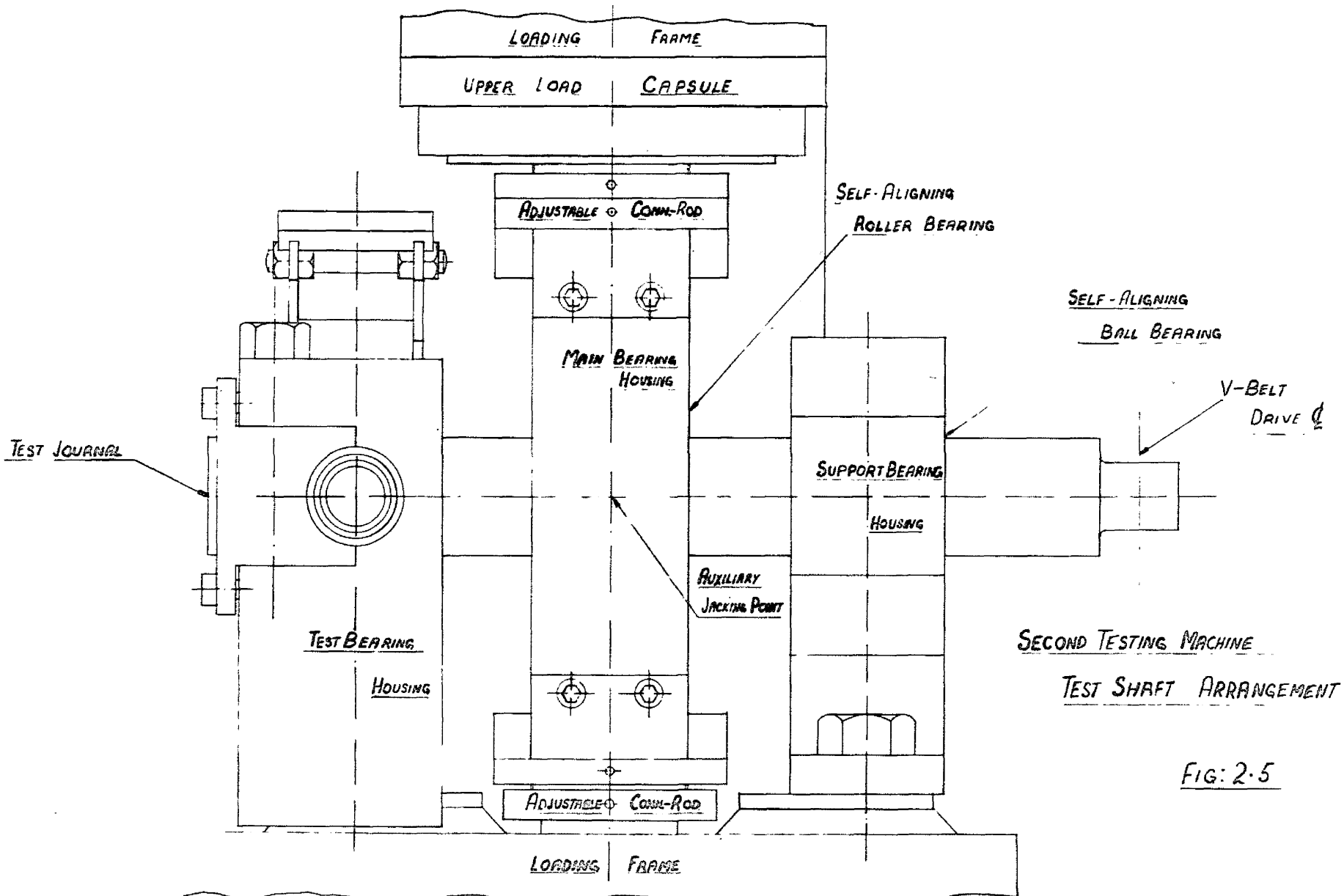

SECOND TESTING MACHINE

TEST SHAFT ARRANGEMENT

FIG: 2·5

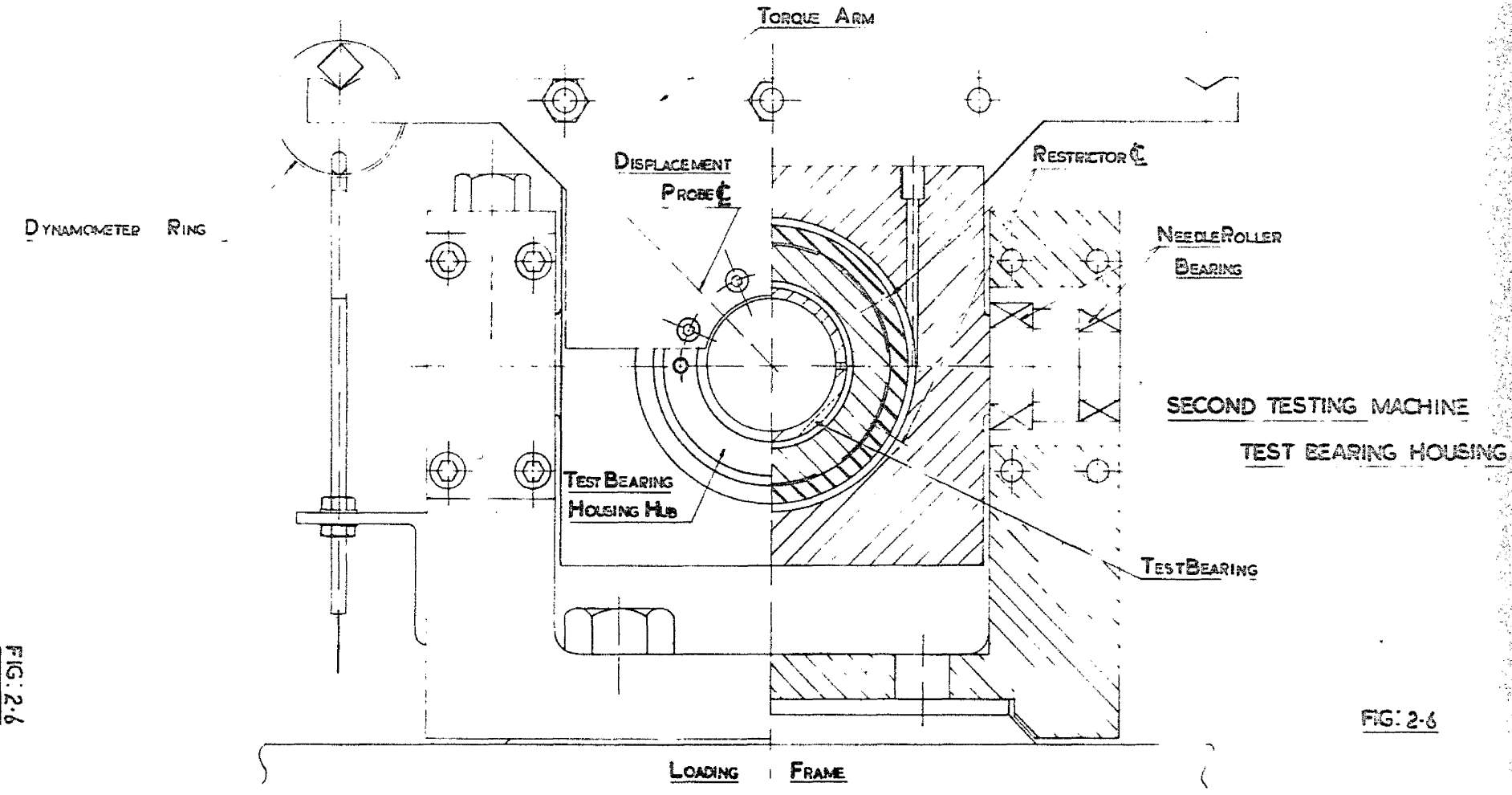
TORQUE ARM
DISPLACEMENT PROBE ℄
RESTRICTOR ℄
DYNAMOMETER RING
NEEDLE ROLLER BEARING
SECOND TESTING MACHINE
TEST BEARING HOUSING
TEST BEARING HOUSING HUB
TEST BEARING
LOADING FRAME

FIG: 2-6

FIG: 2-6

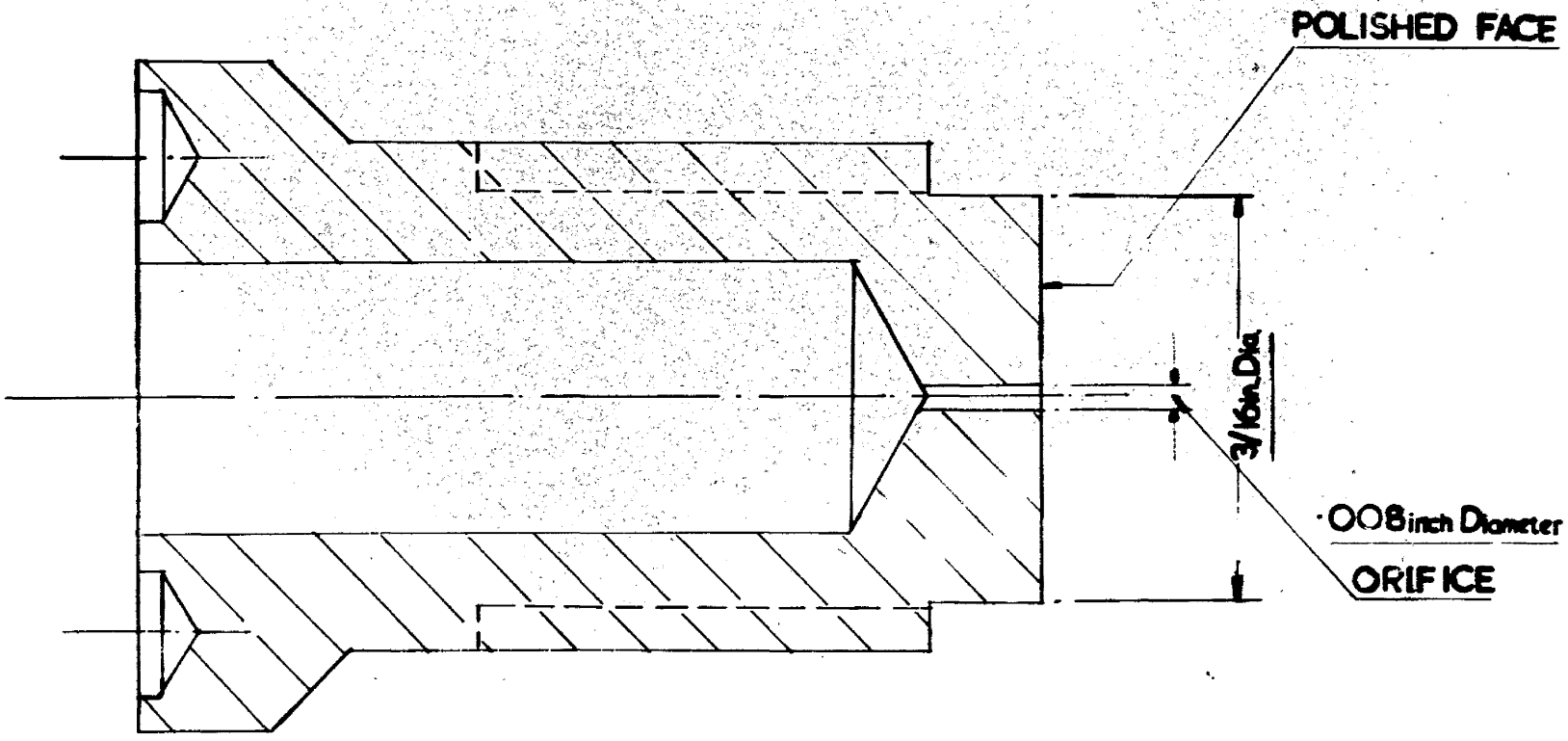

ORIFCE TYPE RESTRICTOR

FIG:2·7

FIG:2·7

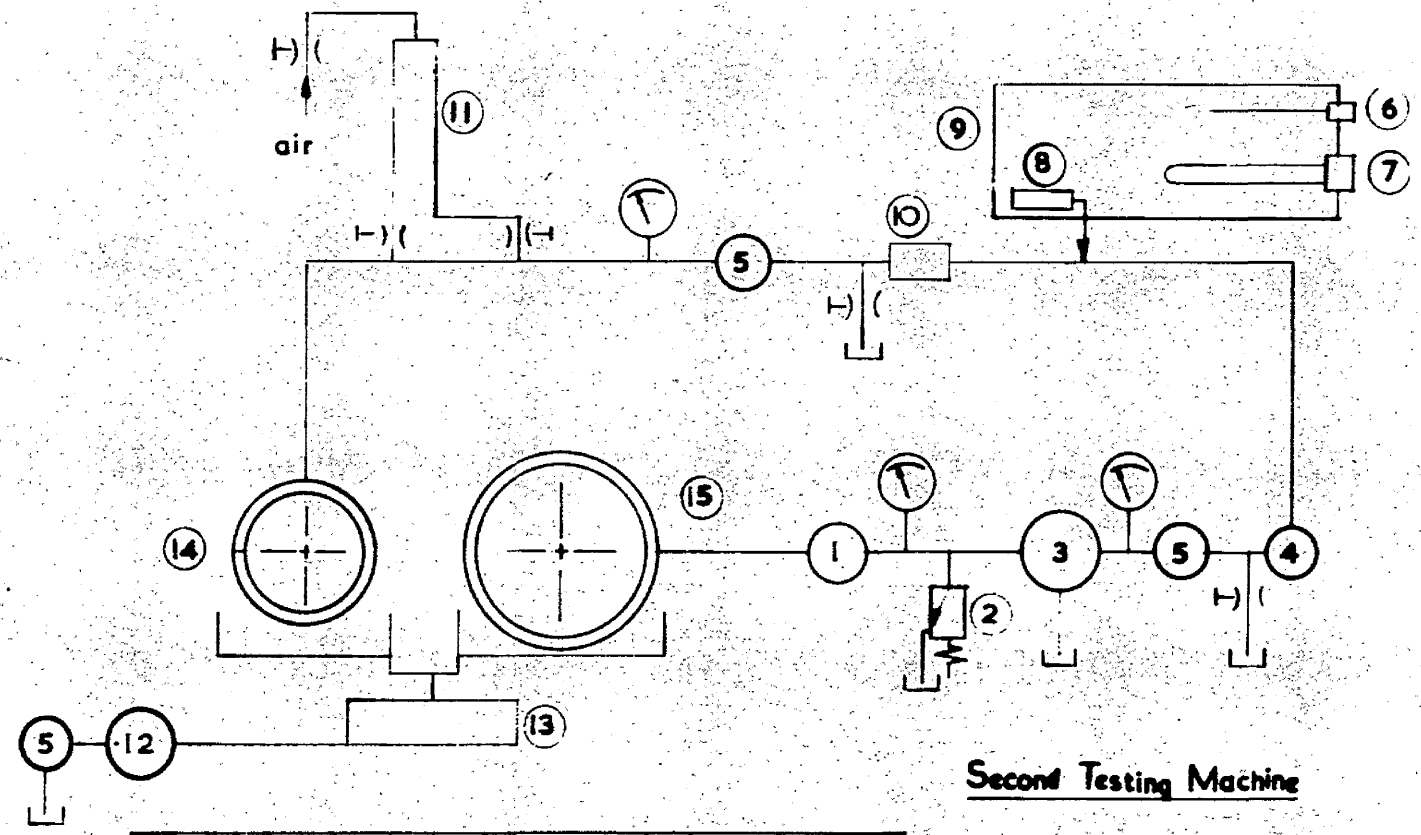

Second Testing Machine

Lubricating Oil System

1	1μ Filter	6	Thermostat	11	Manometer
2	Relief Valve	7	Heater	12	Cent. Pump
3	H.P. Pump	8	Strainer	13	Dry Sump
4	L.P. Pump	9	Oil Tank	14	Test Bearing
5	5μ Filter	10	Imo Pump	15	Ext Pres Bearing

FIG: 2·8.

FIG: 2·8.

ESCAPEMENT MECHANISM

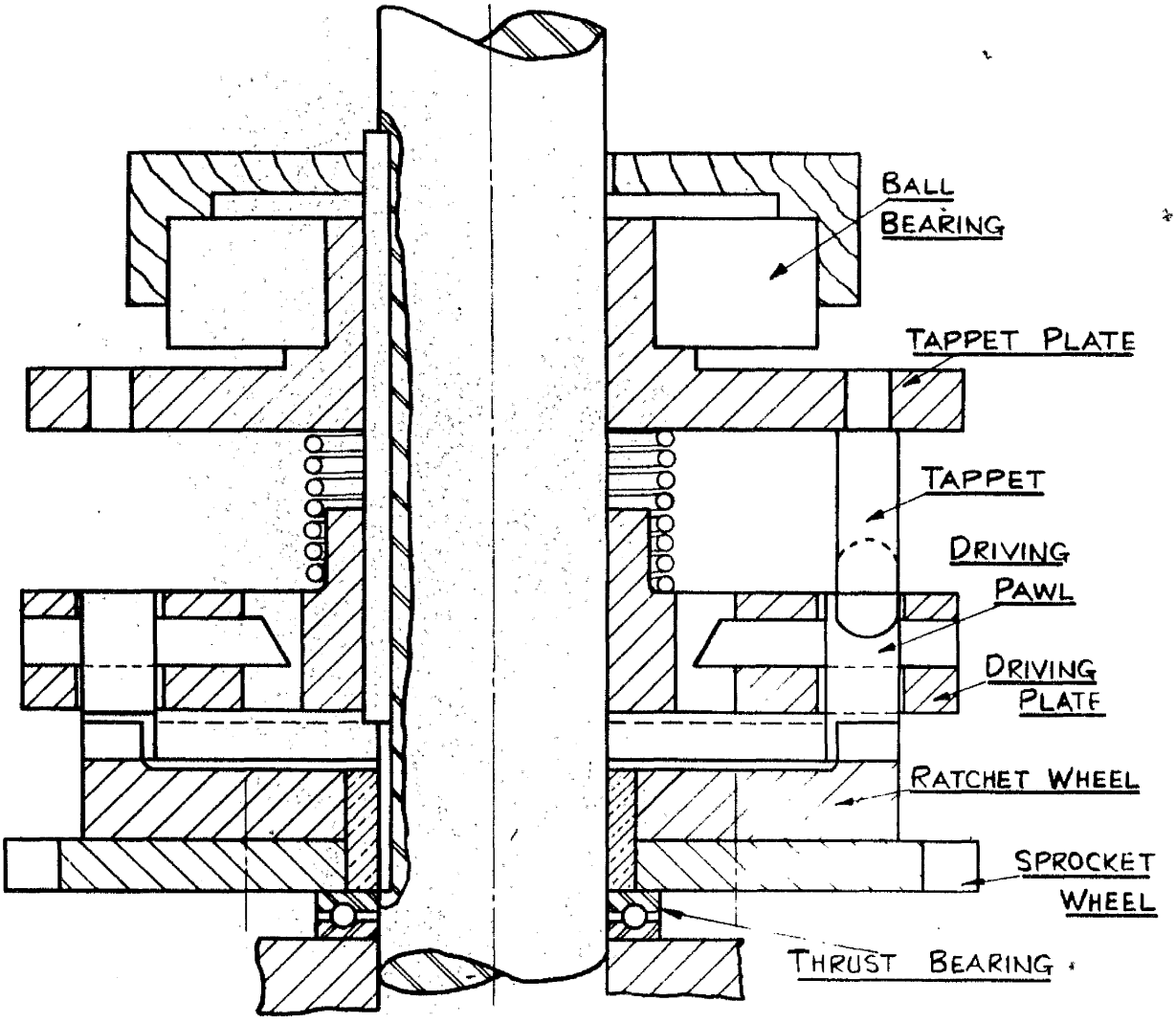

FIG: 2·9

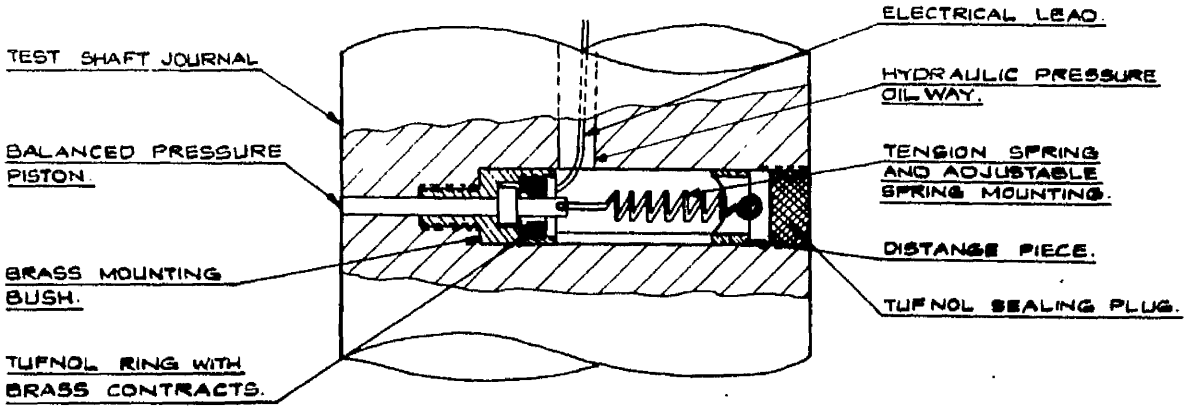

FIG. 2.10

BALANCED PRESSURE PISTON MK. 1.

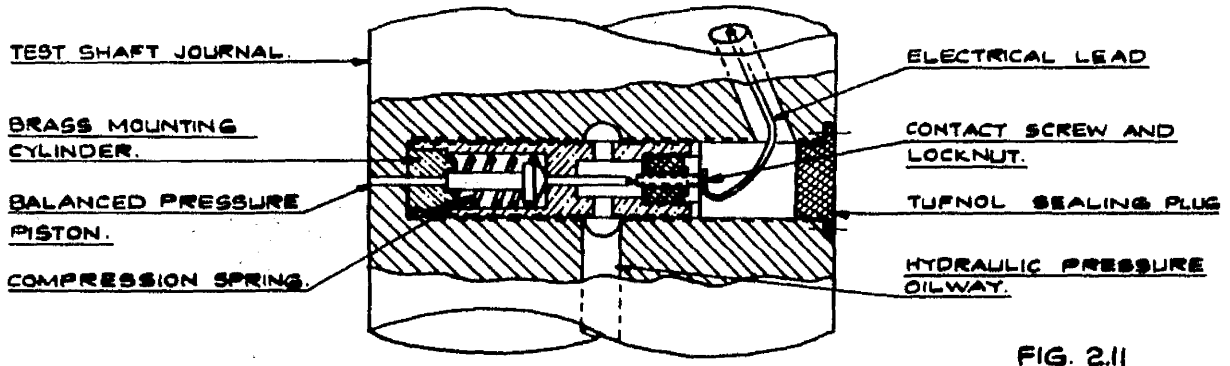

FIG. 2.11

BALANCED PRESSURE PISTON MK. 2.

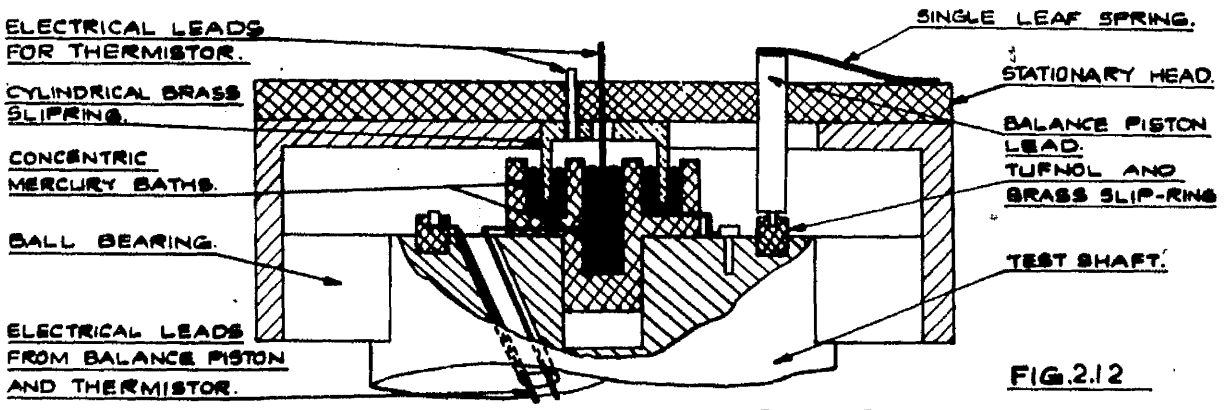

FIG. 2.12

SLIP RING ASSEMBLY.

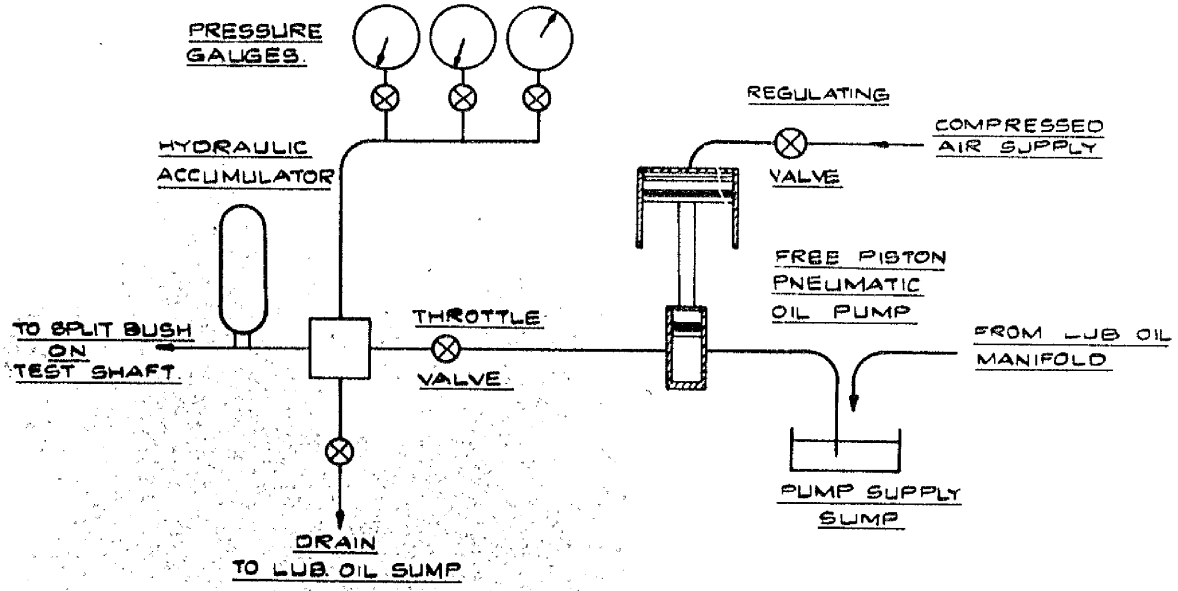

BALANCE PISTON HYDRAULIC PRESSURE SYSTEM. FIG. 2.13

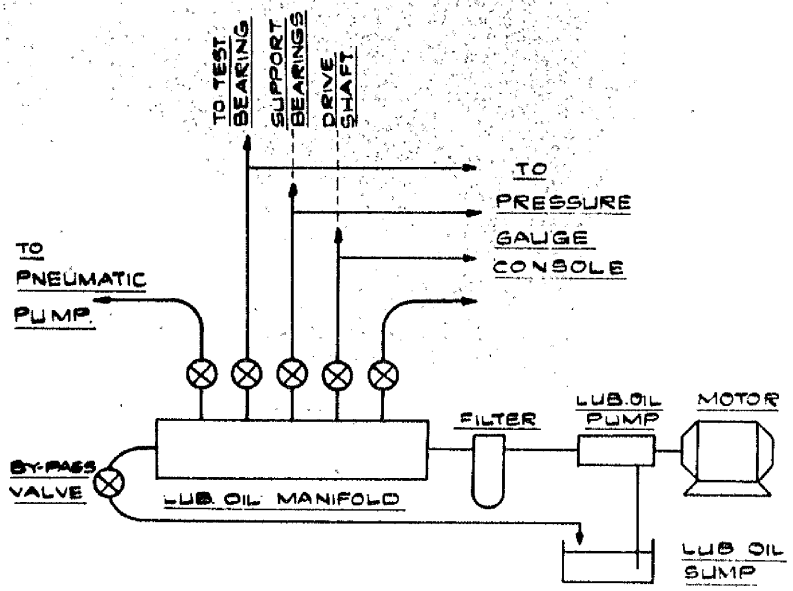

LUBRICATING OIL SUPPLY SYSTEM. FIG. 2.14

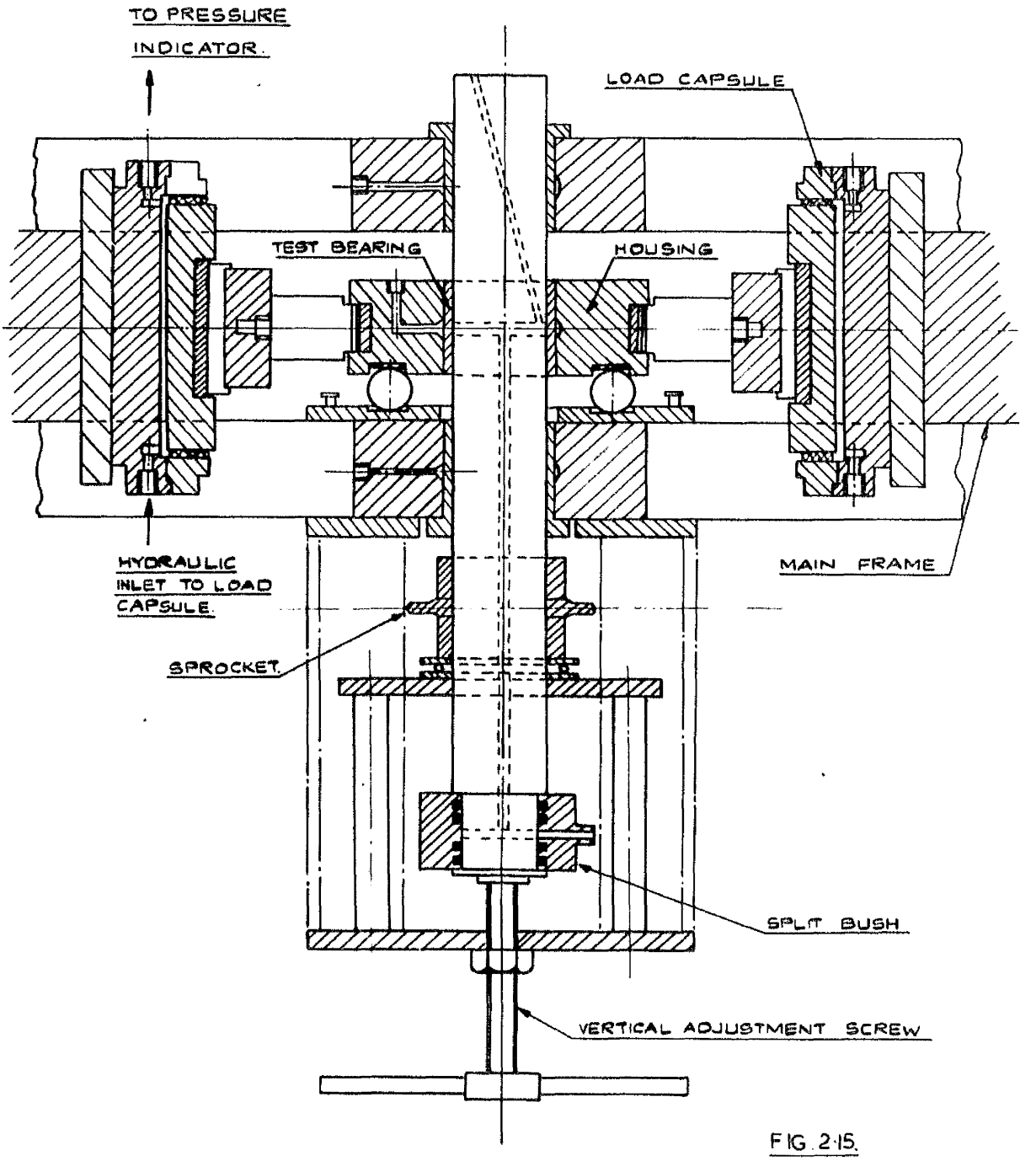
TO PRESSURE INDICATOR.
LOAD CAPSULE
TEST BEARING
HOUSING
HYDRAULIC INLET TO LOAD CAPSULE.
MAIN FRAME
SPROCKET
SPLIT BUSH
VERTICAL ADJUSTMENT SCREW

FIG. 2·15.

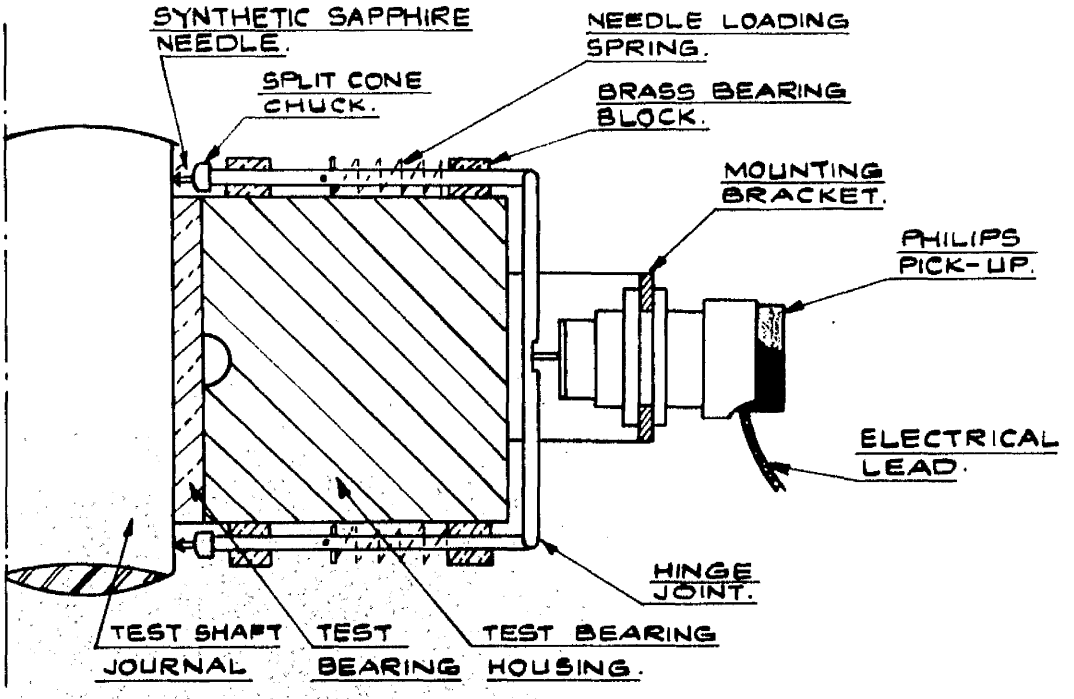

DISPLACEMENT PICK-UP AND LEVER SYSTEM.

FIG: 2·16

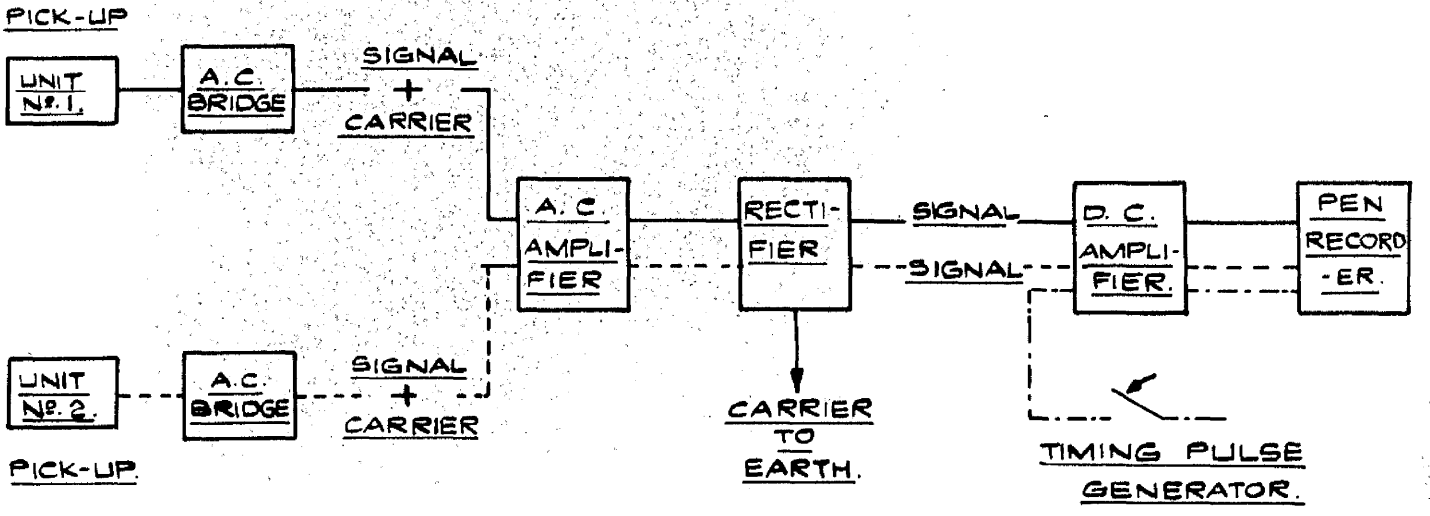

DISPLACEMENT PICK-UP AND PEN RECORDER CIRCUIT.

FIG: 2·17

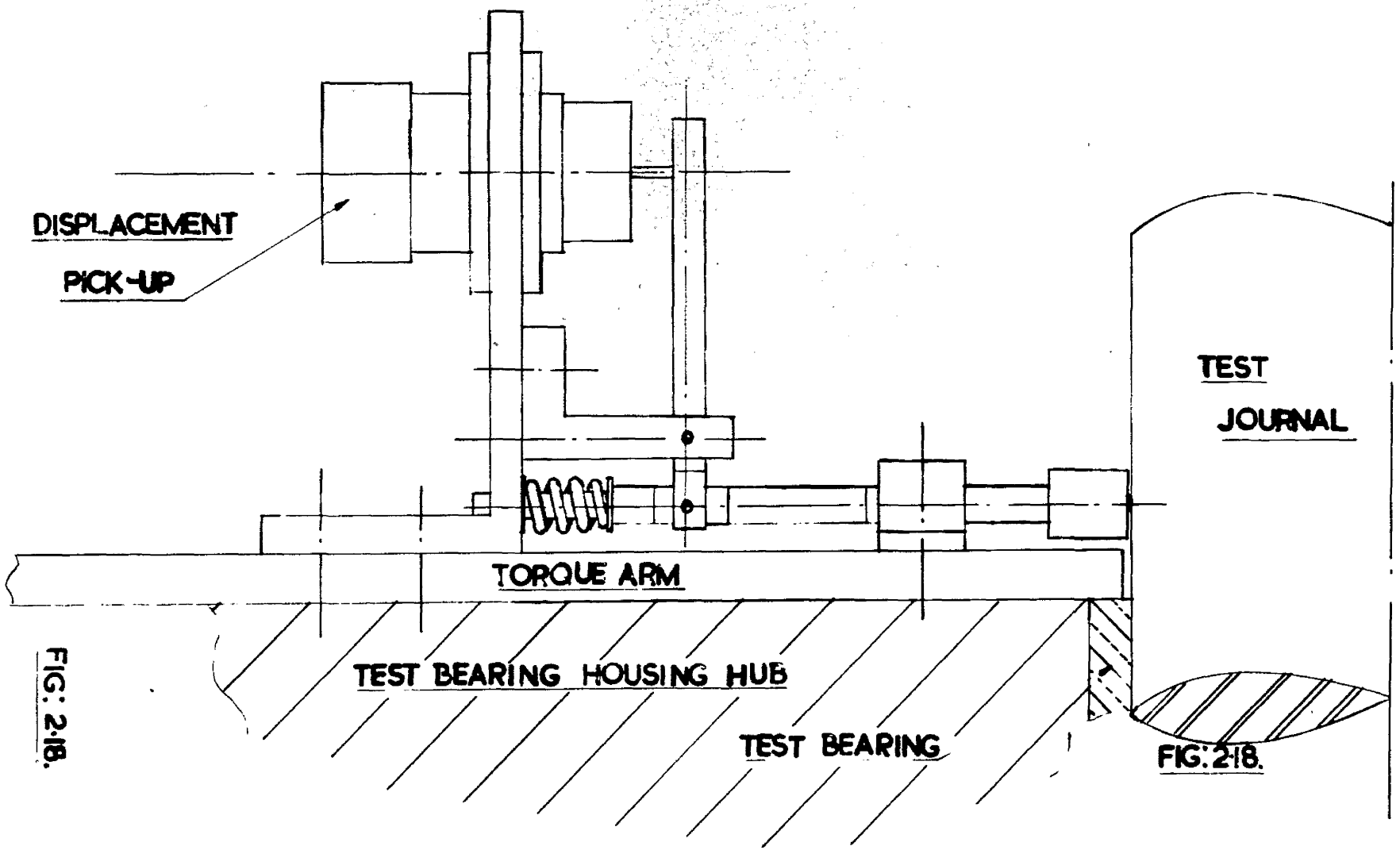

FIG: 2.18.

FIG: 2.18.

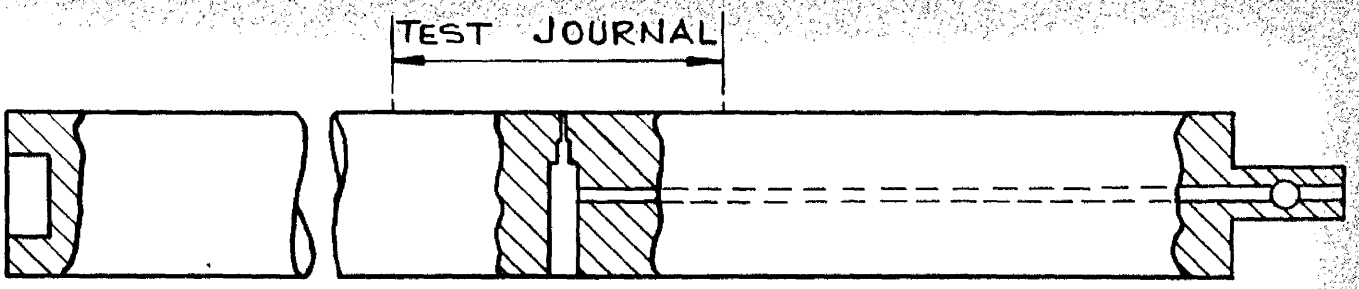

TEST SHAFT FOR MK1 BALANCE PISTON FIG:2·19

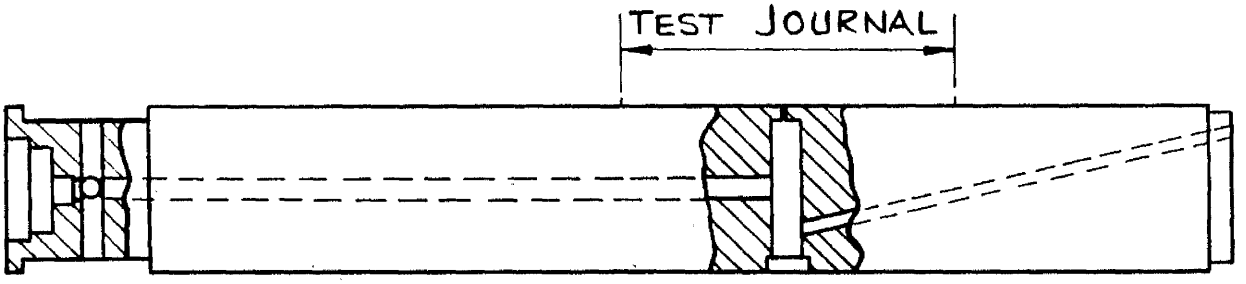

TEST SHAFT FOR MK 2 BALANCE PISTON

FIG:2·20

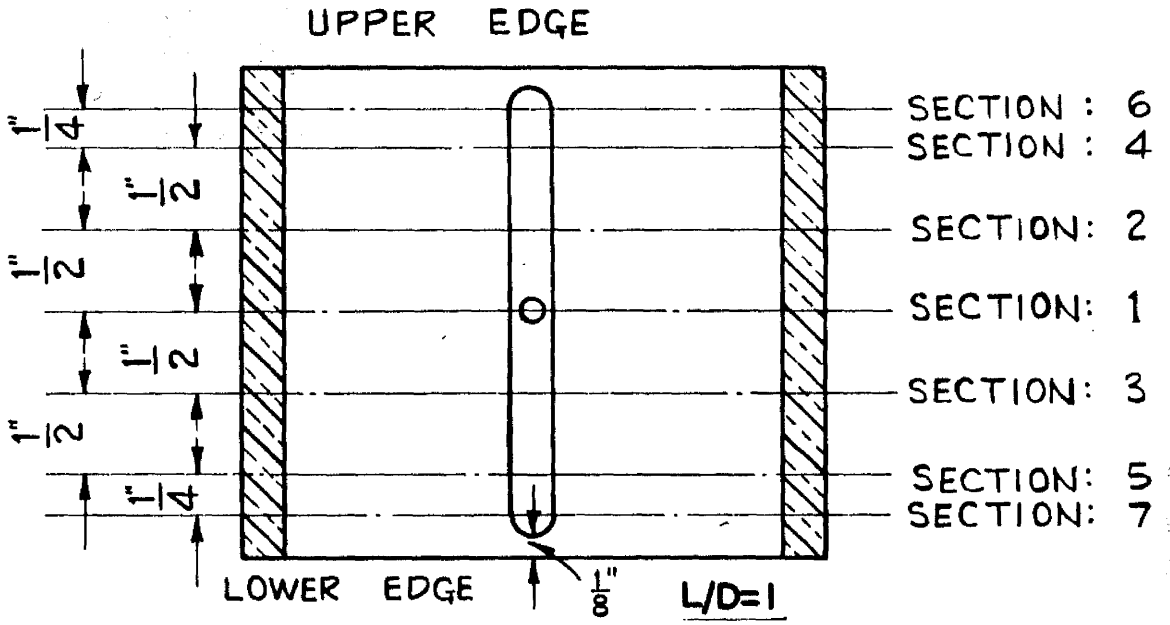

PHOSPHOR BRONZE TEST BEARING BUSH FIG.2·21

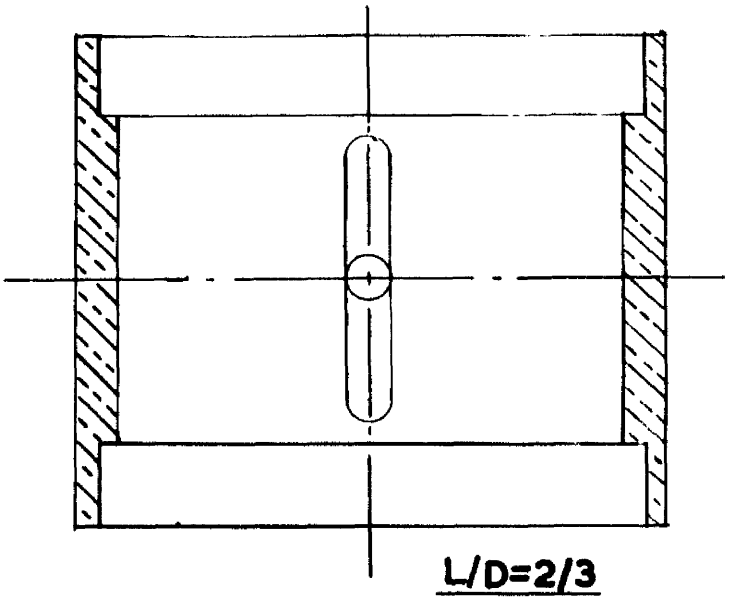

L/D=2/3

PHOSPHOR BRONZE TEST BEARING BUSHES

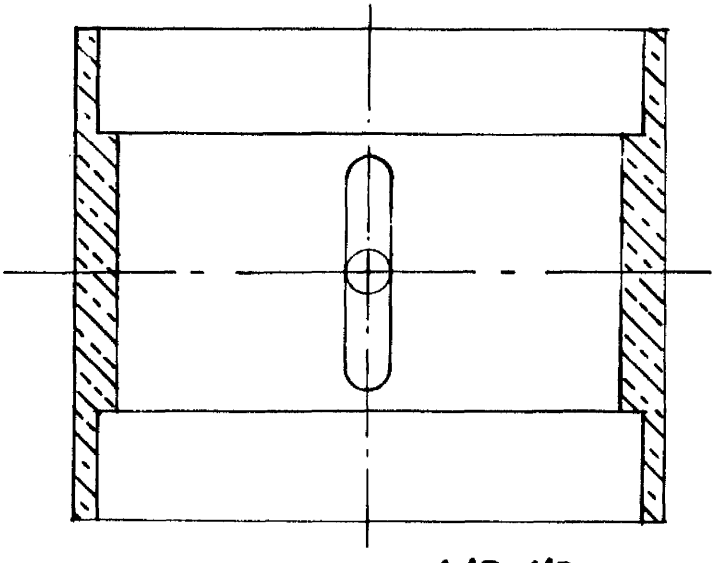

L/D=1/2

FIG: 2·22

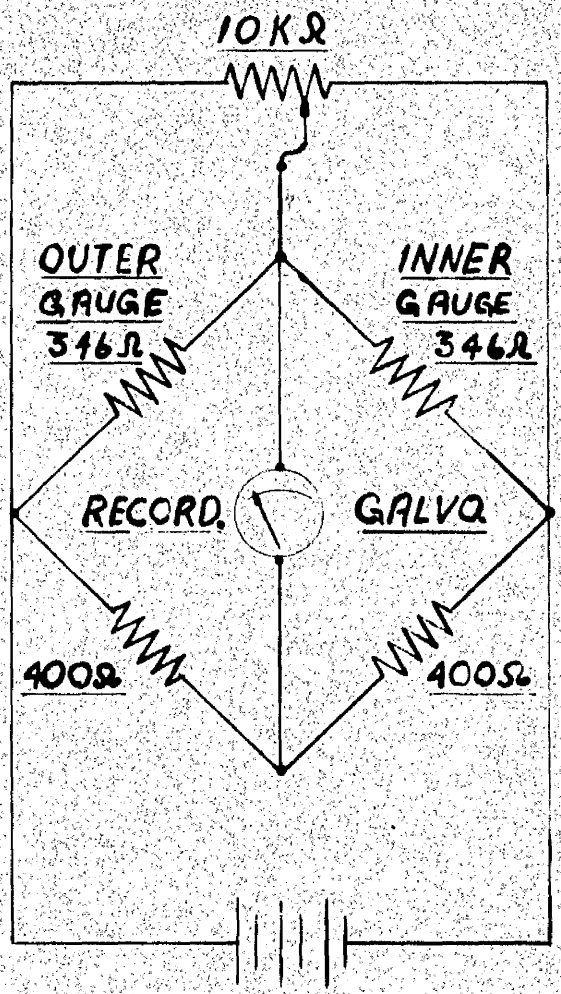

STRAIN BRIDGE FOR DYNAMOMETER RING.

STRAIN GAUGE FACTOR: OUTER = 108

INNER = 108·5

FIG. 2·23

CHAPTER III

3. Experimental Procedure

3.1 Bearing Size

The diameter of each test journal was accurately determined on a comparator by taking measurements in a series of planes at 0.5 inch intervals along the length of the journal. The variation in diameter in all planes of both test shafts was found to be less than 0.00005 inches, and the mean diameter was established at 3.0002 and 2.9966 inches for the test journals used in the First and Second Testing Machines respectively.

The relevant mean diameter was taken as a datum for each Testing Machine, and the Phosphor Bronze bushes bored in situ to give the required bearing clearances. The finished size of the bearing was compared with a Standard Ring Gauge by means of a bore gauge reading to 0.0001 inches.

3.2 Journal and Bearing Alignment

The first stage in the alignment of the First Testing Machine was the levelling of the plate under the Test Bearing Housing until the upper surface of the housing was parallel to a plane represented by the upper surface of the end support frame. The connecting rods

were then placed in position and the height of the line of thrust of the applied load relative to the Test Bearing Housing adjusted by means of levelling screws under the load capsules. The line of thrust was in its optimum position when the application of equal pressures to diametrically opposed load capsules produced no tilting of the Test Bearing Housing from the previously established position. Any tilting movement was detected by clock gauges reading to 0.0001 inches.

A more exacting alignment procedure was feasible in the Second Testing Machine as the alignment of the Trunnion Bracket and Test Journal remained undisturbed throughout the range of bearings investigated.

The object was initially to set the Test Shaft Axis parallel to the machined pads on the bedplate of the load frame. To this end, an equal pressure was applied to the load capsules and packing shims placed under the Ball Bearing Housing until the test journal centreline was parallel to the front bedplate pad. The desired journal level was established by comparing the height of the journal at various positions along a 6 inch test length with the height of slip gauges mounted on the bedplate pad. At a height of 7.7894 inches the journal axis was found to be parallel to the bedplate.

Previous examination on a surface table indicated that the axis of rotation of the test bearing housing in the trunnion bracket was 7.7465 inches above the clamping face, and packing; .045 inches thick, was placed between the mating faces before the initial clamping of the trunnion bracket to the bedplate.

At this stage a specially prepared alignment bearing was mounted in the trunnion bracket to set the tilting plane of the Test Bearing Housing in a plane normal to the test shaft axis before final clamping of the bracket to the bedplate of the loading frame. The alignment bearing had a diameter of 3.0 inches and length of 2.0 inches, and incorporated two pressure tappings positioned $\pm$ 0.25 inches from the centre of the bearing in the vicinity of the maximum oil film pressure. The optimum bracket position existed when the film pressures at the measuring points were equal and increased in equal increments for a range of static loads, applied with the journal running at a constant speed.

This type of bearing constitutes the most sensitive alignment tool available to the bearing investigator and showed its value in the Second Testing Machine when it was possible to place a half length bearing in the housing and run a complete test series with no need for further adjustment to the alignment of the trunnion bracket.

3.3 Dynamic Load Operation

Throughout the current investigations two diametrally opposed load capsules were used in the testing machines to apply a range of alternating pulsating, and static loads.

The mass of air in the system and the ram-pump inlet pressure controlled the magnitude and cyclic variation of the load in the First Testing Machine. To ensure that the applied load did not vary from a prescribed form throughout the prolonged period of up to ten days required for a seven section pressure survey, thorough and prolonged bleeding of the hydraulic system was required. This was readily achieved by venting the system through the 3-way cocks of the Peak Pressure Indicators which were mounted at the highest points on the testing machine.

Both ram pumps were connected to a common manifold so that the mass of air retained in the accumulators forms the only means of balancing any variation in the magnitude of the alternating loads due to variations in the elasticity of the individual load capsule - ram pump circuits.

Several trial runs were required to achieve the critical load balance as the hydraulic system had to be reduced to atmospheric

pressure to ensure that the poppet valve in the accumulator was closed, before the charging pressure in the air bag could be adjusted. Once the required balance was attained, however, it remained unaltered throughout a prolonged test period.

The air bag in the one quart accumulator attached the ram pump inlet manifold was charged to a pressure equal to 50% of the manifold pressure required for a given test condition.

In applying dynamic loads to the test bearing housing in the First Testing Machine the following routing was observed:-

1) Set the oil supply pressure to the test bearing at 40 p.s.i.g.

2) Apply the base pressure to the inlet manifold with the priming valves open and start the drive motor.

3) Apply the dynamic load by simultaneously closing the priming valves on Diametrically opposed capsules.

This procedure was reversed when stopping the machine under normal running conditions.

The three parameters which controlled the magnitude of the applied load in the Second Testing Machine, were the ram-pump inlet pressure, the mass of air in the ram-pump accumulators, and

the variable throw of the ram-pump eccentrics. The reproducibility of load conditions was not so critical in this testing machine as pressure surveys were not required and the load variation was simultaneously recorded with other bearing variables.

The normal procedure was to thoroughly bleed the system paying particular attention to the bleeding of the differential pressure transducer, and charge the ram pump accumulator air bags to 40 p.s.i.g. The throw of each ram pump eccentric was then adjusted to give the same maximum pressure in opposing load capsules for a given ram-pump inlet pressure.

The routine detailed below was followed in setting up Dynamic Loads on the Second Testing Machine.

1) Start the header tank circulation pumps and switch on the electric oil heater.
2) When the oil supply has reached the required temperature start the dry sump return pump and set the oil supply pressure to the test bearing at 30 p.s.i.g.
3) Set the supply pressure to the externally pressurised bearing at that value, in the range 1000 to 2000 p.s.i.g., which preliminary tests have shown to be suitable for the anticipated load.

4) Start the test shaft drive and lubricant pump for the ram-pump eccentrics.

5) Start the eccentric drive motor and raise the ram-pump inlet pressure to the required level.

6) Apply the dynamic load by closing the priming valve between the ram pump outlets.

This routine was reversed on stopping the machine.

The time required to reach steady temperature conditions was a more critical problem under the relatively short duration tests required for journal displacement measurements than under the prolonged running at a given load condition required for the oil film pressure surveys.

In the First Testing Machine a settling period of 45 minutes was allowed after a change in applied load, when displacement measurements were being recorded.

The temperature measuring probes of the Second Testing Machine provided a clear indication of the steady state conditions in the Test Bearings. The ability of this machine to run unattended for prolonged periods enabled occasional long term steady state temperatures to be established for various combinations

of loads and journal speeds. In general it was found that on setting up a given load at a journal speed of 300 r.p.m. 40 minutes was required for the bearing temperatures to settle and that after subsequent increases in the journal speed at the same load, a period of 25 minutes was required to establish steady temperature conditions.

3.4 Static Load Operation

The procedures for applying Static Loads follow closely those laid down in § 3.3.

In the First Testing Machine the ram-pump inlet ports were sealed off for static load running by clamping the pistons at Bottom Dead Centre. A constant pressure was then applied to the Inlet Manifold by a hand pump and the priming valves closed when their associated capsules reached a pressure corresponding to the required load. The same procedure applied to the Second Testing Machine, except that each ram-pump outlet was sealed off by an isolating valve.

3.5 Load Phasing

The Load Phasing Switch was driven from the ram-pump camshaft of the First Testing Machine, with the zero position

of its Protractor Scale set to coincide with the Top Dead Centre position of a known ram-pump. The relevant magnitude of the applied load at which the switch was closed was then determined from the recordings of the cyclic variation of the applied load detailed in § 3.9.

A load phasing indicator, which was driven from the ram-pump camshaft of the Second Testing Machine, was used to put sixteen load phase marks per cycle on the journal path displayed on the X-Y oscilloscope. The indicator was set with the reference mark coincident with the maximum value of load applied by the upper load capsule.

3.6 Angular Position of the Balanced Pressure Piston

The datum position of the balanced pressure piston was established by raising and rotating the test shaft until the piston end was visible above the test housing and set in an axial plane coincident with the oil inlet grooves. With the test shaft held in this position, the camshaft set in the zero phase position, and the indexing mechanism driving the zero tooth, the drive chain was secured to its sprockets. The true angular position of the balanced pressure piston Θ degrees, when the load phase was set

at zero degrees, was indicated by the angle (360-B) degrees, where B represents the angular position of the driven tooth of the indexing mechanism. The negative sign indicates that the indexing action moved the position of the piston in a direction opposite to that of the rotating test shaft. At other values of load phase, the Balance Piston Position was given by;

$$\Theta = (360 - B + F) \text{ degrees.}$$

3.7 Measurement of Oil Film Pressures

Variation of the Pressure Differential across the Balanced Pressure Piston produced the following range of signals in the attached headset.

When the pressure applied to the inner end of the balance piston produced a force which was less than the combined forces from the film pressure at the survey point acting on the outer end of the balance piston and the compression spring, a steady series of signals could be detected in the headset, as the phasing switch closed once per load cycle. The signals became intermittent as the applied back pressure was increased, and the piston reached a balance point, and ceased on further increase of the applied back pressure.

The balance pressure P_b was taken as the mean value in that narrow band of pressures within which intermittent signals were detected.

The film pressure P_f at the survey point was given by:- $P_f = P_b - P_a$, where P_a was the atmospheric datum pressure.

The Atmospheric Datum Pressure is controlled by the compression spring incorporated in the balance piston assembly Fig 2.11 and was that applied backing pressure at which the piston was in balance when detecting atmospheric pressure. The magnitude of this value of backing pressure and the maximum travel of the balance piston were adjusted and preset by operating the piston in a calibrating fixture before insertion in the test shaft. Each group of pressure measurements in a large survey was preceded and succeeded by an in situ check of the Atmospheric Datum Pressure. This was achieved by raising the test shaft until the balance piston was clear of the Test Bearing Housing and measuring the backing pressure required to break the balance piston circuit.

The survey points in the bearing were situated at 20 degree intervals around each bearing section with intermediate points at 10 degree intervals where finer details of the pressure variation

were required. The pressure at each survey point was measured at load phase intervals of 30 degrees.

The axial location of the Balance Piston in the Test Housing was determined by measuring the height of the upper surface of the test shaft above the reference plane represented by the upper surface of the end support frame. To facilitate this procedure a set of height gauges were machined each representing one of the 7 sections surveyed in the bearing.

3.8 Measurement of Journal Displacement

The problems involved in measuring quantities which vary cyclically can be considerable as the recording system distorts the representation of the measured variable when operating at frequencies close to its own natural frequency. At the time of the initial displacement measurements on the First Testing Machine, instrumentation for continuous recording was limited in this field of bearing research. The considerable advances in the design of Ultra-Violet Recorders in the intervening period produced a recording instrument for use in the Second Testing Machine which incorporated a variety of interchangeable galvanometers. These galvanometers have a range of natural frequencies from 30 to 500

cycles per second, but their sensitivity is inversely proportional to their natural frequency.

Galvanometers with a natural frequency of 160 cycles per second and a useful recording range of 0 to 100 cycles per second have been used in the simultaneous recording of all variables measured on the Second Testing Machine. Every journal path was displayed and photographed on an X-Y oscilloscope and frequent comparisons made with the path plotted from the co-ordinates presented by the U-V recorder, to verify that the recording system was not superimposing a self generated variation. A typical comparison is shown on Fig 3.1.

Each Displacement Pick-Up-Direct Reading Bridge pair was calibrated as a measuring unit by mounting the displacement pick-up in a fixture incorporating a micrometer gauge. A mean position was selected on the micrometer, and the bridge progressively balanced until the galvanometer zero position was unaltered at all six gain settings of the bridge amplifier. The gain of this differential amplifier was then balanced to give the same galvanometer deflection about the centre zero position for equal displacements of the pick-up above and below the selected mean position of the micrometer. The

zero position was then re-examined and the process of balancing repeated.

A different technique was required in mounting the Displacement Pick-Ups in their respective testing machines. The Pick-Ups on the First Testing Machine were mounted with their bridges set at minimum gain and the mean position of the transducers set in the position which ensured that all subsequent galvanometer deflections would be on the positive scale. This setting was necessary as the pen recorder used in conjunction with the bridges was not a centre zero instrument. Each record of journal displacement was calibrated by deflecting the Direct Reading Galvanometer to a series of known displacement values and recording the corresponding displacements on the pen recorder chart.

The pick-ups were adjusted in the mountings of the Second Testing Machine until the galvanometer readings were zero with the bridge amplifiers set at minimum gain. No direct calibration of the U-V recorder trace was necessary but the gain of the differential amplifiers of the X-Y oscilloscope were balanced to give an equal beam deflection in all directions for a given pick-up displacement.

The placing of a given journal path within the clearance circle is without doubt the most difficult and critical aspect of journal displacement measurements.

On the First Testing Machine the path of the journal centre was determined from the calibrated pen recorder trace by plotting the recorded co-ordinates on a system of rectangular co-ordinates. The minimum film thickness was then determined by superimposing the clearance circle on the journal path, taking the geometric centre of the path as that of the bearing.

The position of the bearing centre was more difficult to assess under constant load conditions and the following procedure was adopted on the First Testing Machine.

The position of the journal subjected to a given constant load was plotted from the co-ordinates indicated on the Direct Reading Galvanometer, and the process repeated with the same load applied in the opposite direction. This procedure gave two journal centre positions for similar load conditions, and it was assumed that the centre of the clearance circle was coincident with the mid-point of the line joining the two measured positions. The superimposition of the clearance circle on this centre determined the minimum film thickness.

The Second Testing Machine was stopped immediately after each journal path was recorded, and the journal position determined for a series of small loads applied by the load capsules and additional screw jacks. This procedure gave six positions of the journal centre which were coincident with the clearance circle. Before any one of those journal positions was measured great care was taken to ensure that the journal was static i.e. that there was metal to metal contact between the shaft and bearing surfaces. The co-ordinates of each position were recorded, read off directly on the Bridge Galvanometer, and photographed on the X-Y oscilloscope. These co-ordinates accurately established the position of the clearance circle centre within each journal path, and the diameter of the clearance circle at working temperatures from a graphical plot of the galvanometer readings.

3.9 Measurement of Applied Load

The general procedure adopted in measuring applied load was to stop the testing machine after a load variation had been recorded and calibrate the record by applying known static pressures to the load capsules and noting the corresponding recorder deflections.

The recorder deflection for a given pressure applied to the C.A.V.-Ricardo, Photoelectric Pressure Gauge was proportional to the pen recorder amplifier gain and the voltage applied to the light source. When the system had been adjusted to give suitable recorder displacements, it was necessary to ensure that the light source voltage was kept constant during subsequent load measurements.

When a bridge circuit measuring the strain in the connecting rods was used in the First Testing Machine, the strain gauges replaced the displacement pick-ups in the bridge circuits and the recording procedure detailed in § 3.8 repeated with the avoidance of centre zero overlap as before. The strain recorded for any given capsule pressure compared favourably with the strain measured in the same connecting rod when subjected to an equivalent load in a Dead Load Testing Machine. Typical cyclic load variations are shown in Fig 3.2.

The bridge of the differential pressure transducer used in the Second Testing Machine, was balanced at zero pressure differential and adjusted to give equal recorder displacements about the zero position for a range of pressure differentials. A

fixed reference line was set coincident with the zero pressure differential position on the U-V recorder chart, to facilitate the measurement of the recorded load variations. Typical load variations as measured by this system are presented on Fig 4.51 - 4.62.

3.10 Measurement of Bearing Friction

No satisfactory procedure was established for measuring friction on the First Testing Machine.

On the Second Testing Machine it was found advantageous to ensure that the Dynamometer Ring used for friction measurements never operated dynamically with zero strain. This was achieved by hanging a 2 lb.f. dead weight on the torque arm to permanently load the Dynamometer Ring. This ring was removed from its knife edges before the start of each test series, and the strain bridge circuit balanced to give no recorder movement from power off to power on at zero load. The dynamometer ring was then suspended from a suitable knife edge and the recorder displacements noted for a range of known dead loads. Finally a reference line on the recorder was set coincident with a dead load of 2 lb.f. to indicate the true zero load of the system, and the Dynamometer Ring mounted in the torque arm. If at any subsequent time the friction variation indicated

a variation approaching a nett zero load in the system, the Dynamometer Ring was removed and the strain bridge rebalanced before recording was continued.

3.11. Thermocouple Calibration

Every Eureka-Nickel Chromium thermocouple was calibrated in a water bath before use. A typical calibration curve is shown on Fig 3.3.

3.12 Oil Flow Calibration

The metering length of the test bearing oil supply on the Second Testing Machine was calibrated in situ by measuring the flow for a range of known pressure drops. The oil supply was set at a constant pressure of 30 p.s.i.g. and the time required to collect a known volume noted. Difference readings were taken in measuring the volumes, to avoid the problems of cleaning a measuring cylinder which contains heavy oil. The calibration graph is shown on Fig 3.4.

3.13. Pressure Gauge Calibration

Wherever possible Budenberg Standard Test Gauges were used for measuring static pressures. All other pressure gauges were regularly calibrated in a dead weight gauge tester.

3.14 Viscosity of Lubricating Oil

Shell Talpa 40 lubricating oil was used throughout the investigation. The Specific Gravity (S.G.) was deterined from the law S.G. = .905 { 1 - .00036 (T - 60)} where T is the temperature of the oil in degrees Fahrenheit.

The viscosity μ of the oil was determined from

$$\mu = \text{S.G.} (.026N - .40/N) \text{ poise.}$$

Where N seconds is the time required for a given quantity of oil to pass through the orifice of a Redwood II Viscometer. The temperature - viscosity graph for Talpa 40 oil is presented on Fig 3.5.

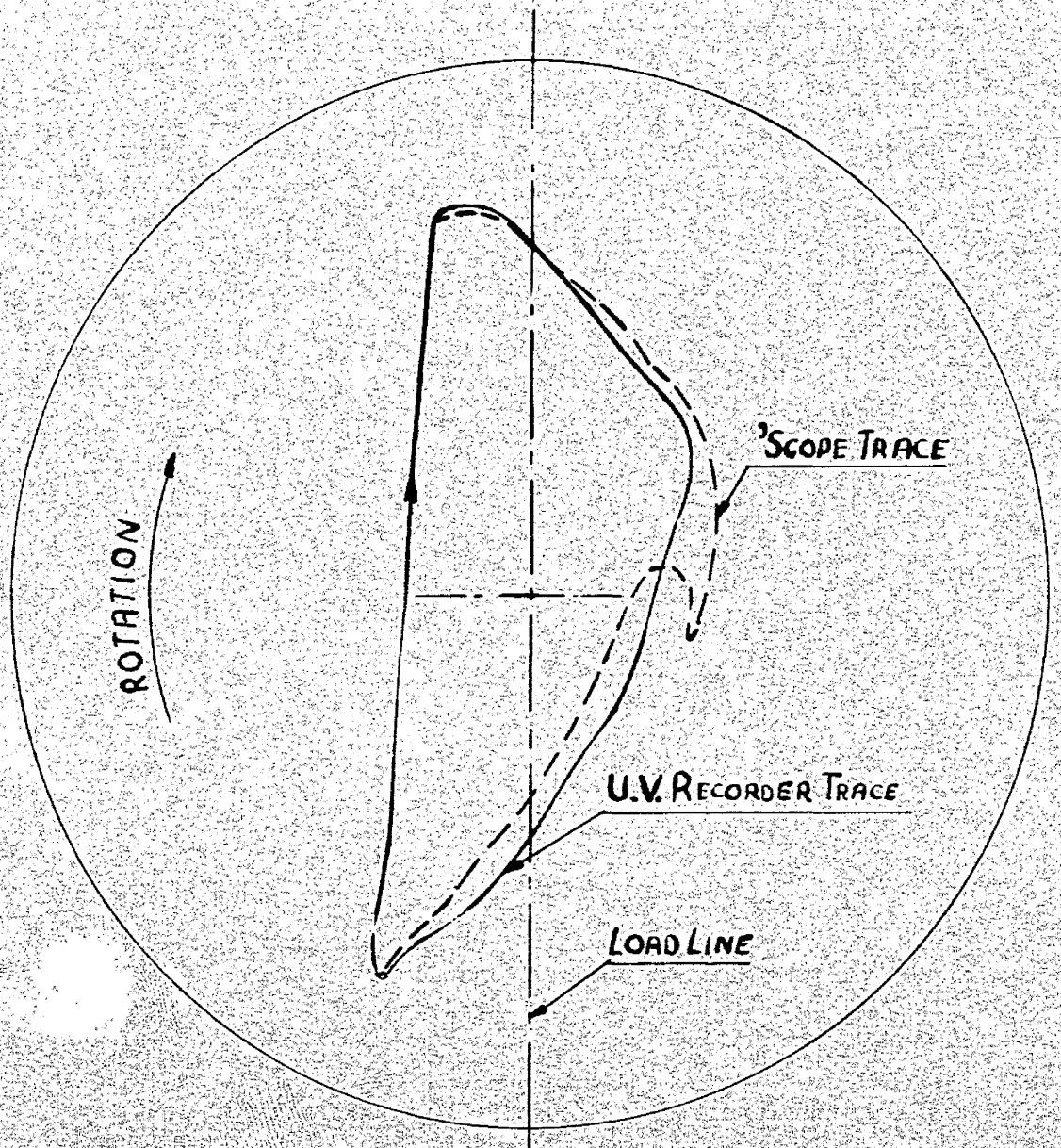

Fig: 3·1

EXPERIMENTAL PROCEDURE
JOURNAL CENTRE PATHS UNDER SAME DYNAMIC LOAD CONDITIONS

$L/D = 2/3$; $\sigma = 1$; $S_M = 0.29$

Fig: 3·1

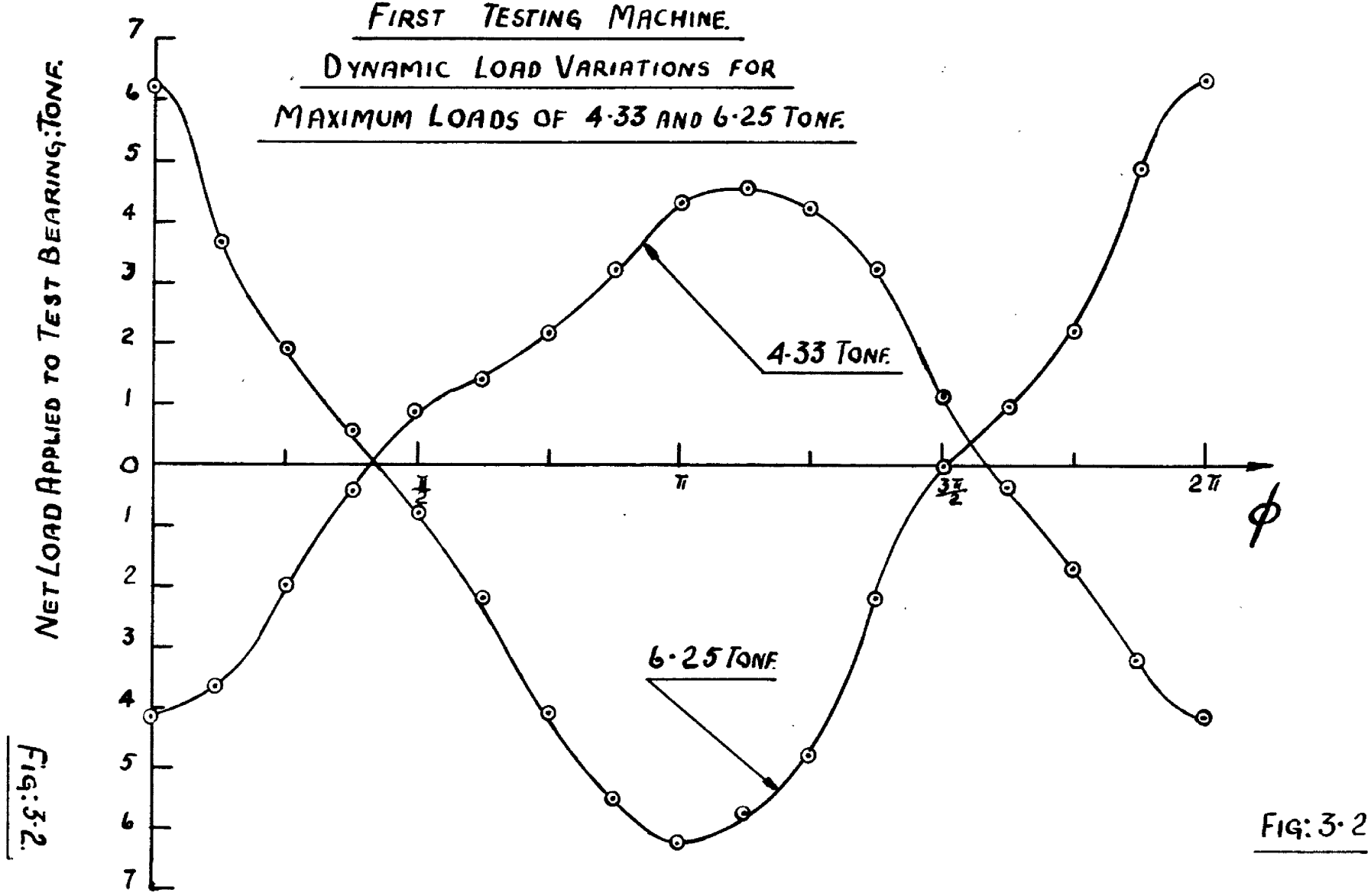
FIRST TESTING MACHINE.
DYNAMIC LOAD VARIATIONS FOR
MAXIMUM LOADS OF 4·33 AND 6·25 TONF.
NET LOAD APPLIED TO TEST BEARING: TONF.
7
6
5
4
3
2
1
0
1
2
3
4
5
6
7
4·33 TONF.
6·25 TONF.
π/2
π
3π/2
2π
φ

FIG: 3·2

FIG: 3·2

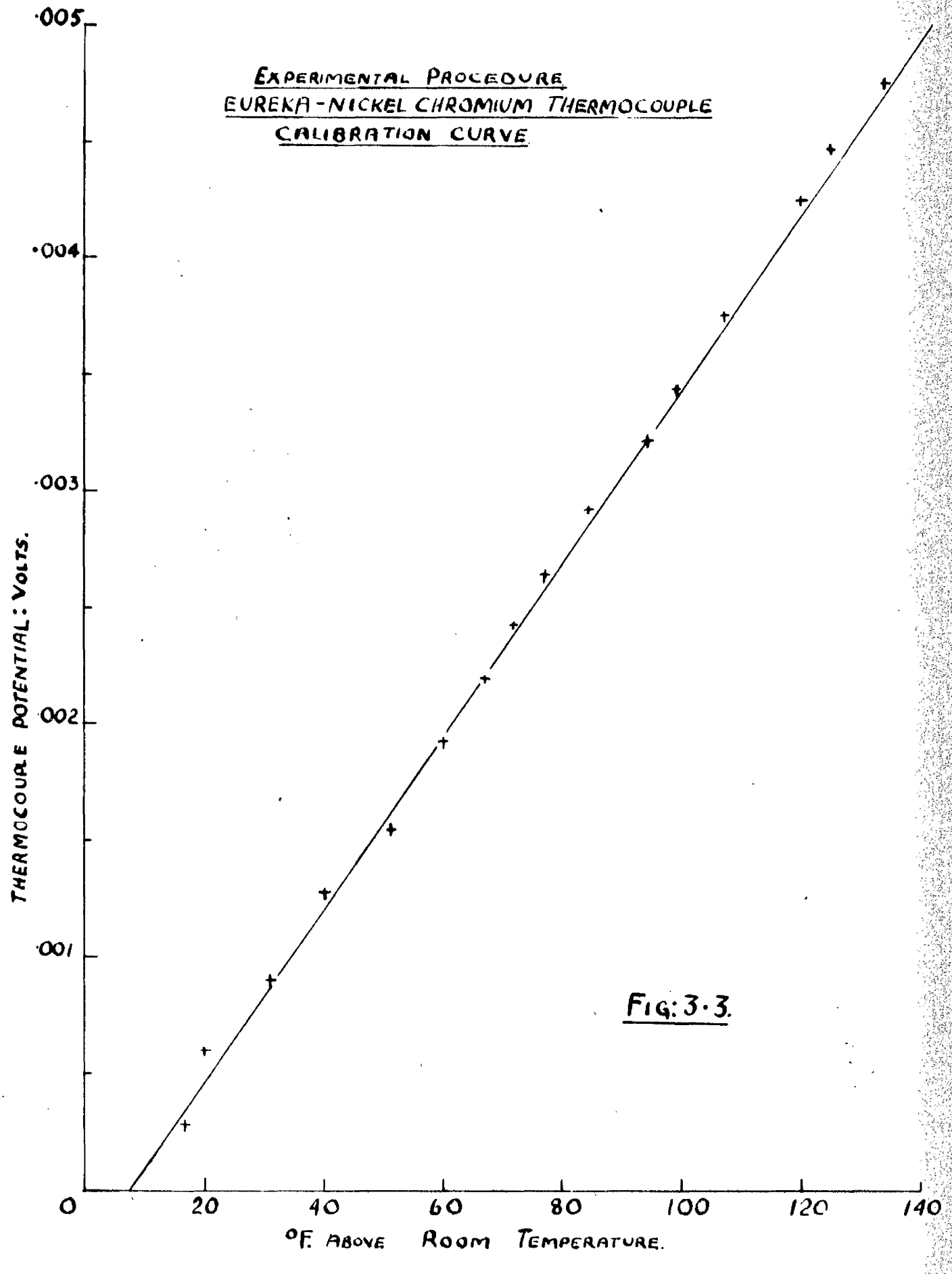
EXPERIMENTAL PROCEDURE
EUREKA - NICKEL CHROMIUM THERMOCOUPLE
CALIBRATION CURVE
·005
·004
·003
·002
·001
0
20
40
60
80
100
120
140
THERMOCOUPLE POTENTIAL : VOLTS.
°F. ABOVE ROOM TEMPERATURE.

FIG: 3·3.

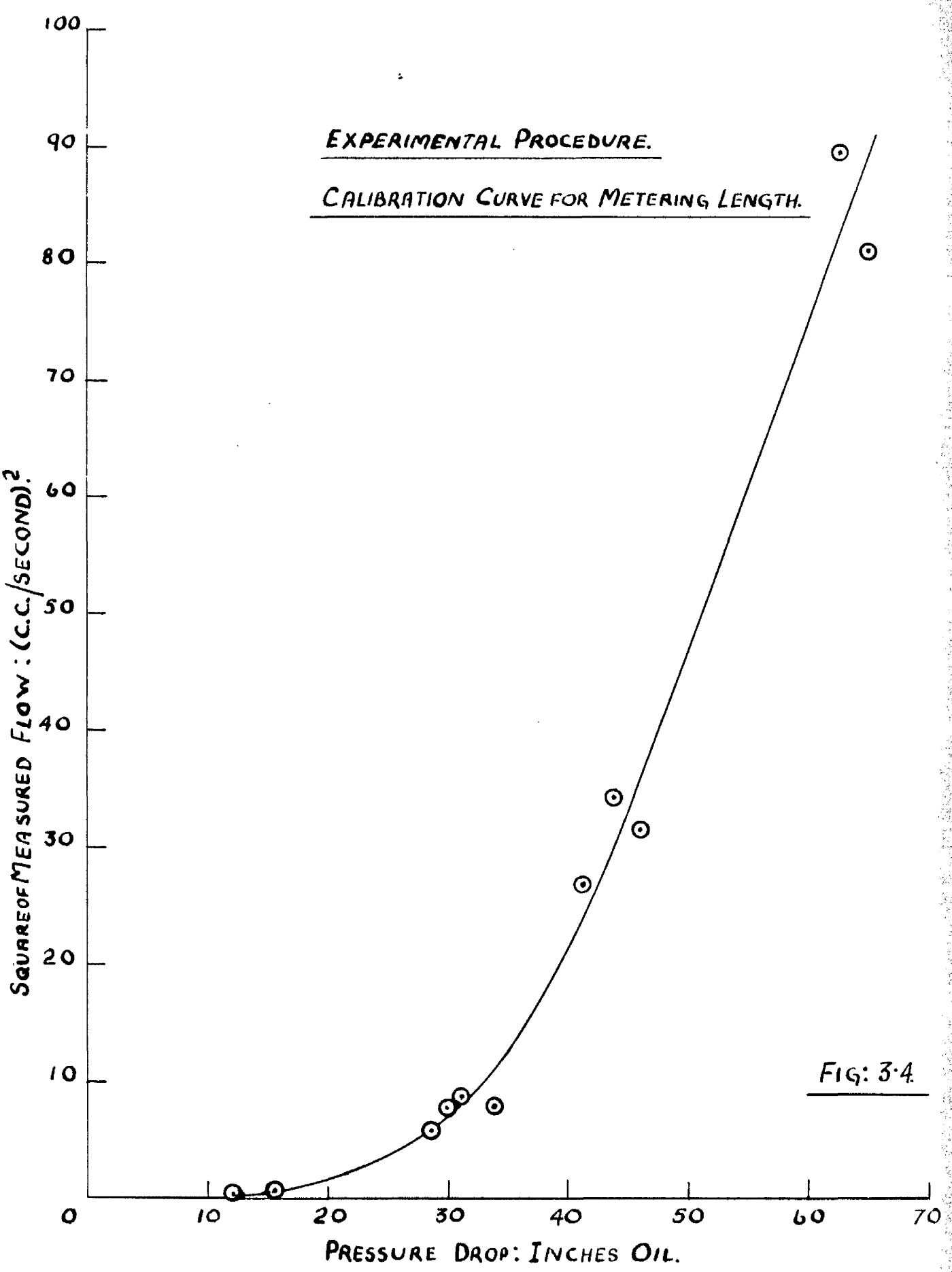
EXPERIMENTAL PROCEDURE.
CALIBRATION CURVE FOR METERING LENGTH.
SQUARE OF MEASURED FLOW : (C.C./SECOND)².
PRESSURE DROP: INCHES OIL.
0
10
20
30
40
50
60
70
80
90
100

FIG: 3·4

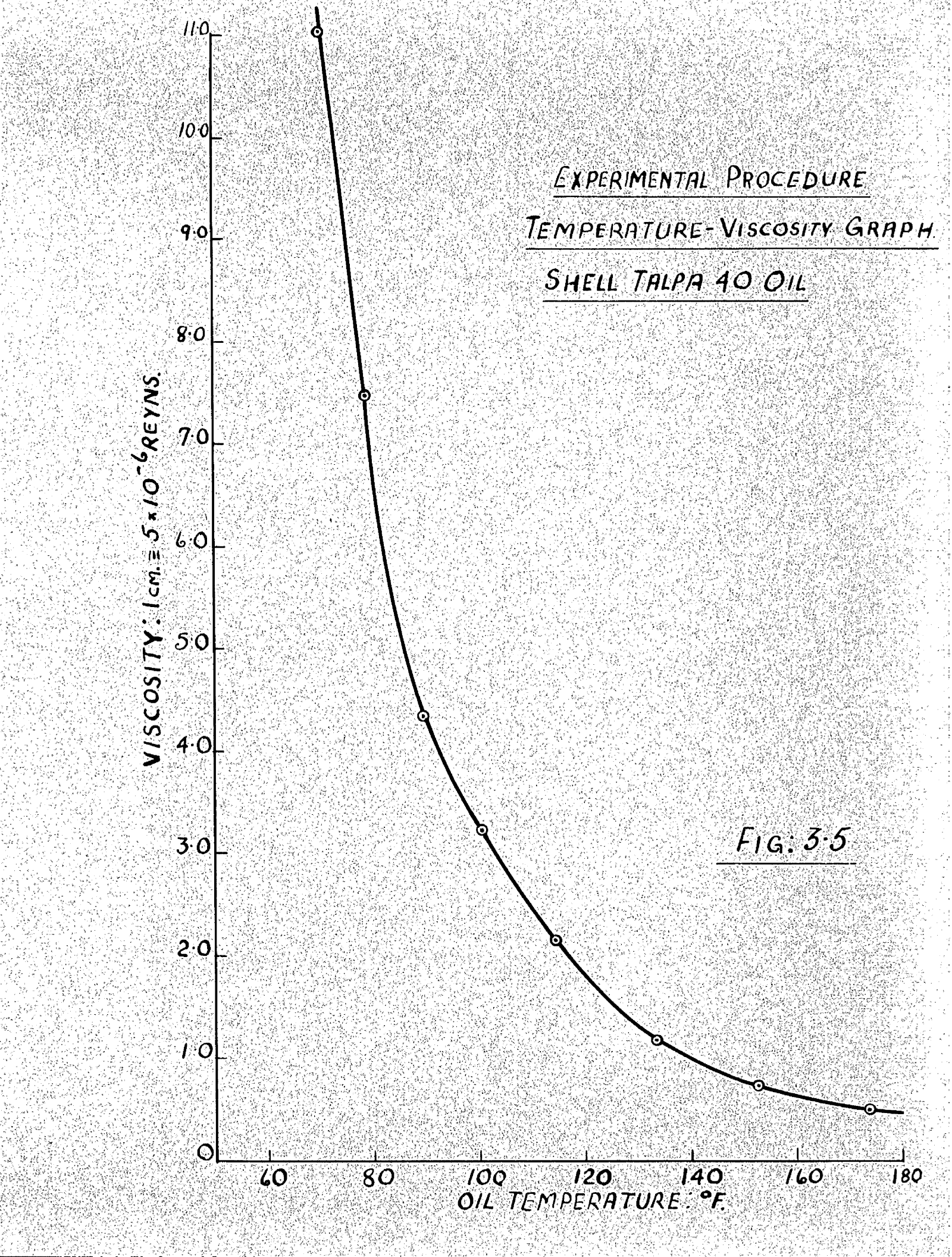
EXPERIMENTAL PROCEDURE
TEMPERATURE-VISCOSITY GRAPH
SHELL TALPA 40 OIL
VISCOSITY: 1 CM. ≡ 5 × 10⁻⁶ REYNS.
11·0
10·0
9·0
8·0
7·0
6·0
5·0
4·0
3·0
2·0
1·0
0
60
80
100
120
140
160
180
OIL TEMPERATURE: °F.
FIG. 3·5

CHAPTER IV

4. Experimental Results and Observations

4.1 Oil Film Pressure Surveys

All pressure surveys presented in this thesis were made in journal bearings, 3 inches diameter and 3 inches long, running in the First Testing Machine at the same speed as the applied load. The surveys are presented under separate headings for bearings supporting Static and Dynamic Loads.

Static Loads

Oil film pressures were surveyed in 360° bearings, with diametral clearances of .0015 and .003 inches as measured at room temperatures, when supporting Static loads of 6.7, 3.35, and 2.23 Tons.f. The oil film pressure reached a maximum value within the convergent clearance space in all but two cases and in all cases the load bearing pressure film was terminated by the axial oil inlet groove. A typical oil film pressure distribution is shown on Fig 4.2 for a load of 6.7 Tons. f. in the larger clearance bearing, and one of the exceptions on Fig 4.1 for a load of 6.7 Tons f. in the smaller clearance bearing.

Dynamic Loads

The bushes detailed above were surveyed when subjected to Dynamic Loads of the form detailed in § 3.9, with maximum amplitudes of 4.33, 5.7, and 6.7 Tons f. on the bearing with the .0015 inch diametral clearance and 6.25 Tons f. on the bearing with the .003 inch diametral clearance. Typical surveys are presented for 7 sections of the former bearing subjected to a maximum load of 4.33 tons f. Fig 4.3a - 4.14b, and for the centre and top three sections of the latter bearing subjected to a maximum load of 6.25 tons f. Fig 4.16 - 4.25. These figures indicate the pressure existing in the oil film at the instant the applied load has the magnitude indicated by the phase angle ϕ. A seven section survey involves the measurement of over 1500 oil film pressures and requires at least 10 days to complete.

The pressure variations of Fig 4.3 - 4.25 are also presented on Fig 4.15a & b and 4.26 a & b using polar co-ordinates for the pressure and its position in the centre section of each bearing. This presentation shows clearly the retention of the load bearing pressure film within an arc bounded by the axial oil inlet grooves situated at $\theta = 0$ and 180°.

The load bearing oil film is stationary during its generation (ϕ = 90 - 180°, and 270 - 360°) in both bearings and is swept through a bearing arc of 25° during its decay (ϕ = 360 - 90°, and 180 - 270°). The oil film pressure peak has insufficient time to travel through the clearance space with the journal, but is fractured and reformed within the same bearing arc.

The oil film pressures existing in the bearing at ϕ = 0, were integrated by graphical means to establish the; Integrated Pressure Load

$$= \left\{\left(\int_{-\frac{L}{2}}^{+\frac{L}{2}}\int_{0}^{2\pi} p \sin\theta \, d\theta \, d\ell\right)^2 + \left(\int_{-\frac{L}{2}}^{+\frac{L}{2}}\int_{0}^{2\pi} p \cos\theta \, d\theta \, d\ell\right)^2\right\}^{\frac{1}{2}}$$

The integrated pressure load was found to vary from 80% of the maximum applied load in the surveys of Fig 4.16 - 4.25, to 104% of the maximum applied load in the surveys of Fig 4.3a - 4.14b.

4.2 Journal Centre Eccentricity

Journal centre eccentricity measurements were made on journals running in both testing machines when supporting either static or dynamic loads in a variety of bearings. The results of these measurements are presented either, as a Polar plot showing

the journal centre position within a circle whose diameter is proportional to the clearance circle, or as a Rectilinear plot of the non-dimensional co-ordinates:- Eccentricity Ratio and Sommerfeld Number or Capacity Number.

The Eccentricity Ratio presents the journal eccentricity as a proportion of the radial clearance of the bearing.

The Sommerfeld Number combines the parameters of Unit Bearing Load (P: lbs f./in^2), Journal Speed (N' r.p.s.), Oil Viscosity (μ. Reyns) and Clearance Ratio (R/c) in a non-dimensional grouping $S = (\frac{R}{c})^2 \frac{\mu N}{P}$. In the case of Static loads P is the load applied to the bearing, while in the case of Dynamic Loads, P is the maximum load applied in any one cycle. To distinguish between these conditions the Sommerfeld Number is denoted in the latter case by S_m.

The current practice of experimenters and theoreticians is to base calculations on the viscosity of the leakage oil as it leaves the bearing. The author prefers to use viscosity values which correspond to the temperatures of the bush adjacent to the point of minimum film thickness. This choice assumes that this value of viscosity corresponds closely to that of the oil film at this point. Oil

viscosities computed on this basis have been used in computations of the Sommerfeld Numbers associated with the experimental work of the Second Testing Machine. Estimated values of viscosity based on measured outlet temperatures have been used in the computations of earlier experimental work. The radial clearance value used in the computation of Sommerfeld Number and Eccentricity was based on measurements taken at room temperature for all computations associated with the First Testing Machine. Non-dimensional parameters for the Second Testing Machine are based on bearing clearances measured in situ immediately after each test run.

Sommerfeld Numbers can be modified to give a suitable comparison of the performance of a range of short bearings; The modified Sommerfeld Number is known as the

$$\text{Capacity Number: } C_n = S\left(\frac{L}{D}\right)^2$$

Static Loads

Journal eccentricity measurements were made in both; a) The First Testing Machine on the full length bearings detailed in § 4.1 for a range of static loads from 0 - 6.7 Tons f and speeds

from 150 - 340 r.p.m. and b) The Second Testing Machine on bearings of .003 in. diametral clearance and L/D ratios of 1 and 2/3 for a range of static loads from 0 to 4.38 tons f. and speeds from 300 to 1000 r.p.m.

Typical polar plots of the journal centre under these conditions are presented on Fig 4.27 - 4.29, and 4.32 - 4.33. All measurements made under Static Loads are summarised in the Rectilinear Presentation of Fig 4.30, 4.31, and 4.34

The irregular journal centre paths of Fig 4.27 - 4.29 and the regular paths of Fig 4.32 and 4.33 indicate a major difference in journal behaviour under similar conditions. The author interprets this difference as an indication of the restraint placed on the test bearing housing by the loading mechanism of the First Testing Machine. This restraint should not affect the values of minimum film thickness as the journal will move until the film pressure supports the applied load. This restraint will affect the position of the load bearing pressure film within the clearance space.

In all cases examined the journal centre was close to that of the bearing at zero load, but never coincident with it.

The summarised results for a .0015 in. dia. clearance bearing Fig 4.30, fall on separate curves for speeds of 190 and 340 r.p.m. with a scatter of results at 240 r.p.m. Similar tendencies are demonstrated in the .003 in. dia. clearance bearing Fig 4.31, with separate curves for speeds of 150 - 190 r.p.m. and 240 r.p.m. with a scatter for values measured at a speed of 340 r.p.m.

The summarised results for measurements on the Second Testing Machine Fig 4.34, fall on a single curve for a given L/D ratio, for all loads and speeds investigated.

Dynamic Loads

The successive positions of the centre of a journal supporting Dynamic Loads were recorded in both Testing Machines. The principal problem in the evaluation of the results recorded on the First Testing Machine was created by the location of the balance piston cylinder in the test shaft. This caused a variation in the bending stiffness in any given plane as the test shaft rotated. Thus, despite the recording of the mean axial journal position, the superimposed bending variable resulted in journal centre paths which never seemed to close, or follow any identifiable pattern.

The journal positions in the .0015 inch clearance bearing were recorded when supporting dynamic loads of 2.12, 3.8, and 6.7 Tons f. at speed ratios; σ = 1, 1.42, 1.79, where σ is the ratio of the load frequency to the journal speed. Similar measurements were made with the journal in the .003 inch clearance bearing supporting six different Dynamic Loads up to 6.7 tons f, and four speed ratios from σ = 1 to 2.27.

Typical journal paths are shown in Fig 4.32 and 4.33 for the same load conditions as those of the film pressure surveys of § 4.1.

No difficulty was experienced in interpreting the results from the Second Testing Machine as the mounting of the test bearing gave the journal a simply supported condition with negligible bending effect.

The perennial problem of accurately placing the path within the clearance circle recurred under certain circumstances. The procedure detailed in § 3.8 was successful in indicating, in situ, the diameter of the clearance circle, but the quantity of oil cascading from the Externally Pressurised Bearing, during the simultaneous recording of friction and journal displacement, was sufficient to establish a small oil film under the probes. As long

as the journal speed was constant, the presence of this film had no effect on the recorded journal path. When the journal was stopped for clearance circle measurements, this film broke down causing a shift in the position of the clearance circle centre. [Displacement transducers are now on hand which avoid this problem] . Under these circumstances it has been assumed that the film has the same thickness at the extreme ends of the journal path.

The movement of the journal in bearings with a .003 inch diametral clearance, diameter of 3 inches, and lengths of 3, 2, and 1½ ins, were recorded for a range of Dynamic Loads up to a maximum of 4 Tons f. at speed ratio σ = 1, 0.5, 0.33. The Variation of the load with time is illustrated on Fig 4.51 - 4.62.

The various speed ratios were achieved by varying the journal speed, not the load frequency. This means that the wedge action varies in a range of tests with constant value of maximum applied load, as does the Sommerfeld Number which is dependent on journal speed.

Typical journal paths for the full length bearing at various speed ratios are presented as polar plots on Fig 4.37 - 4.39 and on

Fig 4.37 - 4.39 for the half length bearing. Although the paths presented above Fig 4.37 - 4.39, show a single closed loop, this condition was not always observed. When the journal centre took a small number of cycles to repeat any given cycle of events, the variation in path configuration took place during the period of increasing load and generally the journal centre passed through the same point of minimum film thickness.

The journal running at a Speed Ratio $\sigma = 1$, and Sommerfeld Number $S_M > 0.2$ in a full length bearing followed the same path either every load cycle or every other load cycle. With two exceptions the journal path repeated every 15 to 20 cycles at Sommerfeld Number $S_M < 0.2$. The exceptions were cases of 52 cycles at $S_M = .105$ and 118 cycles at $S_M = .177$. These exceptions were not the result of unrepeatable conditions for a given bearing - journal set up, though it must be admitted that the same bearing after dismantling and reassembly in the housing did not produce the above exceptions. These two cases were unusual not only in the large number of cycles to repeat the same path but also in the fact that during the prolonged period of cycles the journal path slowly changed from a small to a large ellipse.

At speed ratio σ = 0.5 the journal path at no time indicated zero film thickness, but was elliptical in form repeating every 5 to 10 cycles at $S_M < 0.2$ and every cycle $S_M > 0.2$.

A speed ratio of σ = 0.33 produced paths which repeated every 3 to 6 cycles independent of Sommerfeld Number. In this case the variation was frequently caused by a small loop rotating round the general elliptical shape of the journal centre path.

The above observations apply to the half length bearing with two exceptions to the general rule. At $\sigma = 1$ and $S_M = .025$ the journal path repeated every 55 cycles with no noteworthy change in ϵ max. At $\sigma = 1$ and $S_M = .2293$, the journal path repeated every 120 cycles with an initially small trace reducing to a spot over half this cyclic period.

These exceptions will be discussed in § 5.2.

The results for all bearing tests are summarised on Fig 4.40 - 4.42 as rectilinear plots of Eccentricity Ratio versus Sommerfeld Number : Presentation of Dynamic Results to a base of Capacity Number did not produce a single line law similar to that found under Static Load conditions. Preliminary recordings under pulsating loads were carried out in the 2 inch long bearing. None of

the speed ratios examined exhibited zero load capacity. Due to the narrow band of unit loads $.500 \leqslant P \leqslant 1200$ examined, no conclusion could be drawn from the journal centre displacements.

4.3 Bearing Friction Measurements

The friction between the connecting rod and the test housing of the First Testing Machine prevented the detection of bearing friction under all load conditions. The Bearing Friction Variable used in the non-dimensional presentation of experimental results is based on friction measurements made in the Second Testing Machine. The measured coefficient of friction (F), the Bearing Radius (R), and the radial clearance (c) combine to form the Bearing Friction Variable; F(R/C).

Static Loads

The experimentally determined friction coefficients presented on Fig 4.46, fall on a single straight line for the range of speeds and loads examined in the full length bearing. Similar results are presented on Fig 4.46 for the half length bearing. The scatter of results about the best line increases as the force balancing the friction torque reduces to 0.5 lb. f. Throughout the range of loads tested, the coefficient of friction showed no tendency to increase

with the load; the characteristic indication of the breakdown of the hydrodynamic film exhibited by McKee and McKee[57]; and Le Loup.[38]

Dynamic Loads

The cyclic variation of the friction force acting on the surface of the bearing was simultaneously recorded with the co-ordinates of the journal centre and the applied dynamic load.

The friction variation reached a maximum value at a time related to the instant of maximum applied load and independent of the bearing length and speed ratio. The amplitude between the peak and trough values of the variation depends on the magnitude of the applied load and the speed ratio Fig 4.51 - 4.62. The lightly loaded cases at σ = .5 and .33, Fig 4.54 and 4.56 do not comply with the above pattern of friction variation. Examination of equipment when these measurements were made, confirmed normal working conditions.

The Coefficient of Friction was determined by integrating the friction force over ten consecutive load cycles, to establish a mean value of friction force, and dividing this by the mean value of applied load over the same period.

The results of measurements made on full and half length bearings for a range of Applied Dynamic Loads are summarised on Fig 4.48 - 4.50. These figures show that there was a transition from Hydrodynamic Film lubrication to some form of thin film lubrication within the range of loads examined. This does not imply that a complete breakdown of the film occurred as the journal ran without distress under these conditions.

4.4 Oil Flow Measurements

The results of flow measurements made in the Second Testing Machine are presented in the Non-Dimensional Ratio of the Measured Flow to the Swept Volume, known as the Oil Flow Number

Static Load

The quantities of oil supplied to bearings operated within the range of static loads and speeds indicated in § 4.2 are summarised on Fig 4.63 - 4.65 for bearings with L/D ratios of 1 and 2/3.

Dynamic Loads

Oil flow measurements were made in bearings with L/D ratios of 1, 2/3, ½ supporting a range of Dynamic and Pulsating Loads with speed ratios from σ = .33 to 1.0.

Typical measurements of the oil flow are summarised in Fig 4.66 for full length and half length bearings.

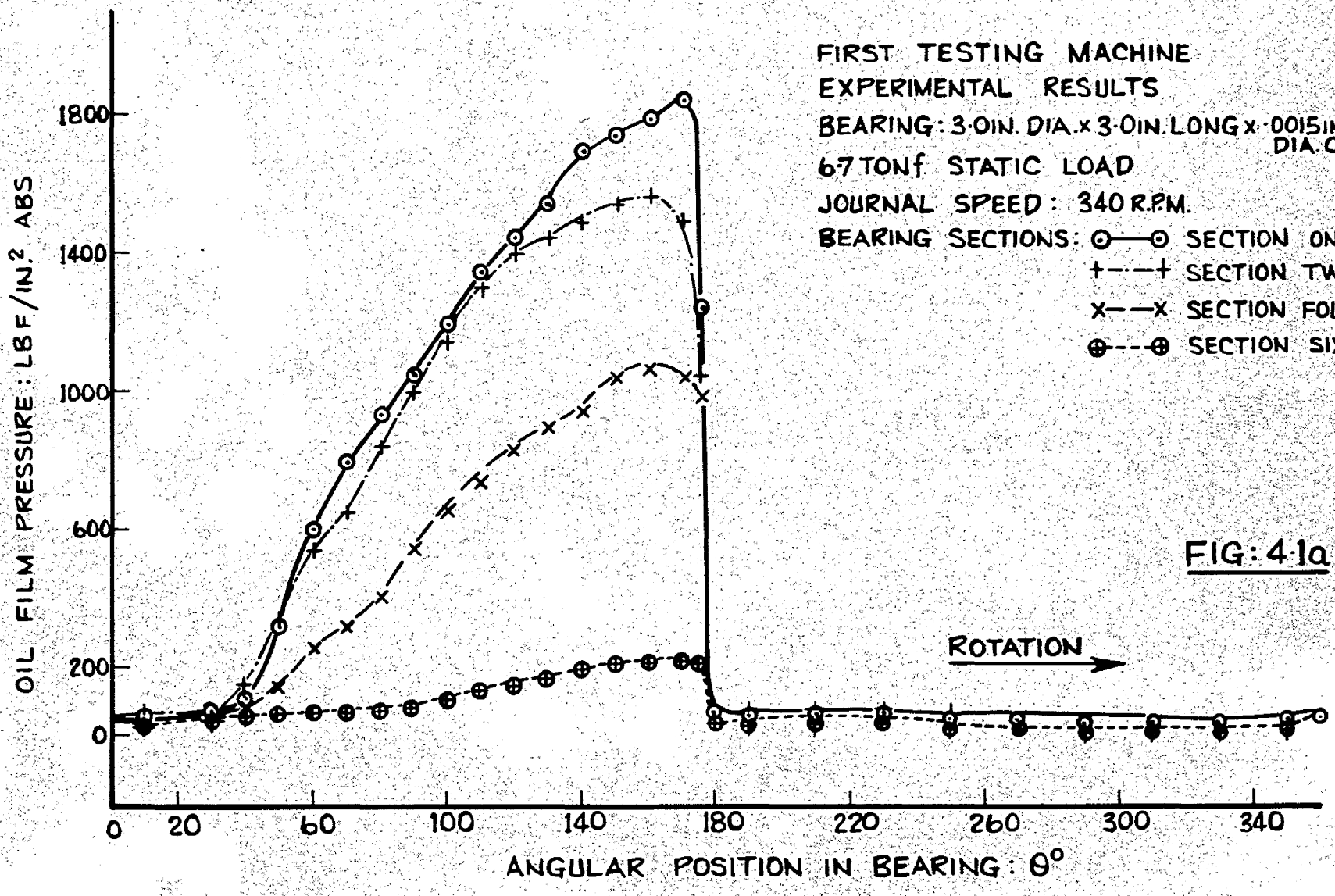
FIRST TESTING MACHINE
EXPERIMENTAL RESULTS
BEARING: 3·0IN. DIA. x 3·0IN. LONG x ·0015IN. DIA. CL.
6·7 TONf. STATIC LOAD
JOURNAL SPEED: 340 R.P.M.
BEARING SECTIONS: SECTION ONE
SECTION TWO
SECTION FOUR
SECTION SIX
FIG: 4·1a
ROTATION
OIL FILM PRESSURE: LBF/IN.² ABS
1800
1400
1000
600
200
0
0
20
60
100
140
180
220
260
300
340
ANGULAR POSITION IN BEARING: θ°

FIG: 4·1a

FIRST TESTING MACHINE
EXPERIMENTAL RESULTS
LOW PRESSURE REGION OF SURVEY
PRESENTED ON FIG: 4·1a.

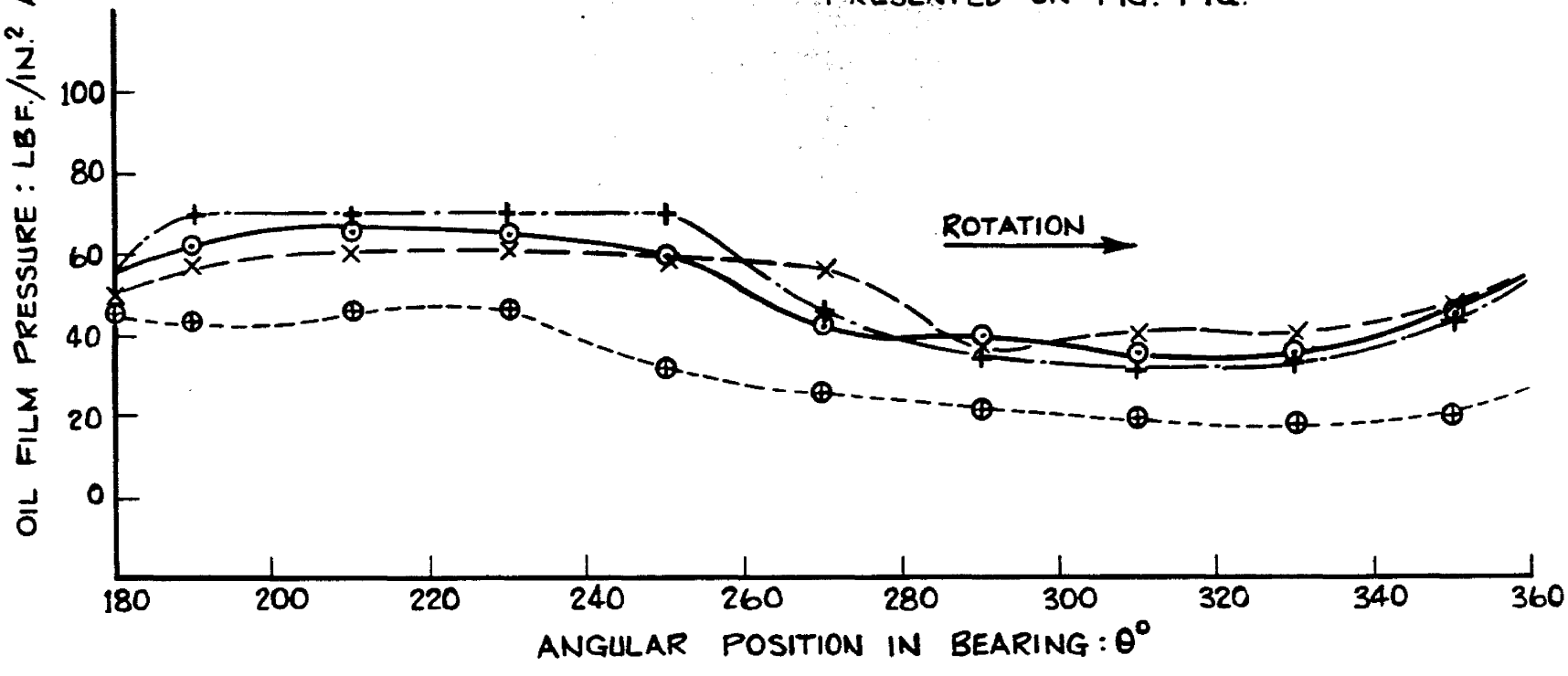

FIG: 4·1b

FIG: 4·1b

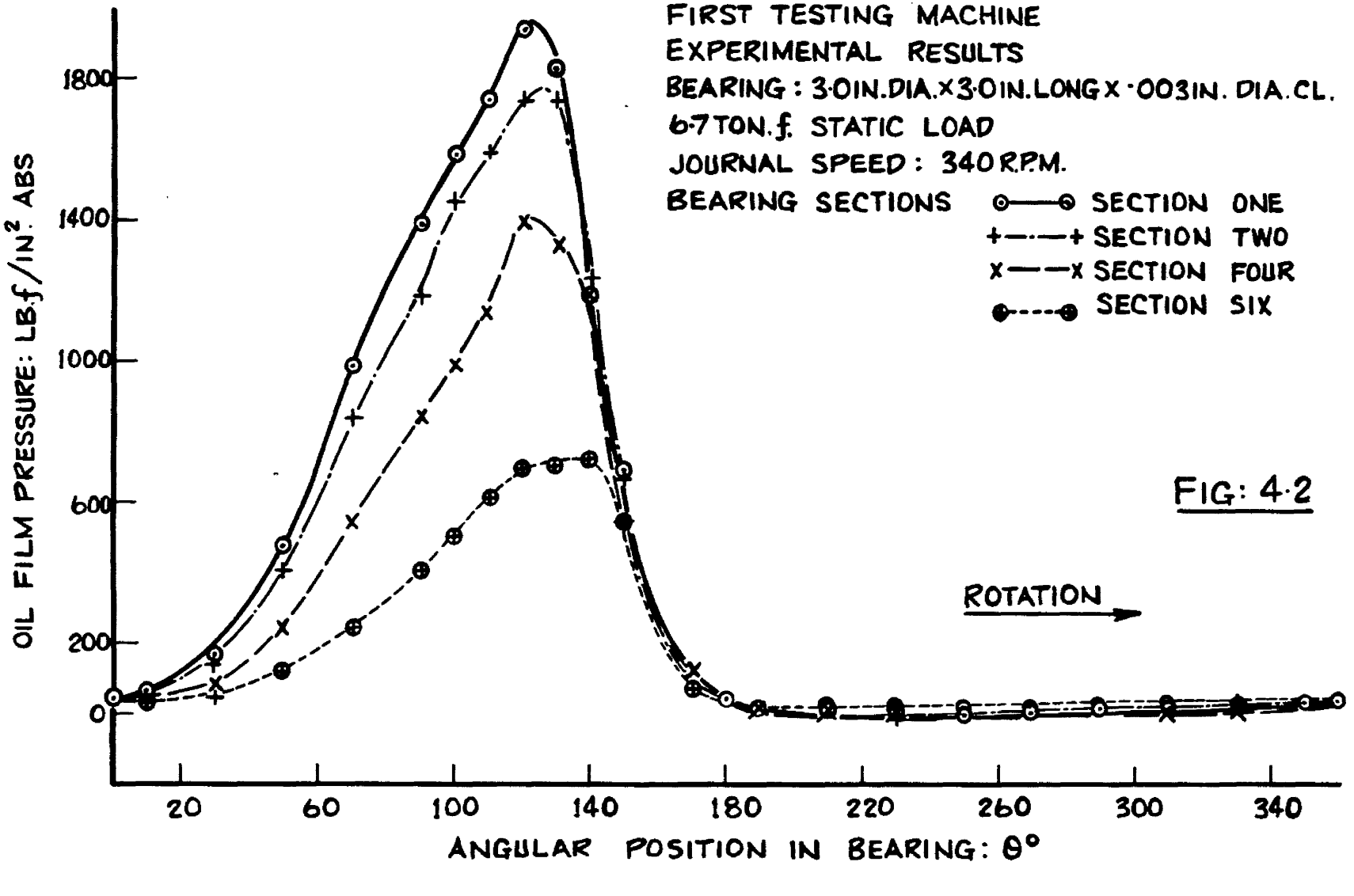
FIRST TESTING MACHINE
EXPERIMENTAL RESULTS
BEARING : 3·0IN.DIA.×3·0IN.LONG×·003IN. DIA.CL.
6·7 TON.f. STATIC LOAD
JOURNAL SPEED : 340 R.P.M.
BEARING SECTIONS
SECTION ONE
SECTION TWO
SECTION FOUR
SECTION SIX
FIG: 4·2
ROTATION
OIL FILM PRESSURE: LB.f/IN.² ABS
1800
1400
1000
600
200
0
20
60
100
140
180
220
260
300
340
ANGULAR POSITION IN BEARING: θ°

FIG: 4·2

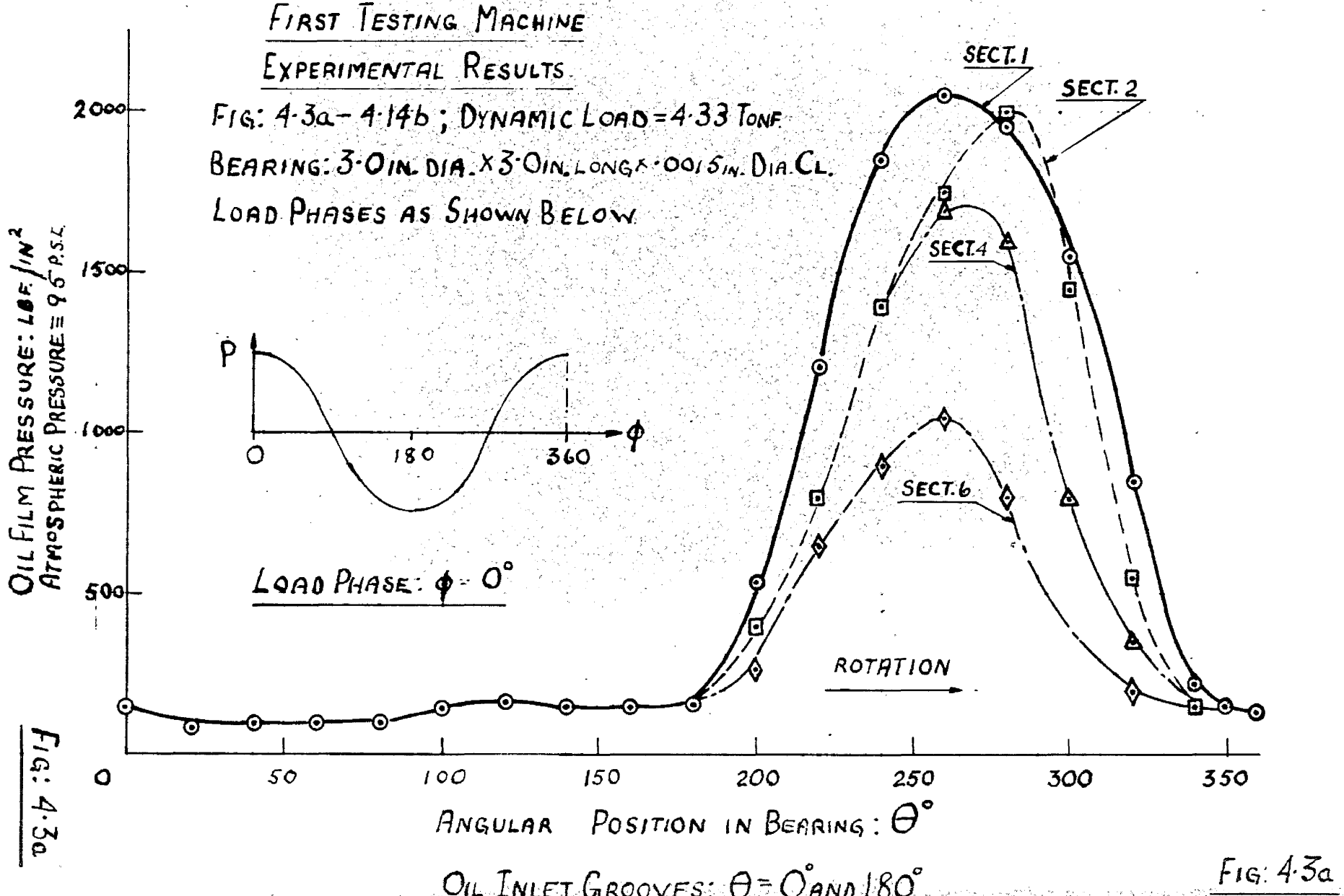
FIRST TESTING MACHINE
EXPERIMENTAL RESULTS
FIG: 4·3a – 4·14b ; DYNAMIC LOAD = 4·33 TONF.
BEARING: 3·0 IN. DIA. × 3·0 IN. LONG × ·0015 IN. DIA. CL.
LOAD PHASES AS SHOWN BELOW
P
0
180
360
φ
LOAD PHASE: φ = 0°
SECT. 1
SECT. 2
SECT. 4
SECT. 6
ROTATION
OIL FILM PRESSURE: LBF./IN²
ATMOSPHERIC PRESSURE = 95 P.S.I.
2000
1500
1000
500
0
50
100
150
200
250
300
350
ANGULAR POSITION IN BEARING: θ°
OIL INLET GROOVES: θ = 0° AND 180°
FIG: 4·3a

FIG: 4.3a

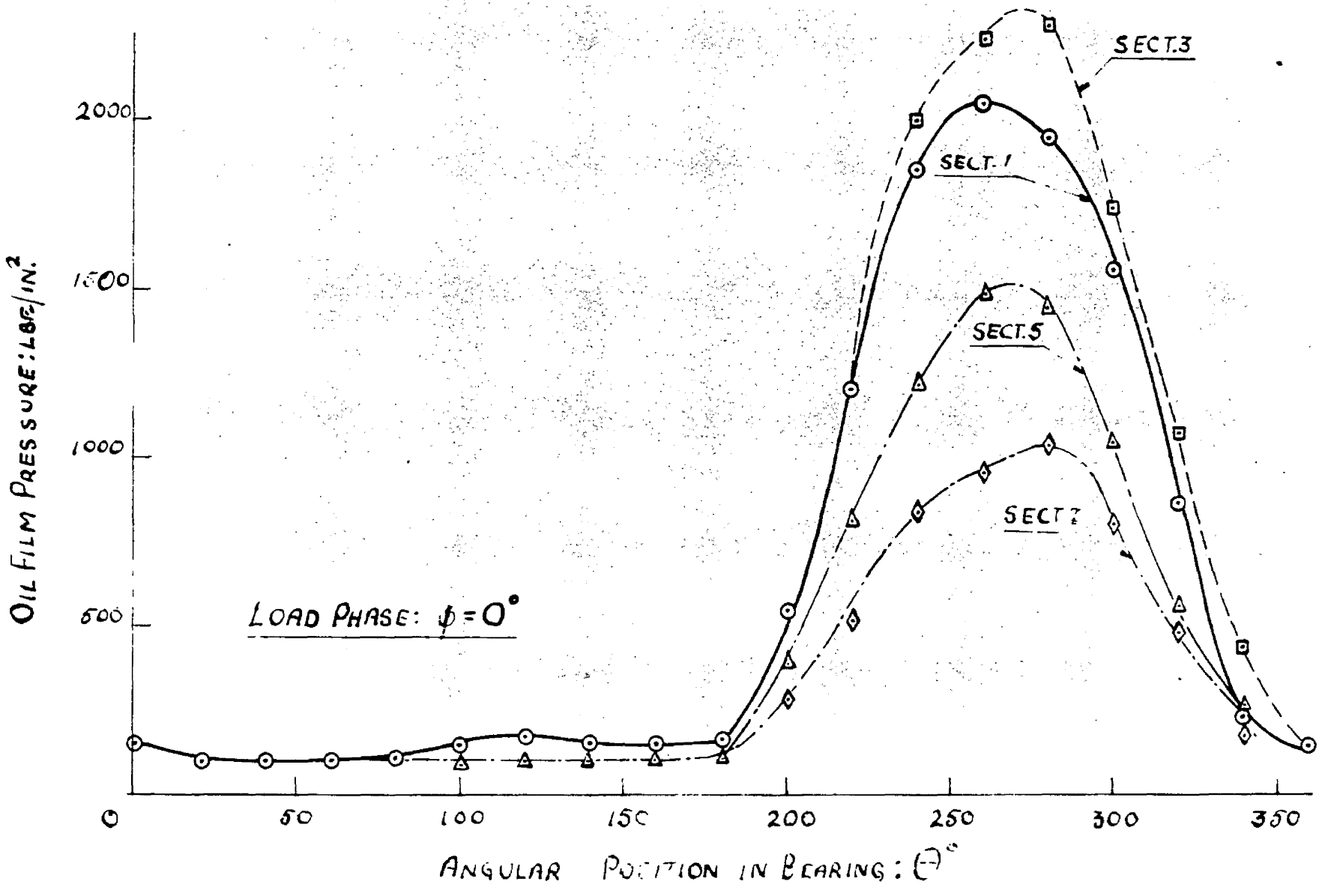
OIL FILM PRESSURE: LBF/IN.²
2000
1500
1000
500
0
50
100
150
200
250
300
350
ANGULAR POSITION IN BEARING: θ°
LOAD PHASE: ψ = 0°
SECT.3
SECT.1
SECT.5
SECT.7

FIG: 4.5

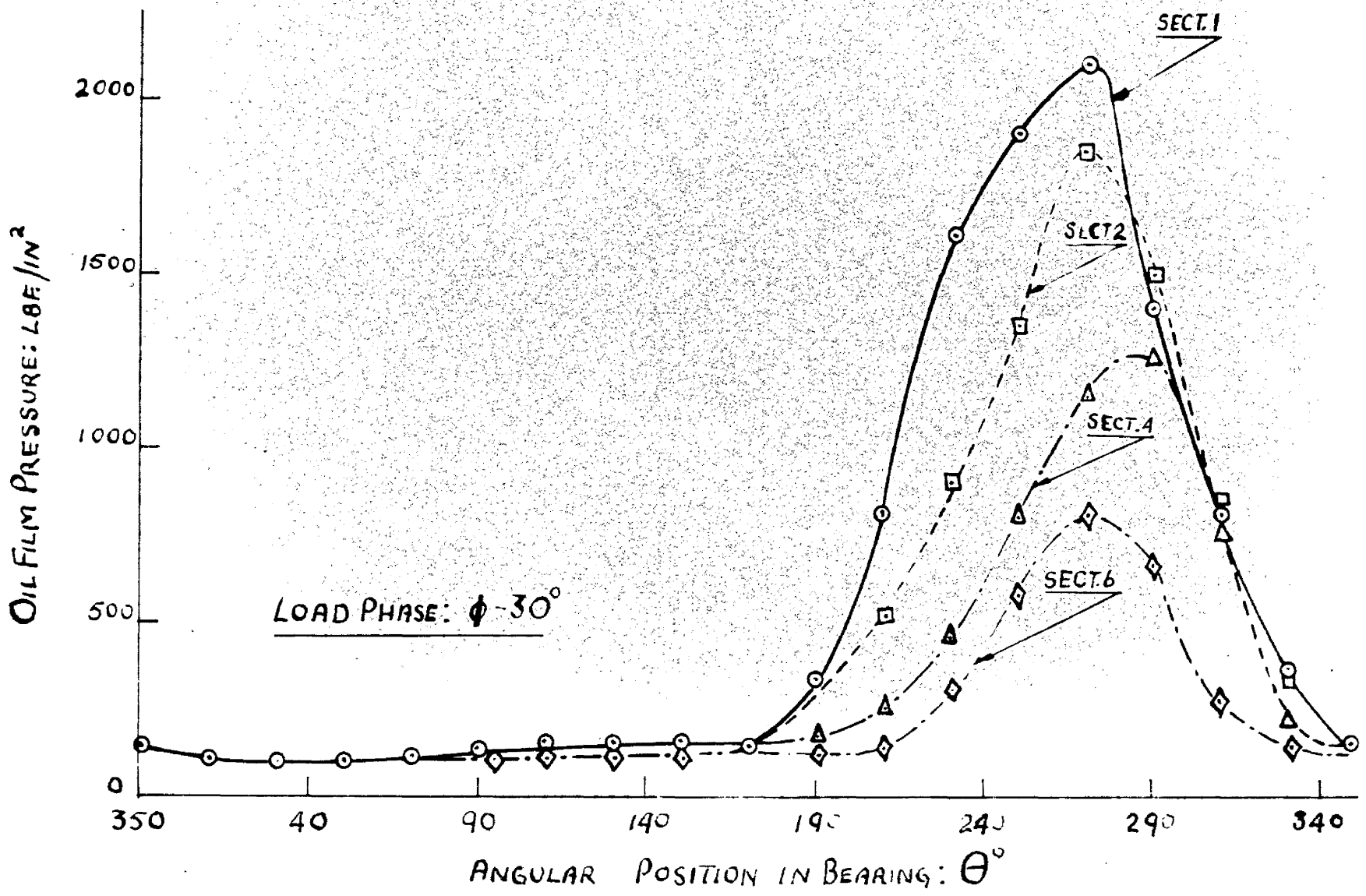
SECT.1
SECT.2
SECT.4
SECT.6
LOAD PHASE: ϕ -30°
OIL FILM PRESSURE: LBF/IN²
2000
1500
1000
500
0
350
40
90
140
190
240
290
340
ANGULAR POSITION IN BEARING: θ°

FIG: 4·4a

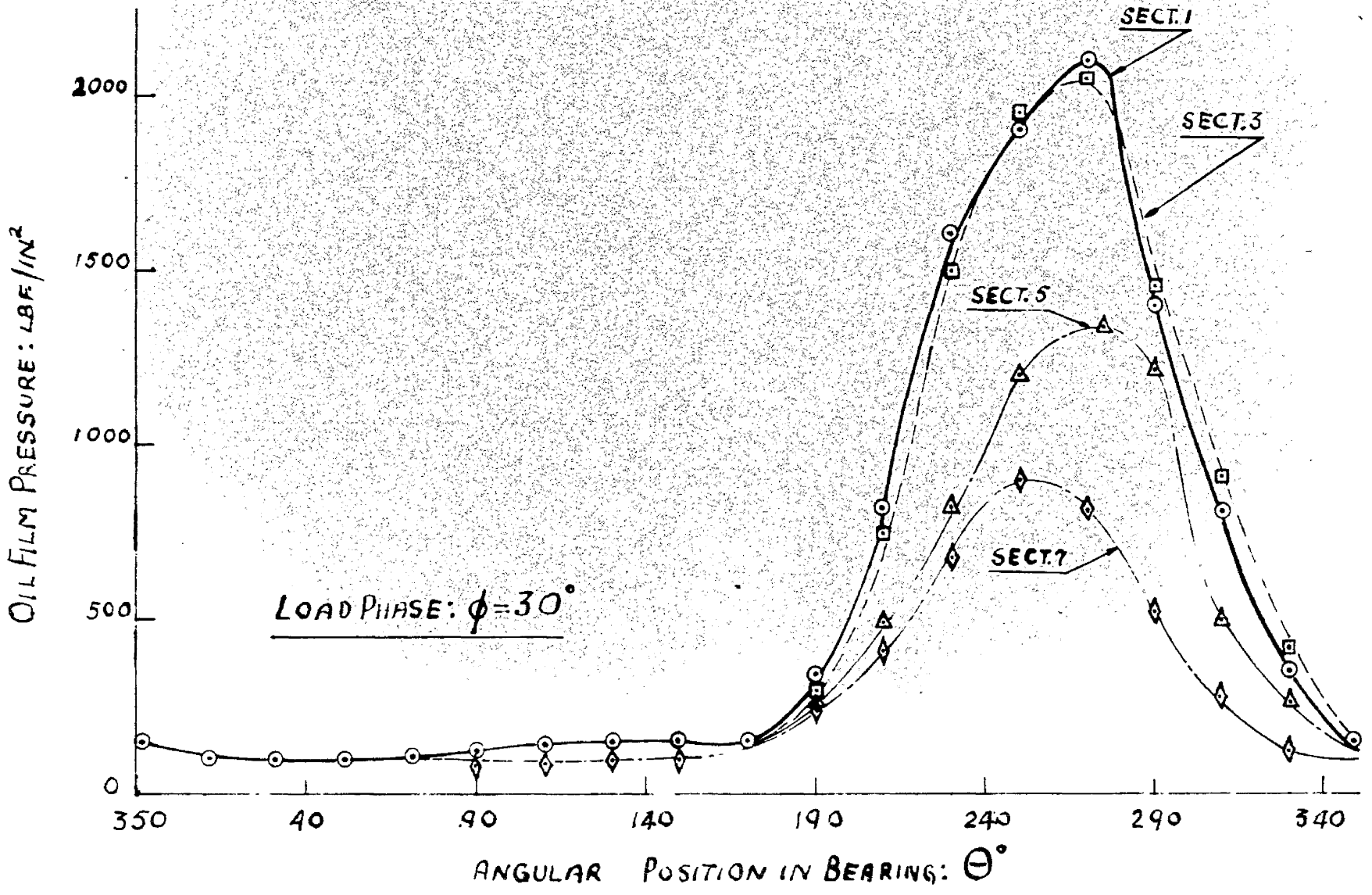
SECT. 1
SECT. 3
SECT. 5
SECT. 7
LOAD PHASE: $\phi = 30^\circ$
OIL FILM PRESSURE: LBF/IN^2
2000
1500
1000
500
0
350
40
90
140
190
240
290
340
ANGULAR POSITION IN BEARING: Θ°

FIG. 4-4b

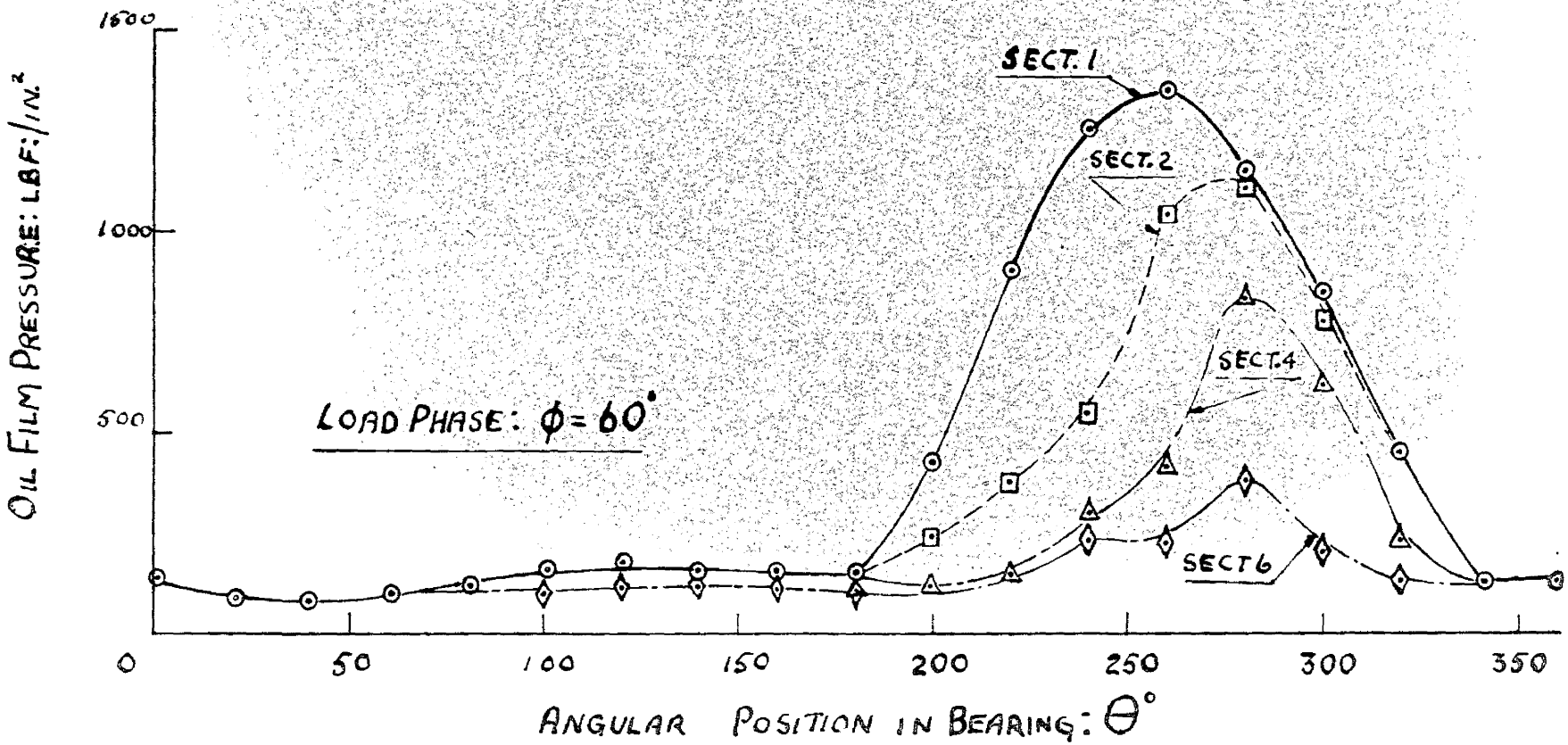
OIL FILM PRESSURE: LBF:/IN.²
1600
1000
500
SECT. 1
SECT. 2
SECT. 4
SECT 6
LOAD PHASE: $\phi = 60^\circ$
0
50
100
150
200
250
300
350
ANGULAR POSITION IN BEARING: θ°

FIG: 4-5a

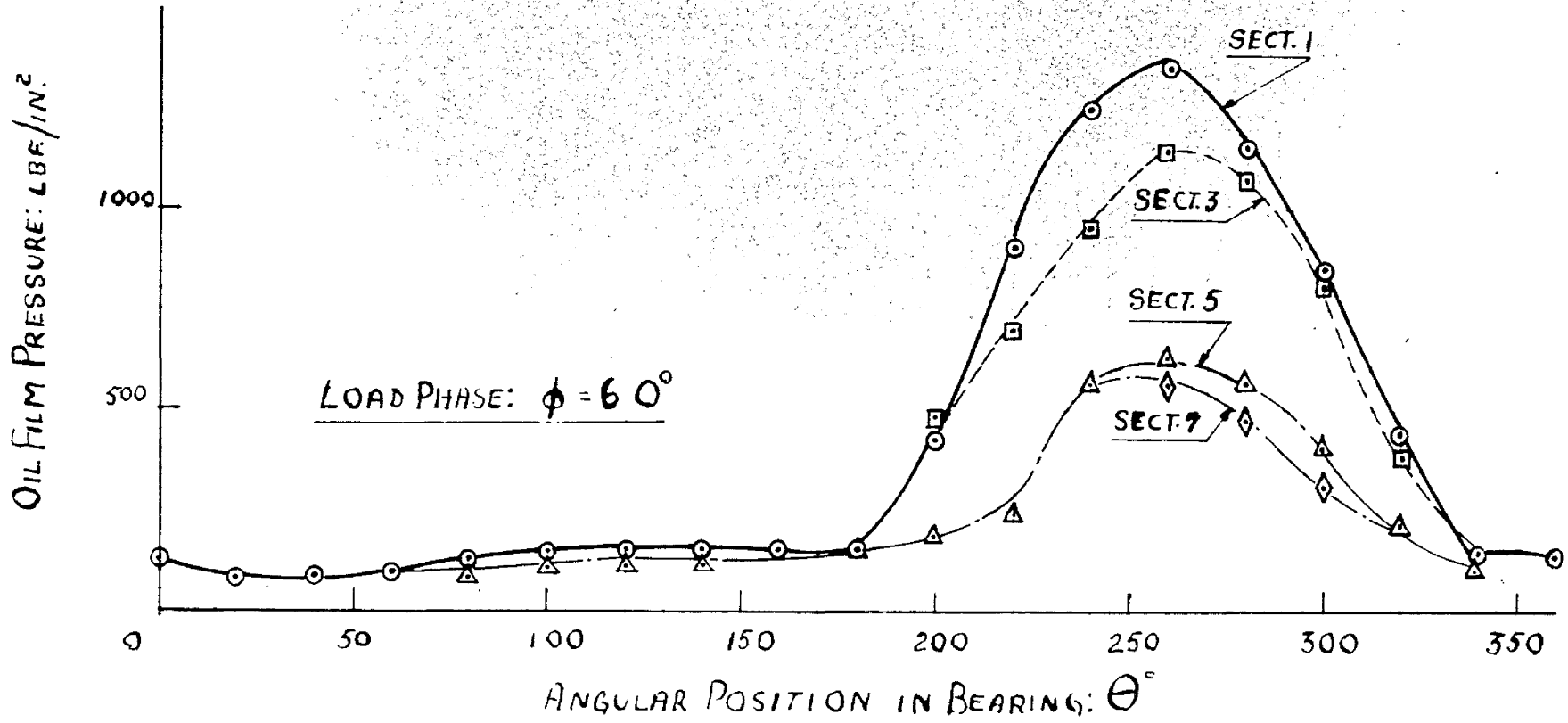
OIL FILM PRESSURE: LBF/IN.²
1000
500
0
50
100
150
200
250
300
350
ANGULAR POSITION IN BEARING: θ°
LOAD PHASE: φ = 60°
SECT. 1
SECT. 3
SECT. 5
SECT. 7

FIG: 4.5b

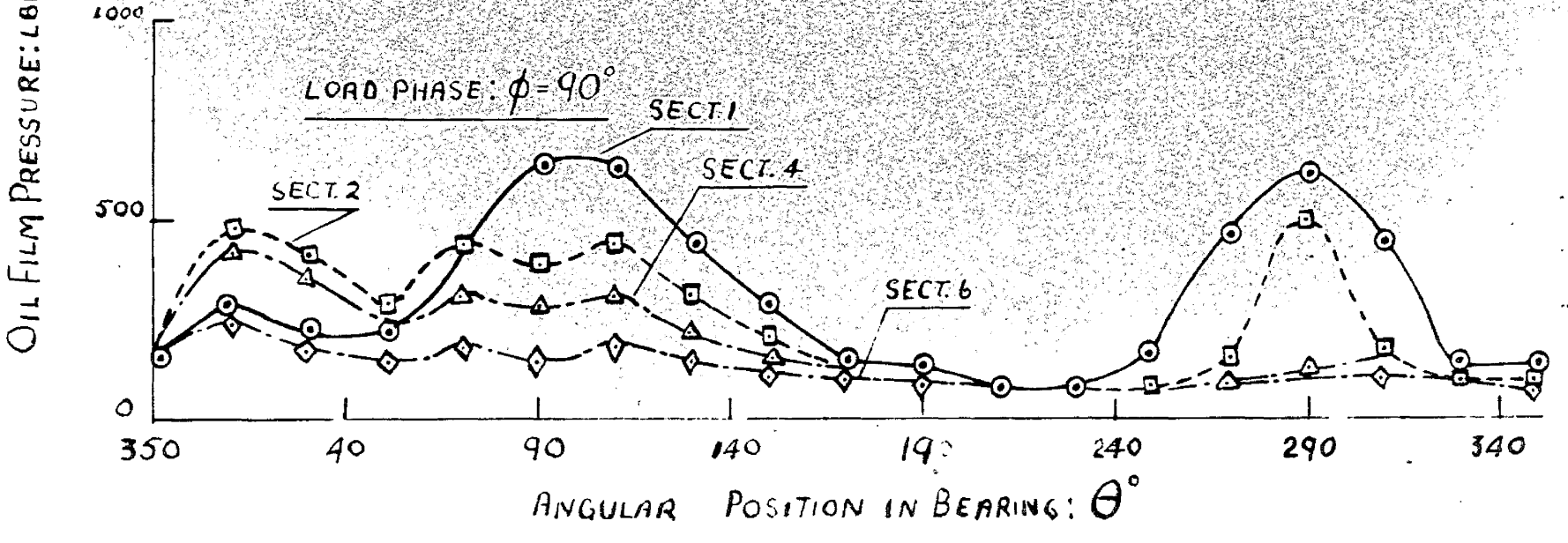
OIL FILM PRESSURE: LBF./IN.²
1000
500
0
LOAD PHASE: $\phi = 90°$
SECT. 1
SECT. 2
SECT. 4
SECT. 6
350
40
90
140
240
290
340
ANGULAR POSITION IN BEARING: $\theta°$

FIG: 4·6a

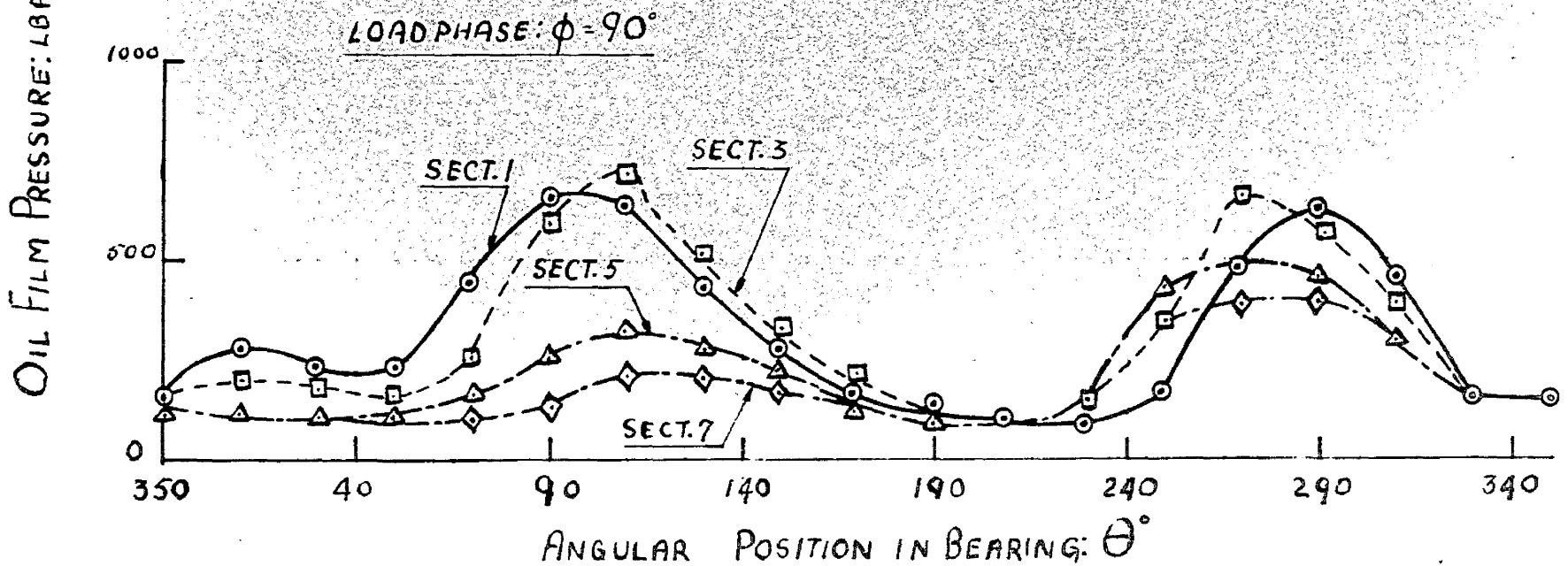
LOAD PHASE: $\phi = 90°$
OIL FILM PRESSURE: LBF./IN²
1000
500
0
SECT. 1
SECT. 3
SECT. 5
SECT. 7
350
40
90
140
190
240
290
340
ANGULAR POSITION IN BEARING: $\theta°$

FIG: 4·6b.

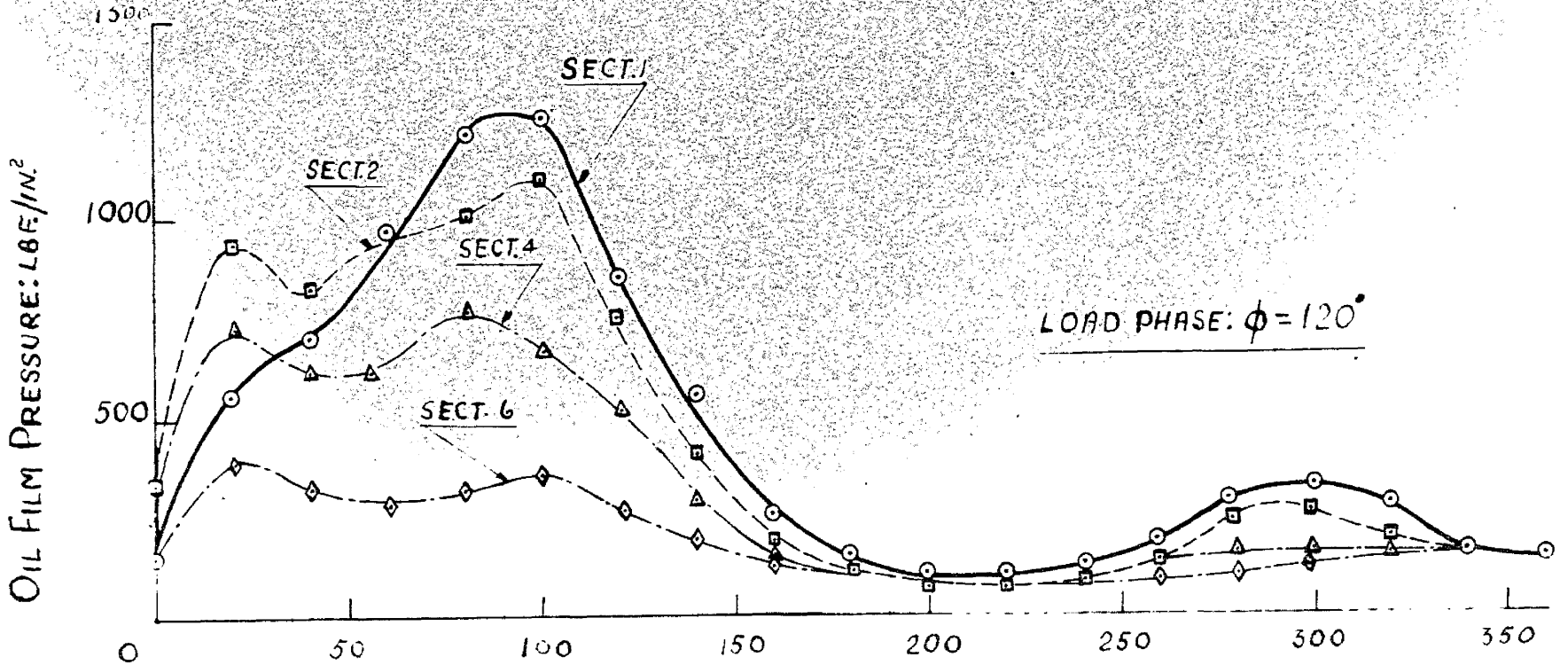
OIL FILM PRESSURE: LBF./IN.²
1500
1000
500
0
SECT.1
SECT.2
SECT.4
SECT. 6
LOAD PHASE: $\phi = 120^\circ$
50
100
150
200
250
300
350
ANGULAR POSITION IN BEARING: θ°

FIG: 4·7a

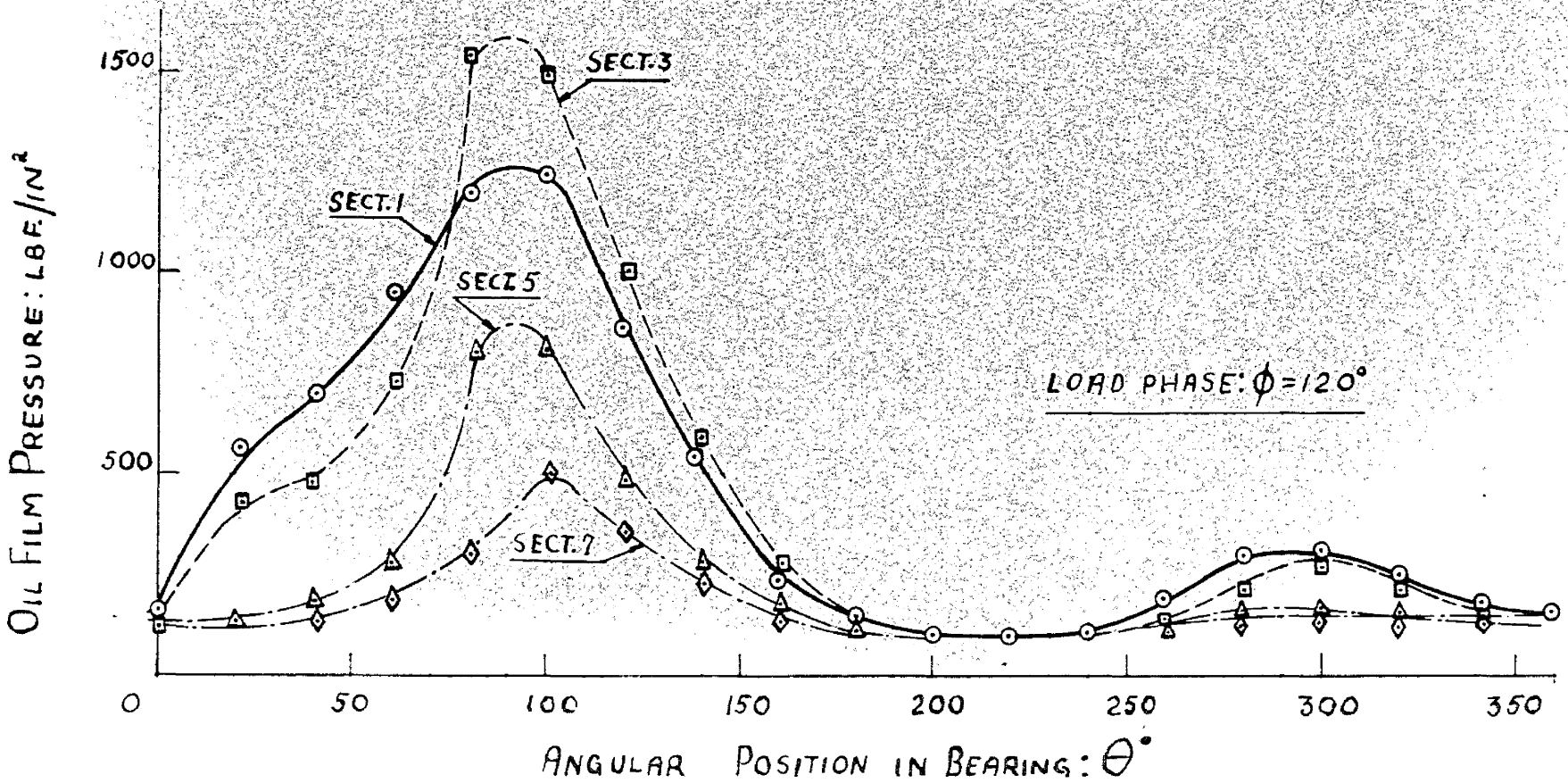
OIL FILM PRESSURE: LBF./IN²
1500
1000
500
0
50
100
150
200
250
300
350
SECT. 3
SECT. 1
SECT. 5
SECT. 7
LOAD PHASE: ϕ = 120°
ANGULAR POSITION IN BEARING: θ°

FIG. 4.7b

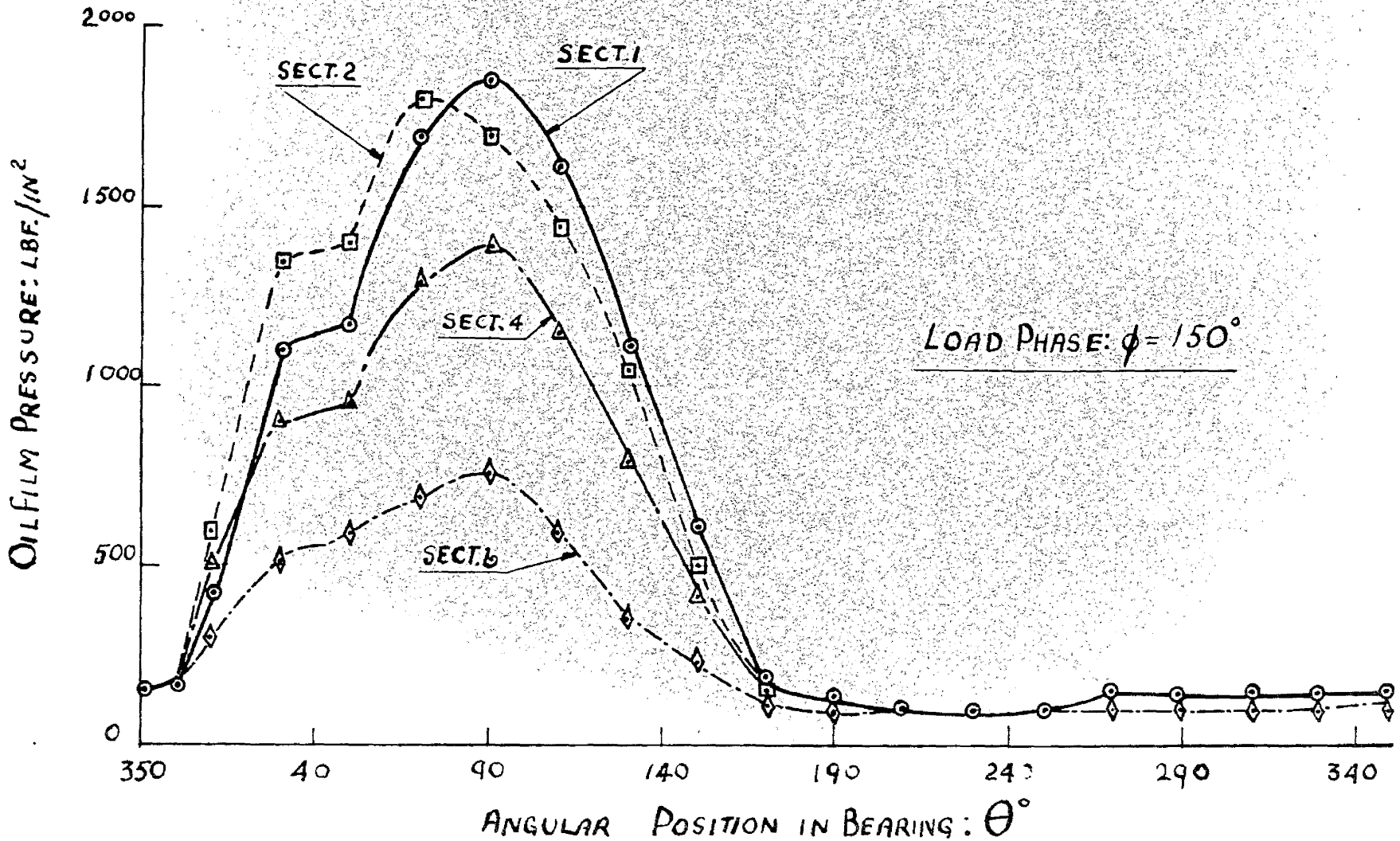
2000
1500
1000
500
0
OIL FILM PRESSURE: LBF./IN²
SECT. 2
SECT. 1
SECT. 4
SECT. 6
LOAD PHASE: φ = 150°
350
40
90
140
190
240
290
340
ANGULAR POSITION IN BEARING: θ°

FIG: 4·8a.

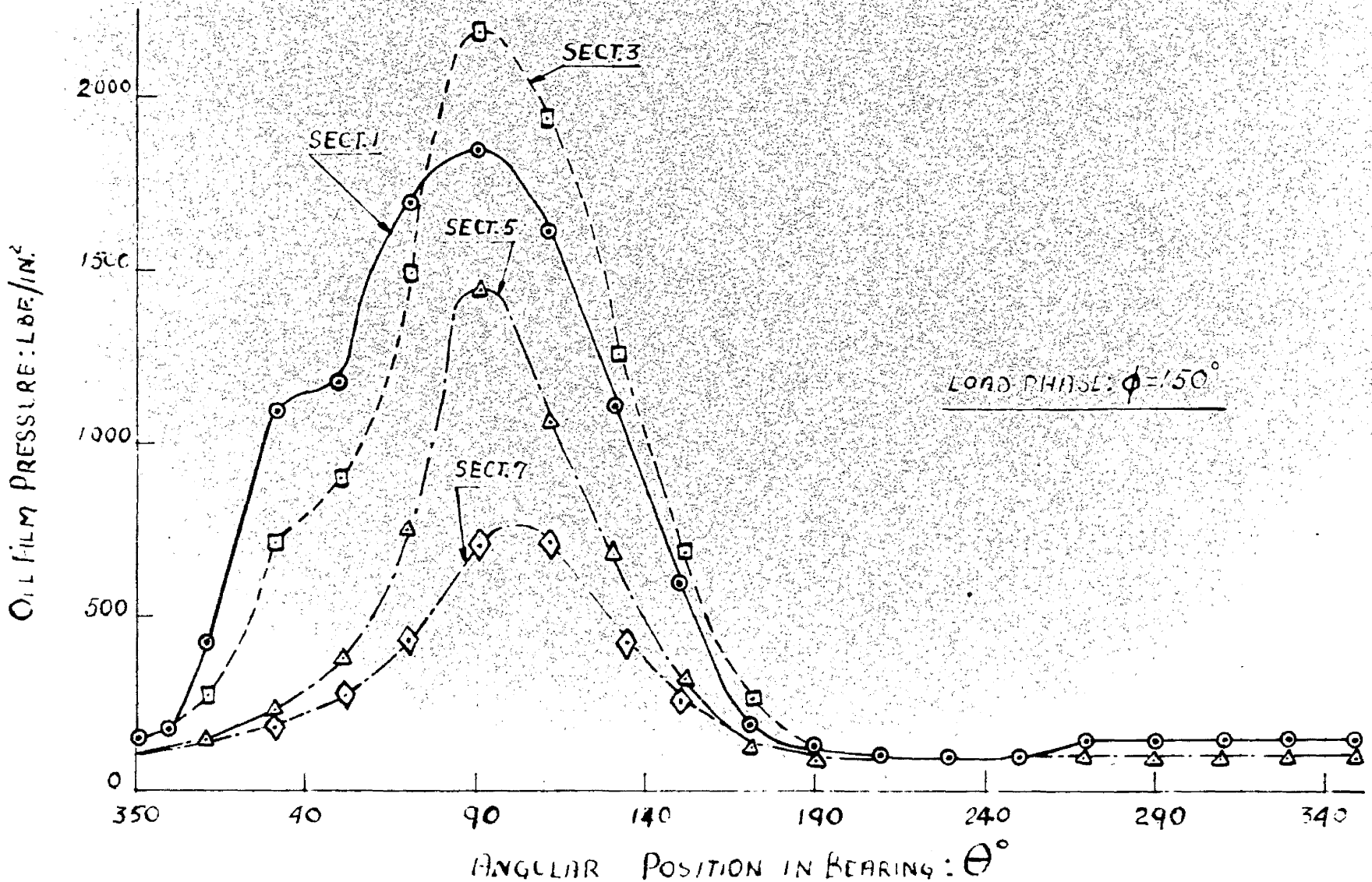
SECT.3
SECT.1
SECT.5
SECT.7
2000
1500
1000
500
0
350
40
90
140
190
240
290
340
OIL FILM PRESSURE: LBF/IN.²
LOAD PHASE: φ=150°
ANGULAR POSITION IN BEARING: θ°

FIG: 48b

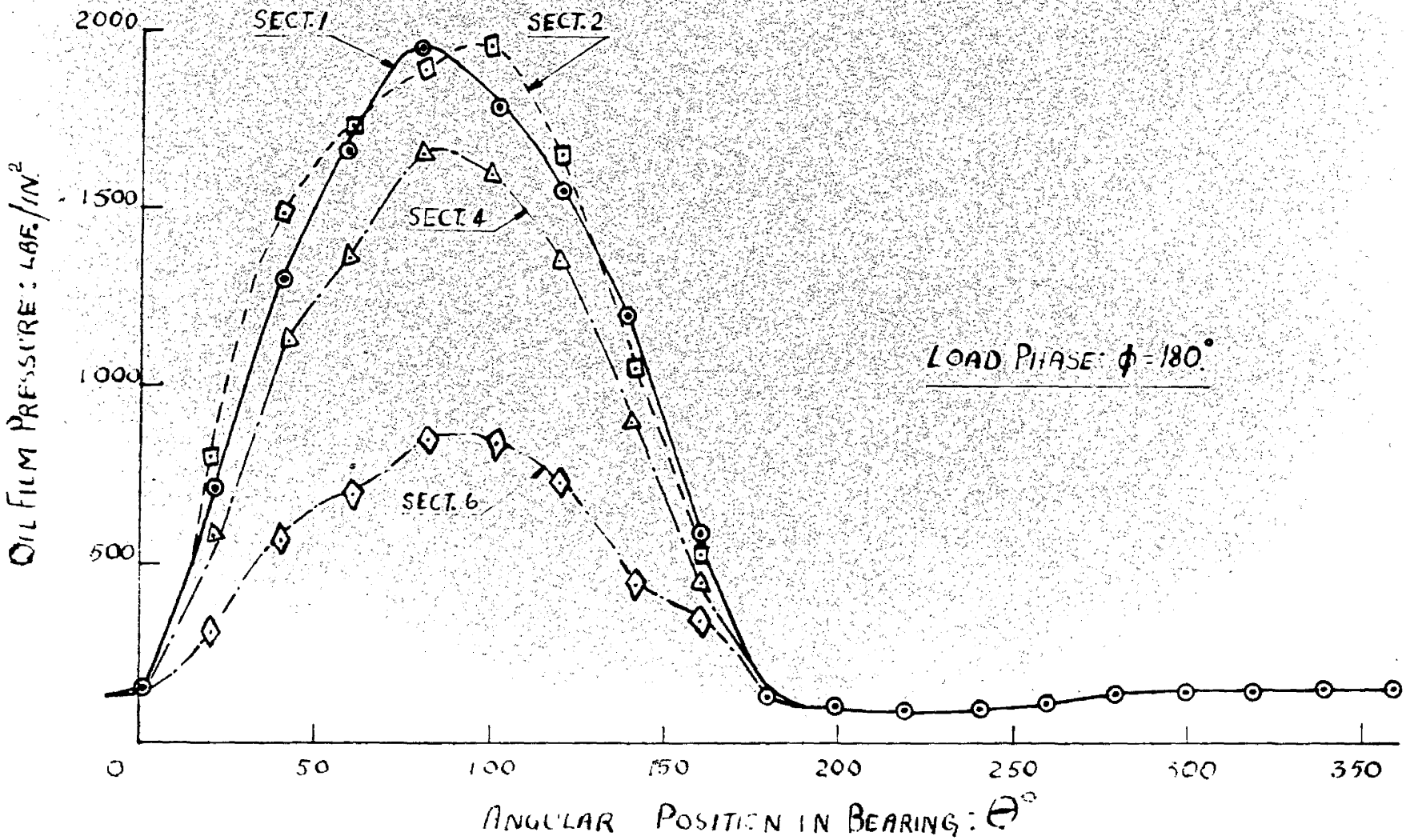
SECT. 1
SECT. 2
SECT. 4
SECT. 6
2000
1500
1000
500
0
50
100
150
200
250
300
350
OIL FILM PRESSURE : LBF./IN.²
ANGULAR POSITION IN BEARING : θ°
LOAD PHASE: φ = 180°

FIG. 4·9a.

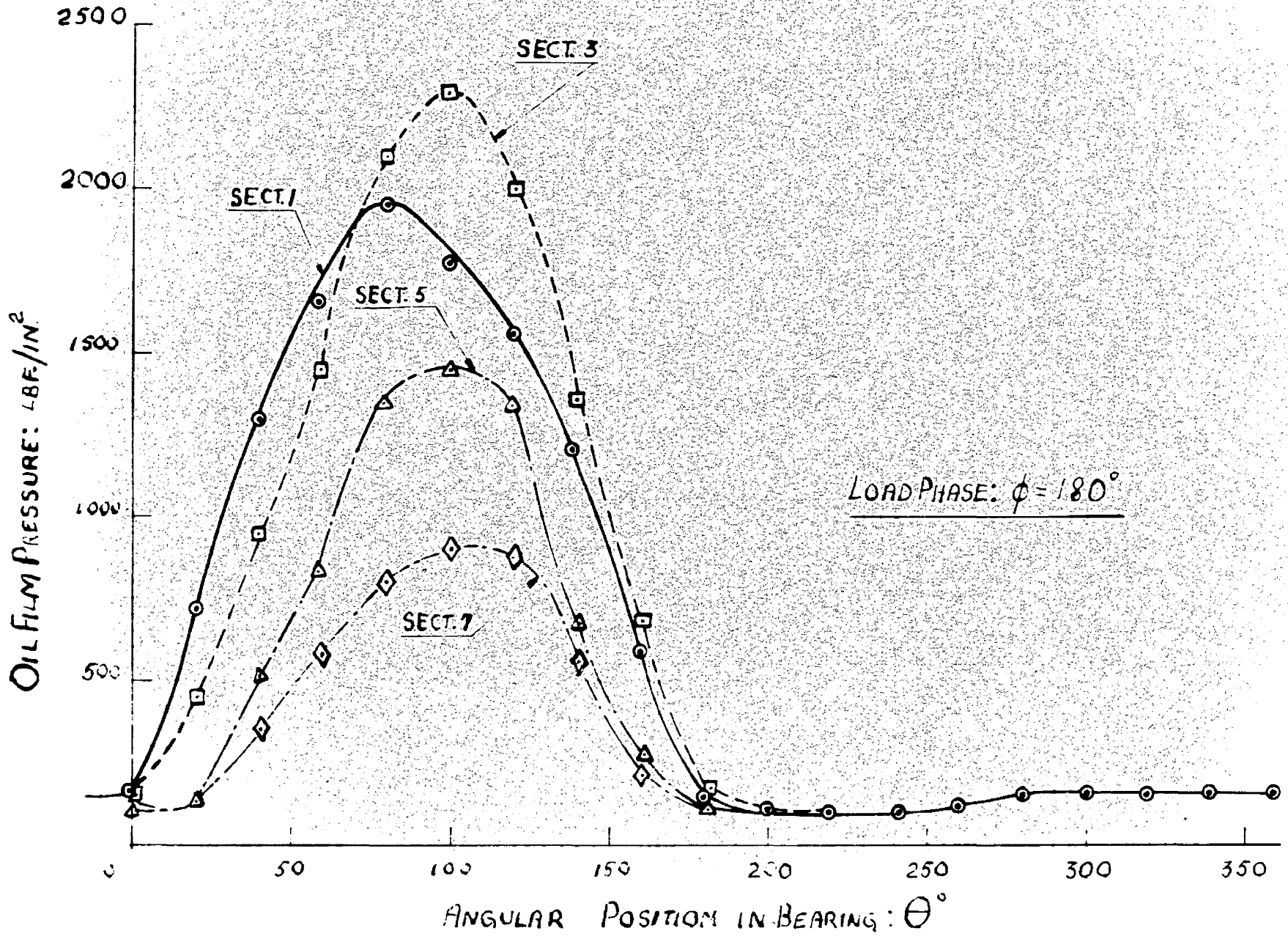
2500
2000
1500
1000
500
0
50
100
150
200
250
300
350
SECT. 3
SECT. 1
SECT. 5
SECT. 7
LOAD PHASE: $\phi = 180^\circ$
OIL FILM PRESSURE: LBF/IN^2
ANGULAR POSITION IN BEARING: θ°

FIG: 4·9b

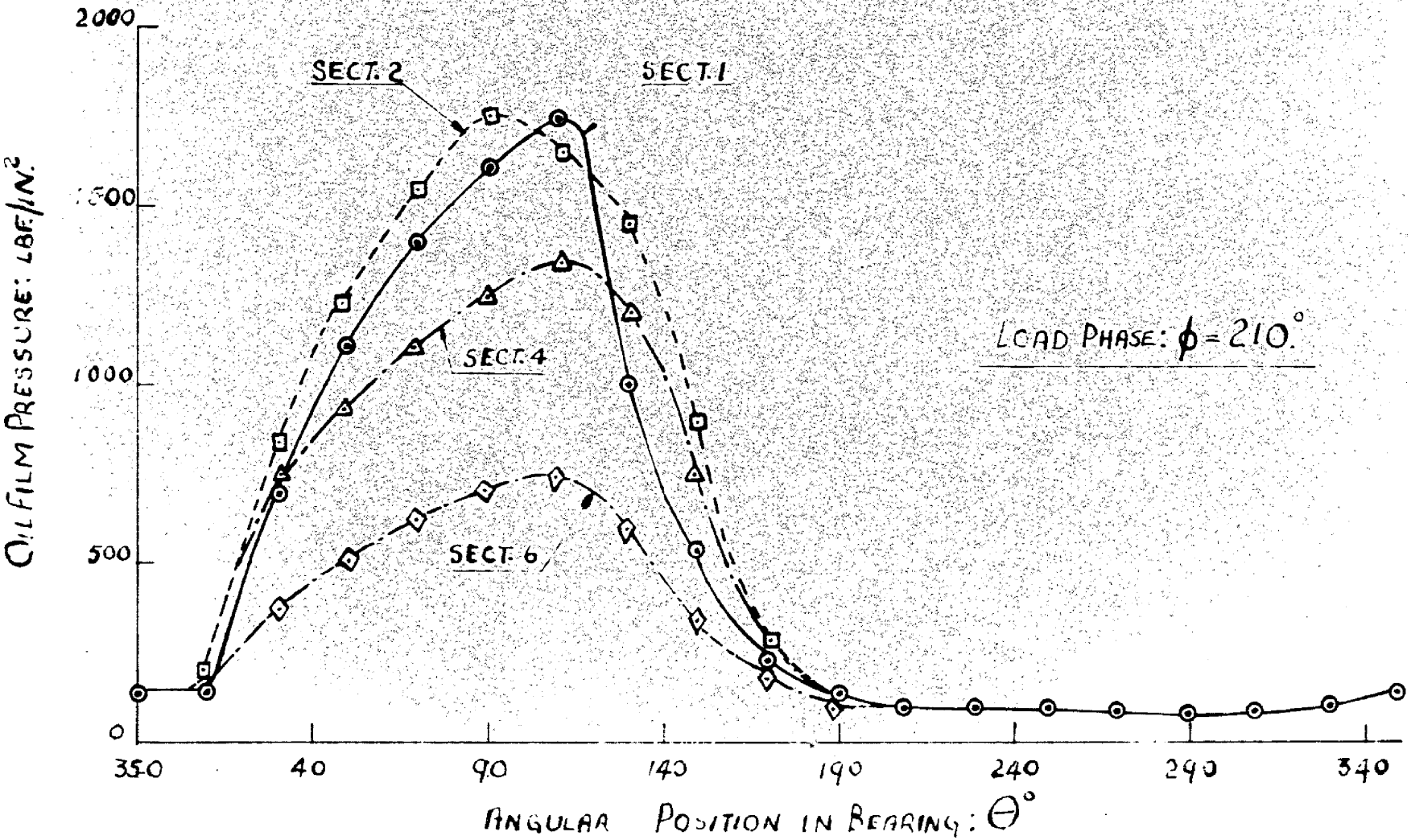
2000
1500
1000
500
0
SECT. 2
SECT. 1
SECT. 4
SECT. 6
LOAD PHASE: $\phi = 210^\circ$
OIL FILM PRESSURE: LBF/IN.^{2}
350
40
90
140
190
240
290
340
ANGULAR POSITION IN BEARING: θ°

FIG: 4·10a

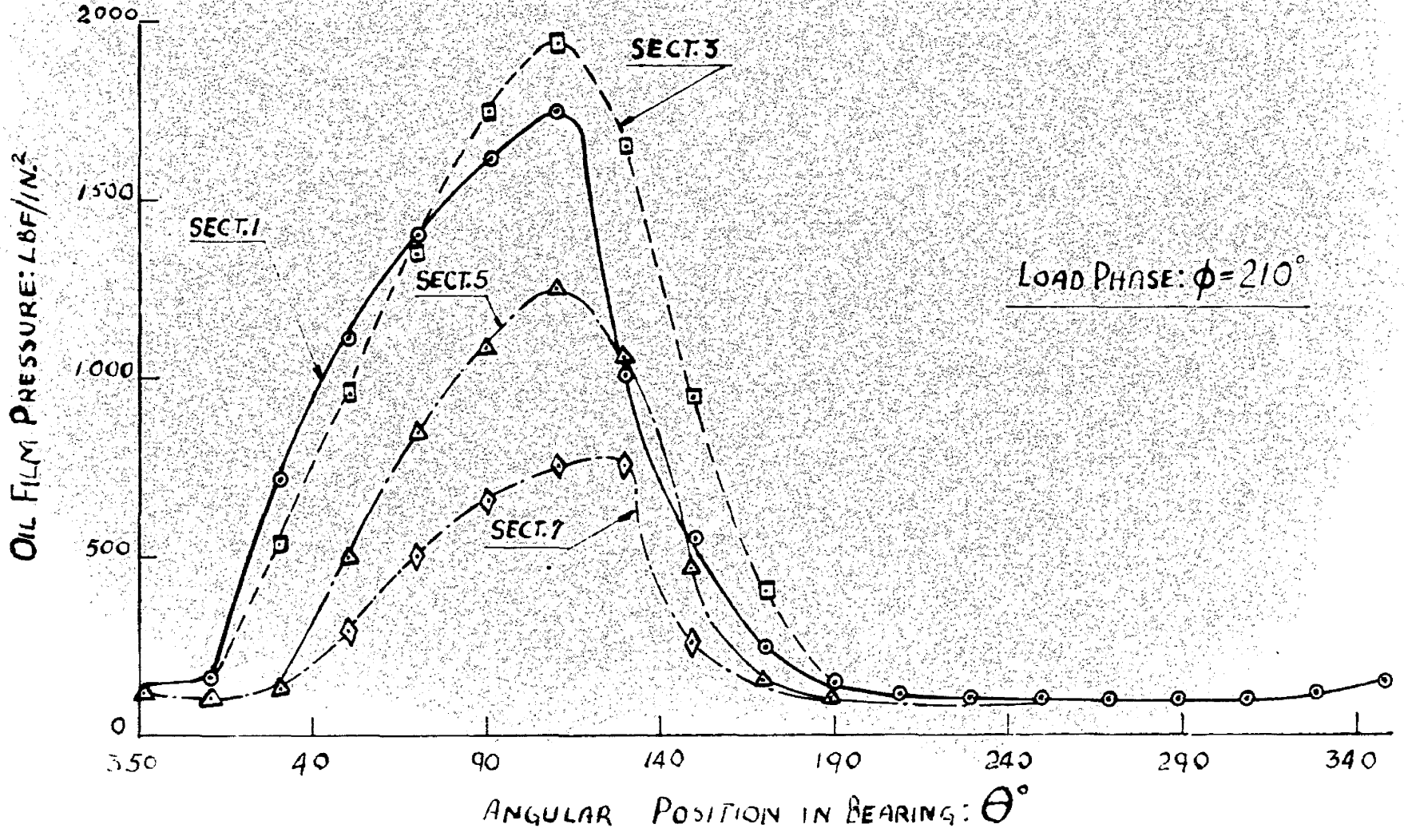
OIL FILM PRESSURE: LBF/IN.²
2000
1500
1000
500
0
SECT. 3
SECT. 1
SECT. 5
SECT. 7
LOAD PHASE: $\phi = 210°$
350
40
90
140
190
240
290
340
ANGULAR POSITION IN BEARING: $\theta°$

FIG: 4·10b

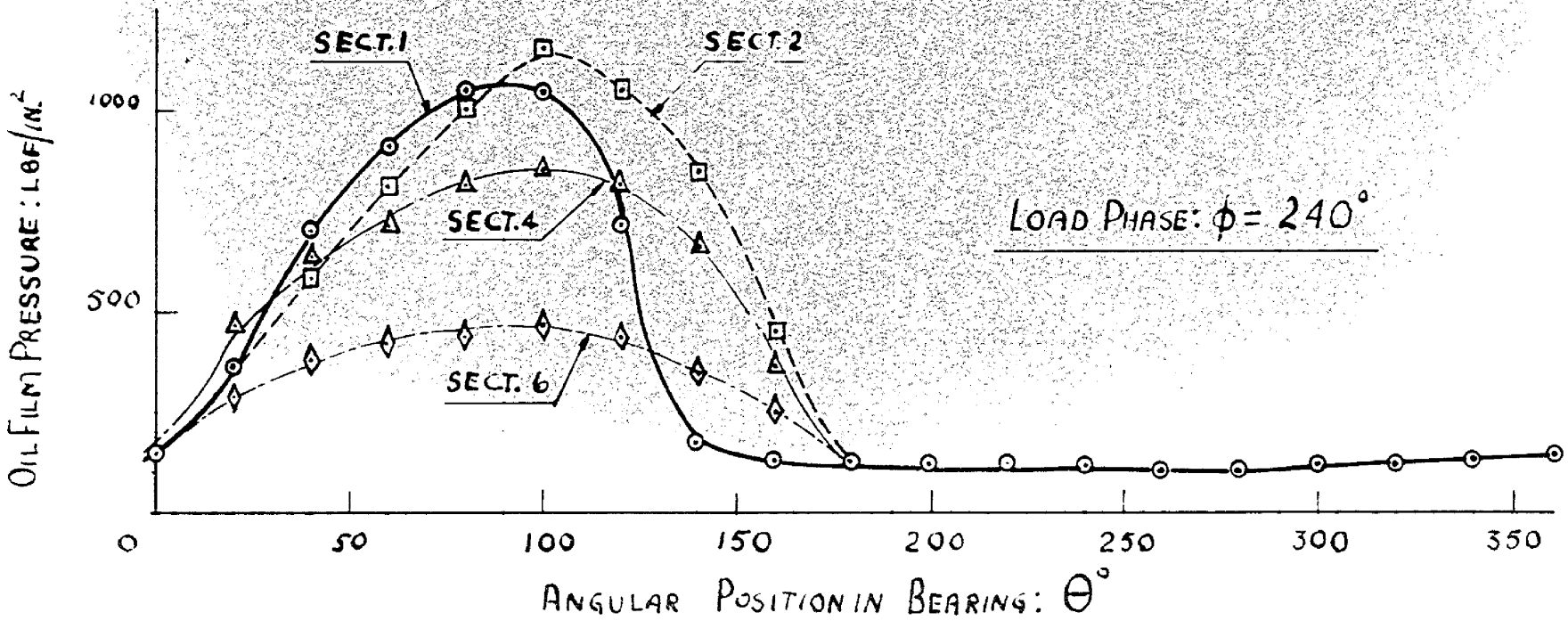
SECT. 1
SECT. 2
SECT. 4
SECT. 6
LOAD PHASE: $\phi = 240^\circ$
OIL FILM PRESSURE: LBF/IN.^{2}
1000
500
0
50
100
150
200
250
300
350
ANGULAR POSITION IN BEARING: θ°

Fig: 4·11a

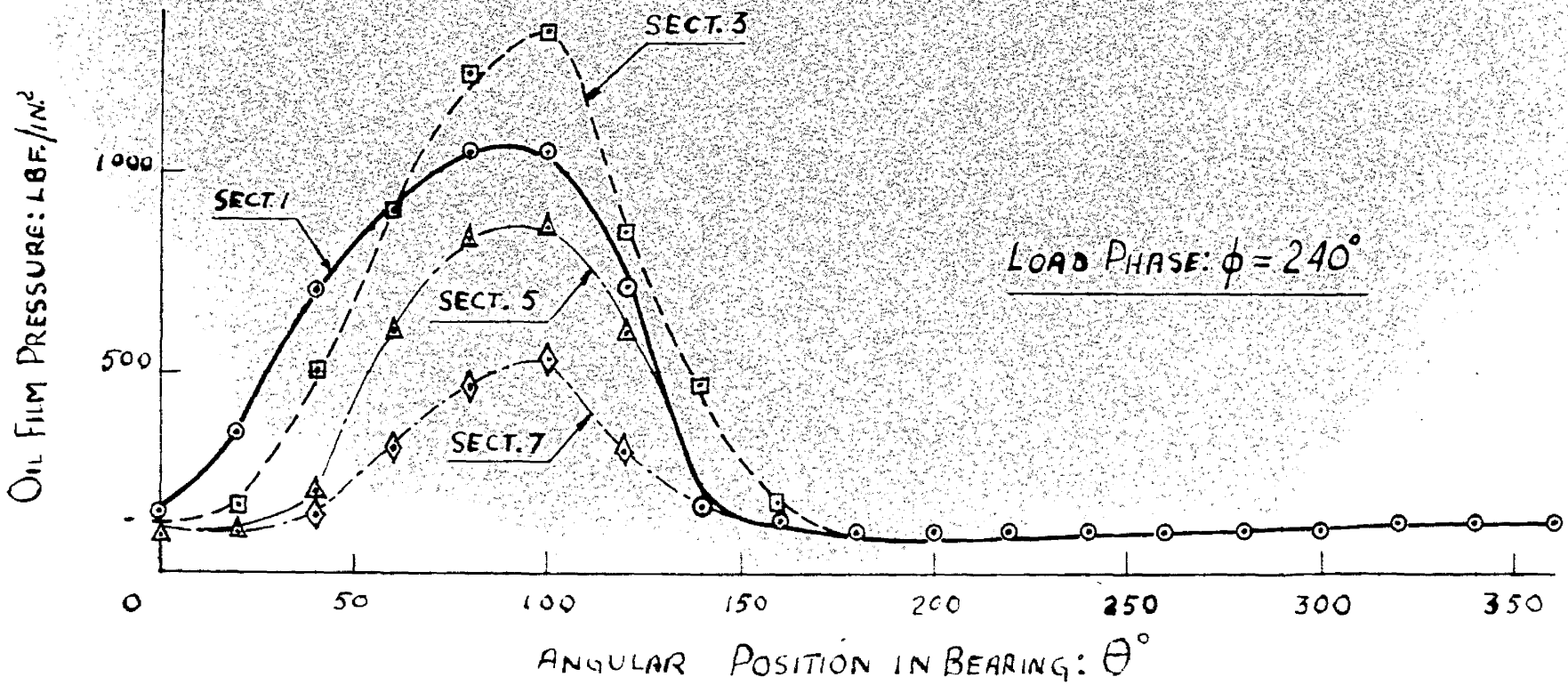
OIL FILM PRESSURE: LBF./IN.²
1000
500
-
SECT. 3
SECT. 1
SECT. 5
SECT. 7
LOAD PHASE: $\phi = 240°$
0
50
100
150
200
250
300
350
ANGULAR POSITION IN BEARING: $\theta°$

FIG: 4·11b

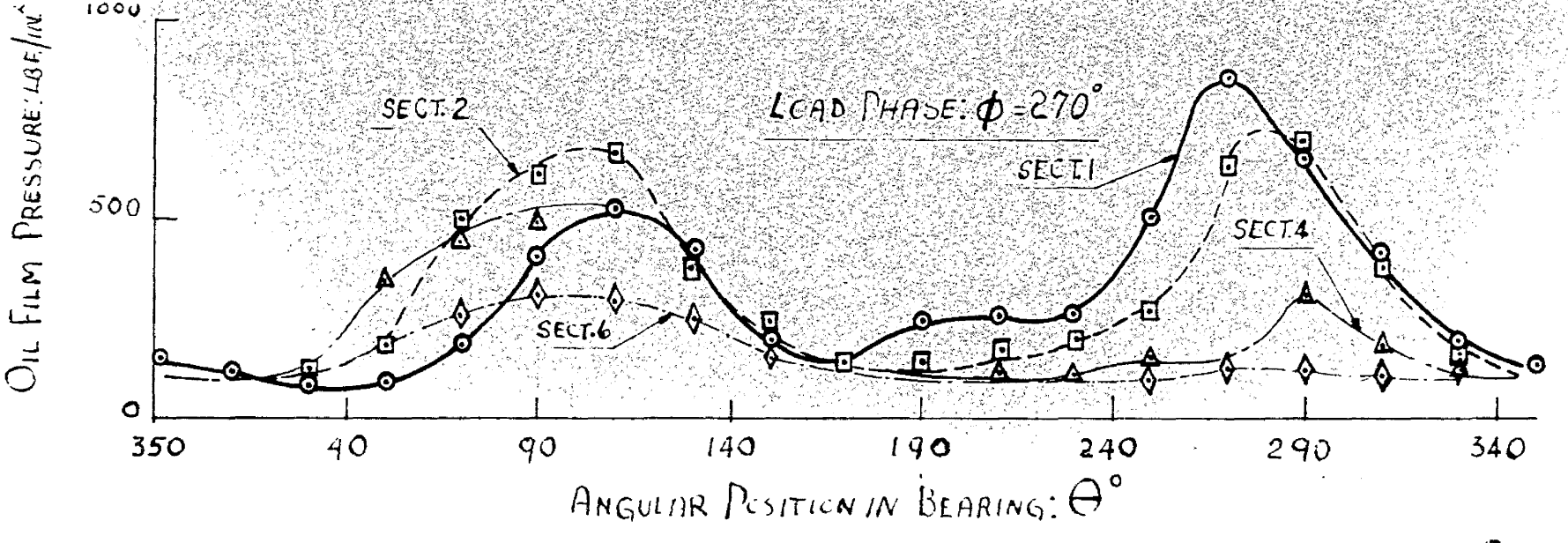
OIL FILM PRESSURE: LBF/IN.²
1000
500
0
SECT. 2
LOAD PHASE: $\phi = 270°$
SECT. 1
SECT. 4
SECT. 6
350
40
90
140
190
240
290
340
ANGULAR POSITION IN BEARING: $\theta°$

FIG: 4·12a

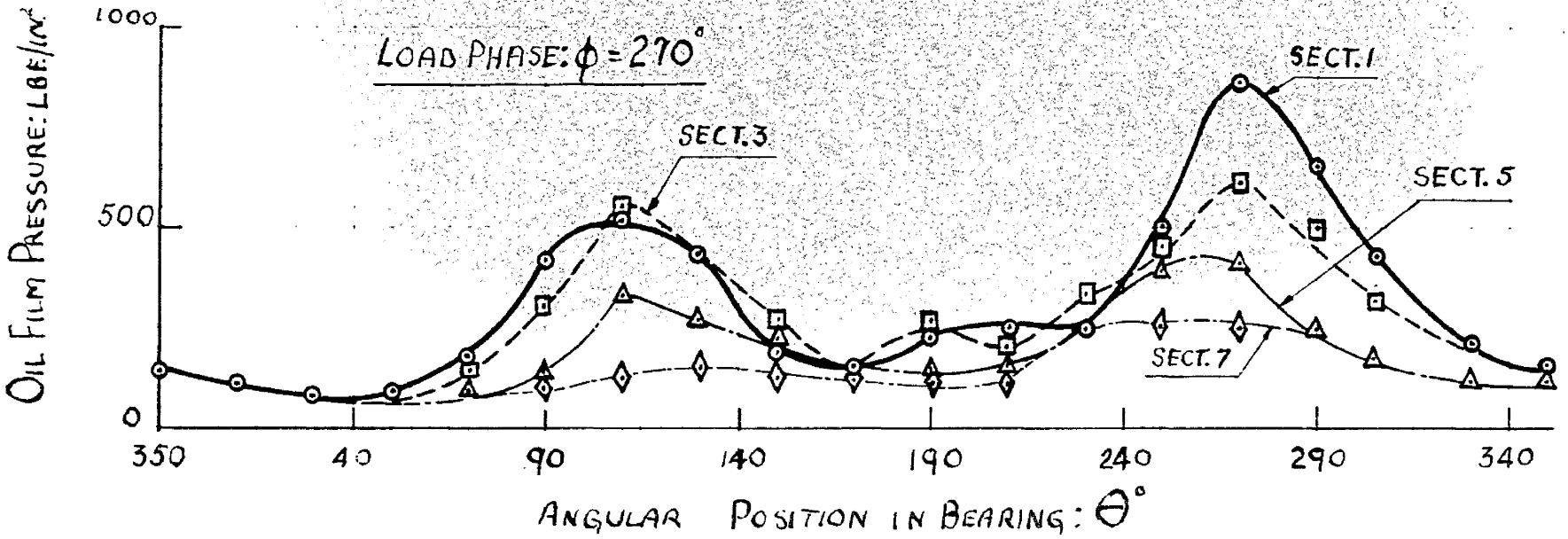
OIL FILM PRESSURE: LBF/IN²
1000
500
0
LOAD PHASE: ϕ = 270°
SECT. 1
SECT. 3
SECT. 5
SECT. 7
350
40
90
140
190
240
290
340
ANGULAR POSITION IN BEARING: θ°

FIG: 4-12b.

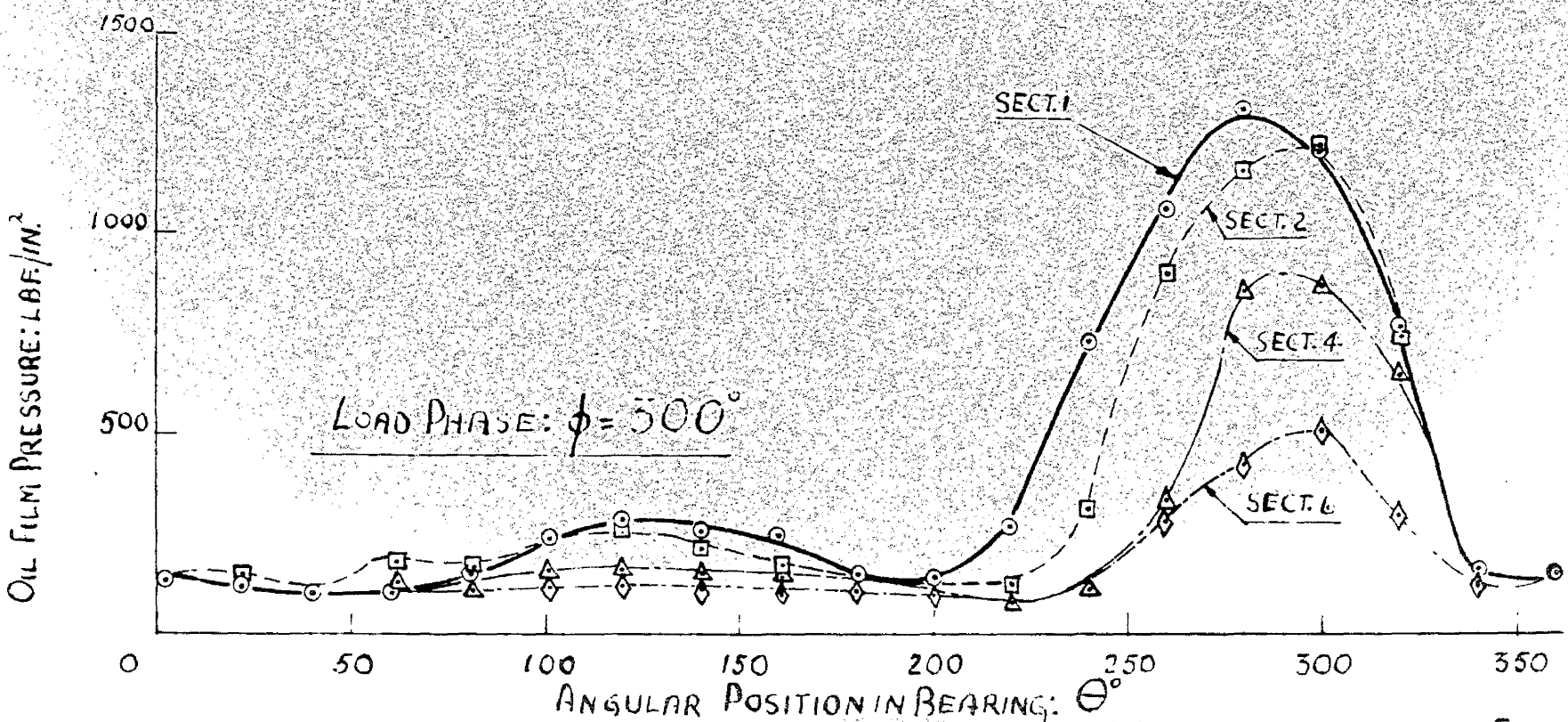
1500
1000
500
0
50
100
150
200
250
300
350
SECT. 1
SECT. 2
SECT. 4
SECT. 6
LOAD PHASE: $\phi = 500^\circ$
OIL FILM PRESSURE: LBF./IN.^{2}
ANGULAR POSITION IN BEARING: θ°

FIG: 4·13a

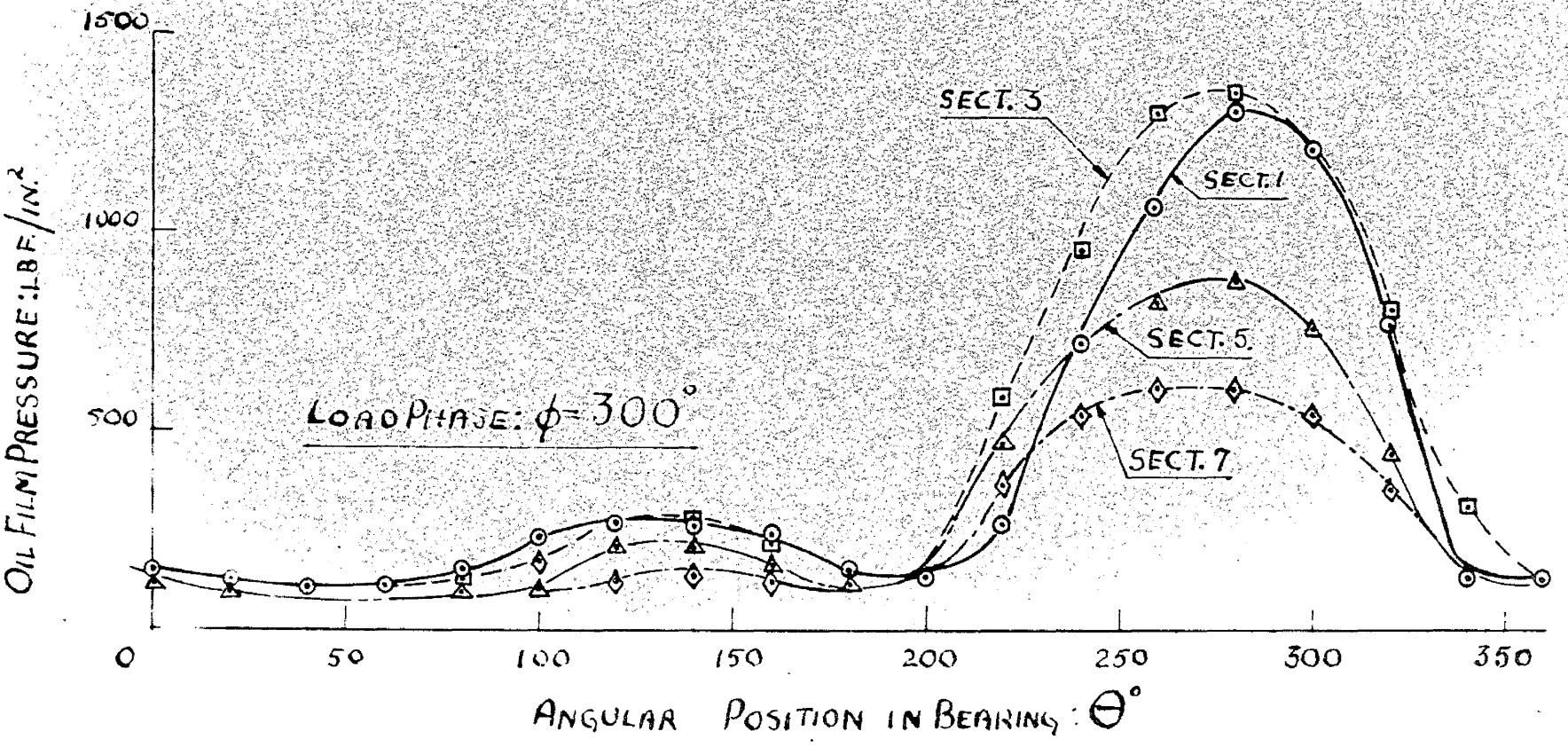
1500
1000
500
OIL FILM PRESSURE: LBF./IN.²
SECT. 3
SECT. 1
SECT. 5
SECT. 7
LOAD PHASE: φ=300°
0
50
100
150
200
250
300
350
ANGULAR POSITION IN BEARING: Θ°

FIG: 4·13b

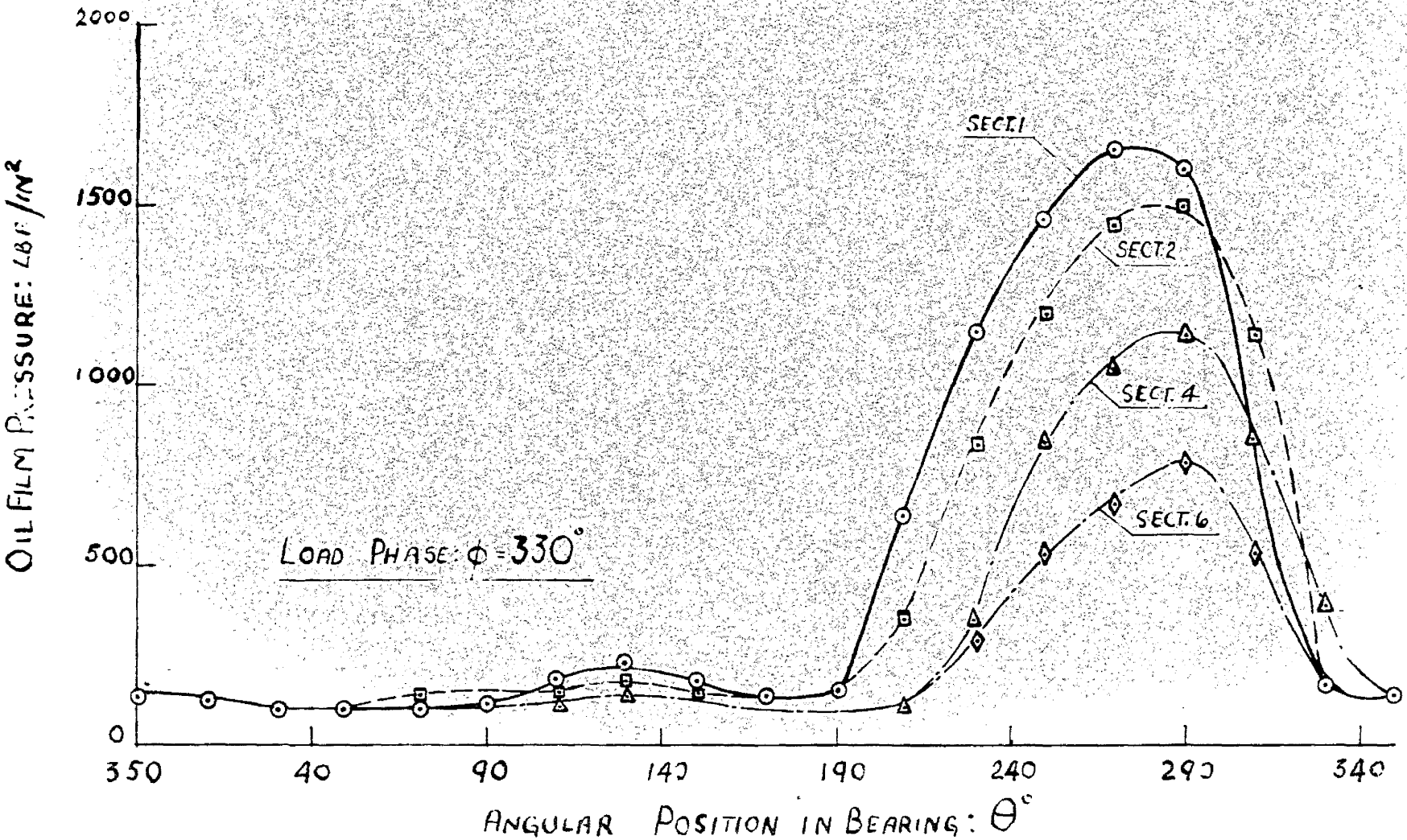
OIL FILM PRESSURE: LBF/IN²
2000
1500
1000
500
0
SECT.1
SECT.2
SECT.4
SECT.6
LOAD PHASE: Φ = 330°
350
40
90
140
190
240
290
340
ANGULAR POSITION IN BEARING: θ°

FIG: 4·14a

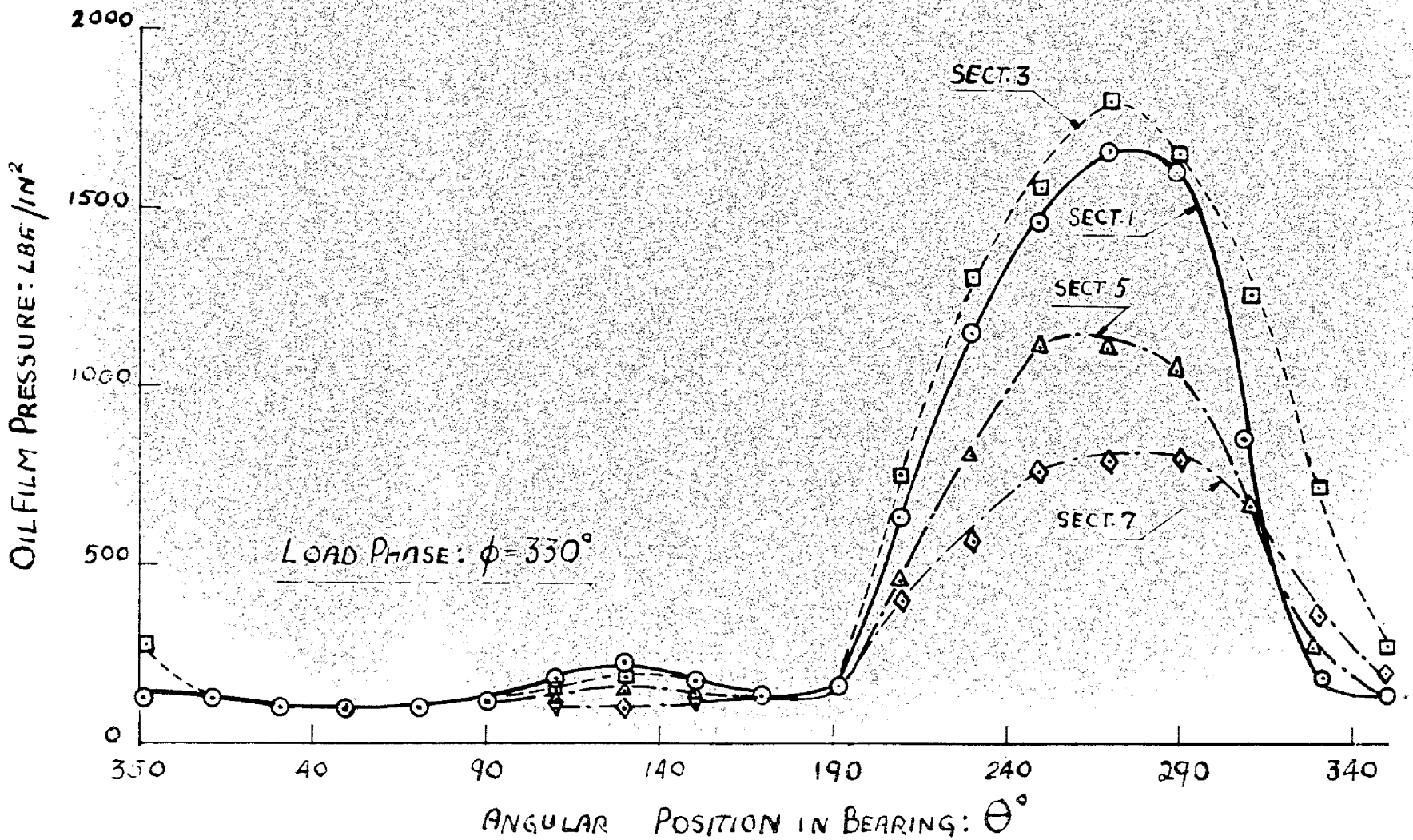
OIL FILM PRESSURE: LBS/IN²
2000
1500
1000
500
0
SECT. 3
SECT. 1
SECT. 5
SECT. 7
LOAD PHASE: φ = 330°
350
40
90
140
190
240
290
340
ANGULAR POSITION IN BEARING: θ°

FIG: 4·14b.

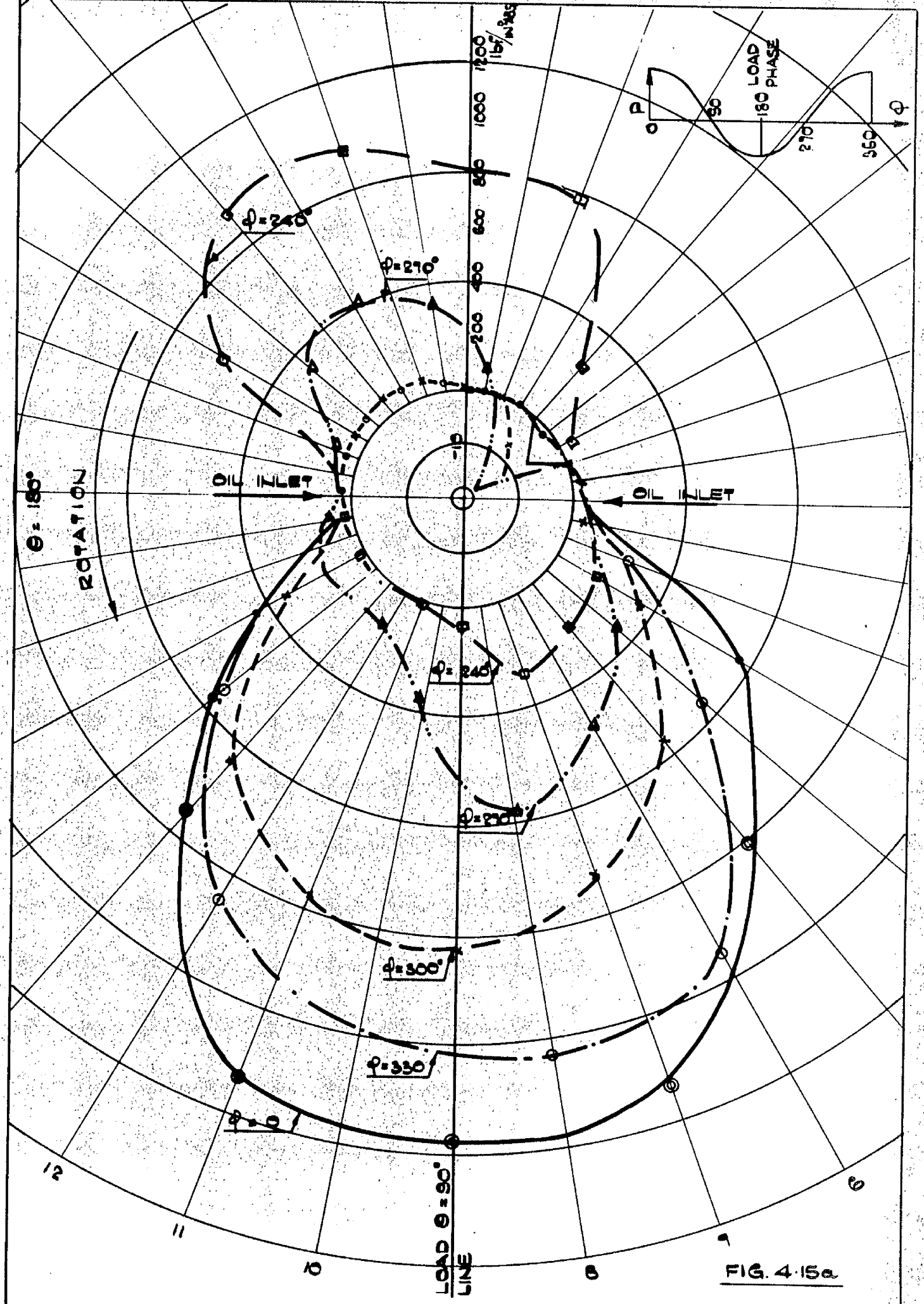
1200 lbf/in²
1000
800
600
400
200
0
LOAD PHASE
P
0
90
180
270
360
φ
φ=240°
φ=270°
φ=300°
φ=330°
φ=0
OIL INLET
OIL INLET
θ=180°
ROTATION
LOAD θ=90°
LINE
12
11
10
9
8
6

FIG. 4·15a

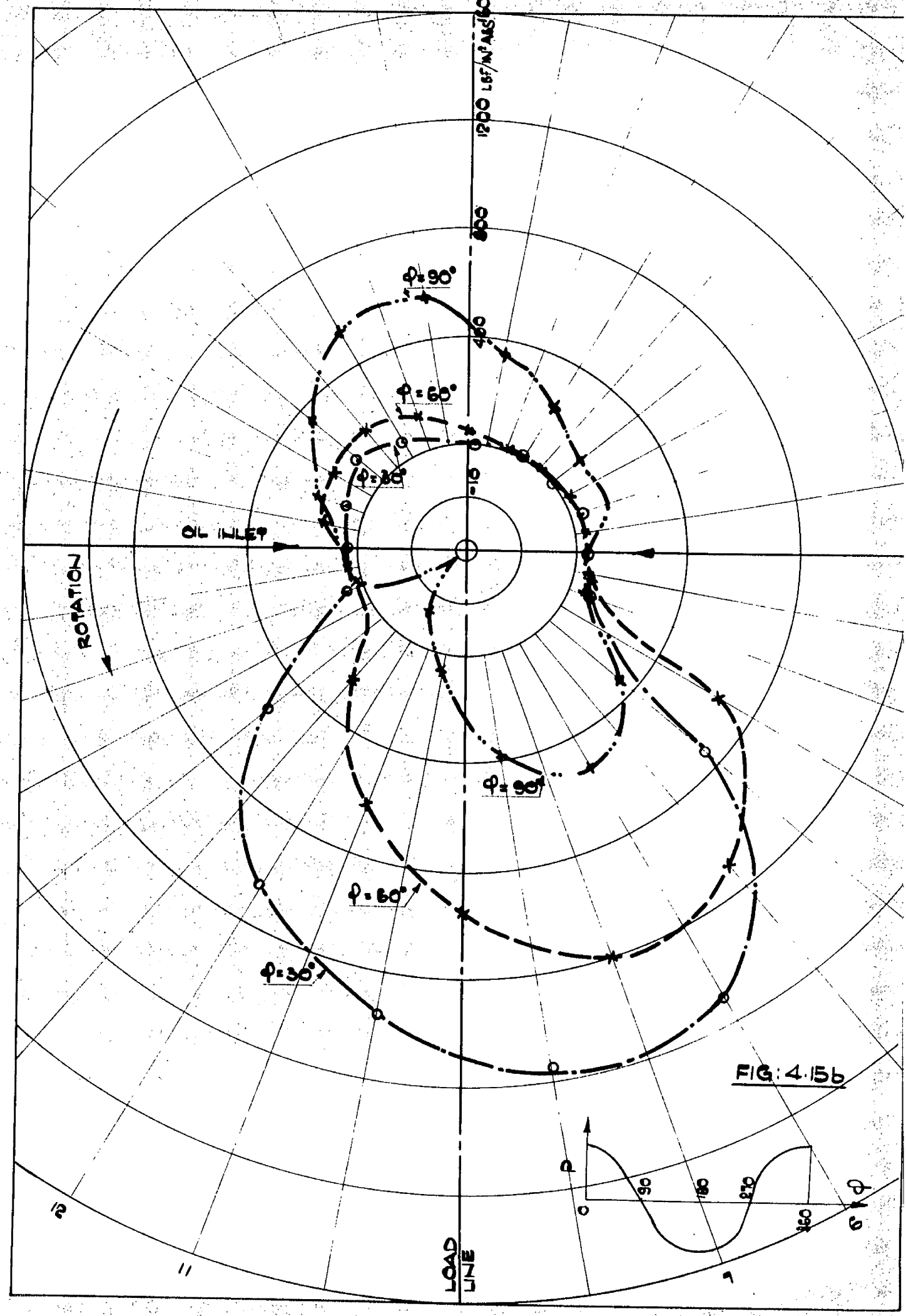
1200 LBF/IN² ABS
800
400
15
φ=90°
φ=60°
φ=30°
OIL INLET
ROTATION
φ=90°
φ=60°
φ=30°
LOAD LINE
12
11
1
P
0
90
180
270
360
θ

FIG: 4.15b

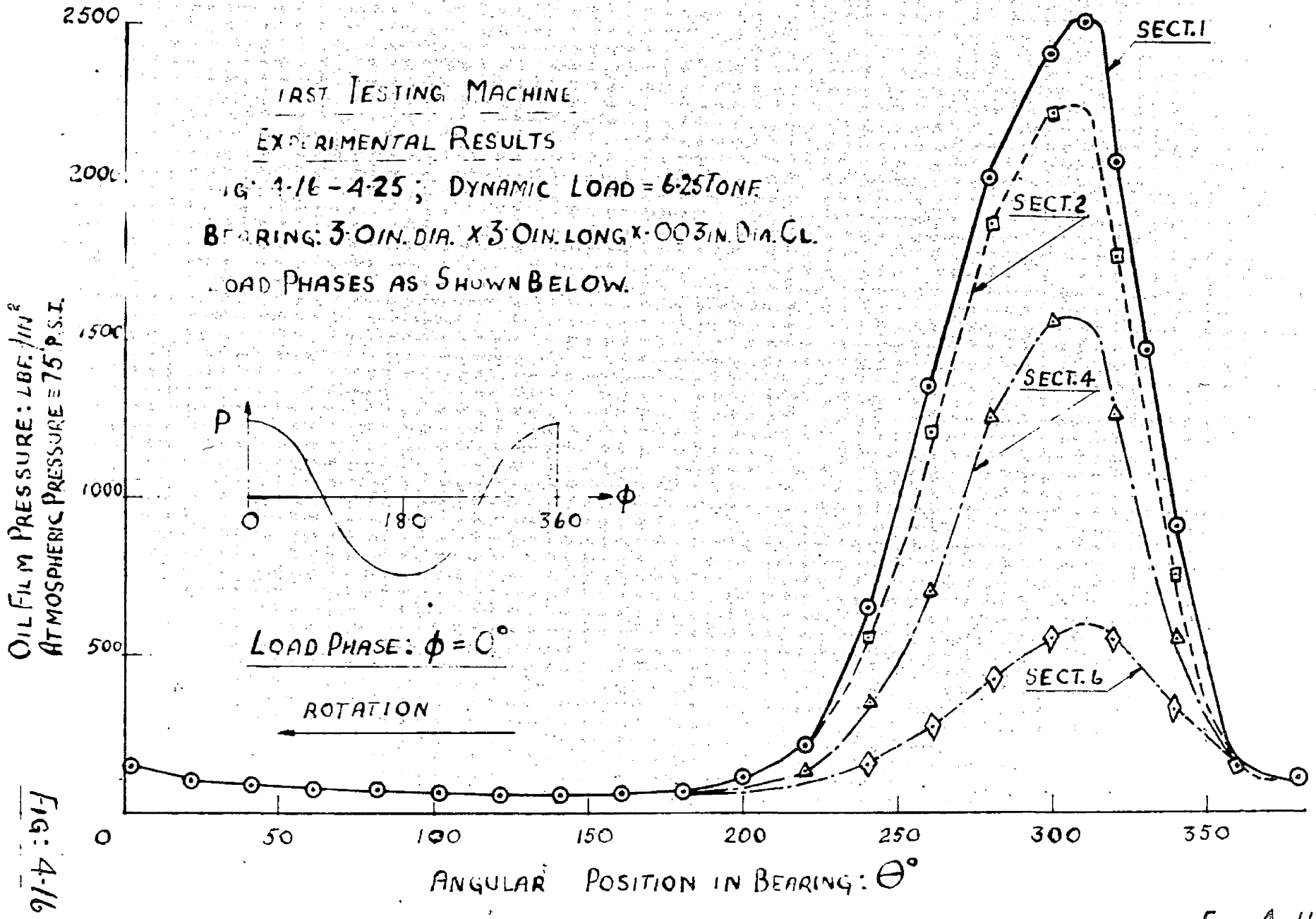
IRST TESTING MACHINE
EXPERIMENTAL RESULTS
G: 4-16 - 4-25 ; DYNAMIC LOAD = 6·25 TONF
BEARING: 3·0 IN. DIA. X 3·0 IN. LONG X ·003 IN. DIA. CL.
OAD PHASES AS SHOWN BELOW.
P
0
180
360
φ
LOAD PHASE: φ = 0°
ROTATION
SECT. 1
SECT. 2
SECT. 4
SECT. 6
OIL FILM PRESSURE: LBF/IN²
ATMOSPHERIC PRESSURE = 75 P.S.I.
2500
2000
1500
1000
500
0
50
100
150
200
250
300
350
ANGULAR POSITION IN BEARING: θ°
OIL INLET GROOVES: θ = 20 AND 200°

FIG: 4·16.

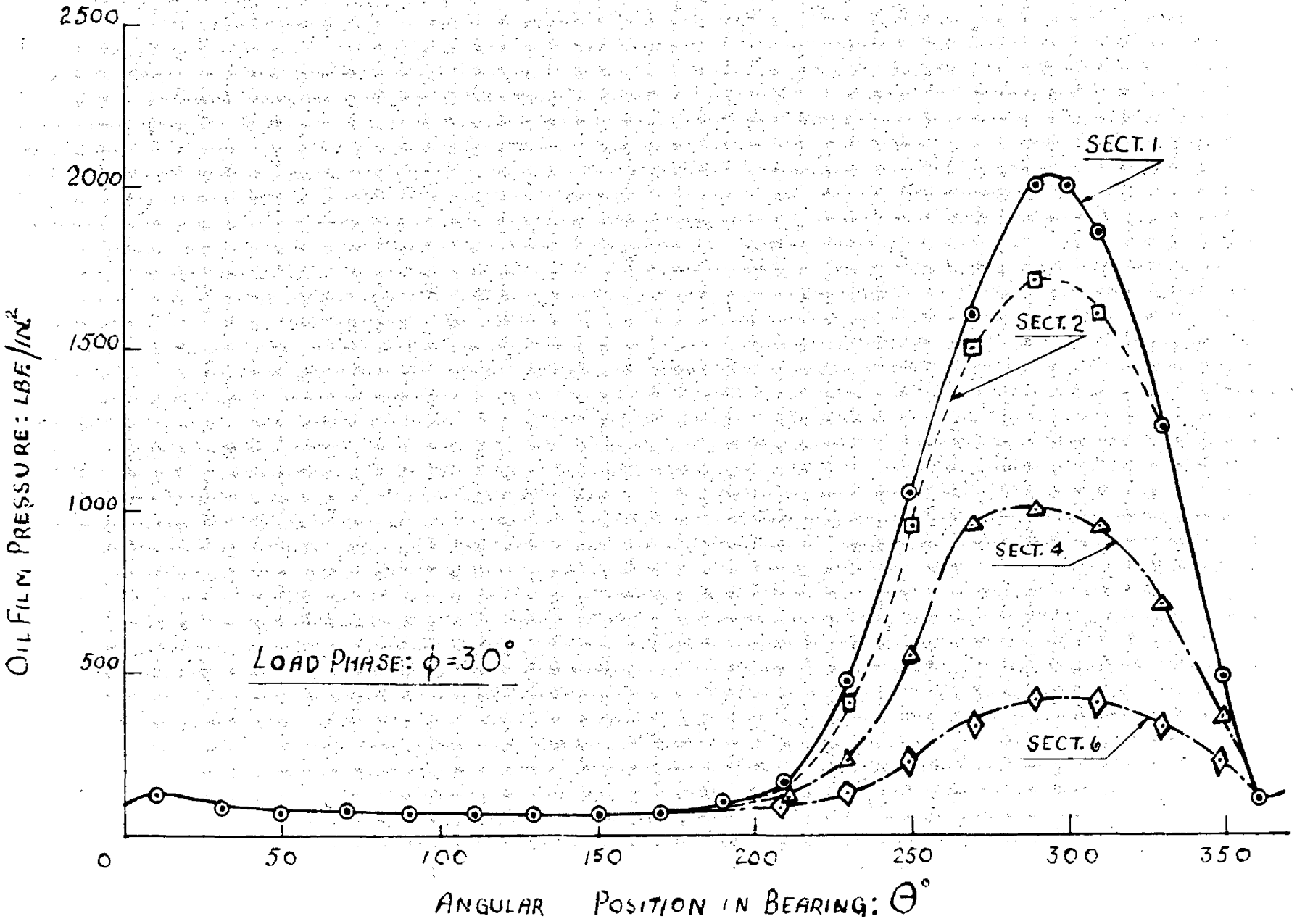
2500
2000
1500
1000
500
0
50
100
150
200
250
300
350
OIL FILM PRESSURE: LBF/IN.²
ANGULAR POSITION IN BEARING: Θ°
LOAD PHASE: φ=30°
SECT. 1
SECT. 2
SECT. 4
SECT. 6

FIG: 4-17

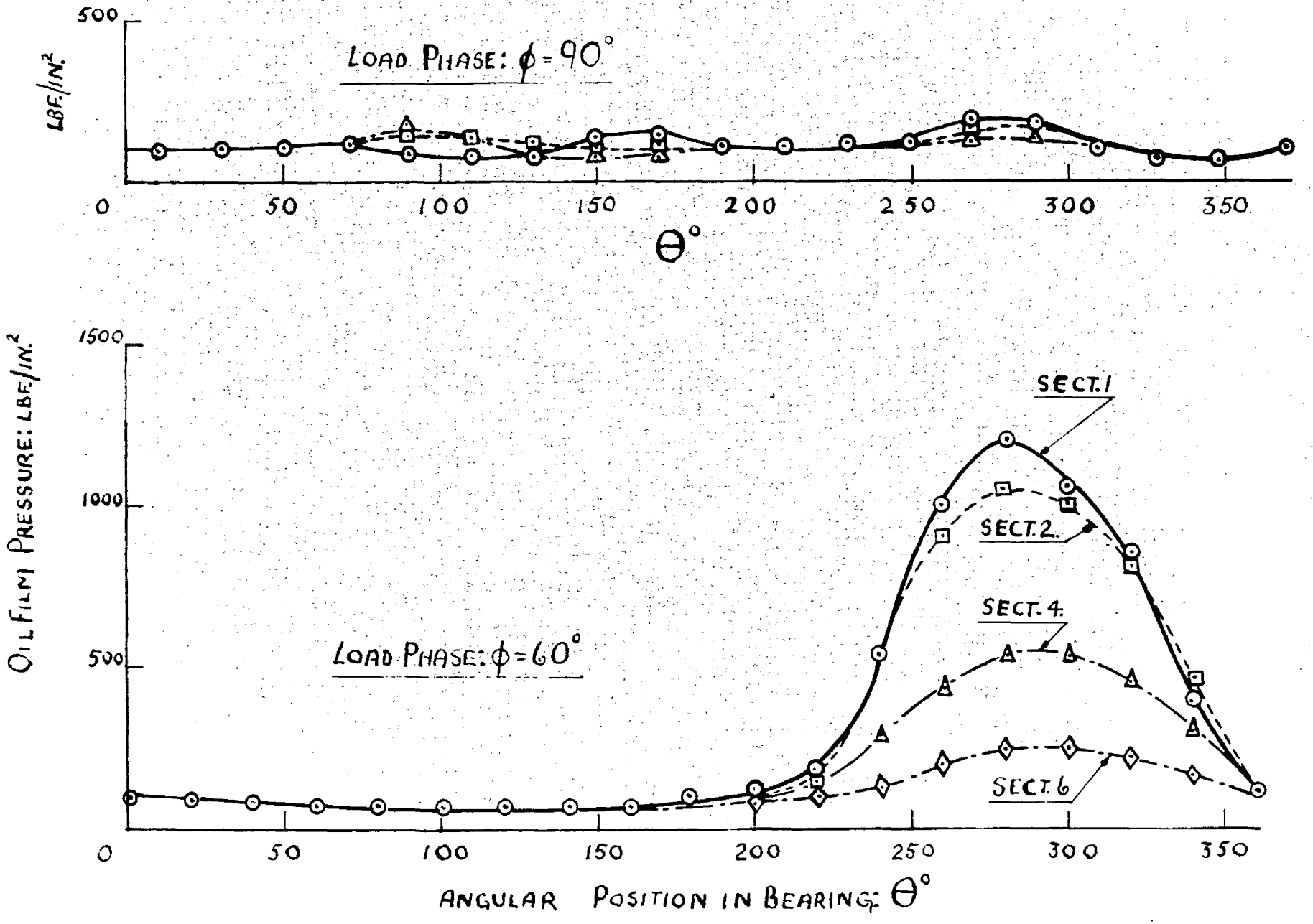
LOAD PHASE: $\phi = 90°$
LBF./IN.^{2}
500
0
50
100
150
200
250
300
350
$\theta°$
OIL FILM PRESSURE: LBF./IN.^{2}
1500
1000
500
LOAD PHASE: $\phi = 60°$
SECT. 1
SECT. 2.
SECT. 4.
SECT. 6
ANGULAR POSITION IN BEARING: $\theta°$

FIG: 4-18.

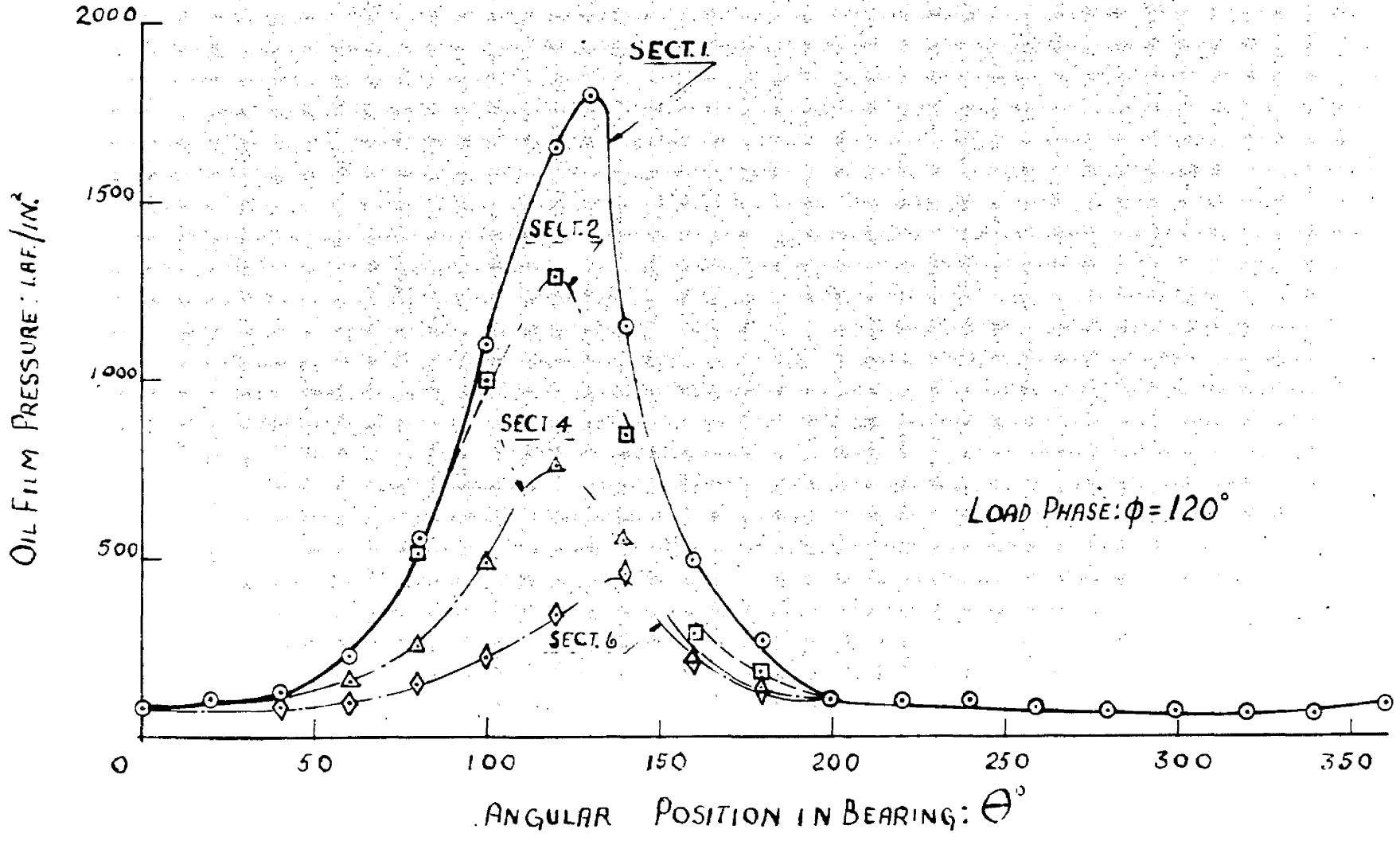
2000
1500
1000
500
0
50
100
150
200
250
300
350
SECT.1
SECT.2
SECT.4
SECT.6
OIL FILM PRESSURE: LBF./IN.²
LOAD PHASE: $\phi = 120°$
ANGULAR POSITION IN BEARING: $\theta°$

FIG: 4·19.

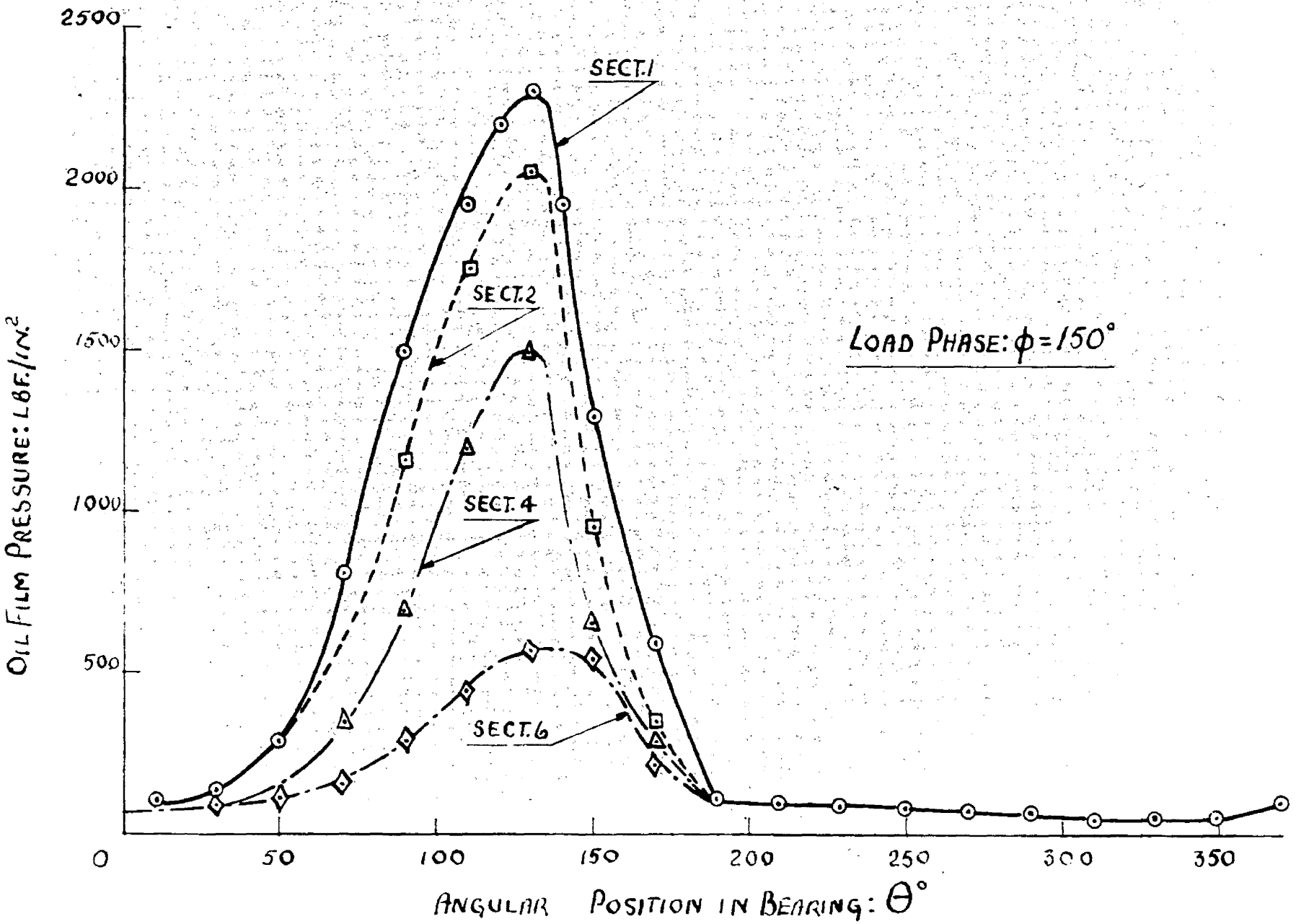
2500
2000
1500
1000
500
0
50
100
150
200
250
300
350
SECT.1
SECT.2
SECT.4
SECT.6
LOAD PHASE: $\phi = 150°$
OIL FILM PRESSURE: LBF./IN.^{2}
ANGULAR POSITION IN BEARING: $\theta°$

FIG. 4-20.

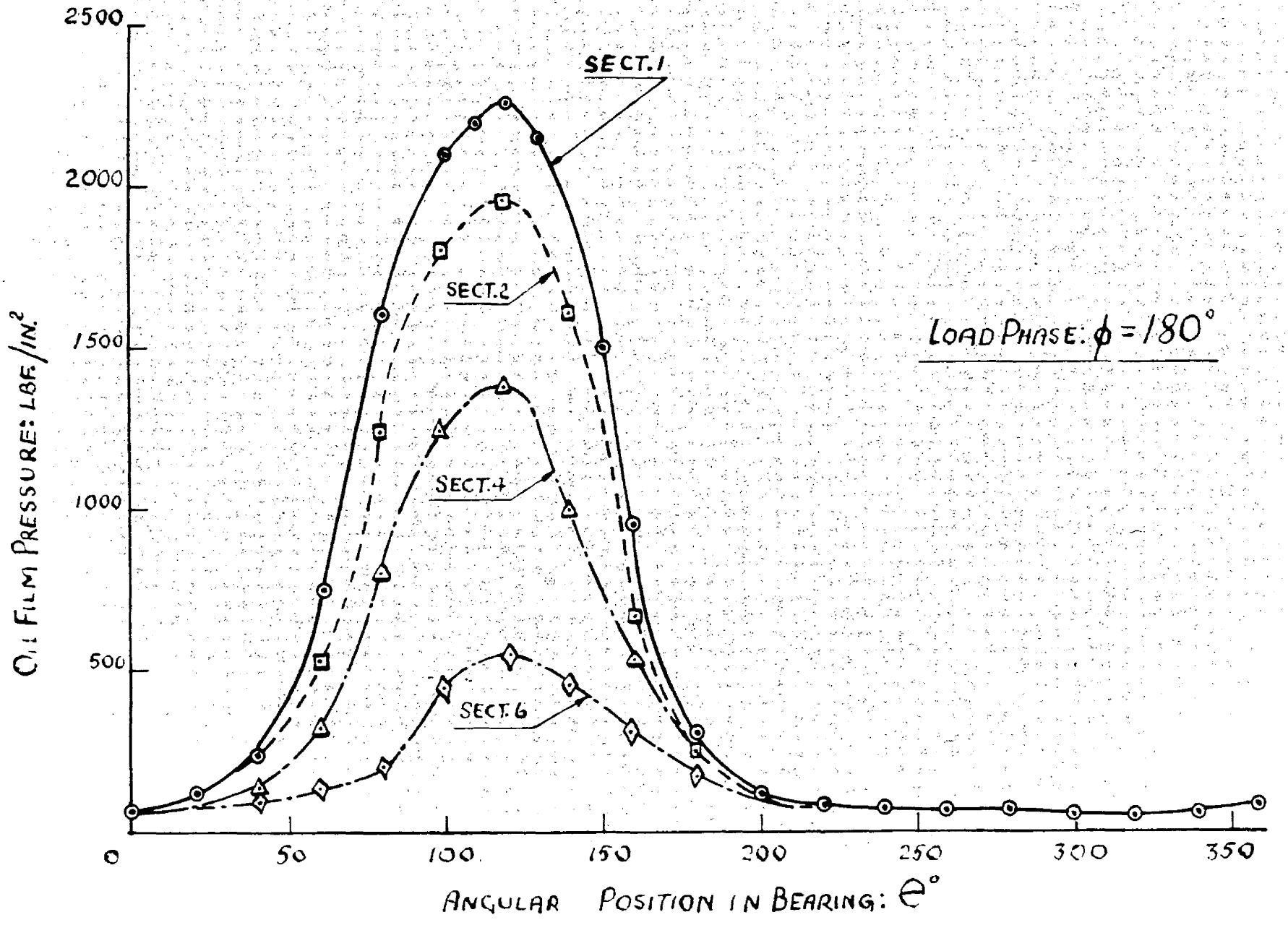
2500
2000
1500
1000
500
0
50
100
150
200
250
300
350
SECT. 1
SECT. 2
SECT. 4
SECT. 6
OIL FILM PRESSURE: LBF/IN.²
ANGULAR POSITION IN BEARING: θ°
LOAD PHASE: φ = 180°

FIG: 4-21

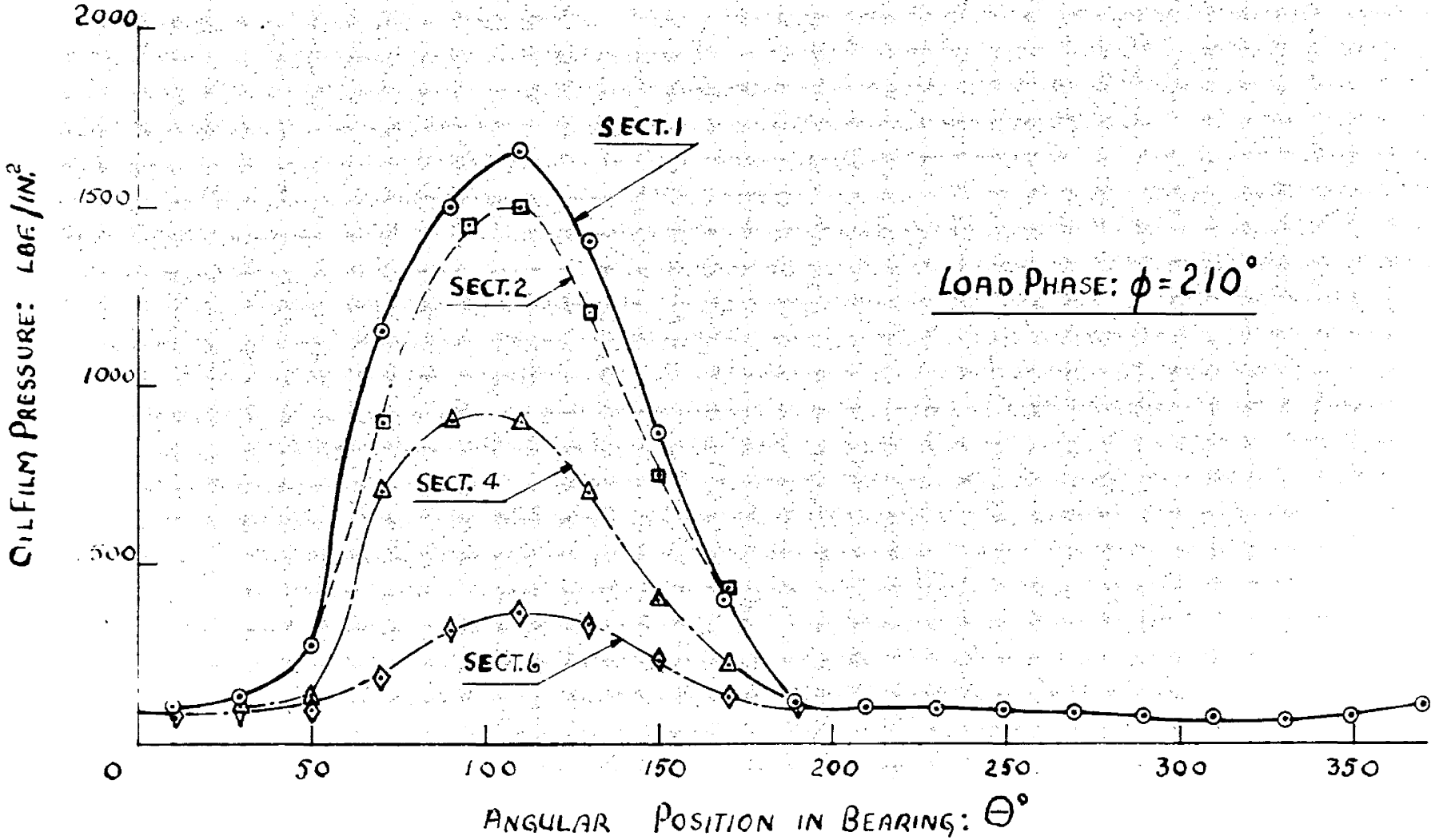
2000
1500
1000
500
0
50
100
150
200
250
300
350
SECT. 1
SECT. 2
SECT. 4
SECT. 6
LOAD PHASE: $\phi = 210°$
OIL FILM PRESSURE: LBF/IN.^{2}
ANGULAR POSITION IN BEARING: $\Theta°$

FIG: 4.22

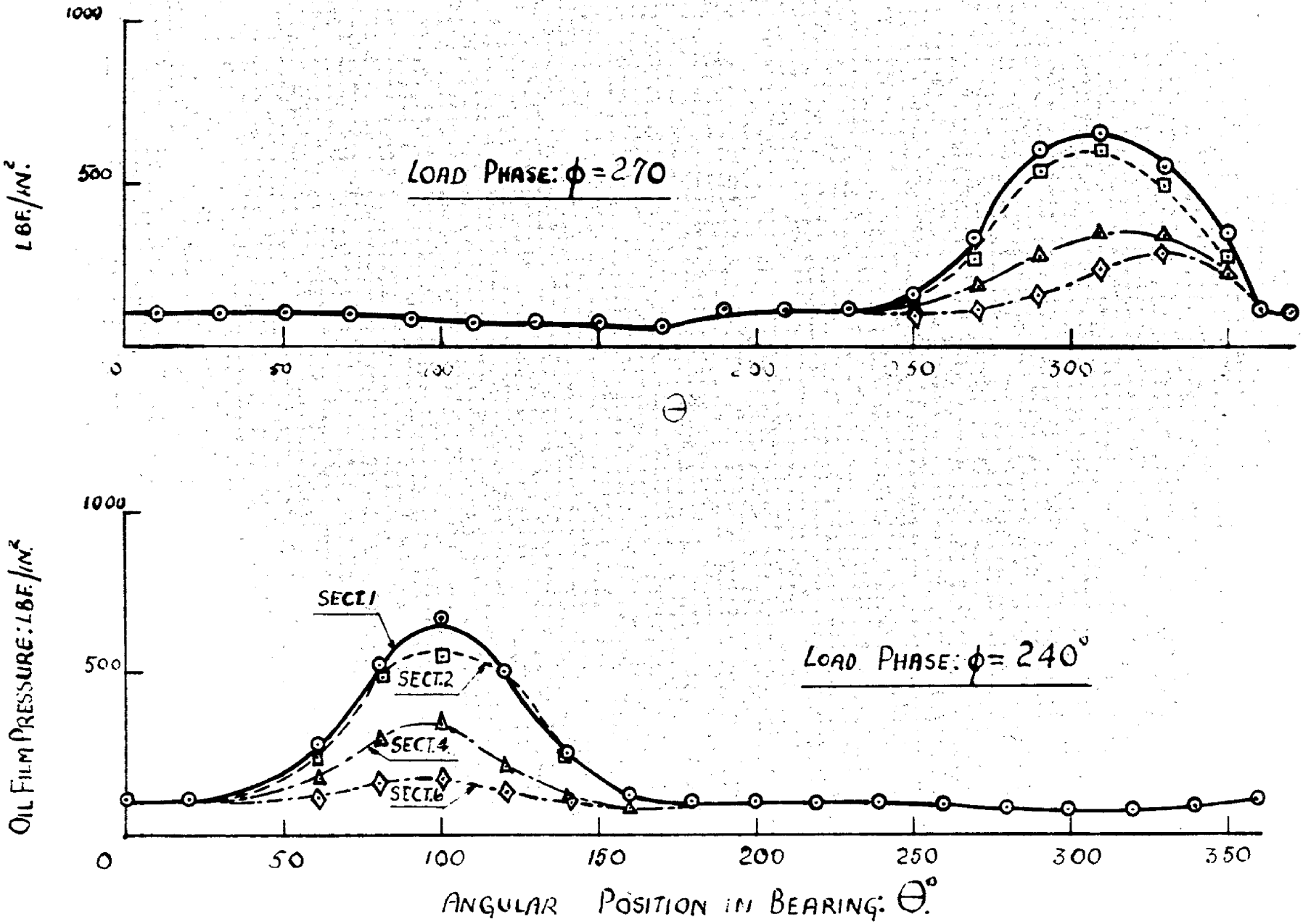
1000
500
LBF./IN.²
LOAD PHASE: ϕ = 270
0
50
100
150
200
250
300
Θ
1000
500
OIL FILM PRESSURE: LBF./IN.²
SECT.1
SECT.2
SECT.4
SECT.6
LOAD PHASE: ϕ = 240°
0
50
100
150
200
250
300
350
ANGULAR POSITION IN BEARING: Θ°

FIG: 4·23.

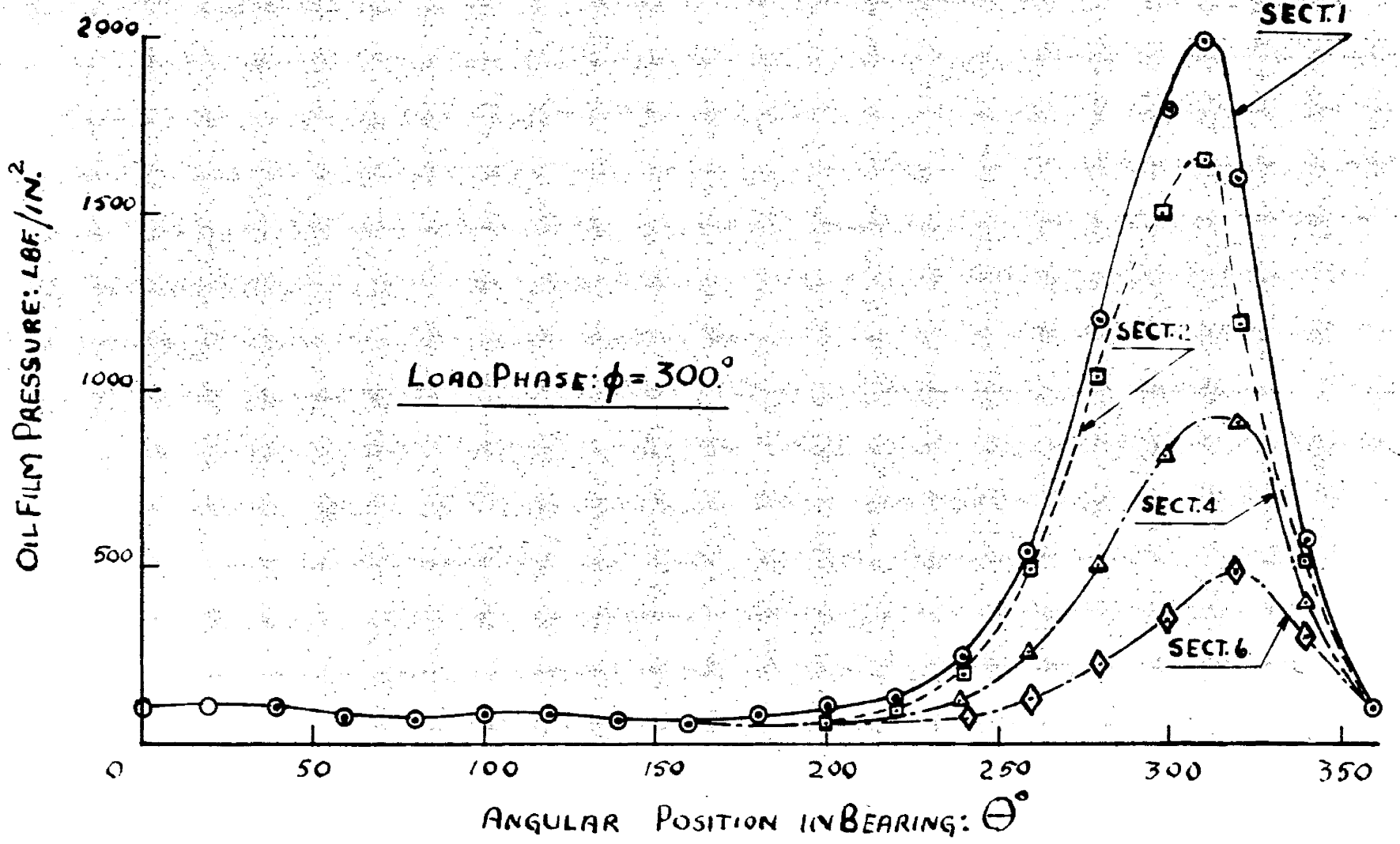
SECT.1
SECT.2
SECT.4
SECT.6
LOAD PHASE: $\phi = 300^\circ$
OIL FILM PRESSURE: LBF/IN.^{2}
2000
1500
1000
500
0
50
100
150
200
250
300
350
ANGULAR POSITION IN BEARING: θ°

FIG: 4·24

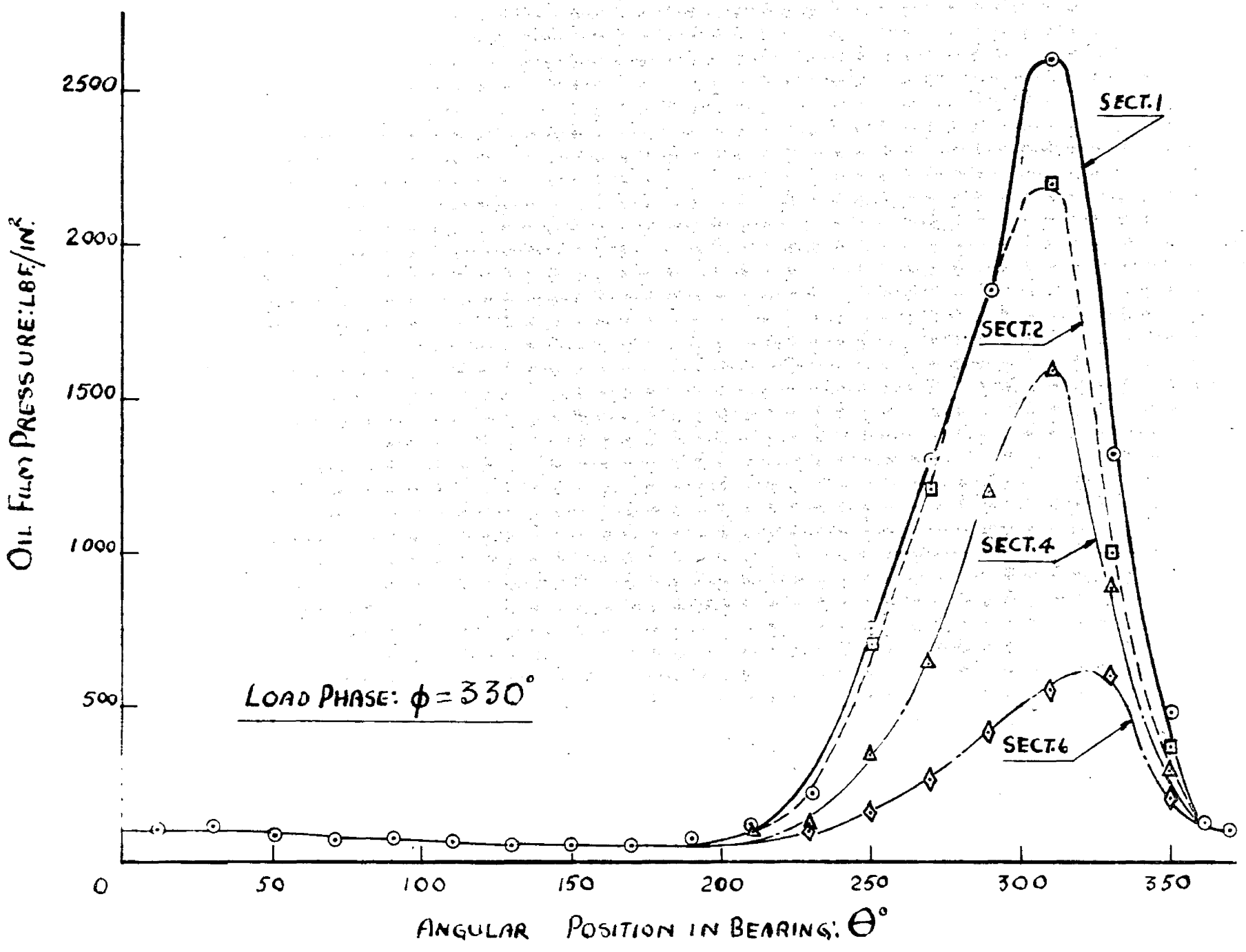
OIL FILM PRESSURE: LBF./IN.²
2500
2000
1500
1000
500
0
50
100
150
200
250
300
350
ANGULAR POSITION IN BEARING: θ°
SECT.1
SECT.2
SECT.4
SECT.6
LOAD PHASE: φ = 330°

FIG: 4.25.

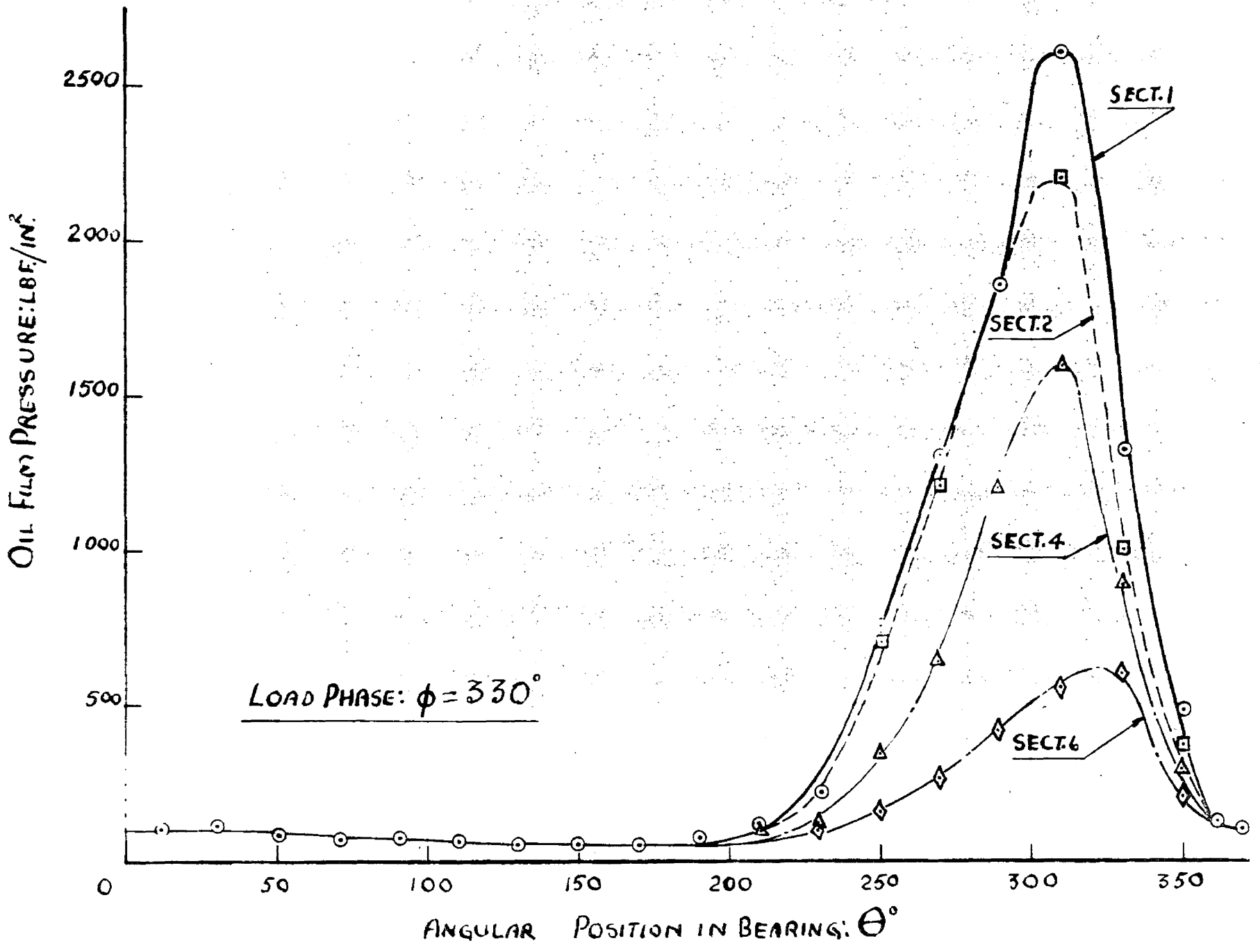
OIL FILM PRESSURE: LBF./IN.²
2500
2000
1500
1000
500
0
50
100
150
200
250
300
350
ANGULAR POSITION IN BEARING: θ°
SECT. 1
SECT. 2
SECT. 4
SECT. 6
LOAD PHASE: φ = 330°

FIG: 4.25.

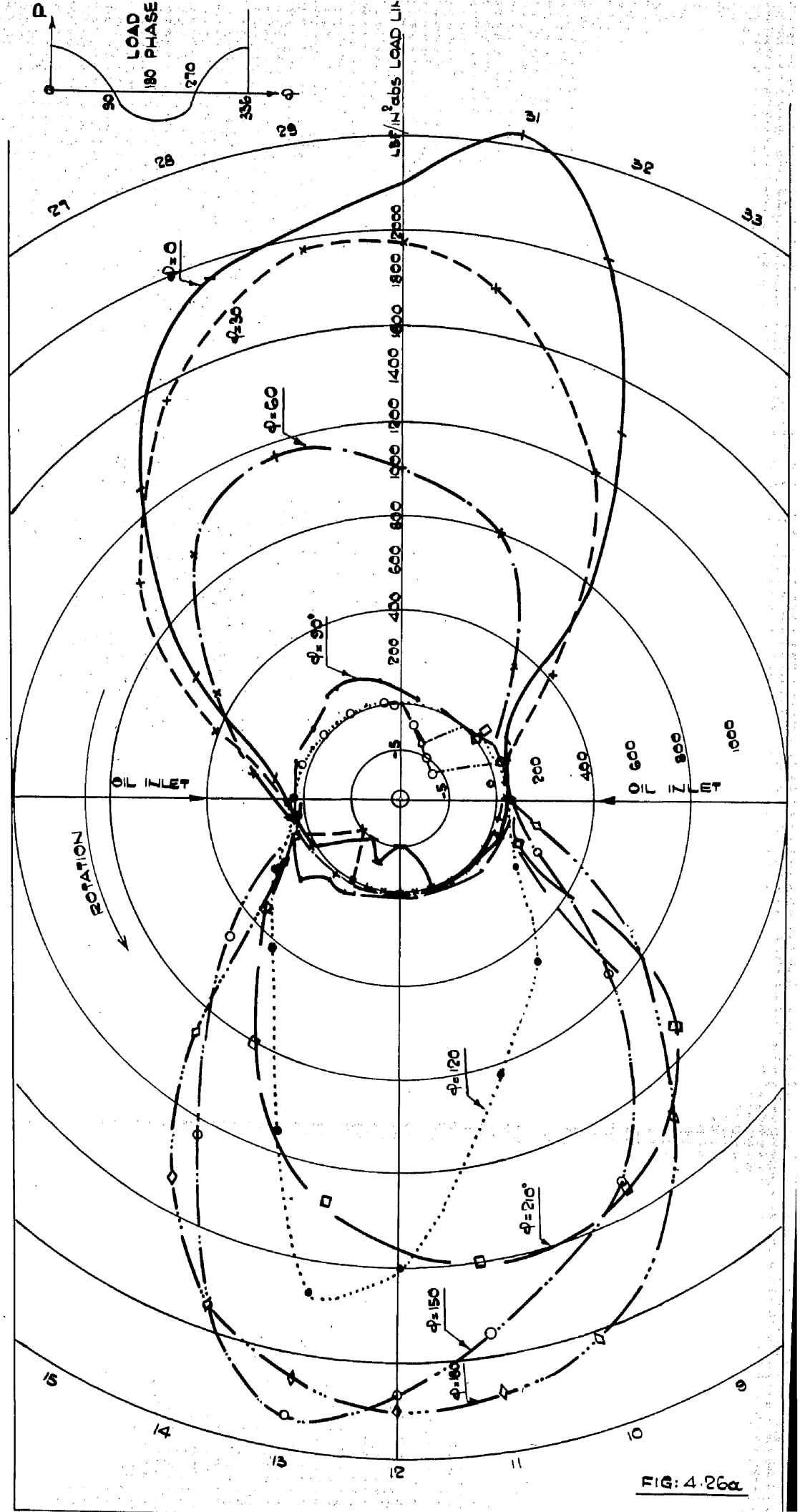
LOAD PHASE
90
180
270
336
φ
LBF/IN² abs LOAD LINE
OIL INLET
OIL INLET
ROTATION
φ=0
φ=30
φ=60
φ=90°
φ=120
φ=210°
φ=150
φ=180
200
400
600
800
1000
1200
1400
1600
1800
2000
-5
0
5
10
11
12
13
14
15
9
27
28
29
31
32
33

FIG: 4.26a

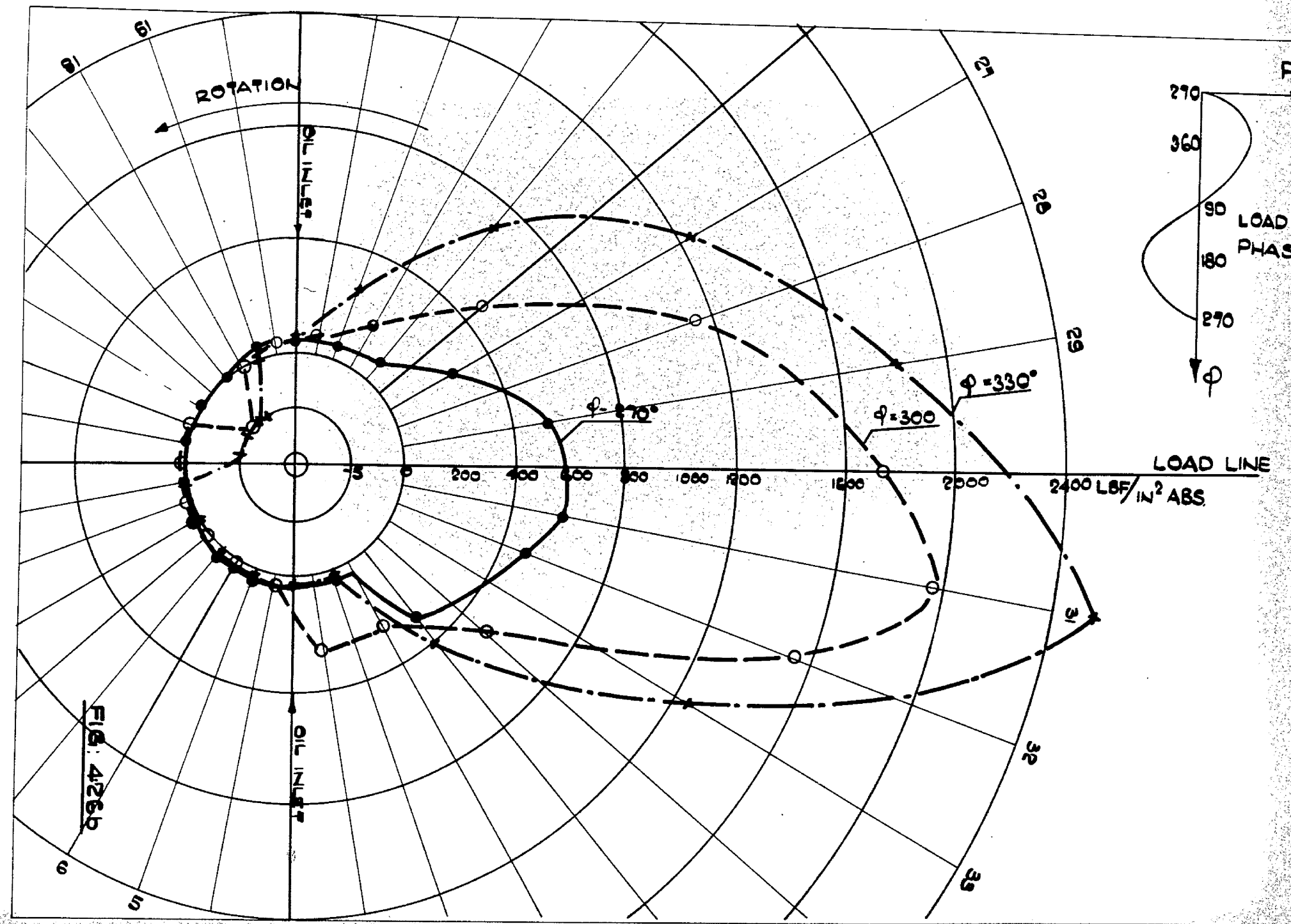
ROTATION
OIL INLET
OIL INLET
LOAD LINE
2400 LBF/IN² ABS.
φ=270°
φ=300
φ=330°
-5
0
200
400
600
800
1000
1200
1600
2000
270
360
90
180
270
φ
LOAD
PHAS
FIG. 4.26b

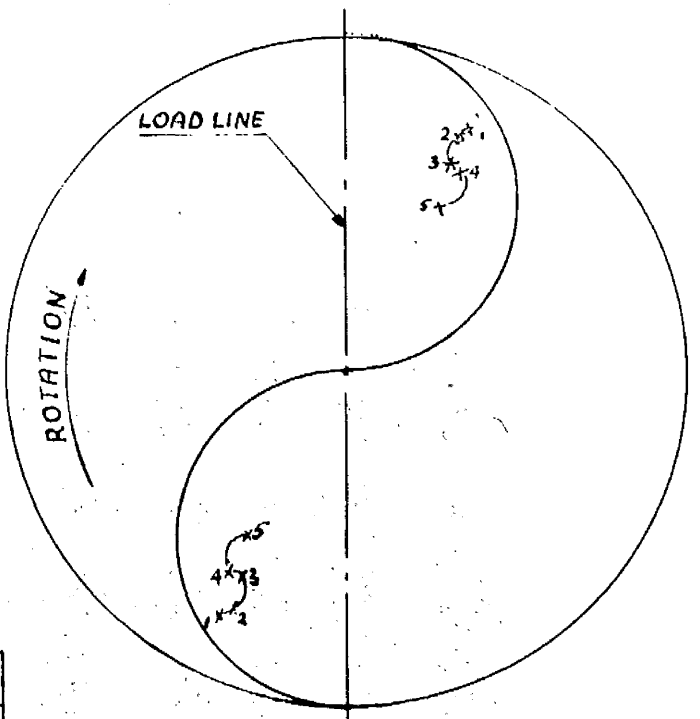

Pt.	P lbf/in²
1	1665
2	1390
3	1110
4	838
5	555

L/D = 1 N = 190 R.P.M.

FIG: 4·27

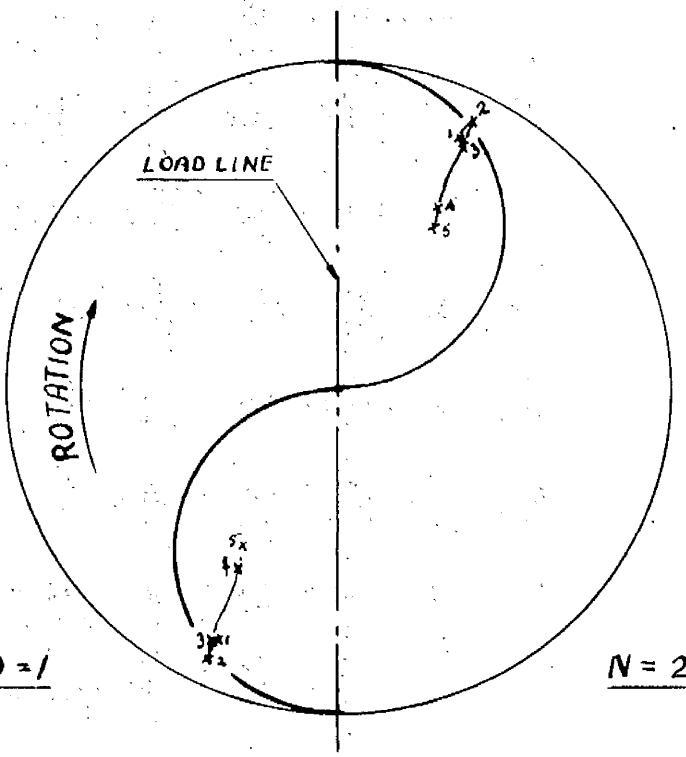

L/D = 1 N = 240 R.P.M.

FIRST TESTING MACHINE
JOURNAL CENTRE PATHS UNDER CONSTANT LOADS

DIAMETRAL CLEARANCE: ·0015 INCHES

FIG: 4·28

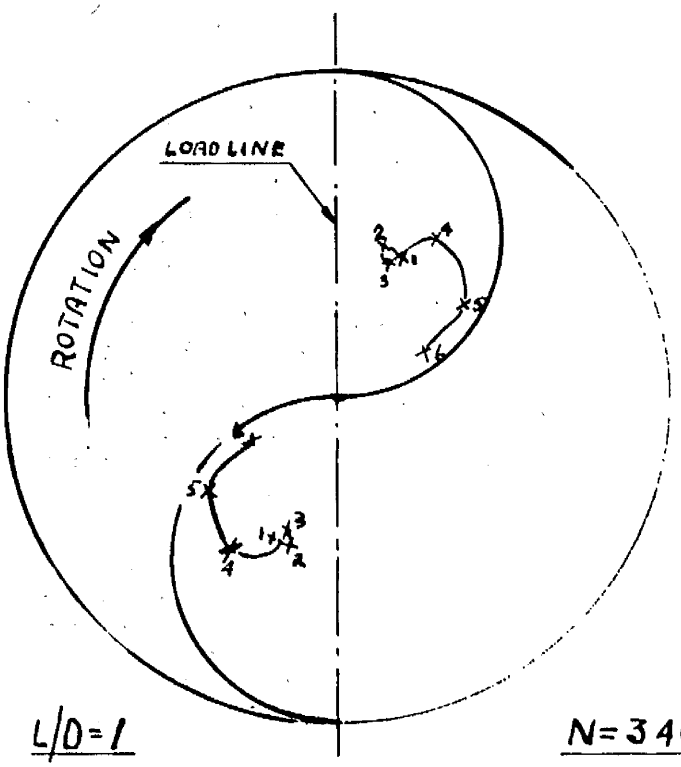

L/D = 1

N = 340 R.P.M.

A.	P_{LBF/IN^2}	Pt.	P_{LBF/IN^2}	Pt.	P_{LBF/IN^2}
1	1665	3	1110	5	555
2	1390	4	838	6	278

FIRST TESTING MACHINE

JOURNAL CENTRE PATHS UNDER CONSTANT LOADS

DIAMETRAL CLEARANCE: .003 INCHES

FIG: 4-29

FIRST TESTING MACHINE

EXPERIMENTAL RESULTS

STATIC LOADS: ·0015" DIA. CL.

EXPERIMENTAL CONDITIONS

LOAD RANGE: 555 → 1665 $^{lbs.f}/_{in^2}$

JOURNAL SPEEDS: ⊕ N = 340 RPM
+ N = 240 RPM
× N = 190 RPM

CLAYTON +JAKEMAN

LOAD RANGE: 500 → 2000 $^{lbs.f}/_{in^2}$

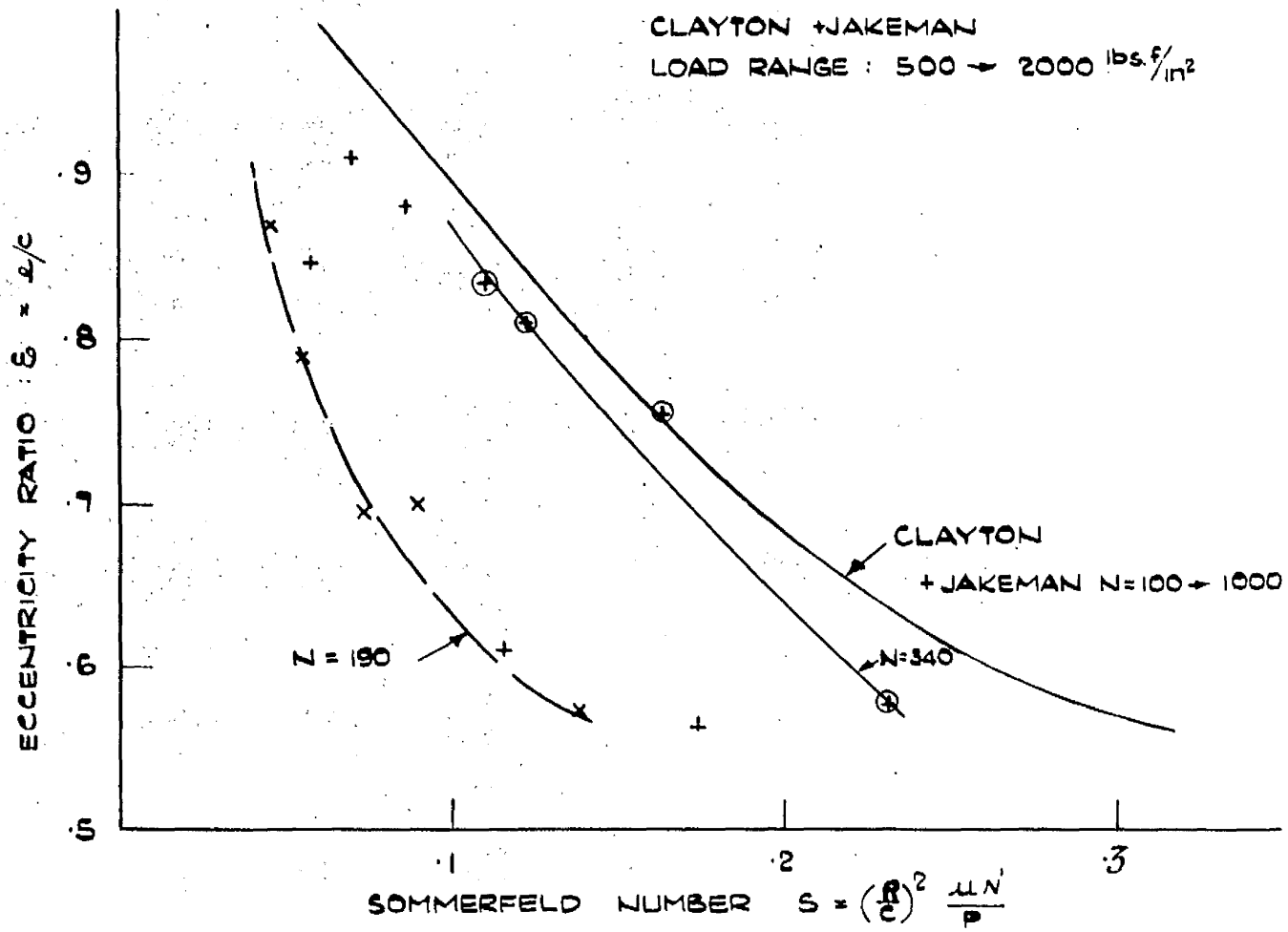

FIG 4 30

FIRST TESTING MACHINE

EXPERIMENTAL RESULTS

STATIC LOADS : ·003 INCH DIA. CL
EXPERIMENTAL : 277 - 1665 lbf/in^2
CLAYTON + JAKEMAN : 500 - 2000 $lbs.f/in^2$
DU BOIS + OCVIRK : 0 - 9000 $lbs.f/in^2$

EXPERIMENTAL JOURNAL SPEEDS:
+ : 340 RPM
× : 240 RPM
⊙ : 190 RPM
⊕ : 150 RPM

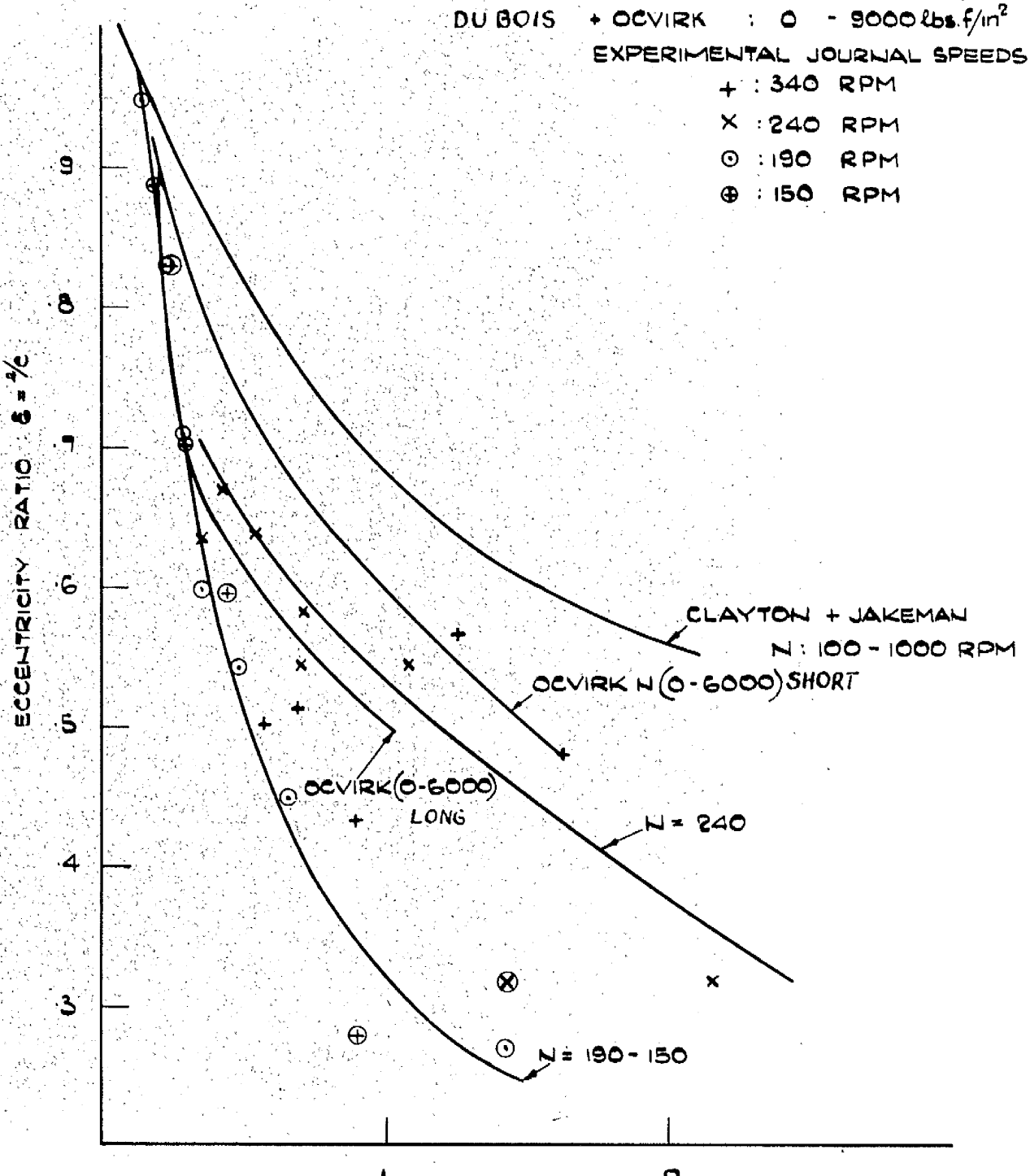

CAPACITY NUMBER $C_n = \left(\frac{R}{c}\right)^2 \frac{\mu N'}{p} \left(\frac{L}{D}\right)^2$

FIG. 4·31

SECOND TESTING MACHINE
EXPERIMENTAL RESULTS.
JOURNAL DISPLACEMENTS UNDER STATIC LOADS.
$\frac{L}{D} = \frac{2}{3}$ JOURNAL SPEED : 300 R.P.M.

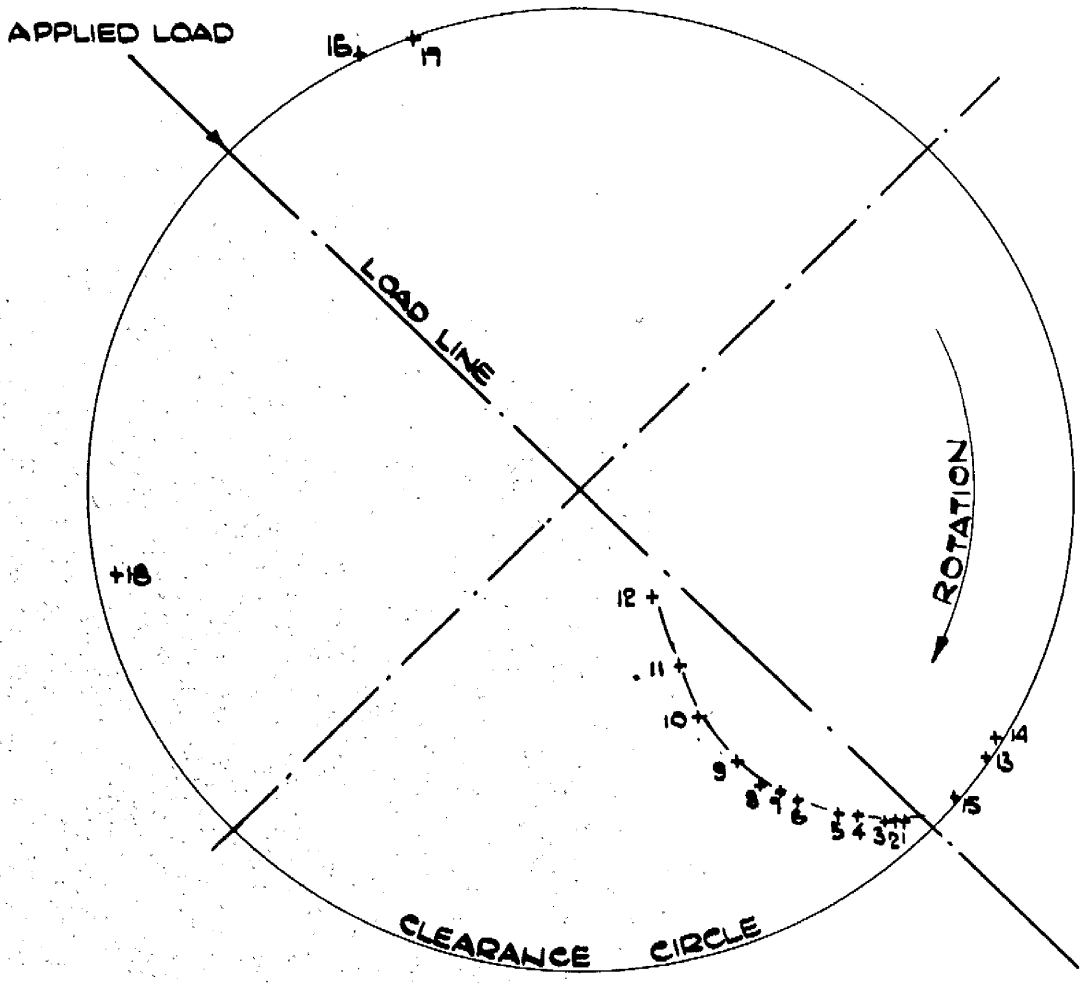

Pt No	P LBF/IN²	Pt No	P LBF/IN²	Pt No	P LBF/IN²
1	1632	5	900	9	186·5
2	1400	6	469	10	93
3	1168	7	373	11	46·7
4	933	8	280	12	0

CLEARANCE CIRCLE
DETERMINED FROM
POINTS : 13-18

FIG. : 4·32

SECOND TESTING MACHINE

EXPERIMENTAL RESULTS

JOURNAL DISPLACEMENTS UNDER STATIC LOADS.

$\frac{L}{D} = \frac{2}{3}$ JOURNAL SPEED : 950 R.P.M.

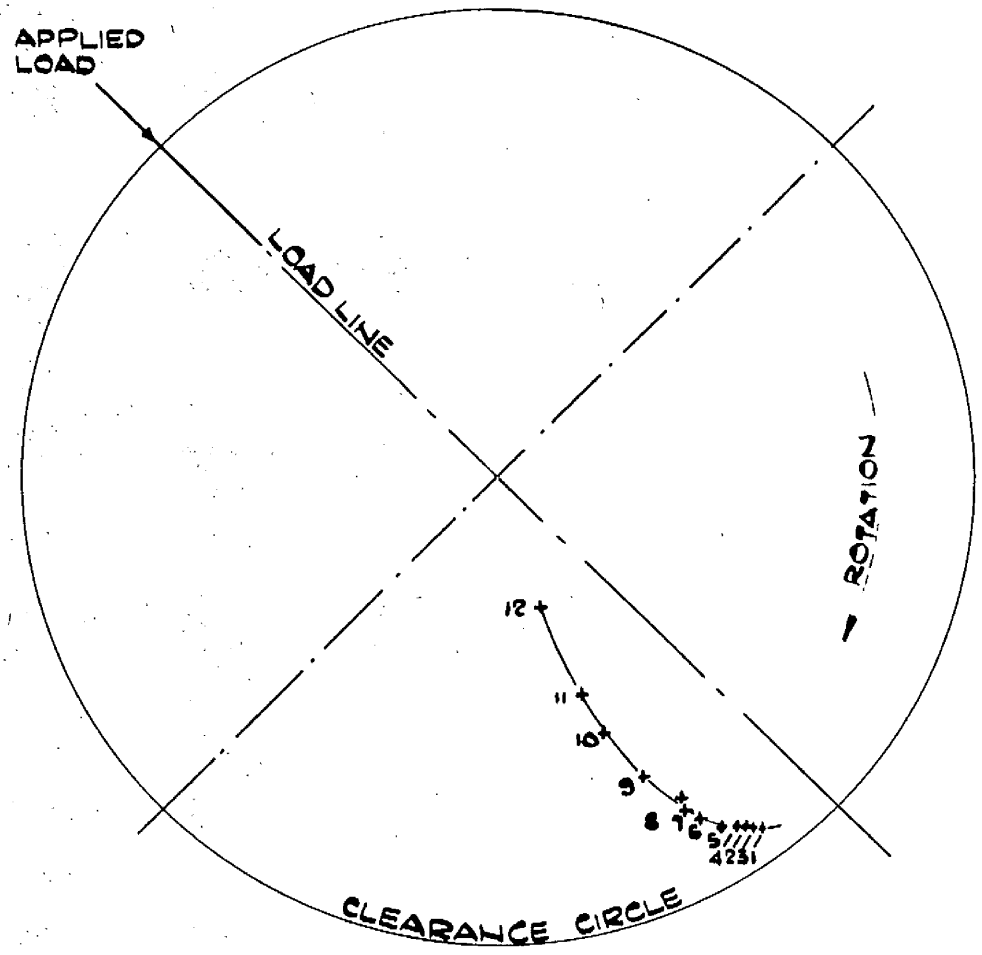

Pt No	P LBF/IN²	Pt No	P LBF/IN²	Pt No	P LBF/IN²
1	1632	5	700	9	186.5
2	1400	6	467	10	93
3	1168	7	373	11	46.7
4	933	8	280	12	0

FIG: 4.33

SECOND TESTING MACHINE

STATIC LOADS

COMPARISON OF EXPERIMENTAL RESULTS WITH EXPERIMENTAL RESULTS OF OCVIRK, DU BOIS, AND WEHE. AND CLAYTON AND JAKEMAN.

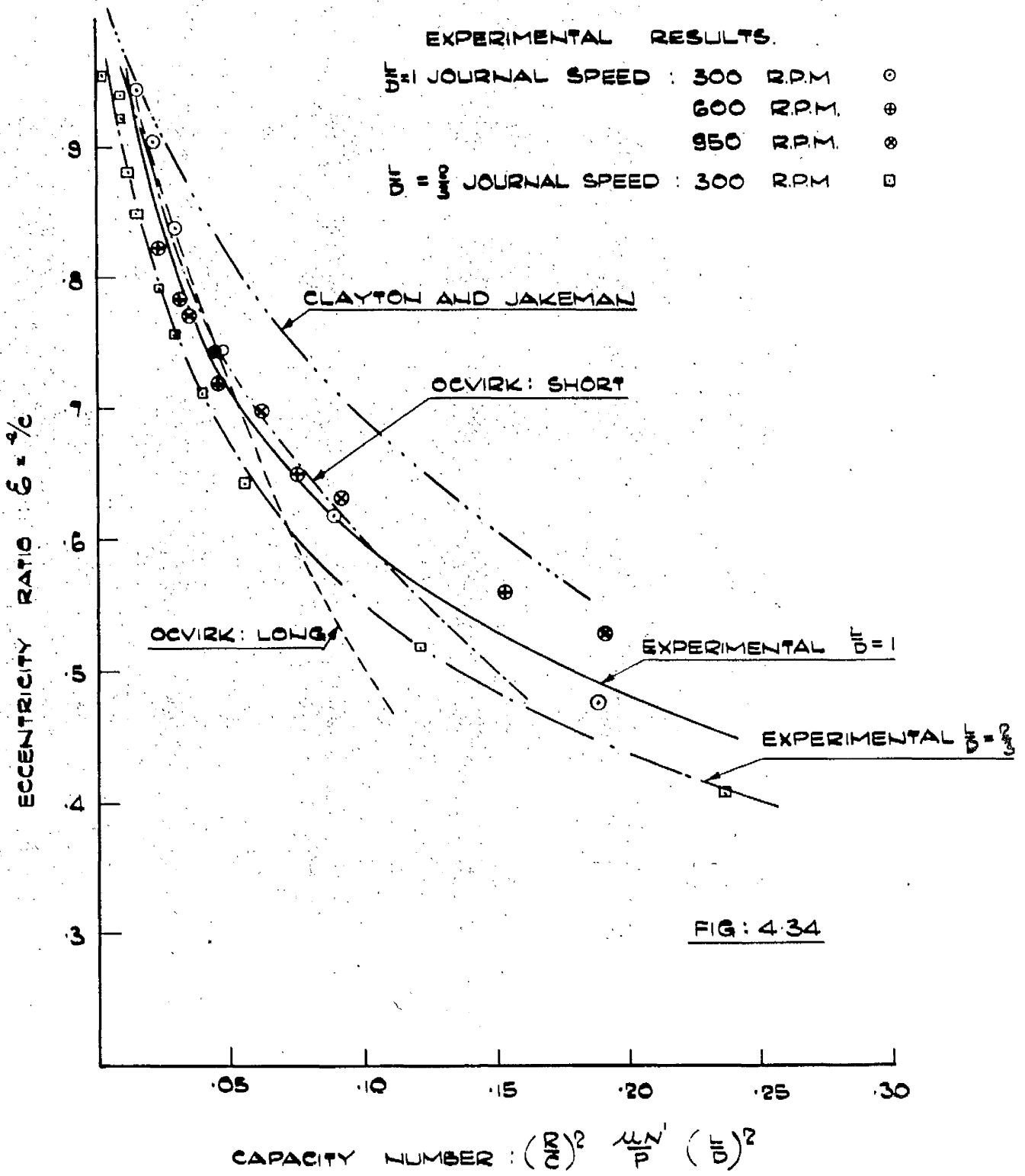

FIG: 4.34

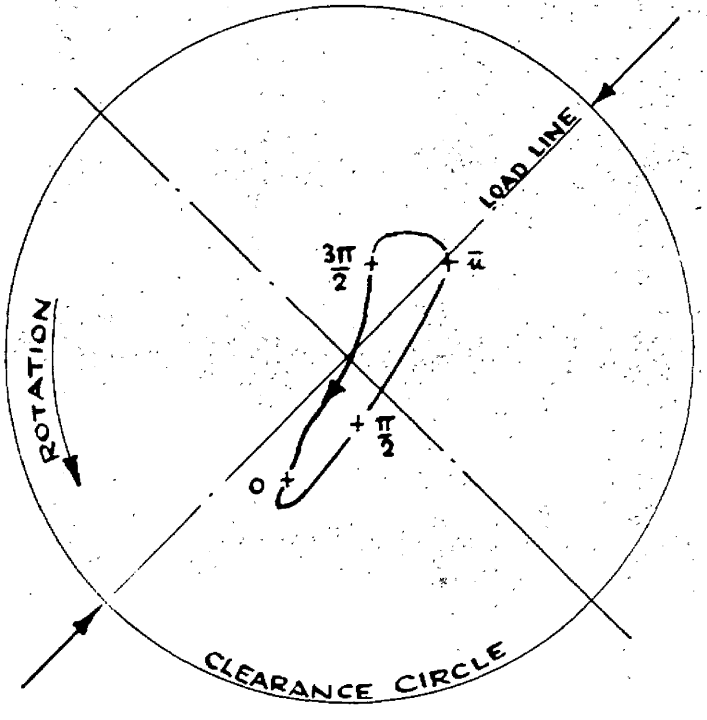

FIRST TESTING MACHINE

EXPERIMENTAL RESULTS

JOURNAL CENTRE PATH UNDER DYNAMIC LOADS

$\frac{L}{D} = 1$ DIA. CLEARANCE : ·0015 INCHES

LOAD CONDITIONS SIMILAR TO THOSE OF PRESSURE SURVEY PRESENTED ON FIG: 4·3–4·15

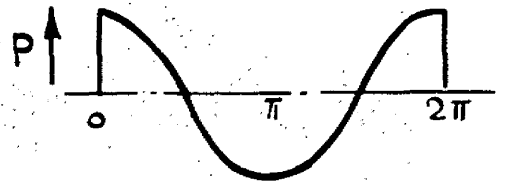

FIG: 4·35.

FIG. 4·35.

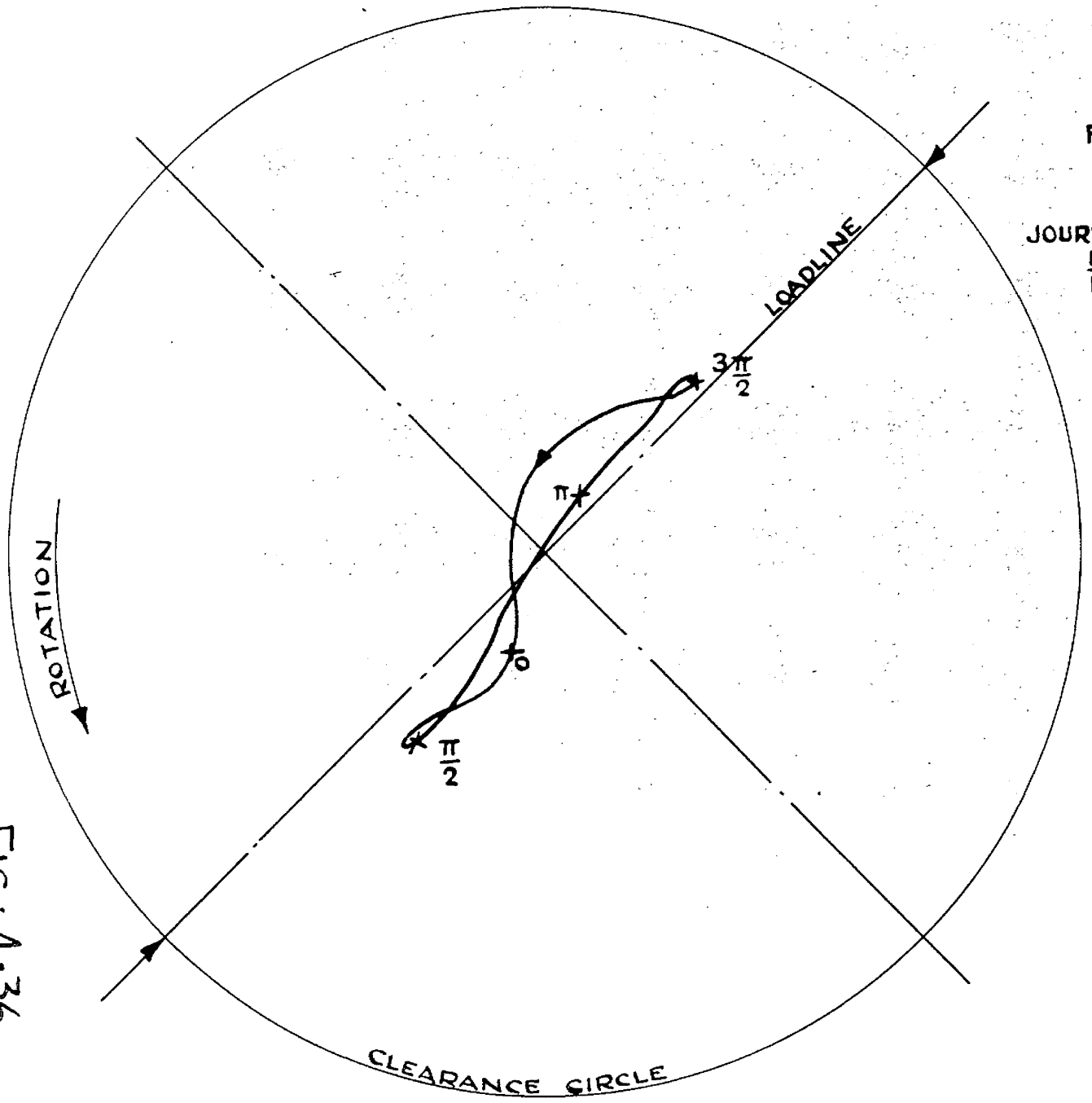

FIRST TESTING MACHINE

EXPERIMENTAL RESULTS

JOURNAL CENTRE PATH UNDER DYNAMIC LOADS.

$\frac{L}{D} = 1$ DIA. CLEARANCE : ·003 INCHES.

LOAD CONDITIONS SIMILAR TO THOSE OF PRESSURE SURVEY PRESENTED ON FIG : 4·16 - 26

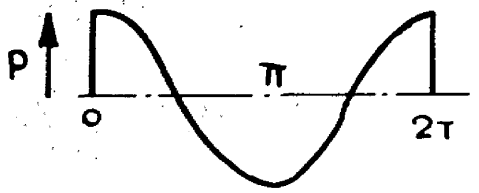

FIG : 4·36

FIG : 4·36

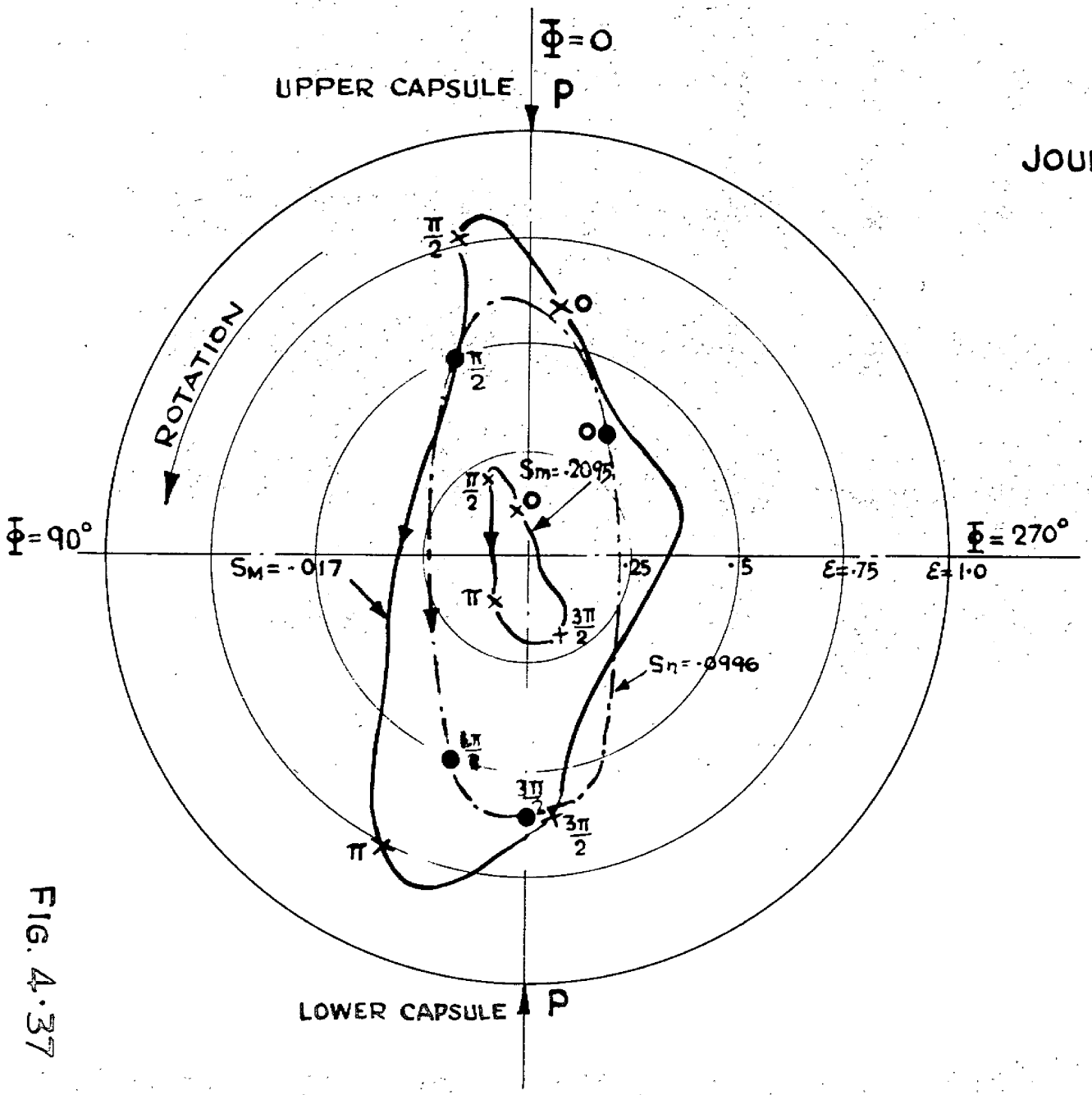

FIG. 4.37

JOURNAL CENTRE PATHS

$\frac{L}{D} = 1 \quad \sigma = 1.0$

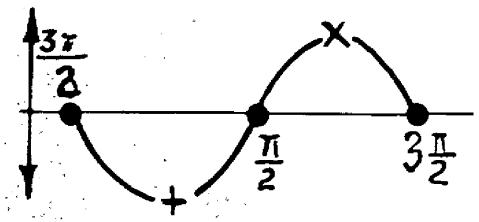

FIG : 4.37

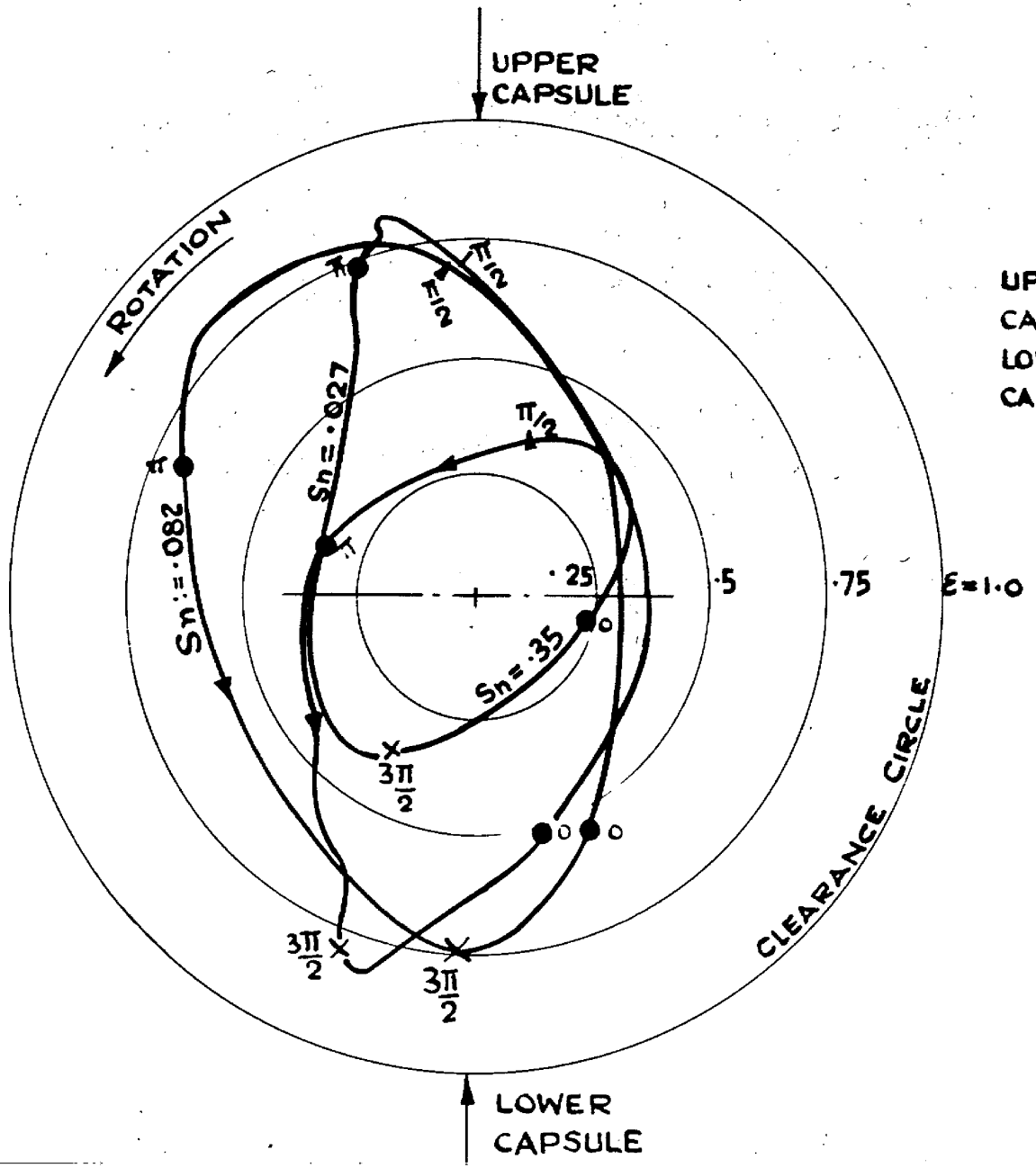

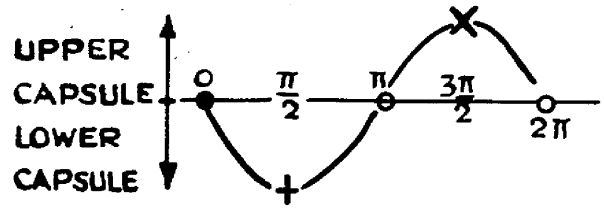

JOURNAL CENTRE PATHS
$\frac{L}{D} = 1 \quad \sigma = .5$

FIG: 4·38

FIG. 4·38

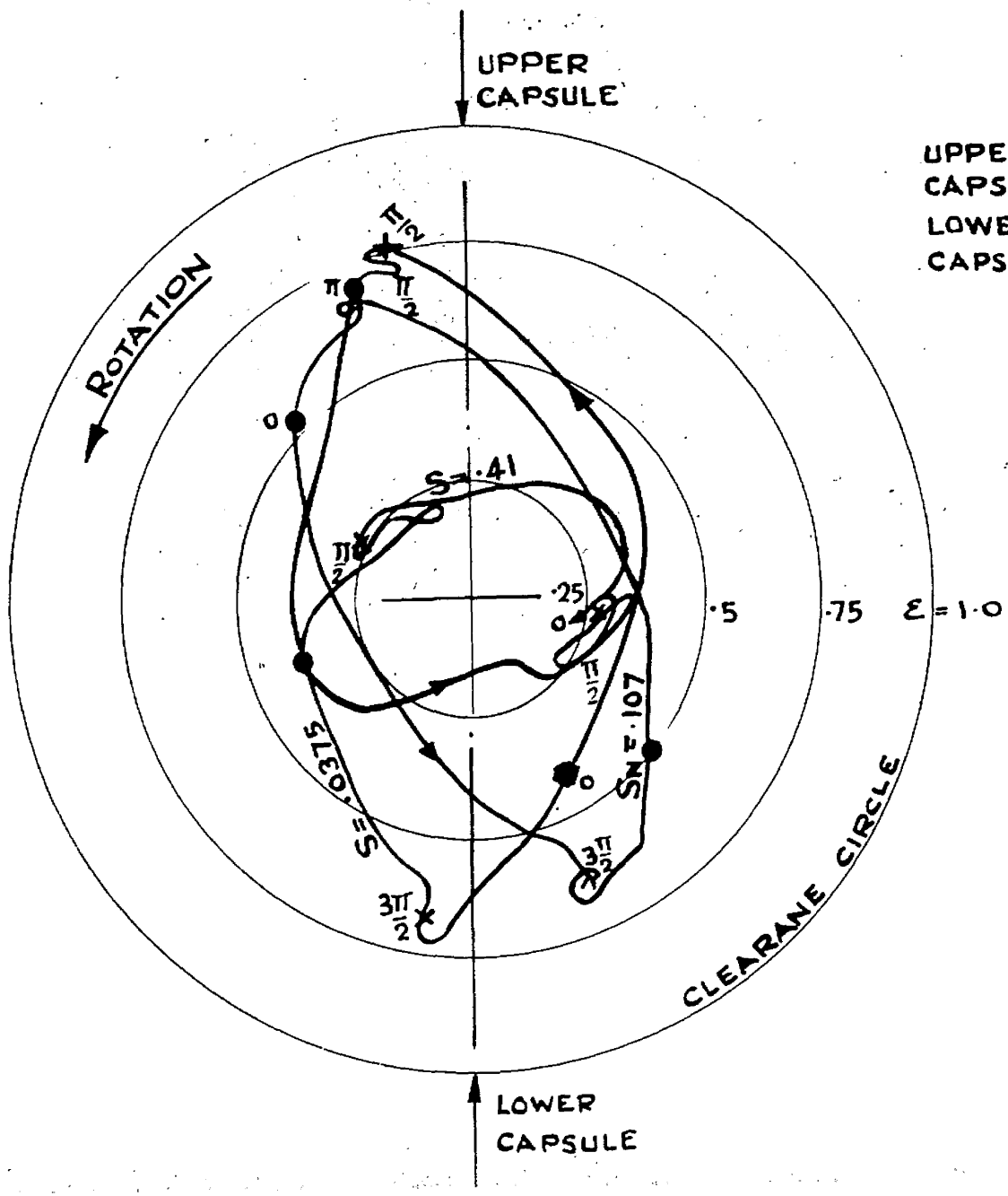

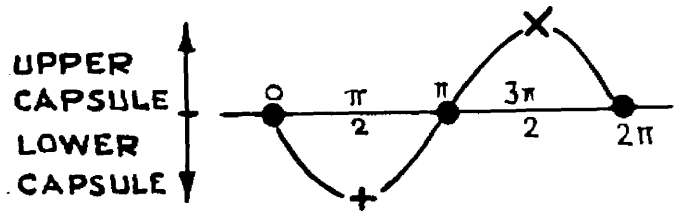

JOURNAL CENTRE PATHS

$\frac{L}{D} = 1 \quad \sigma = .33$

FIG. 4·39

FIG. 4·39

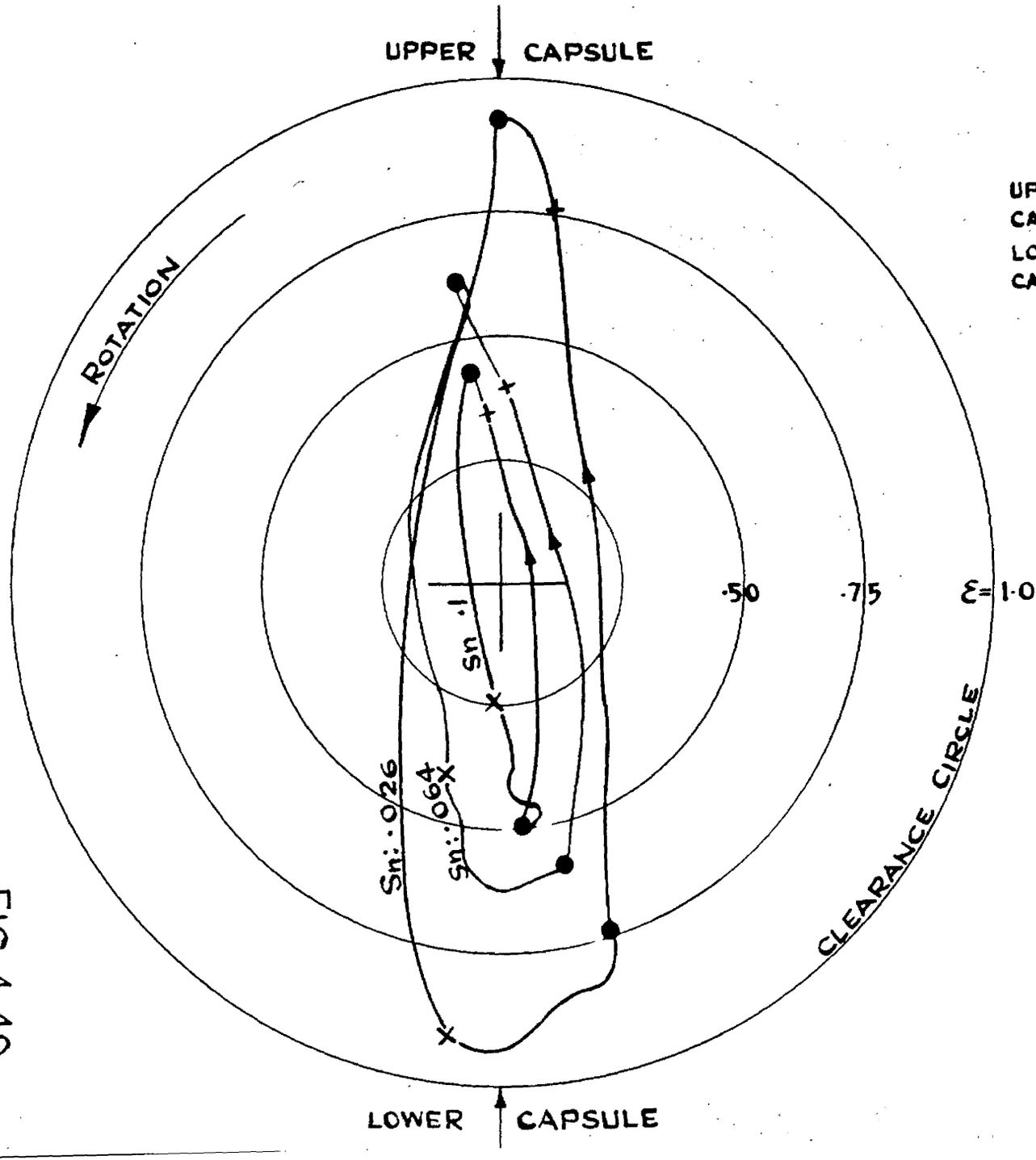

FIG. 4·40

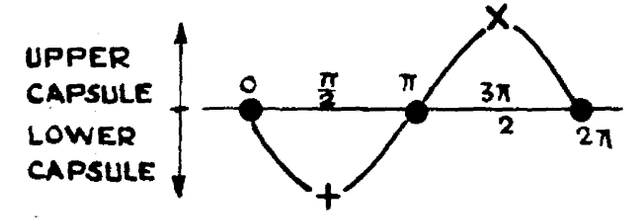

JOURNAL CENTRE PATHS

$\frac{l}{D} = \frac{1}{2}$ $\sigma = 1$

FIG:4·40

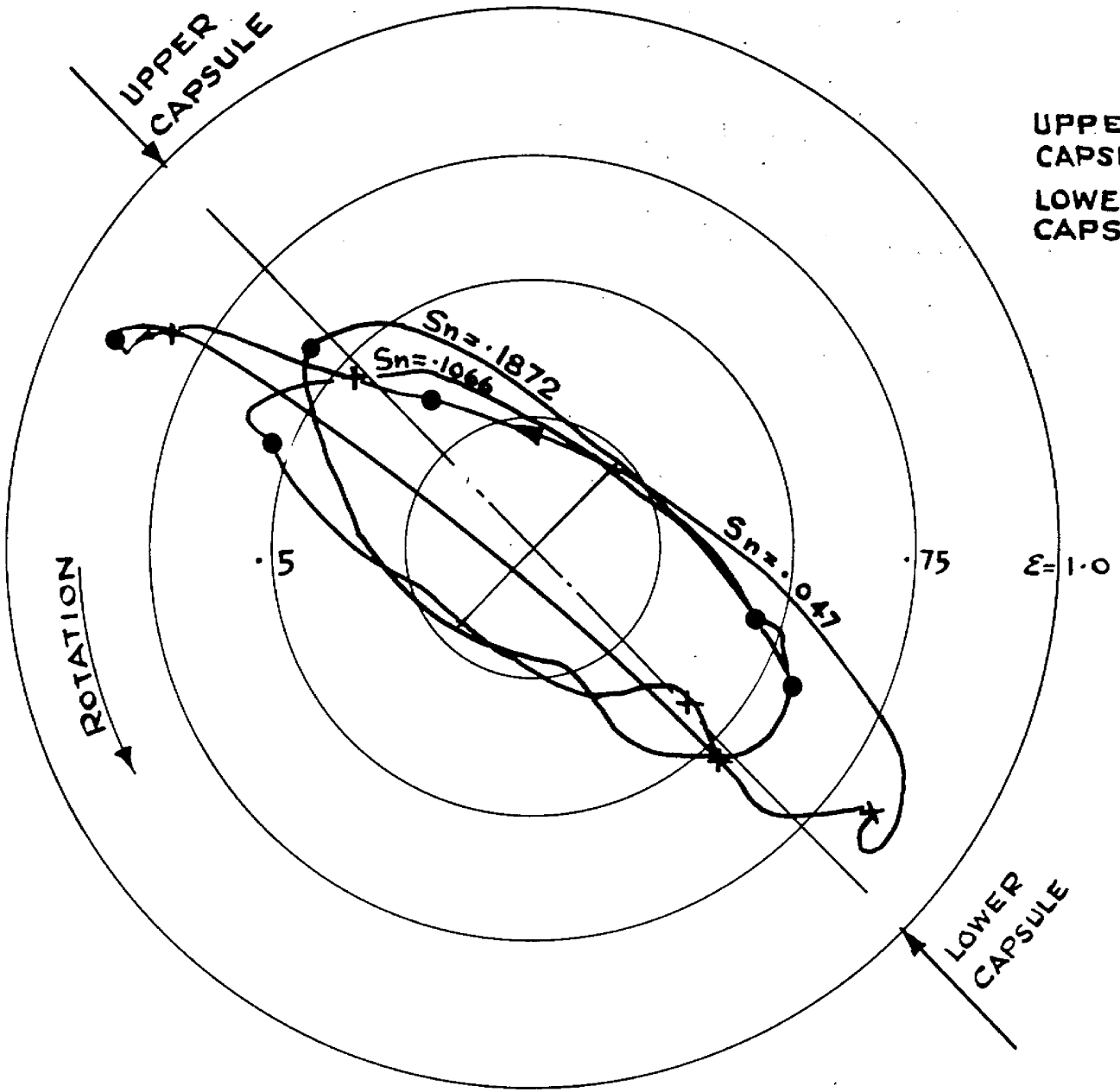

FIG. 4·41

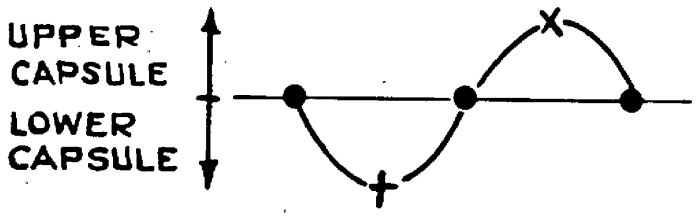

JOURNAL CENTRE PATHS

$\frac{L}{D} = \frac{1}{2}$; $\sigma = \frac{1}{2}$

FIG 4·41

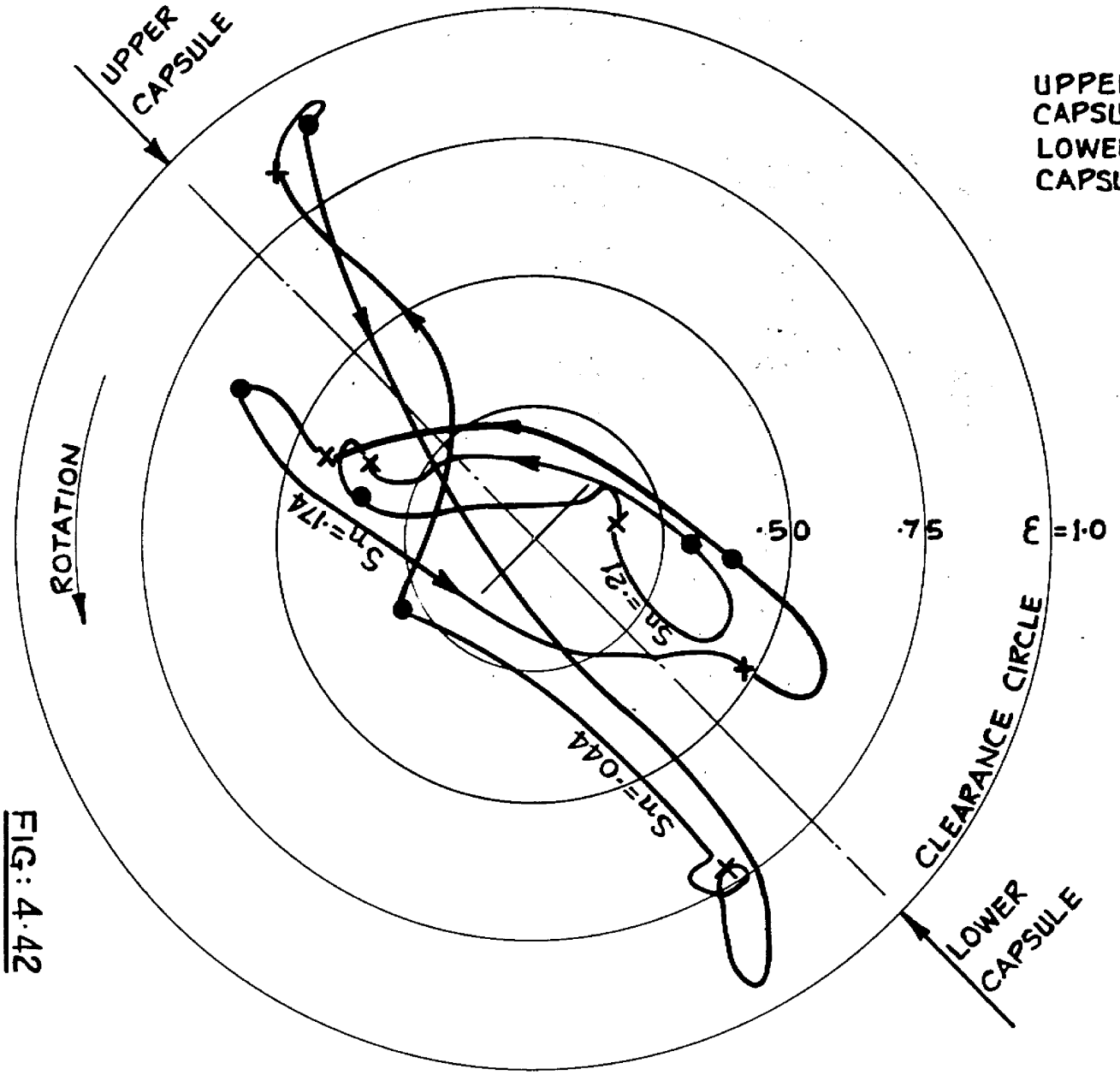

FIG: 4·42

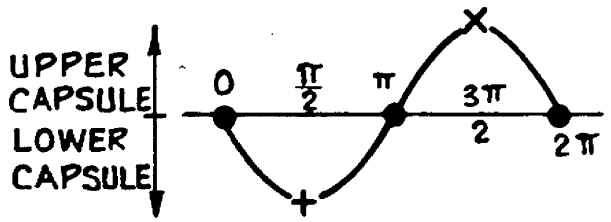

JOURNAL CENTRE PATHS

$\frac{L}{D} = \frac{1}{2}$; $\sigma = \cdot 33$

FIG: 4·42.

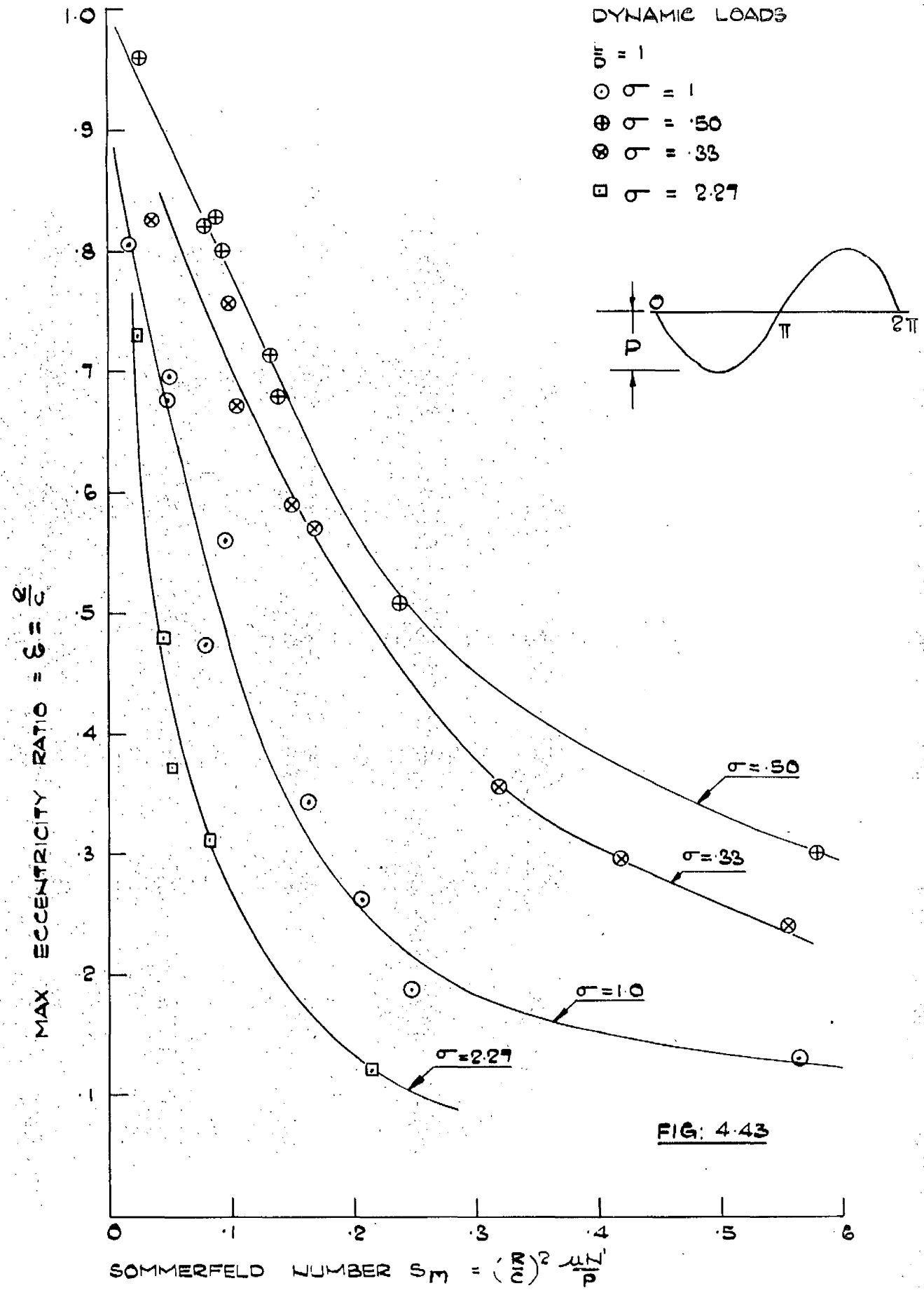
EXPERIMENTAL RESULTS
DYNAMIC LOADS
$\frac{D}{C}$ = 1
⊙ σ = 1
⊕ σ = ·50
⊗ σ = ·33
⊡ σ = 2·29
P
0
π
2π
MAX ECCENTRICITY RATIO = $\frac{e}{c}$ = ε
1·0
·9
·8
·7
·6
·5
·4
·3
·2
·1
σ=·50
σ=·33
σ=1·0
σ=2·29
0
·1
·2
·3
·4
·5
6
SOMMERFELD NUMBER $S_m = \left(\frac{R}{C}\right)^2 \frac{\mu N'}{P}$

FIG: 4·43

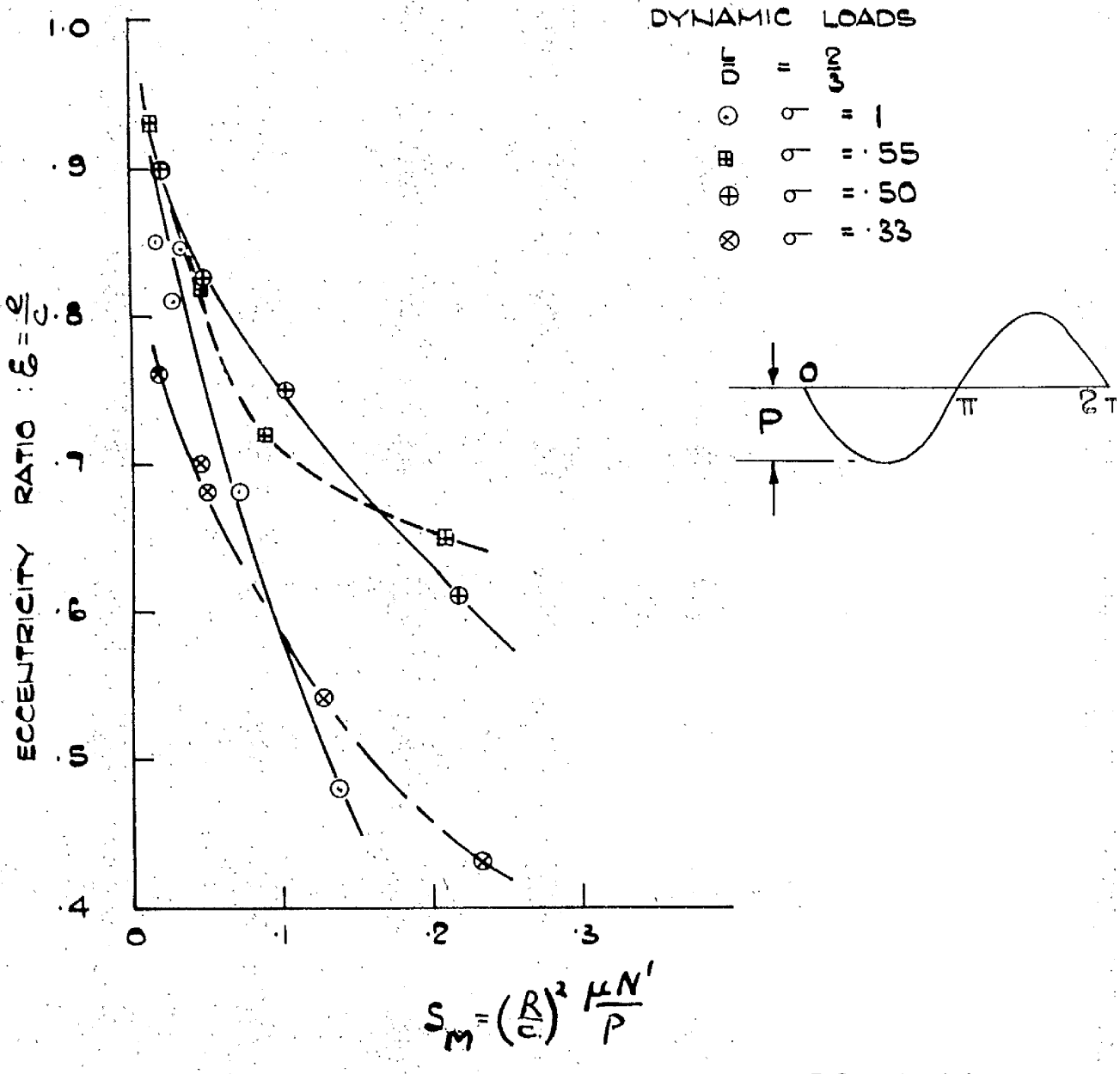
EXPERIMENTAL RESULTS
DYNAMIC LOADS
Dir = Quad
⊙ σ = 1
⊞ σ = .55
⊕ σ = .50
⊗ σ = .33
1.0
.9
.8
.7
.6
.5
.4
ECCENTRICITY RATIO : ε = e/c
0
.1
.2
.3
$S_M = \left(\frac{R}{c}\right)^2 \frac{\mu N'}{P}$
O
P
π
2π T

FIG. 4·44

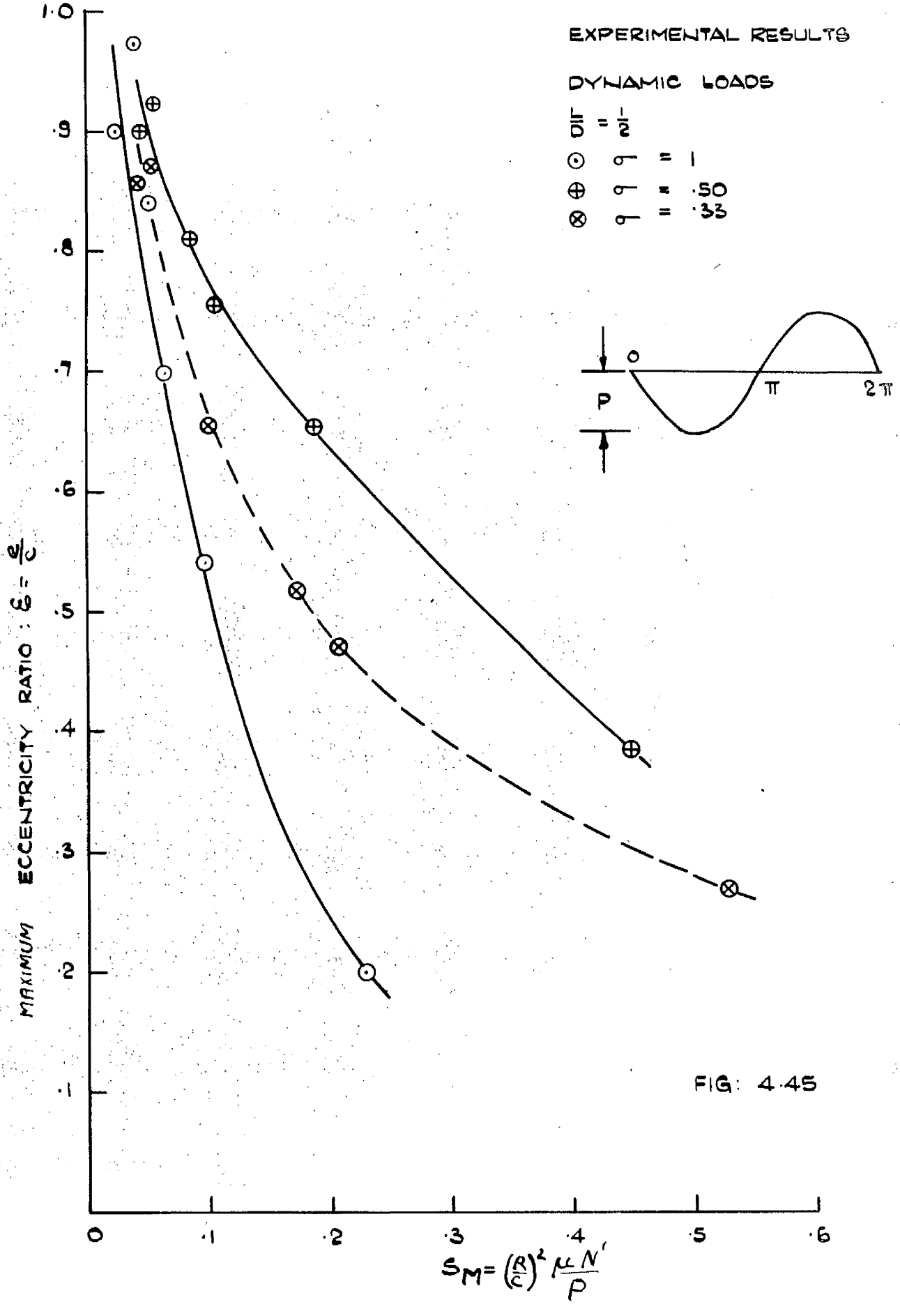
EXPERIMENTAL RESULTS
DYNAMIC LOADS
D/r = 1/2
⊙ q = 1
⊕ q = .50
⊗ q = .33
0
π
2π
P
1.0
.9
.8
.7
.6
.5
.4
.3
.2
.1
MAXIMUM ECCENTRICITY RATIO : ε = e/c
0
.1
.2
.3
.4
.5
.6
$S_M = \left(\frac{R}{c}\right)^2 \frac{\mu N'}{P}$

FIG: 4.45

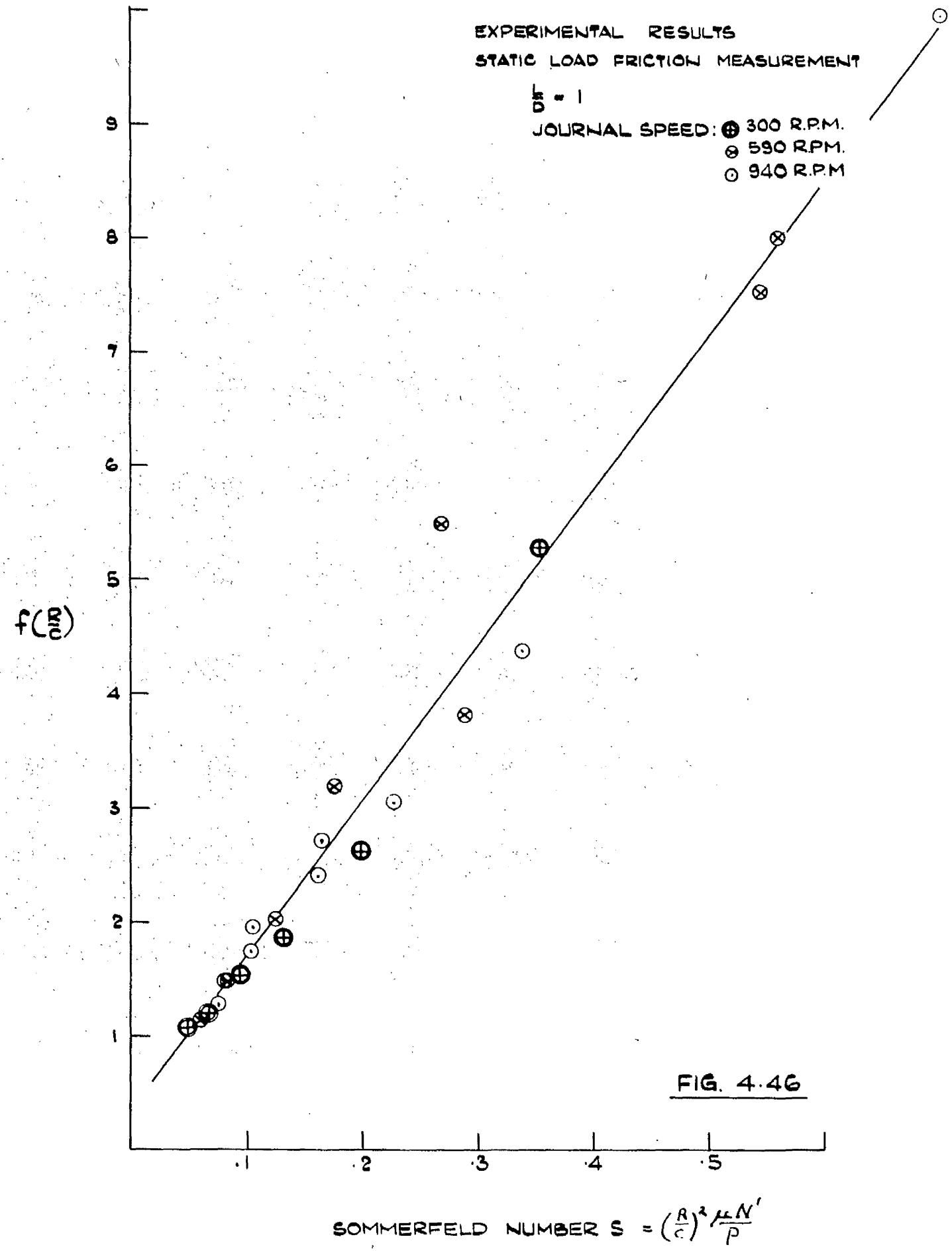
EXPERIMENTAL RESULTS
STATIC LOAD FRICTION MEASUREMENT
L/D = 1
JOURNAL SPEED: 300 R.P.M.
590 R.P.M.
940 R.P.M
f(R/C)
1
2
3
4
5
6
7
8
9
.1
.2
.3
.4
.5
SOMMERFELD NUMBER S = (R/C)² μN'/P

FIG. 4.46

EXPERIMENTAL RESULTS.
BEARING FRICTION UNDER STATIC LOADS
COMPARISON WITH THEORETICAL PREDICTIONS
OF SASSENFELD AND WALTHER FOR $\frac{d/r}{D} = \frac{1}{2}$

⊙: EXPERIMENTAL POINTS FOR $\frac{d/r}{D} = \frac{1}{2}$
JOURNAL SPEED 300 R.P.M.

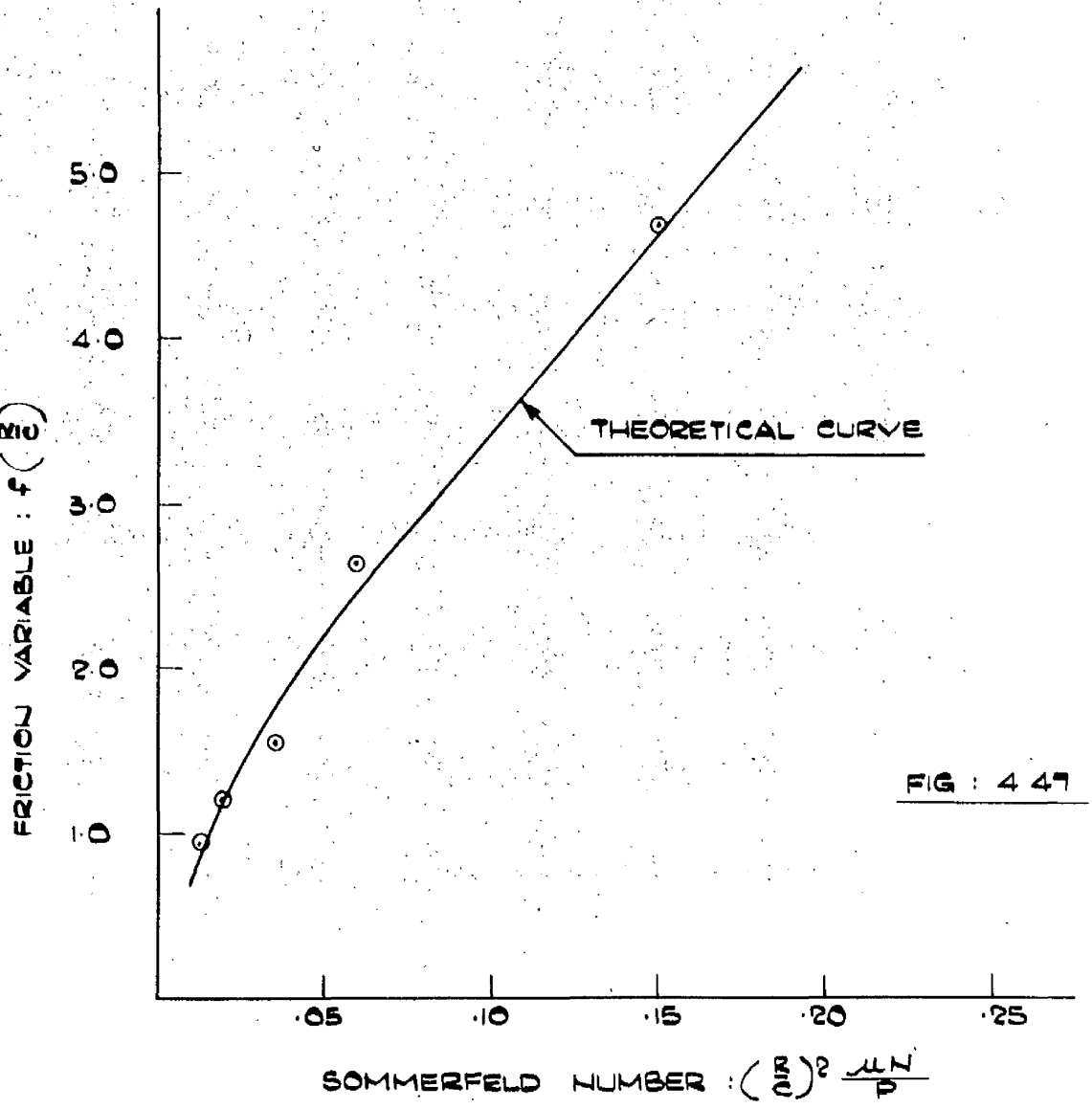

FIG : 4 47

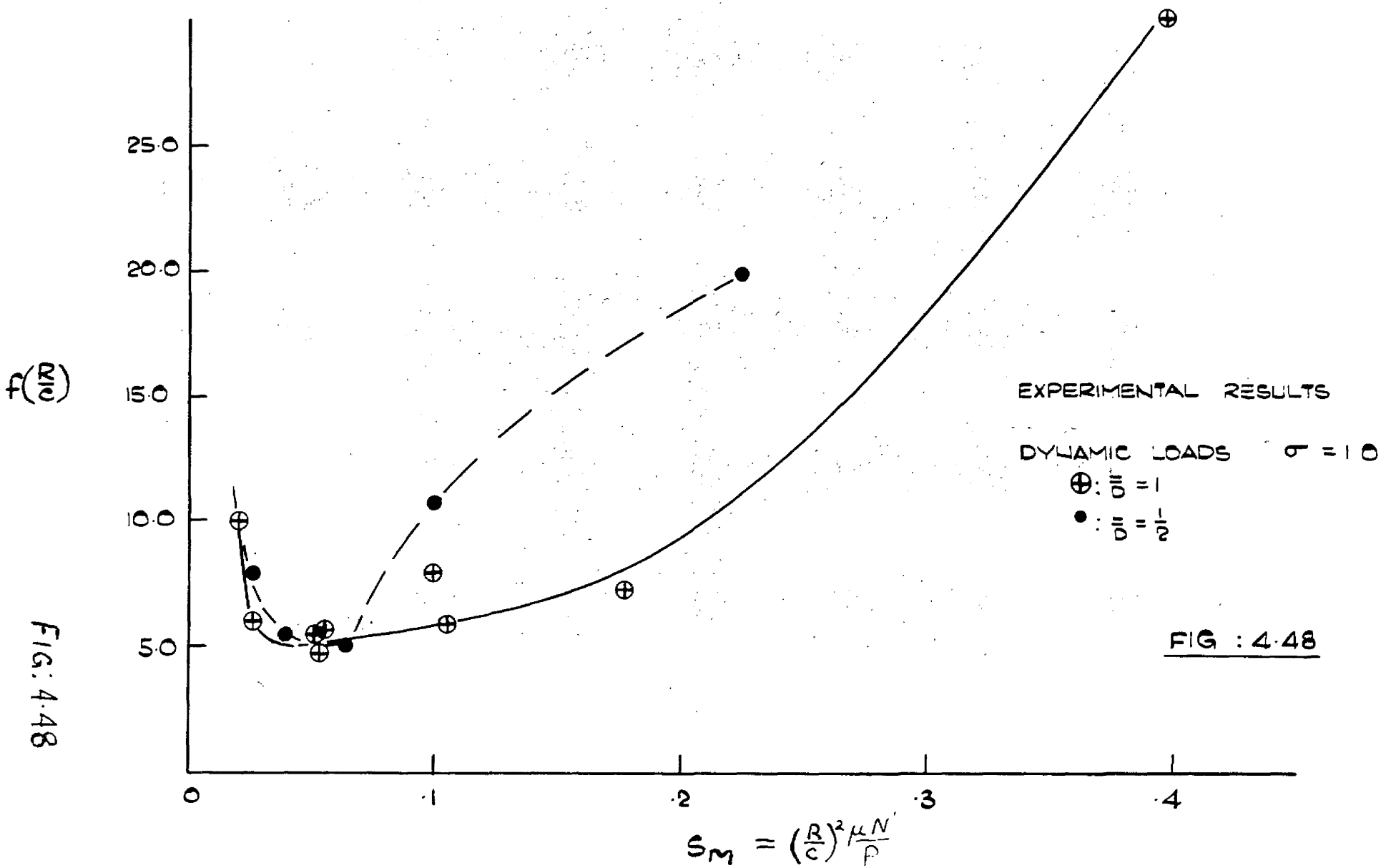

FIG : 4·48

FIG: 4·48

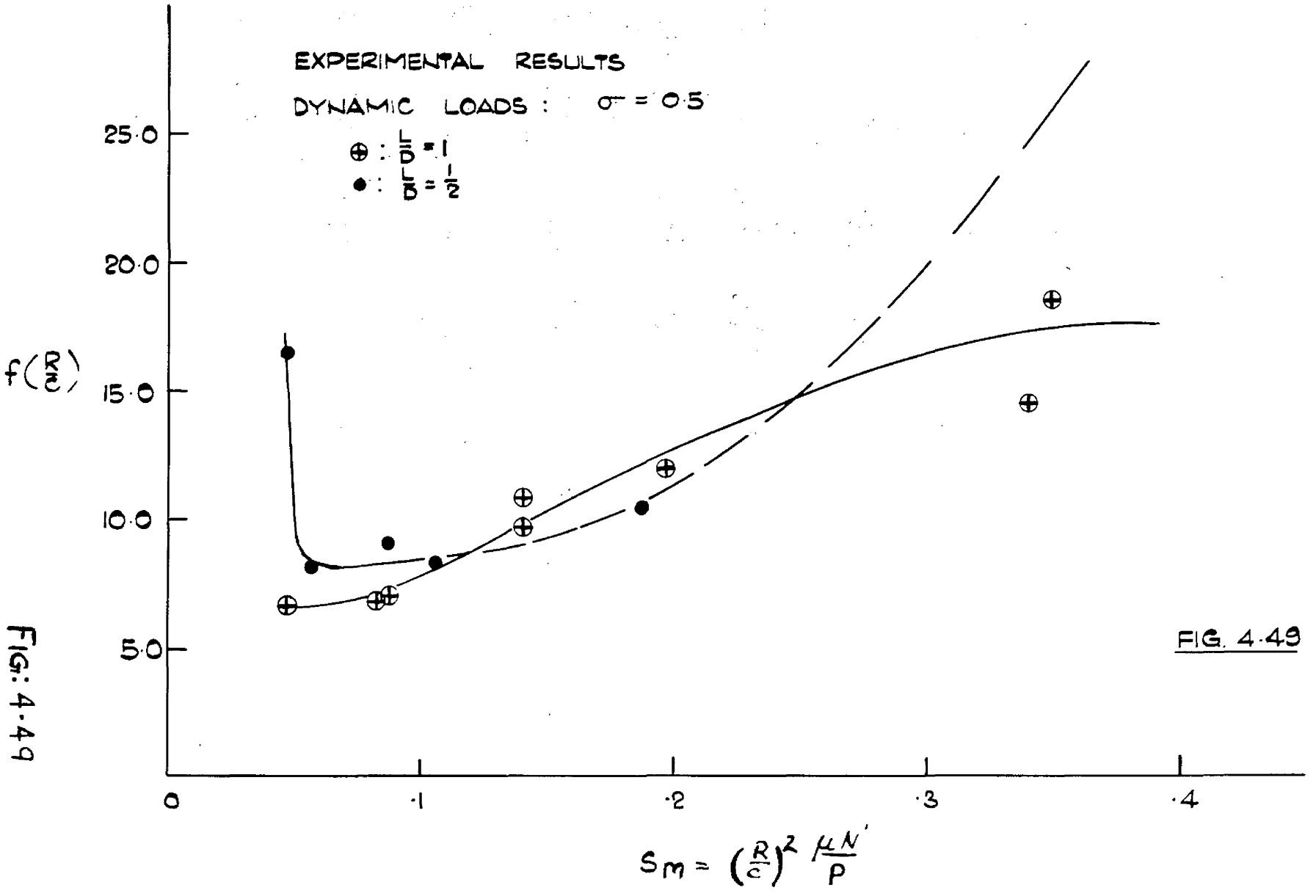

FIG. 4·49

FIG: 4·49

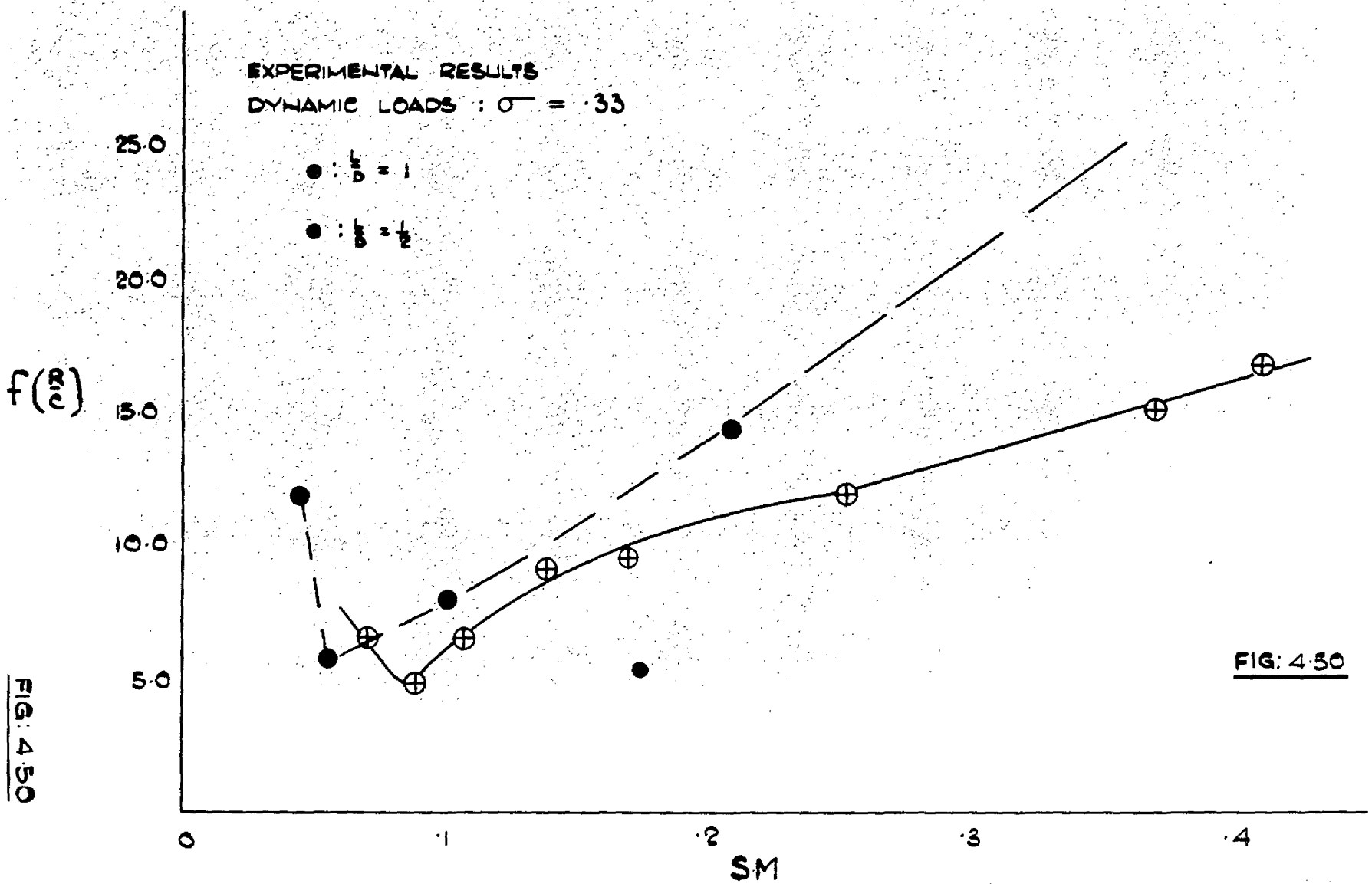

FIG: 4·50

FIG: 4·50

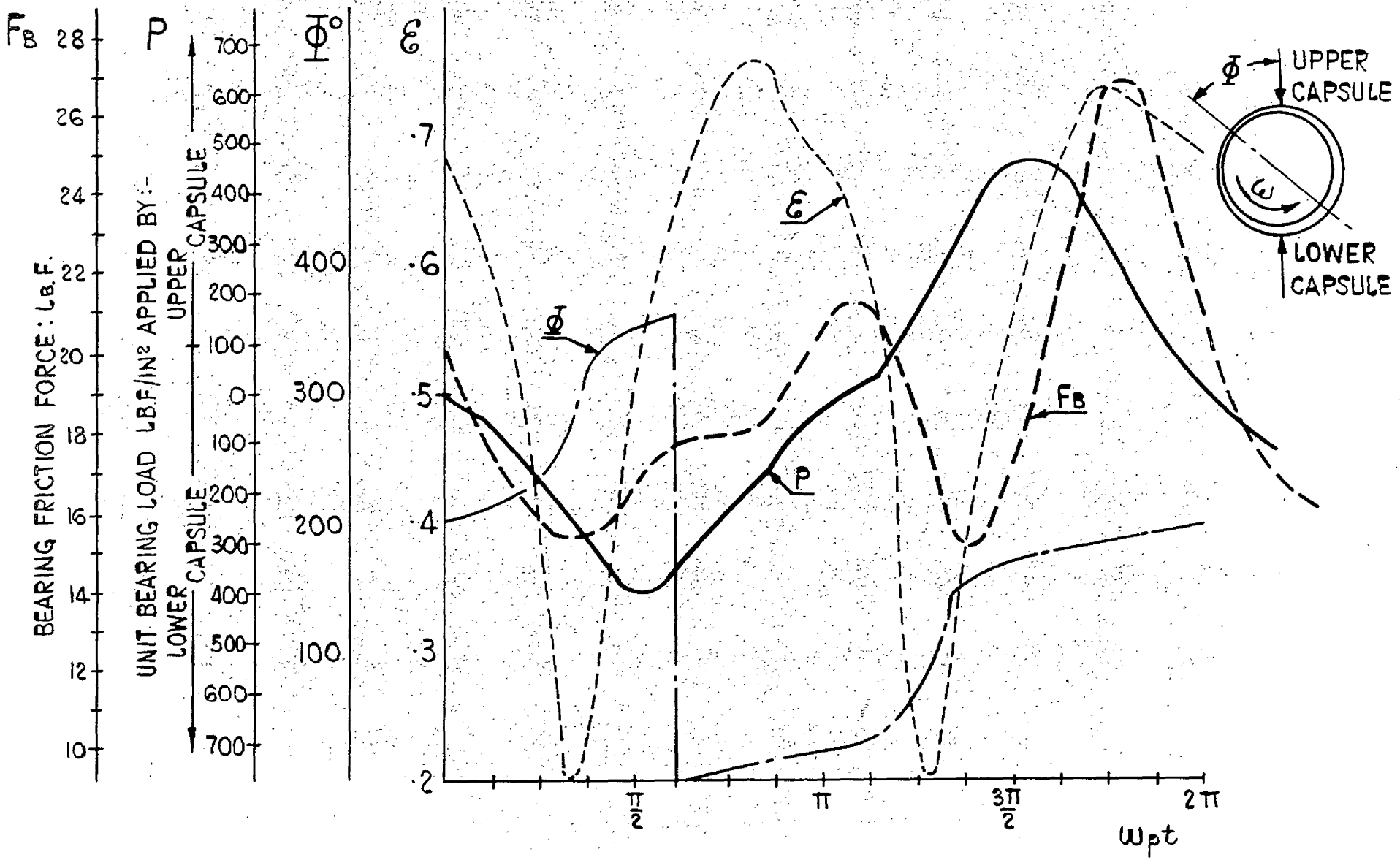

EXPERIMENTAL RESULTS DYNAMIC LOAD $\frac{L}{D} = 1$ $\sigma = 1$ $S_n = \cdot 052$

FIG. 4·51.

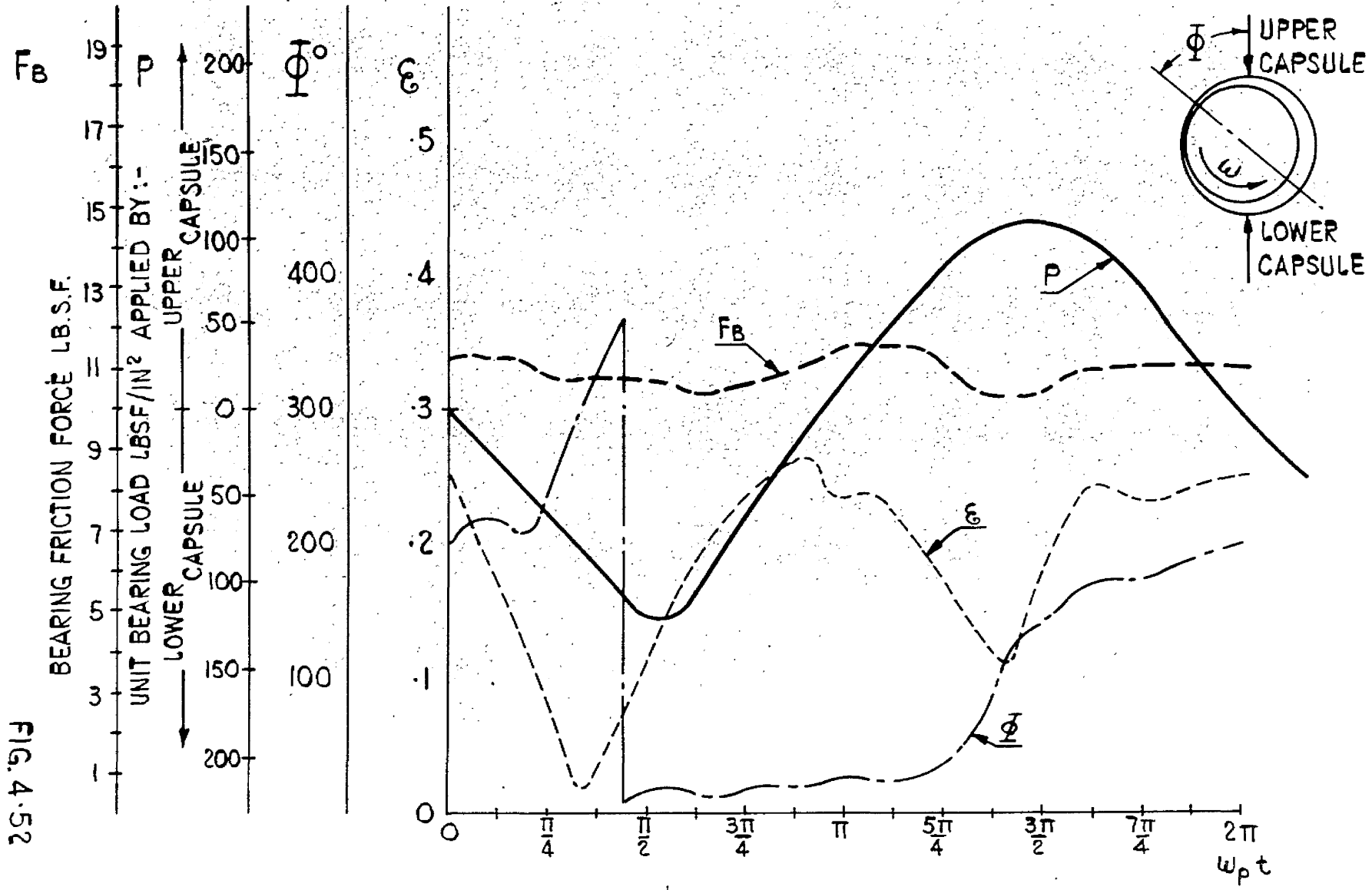

EXPERIMENTAL RESULTS DYNAMIC LOAD $\frac{L}{D}=1$ $\sigma=1$ $S_n:\cdot41$

FIG. 4·52

FIG. 4·52

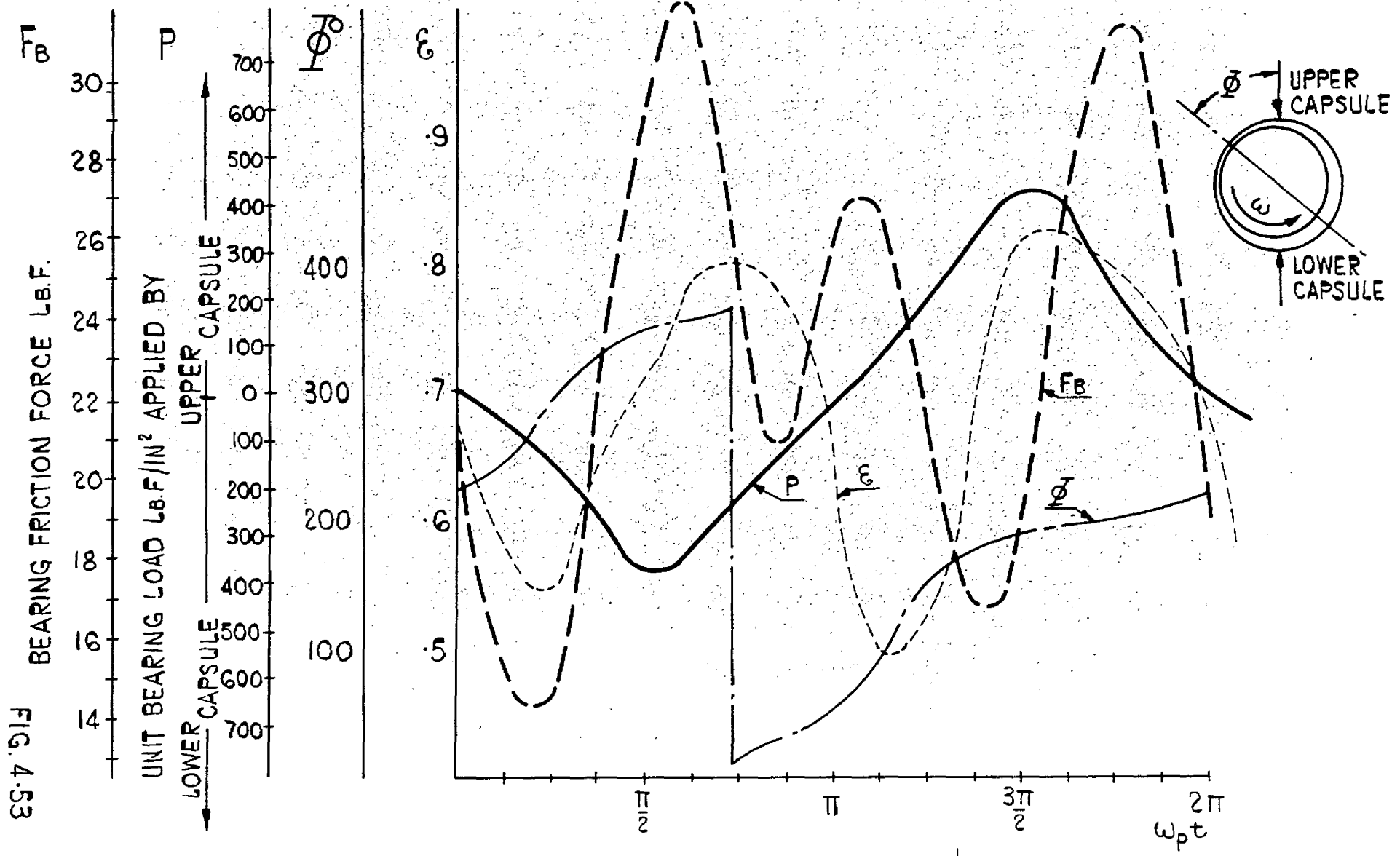

FIG. 4.53

EXPERIMENTAL RESULTS DYNAMIC LOAD $\frac{L}{D} = 1$ $\sigma = .5$ $S_n = .082$

FIG. 4·53

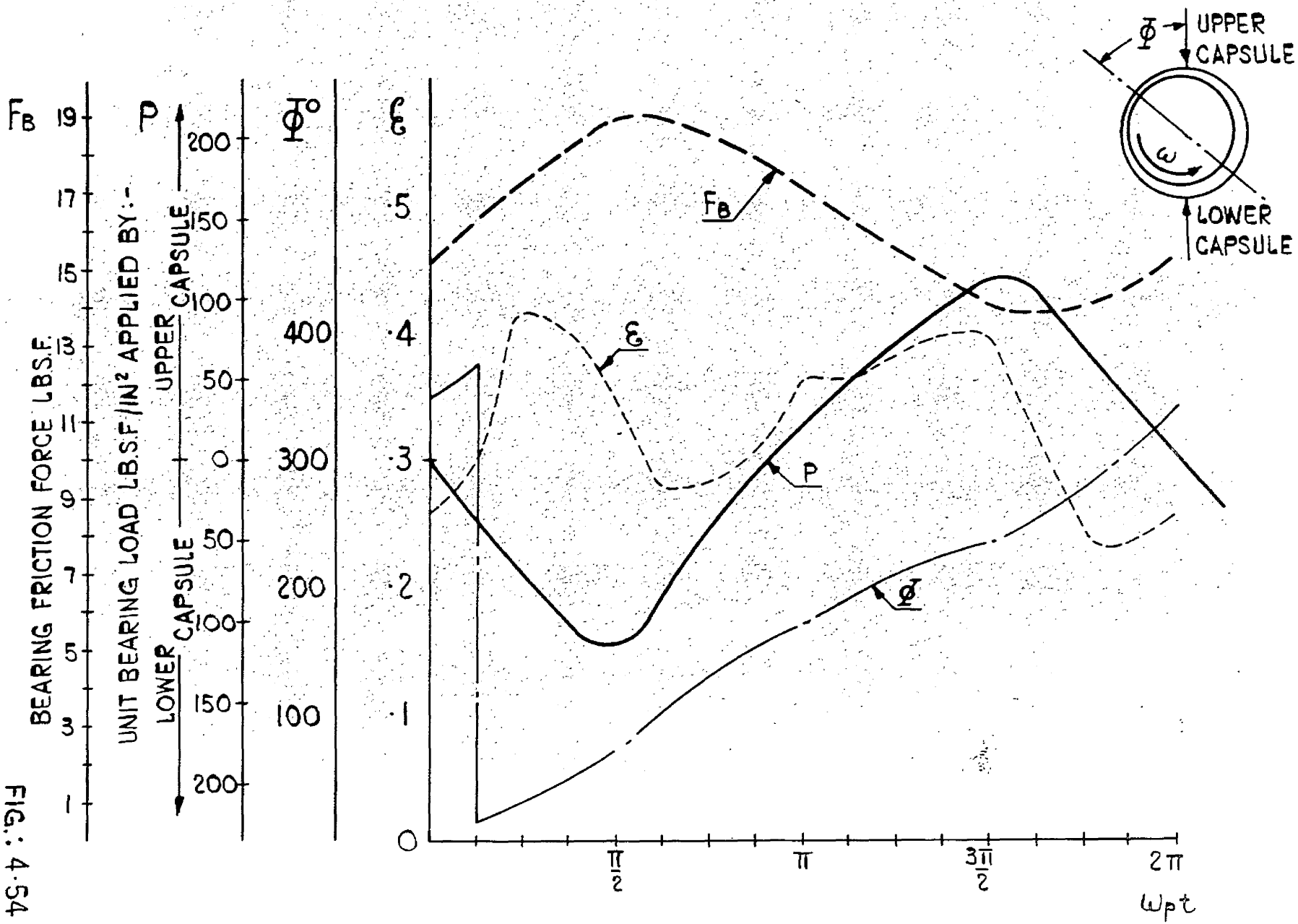

FIG.: 4·54

EXPERIMENTAL RESULTS DYNAMIC LOAD $\frac{L}{D} = 1$ 6 = ·5 S_n = ·35

FIG. 4·54

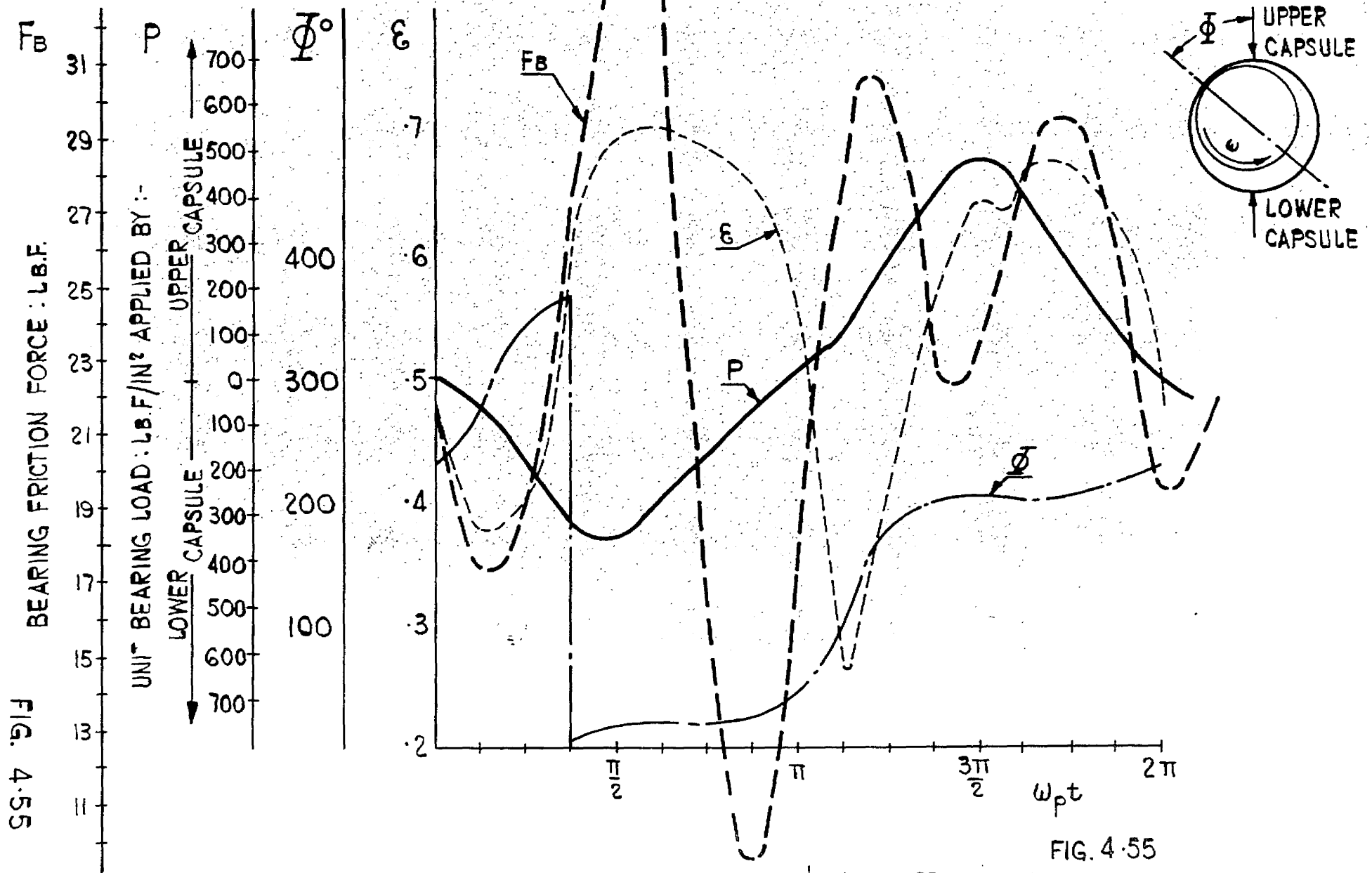

FIG. 4·55

EXPERIMENTAL RESULTS DYNAMIC LOAD $\frac{L}{D} = 1$ $\varepsilon = \cdot 33$ $Sn = \cdot 107$.

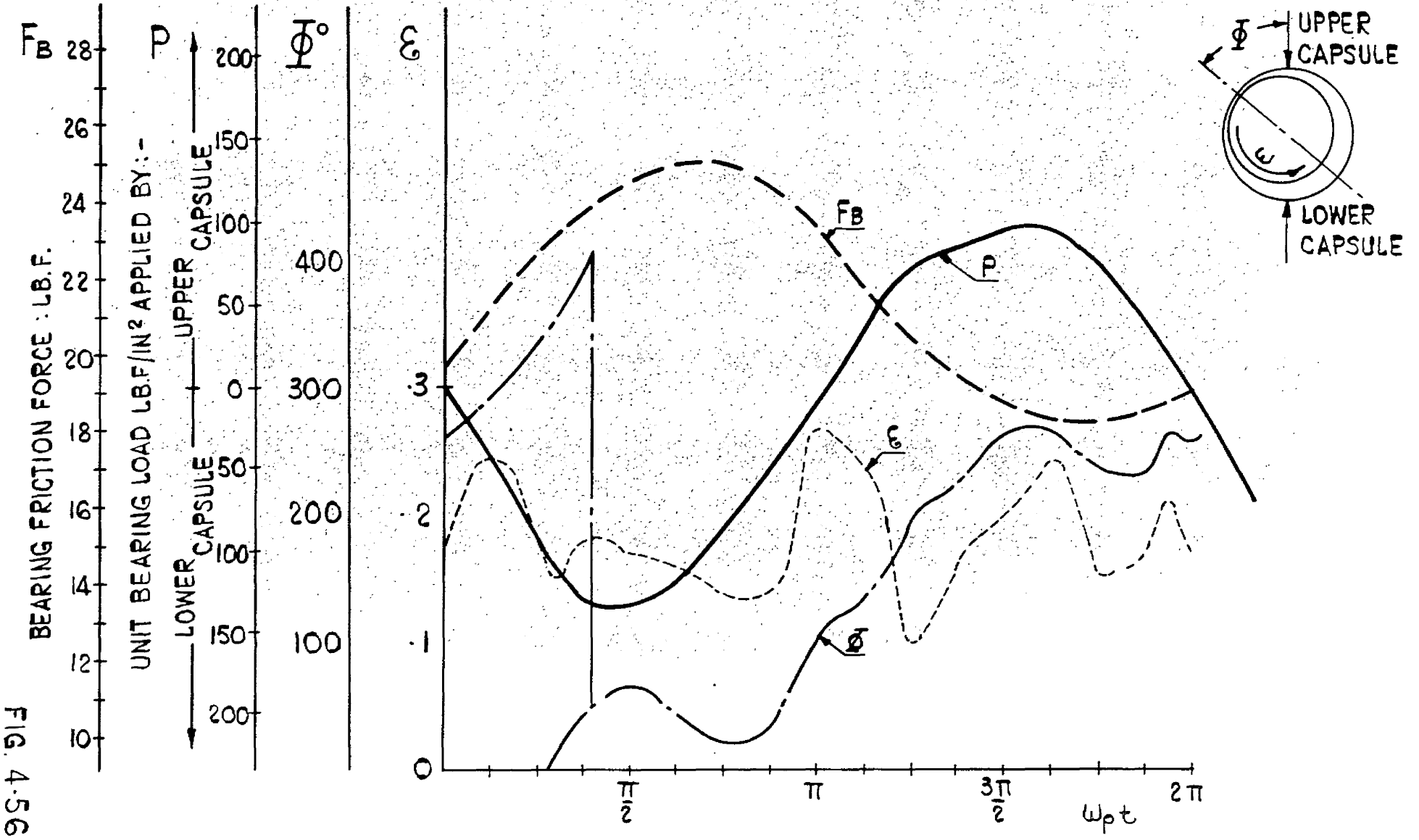

FIG. 4·56

EXPERIMENTAL RESULTS DYNAMIC LOAD $\frac{L}{D} = 1$ $\sigma = \cdot 33$ $S_n = \cdot 41$

FIG. 4·56

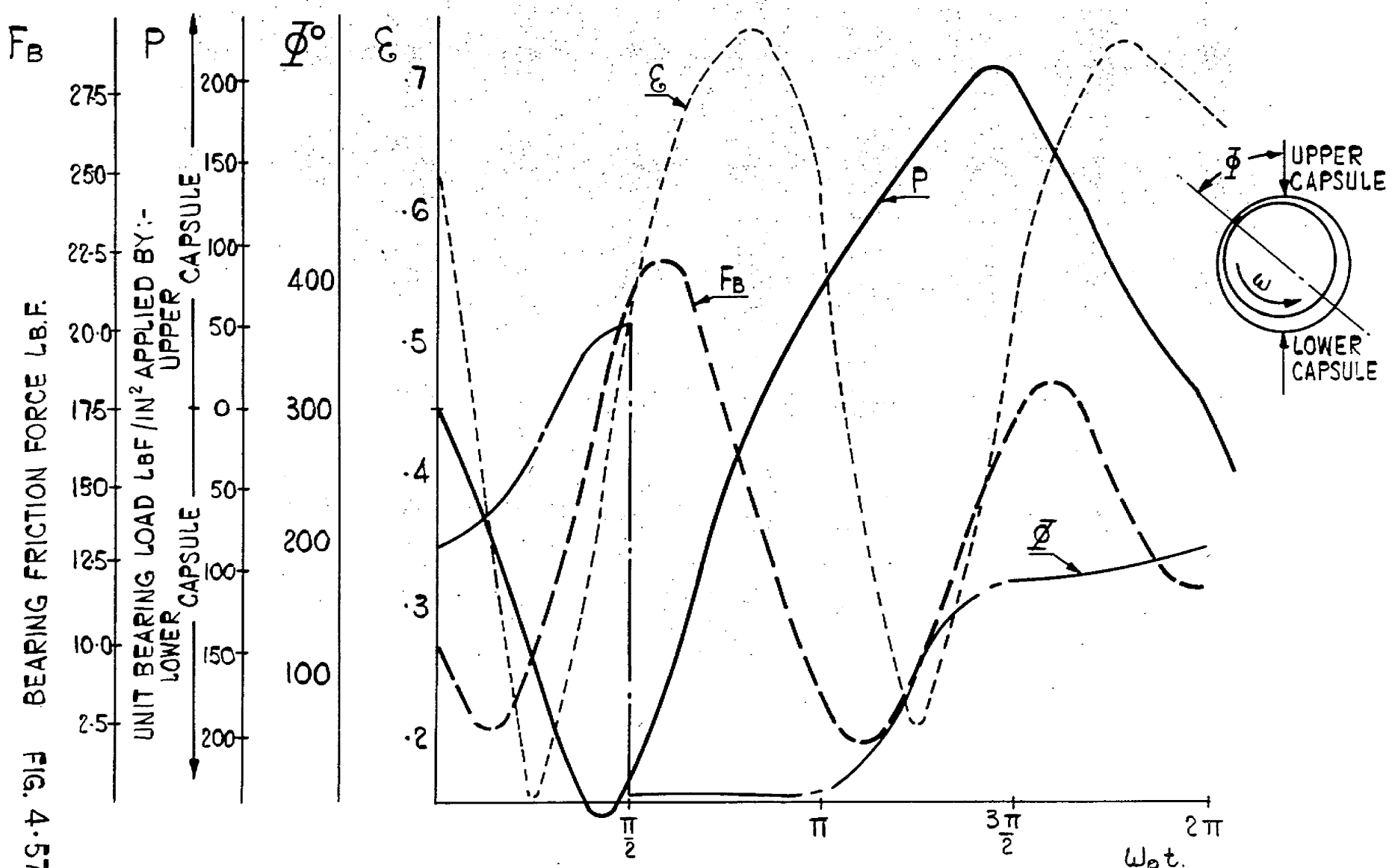

FIG. 4·57

EXPERIMENTAL RESULTS DYNAMIC LOADS $\frac{L}{D} = \frac{1}{2}$; $6 = 1$; $S_n = \cdot 064$. FIG. 4·57.

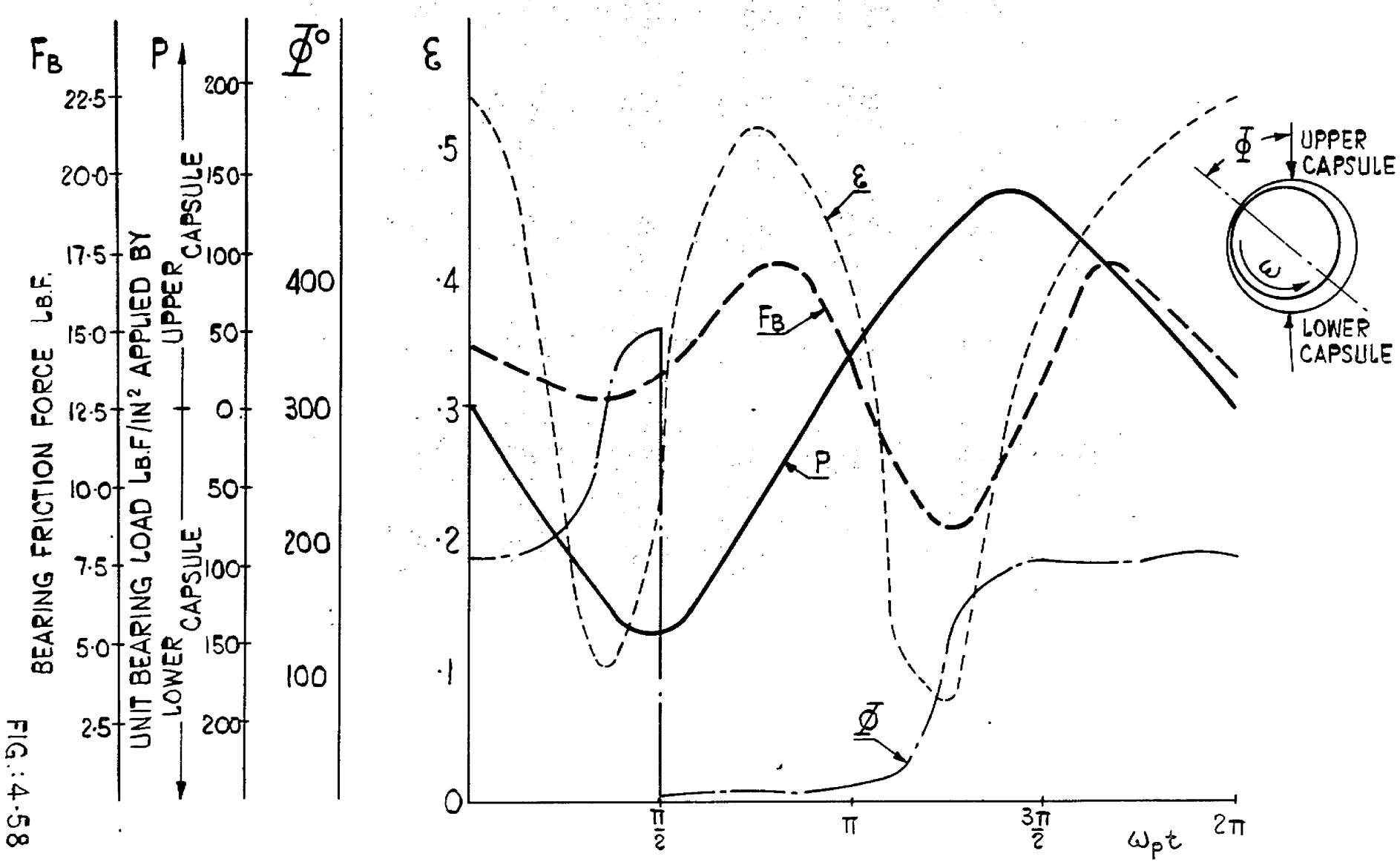

FIG. 4·58

EXPERIMENTAL RESULTS DYNAMIC LOAD $\frac{L}{D} = \frac{1}{2}$; $\sigma = 1{\cdot}0$; $S_n = {\cdot}099$ FIG. 4·58

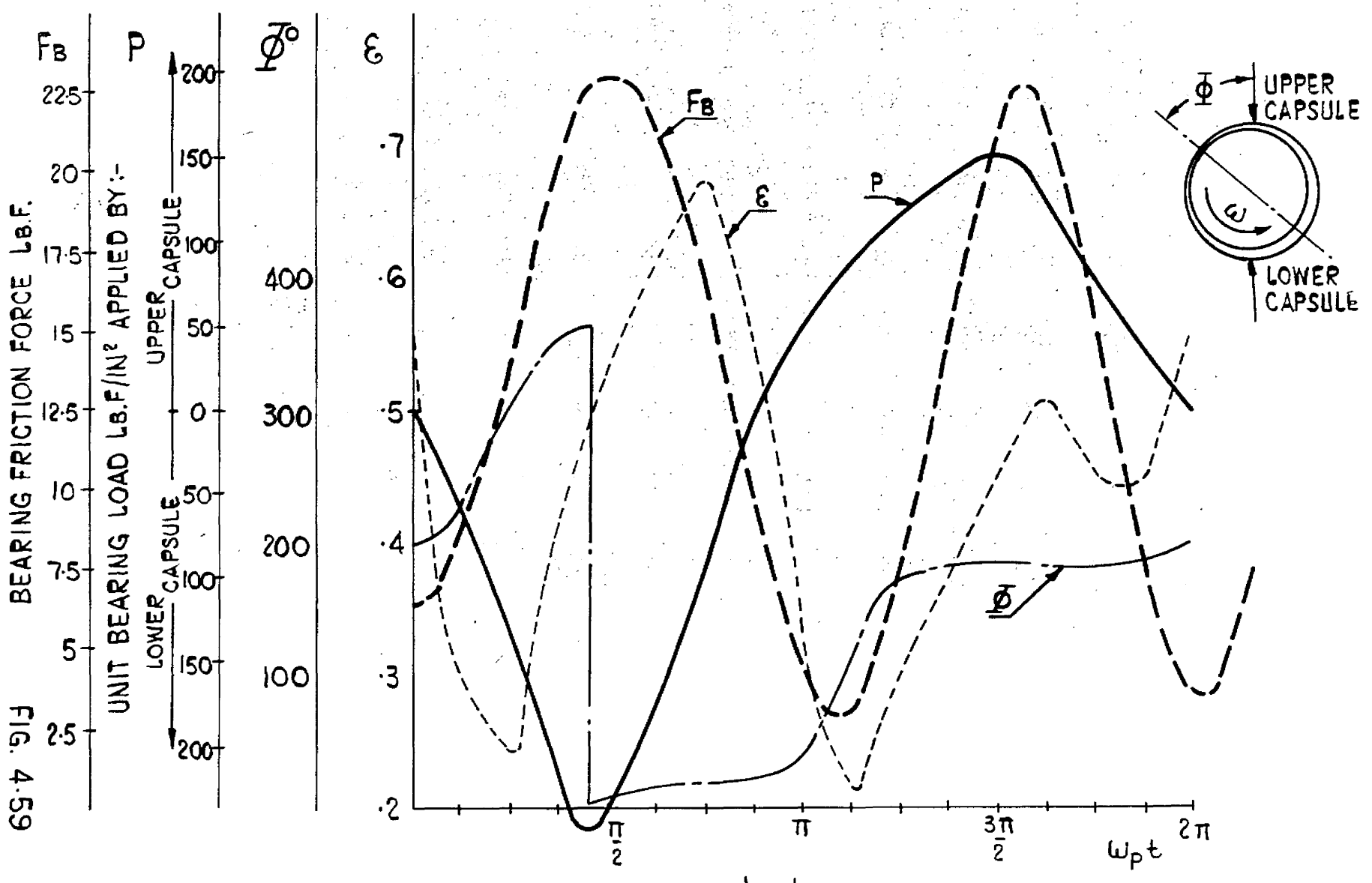

FIG. 4·59

EXPERIMENTAL RESULTS DYNAMIC LOADS $\frac{L}{D} = \frac{1}{2}$; $\sigma = \cdot 5$ $Sn = \cdot 1066$ FIG. 4·59

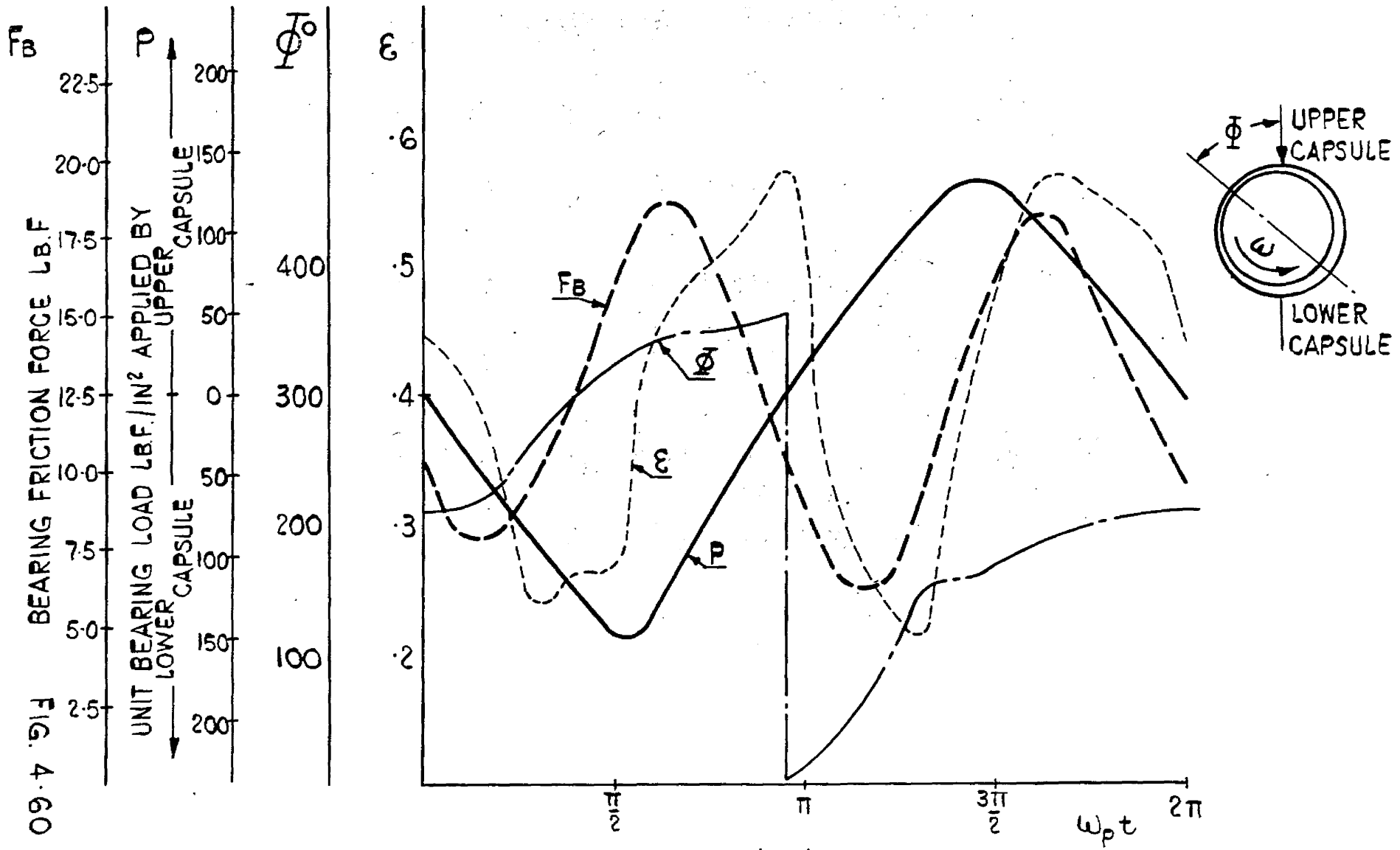

FIG. 4·60

EXPERIMENTAL RESULTS DYNAMIC LOAD $\frac{L}{D} = \frac{1}{2}$; $\sigma = \frac{1}{2}$; Sn = ·1872 FIG. 4·60

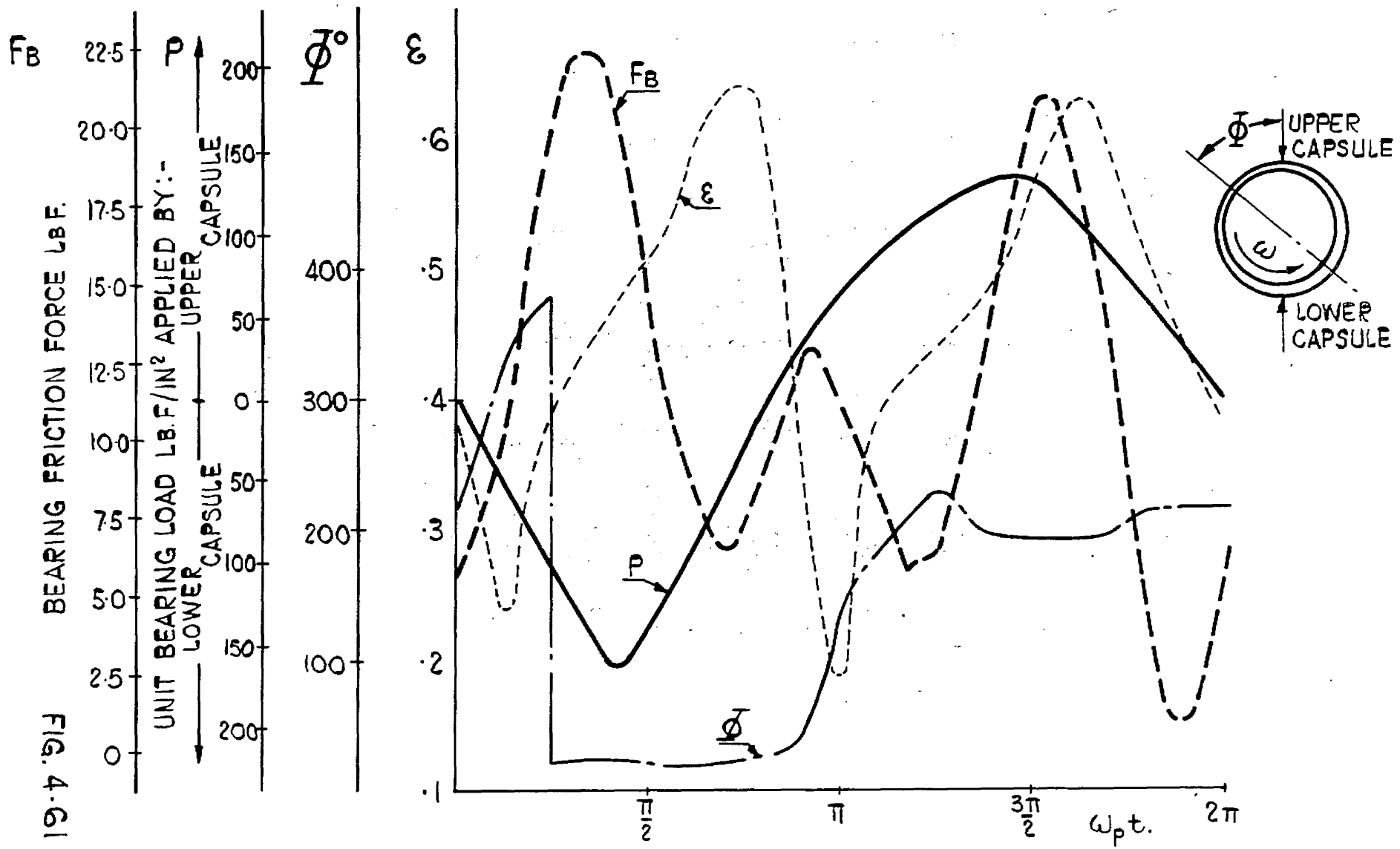

FIG. 4·61

EXPERIMENTAL RESULTS DYNAMIC LOAD $\frac{L}{D} = \frac{1}{2}$ $\sigma = \cdot 33$ $Sn = \cdot 174$ FIG. 4·61

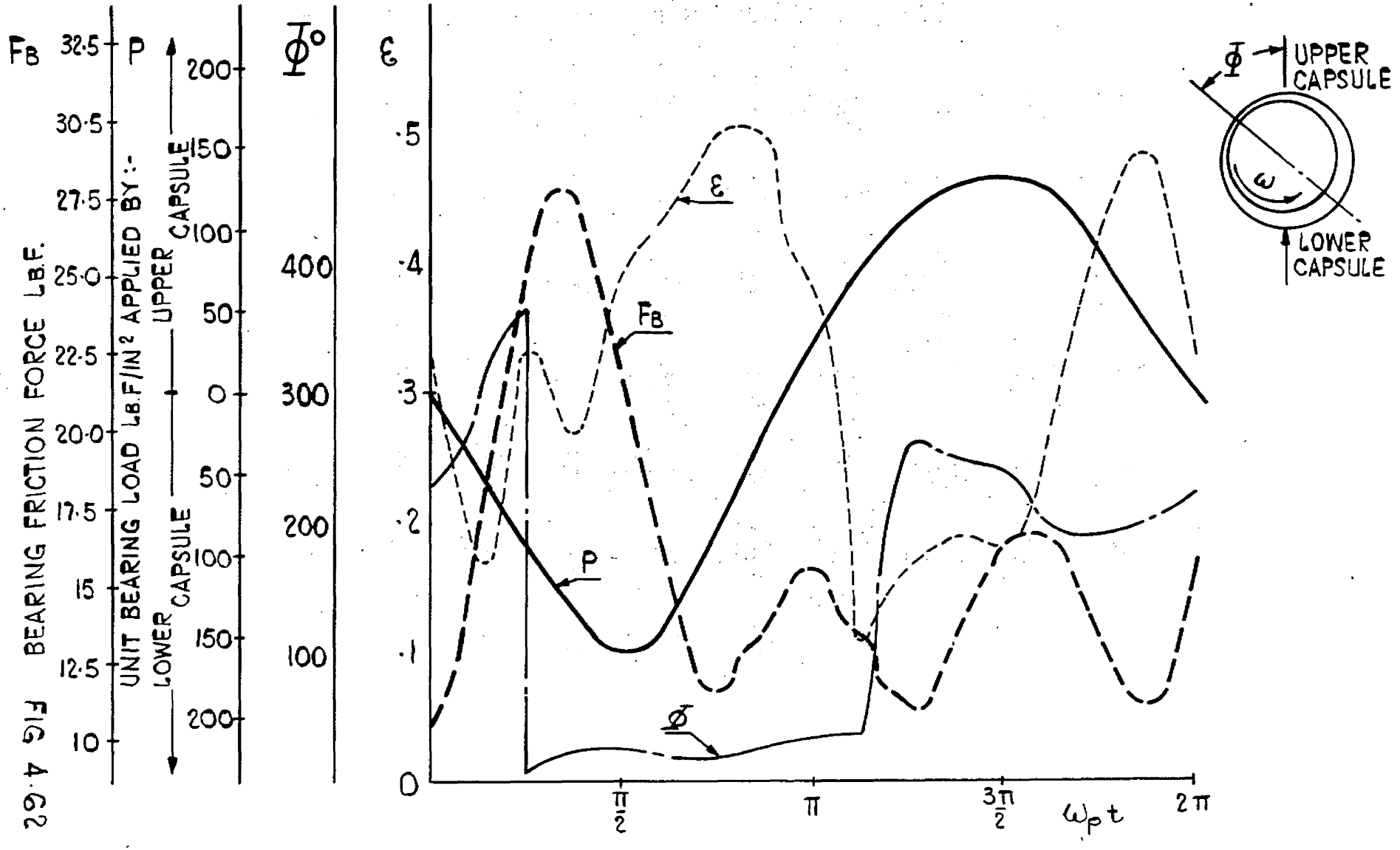

EXPERIMENTAL RESULTS DYNAMIC LOAD $\frac{L}{D} = \frac{1}{2}$; $6 = \cdot 33$ $Sn = \cdot 209$ FIG. 4·62

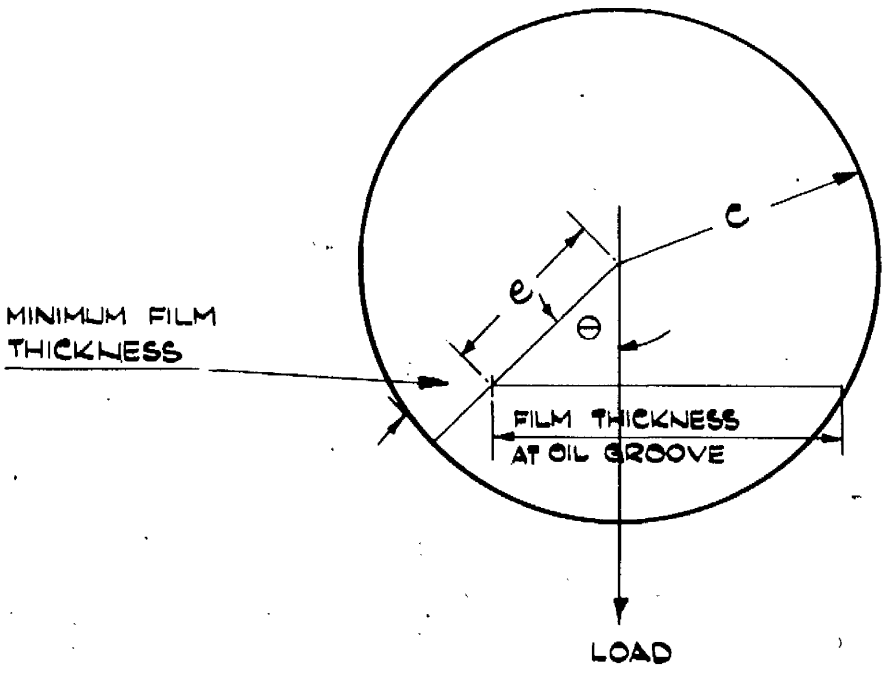

STATIC LOAD
FLOW MEASUREMENTS

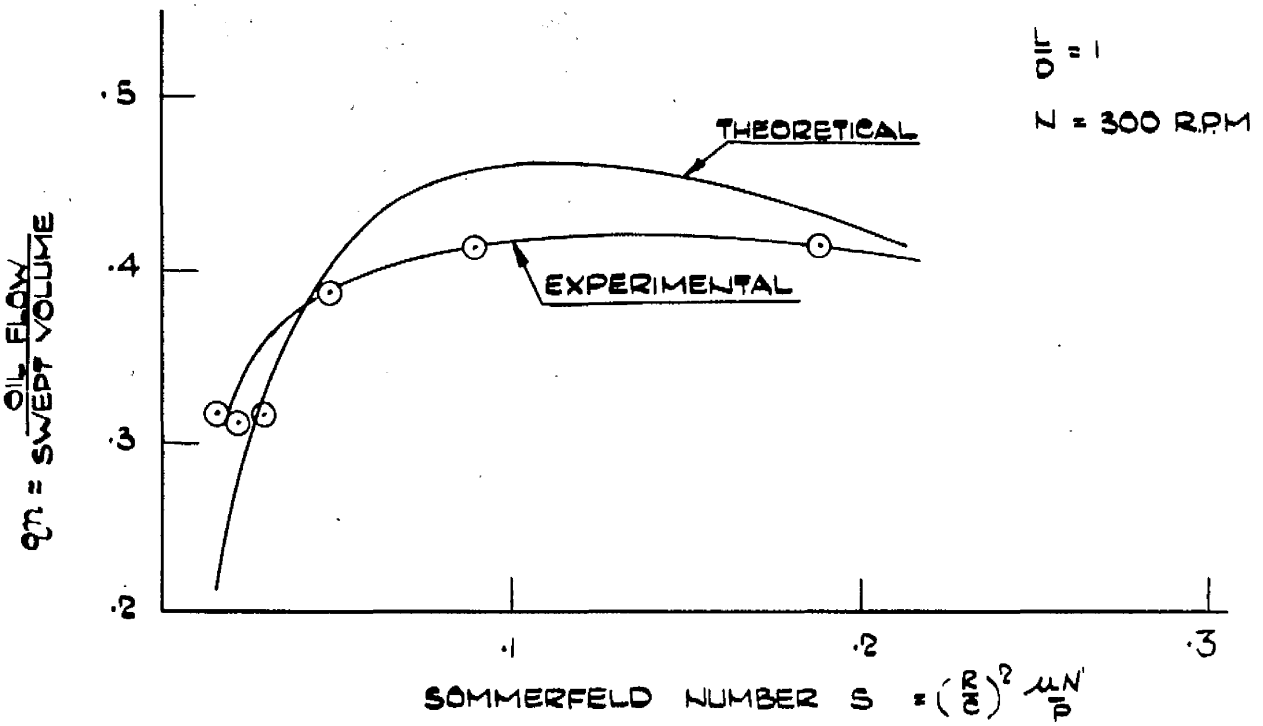

FIG. : 4·63

STATIC LOAD
FLOW MEASUREMENTS

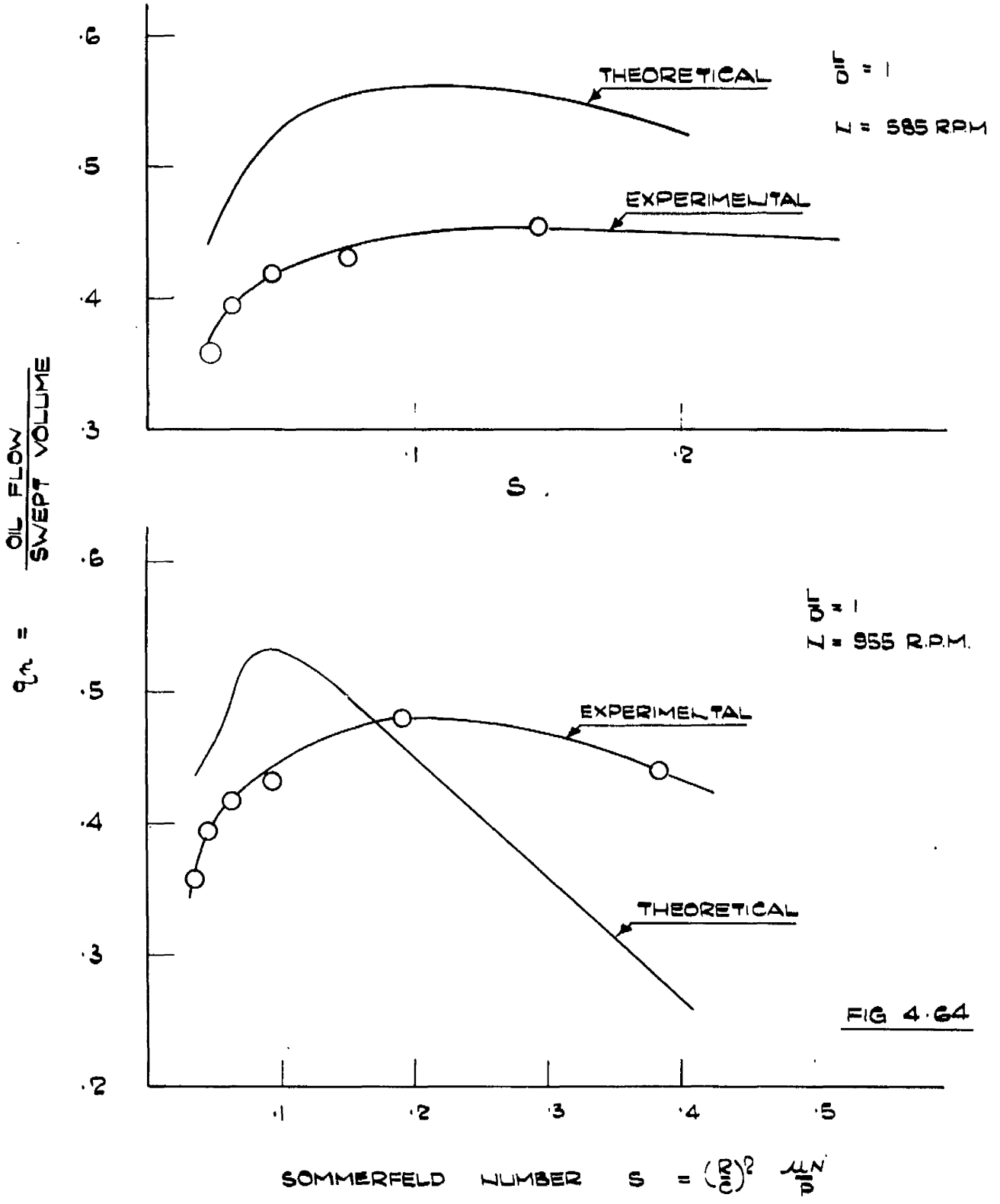

FIG 4·64

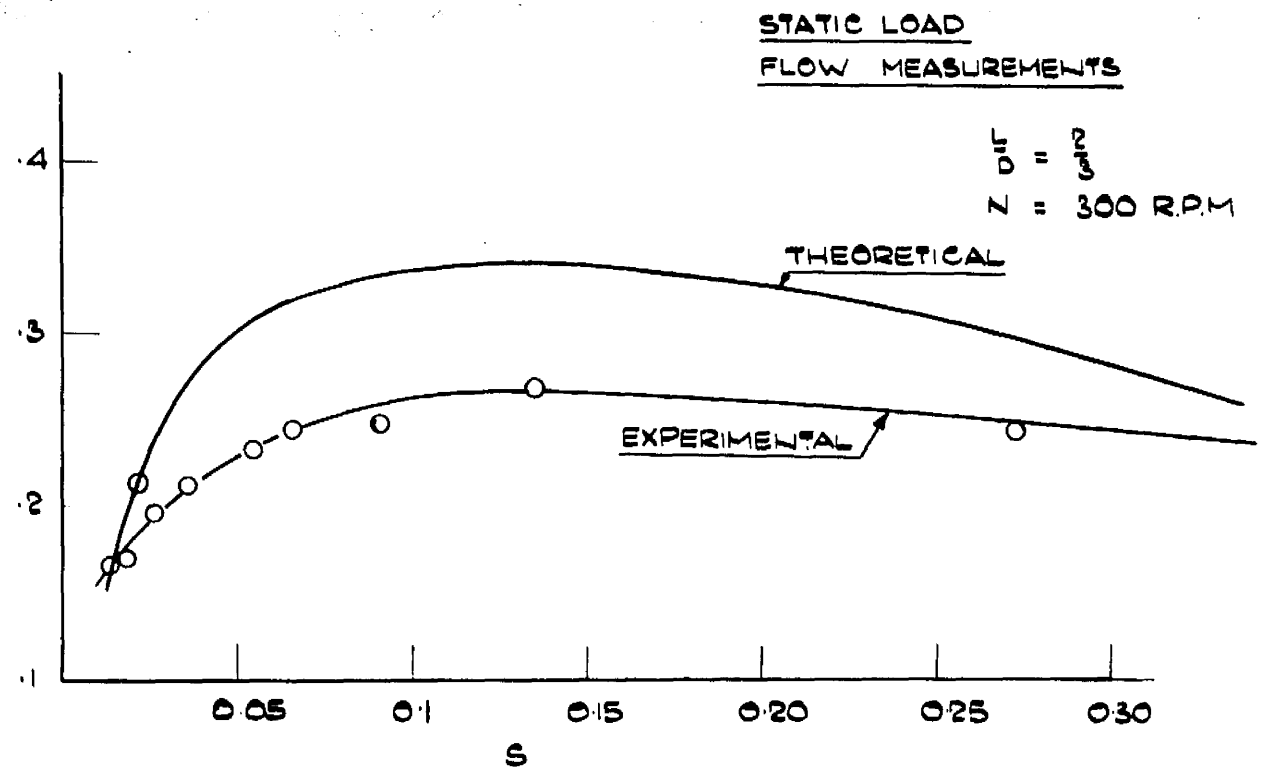

$q_n = \frac{\text{OIL FLOW}}{\text{SWEPT VOLUME}}$

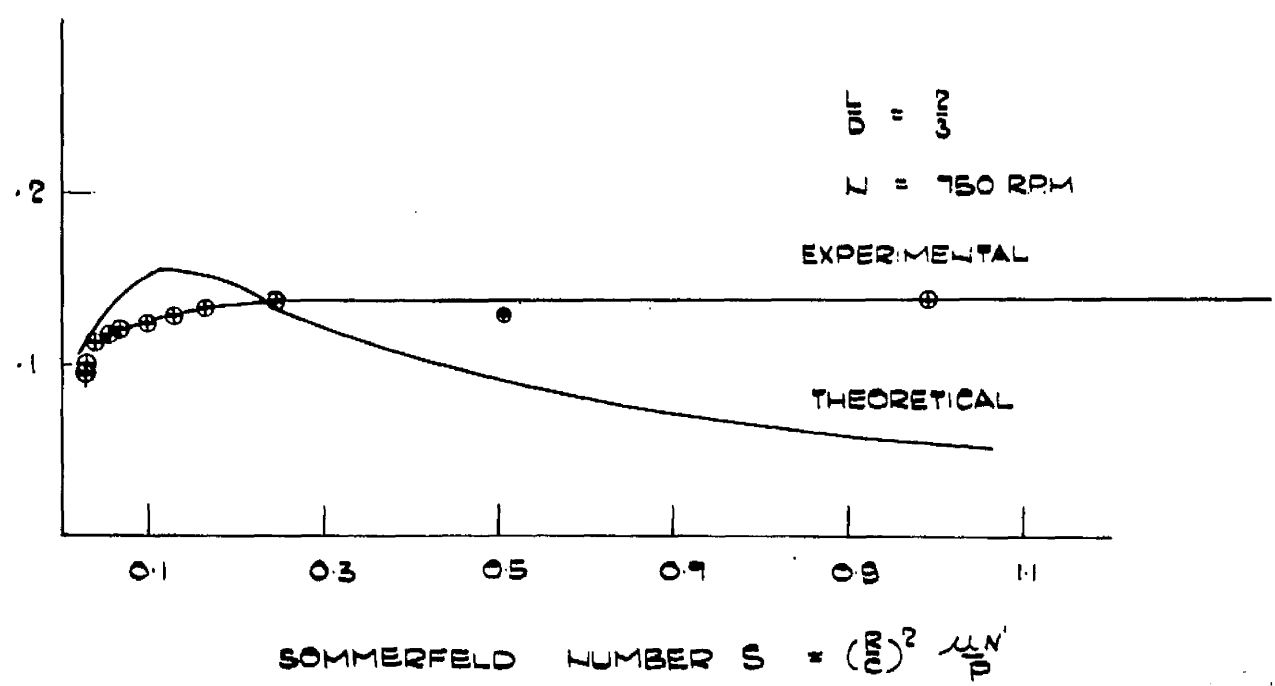

FIG. 4·65

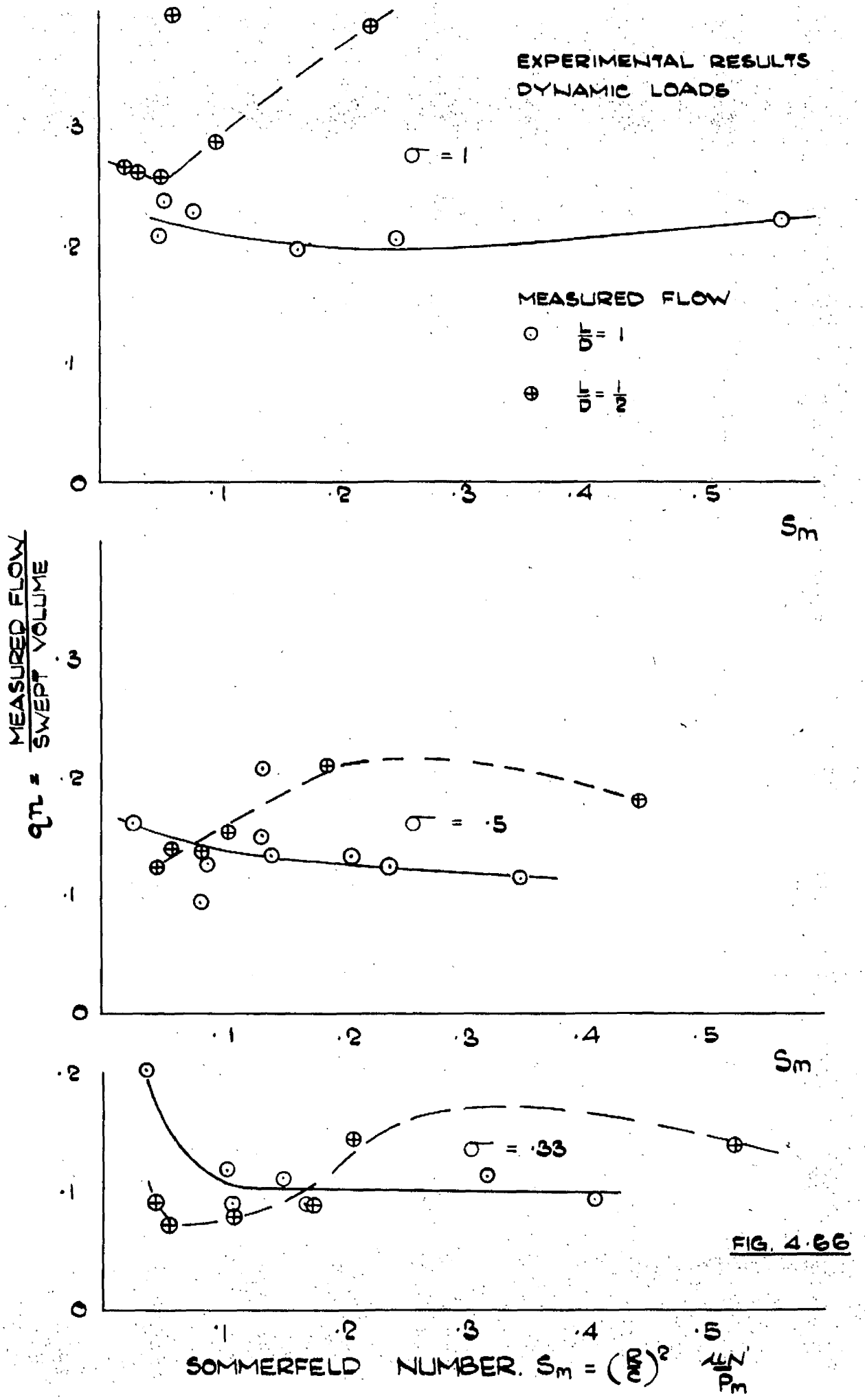
EXPERIMENTAL RESULTS
DYNAMIC LOADS
σ = 1
MEASURED FLOW
L/D = 1
L/D = 1/2
0
·1
·2
·3
·4
·5
Sm
η = MEASURED FLOW / SWEPT VOLUME
σ = ·5
σ = ·33
SOMMERFELD NUMBER. Sm = (R/C)² μN/Pm

FIG. 4·66

CHAPTER V

5. Discussion and Interpretation of Experimental Results

5.1. Pressure Surveys

Theoretical calculations of Statically loaded bearings are based on oil film conditions proposed by either Sommerfeld or Reynolds. The Sommerfeld conditions assume that the pressure in the oil film is a continuous function with positive and negative pressures of equal magnitude. The Reynolds treatment assumes that the pressure in the oil film becomes zero when the slope of the circumferential pressure gradient is zero. In both cases the oil film is said to be complete at the point of maximum film thickness.

The pressure surveys of Fig. 4.1 and 4.2 indicate that none of these conditions exist in an axially grooved full length bearing. In no case was; a) the pressure zero at the point of minimum film thickness as assumed by Sommerfeld, b) the oil film complete at the point of maximum film thickness. The Sommerfeld oil film conditions were found to exist in all but two cases. The film pressure is a continuous function until cavitation takes place at a pressure approaching absolute zero. The cavitated region is terminated

by a combination of converging film and fresh oil from the axial inlet groove.

The exceptions provide an interesting case. The journal centre eccentricities, which were not measured at the time of the pressure surveys indicate no peculiarity at any load throughout the range tested. Yet in the two exceptional cases the film pressures reach a maximum value only 10^{o} of arc before the oil inlet groove and the oil film does not appear to cavitate in the divergent clearance space, Fig 4.1. The position of the pressure peak suggests that the point of minimum film thickness must lie close to the oil inlet groove, i.e. the line along which the journal centre moves makes an angle of 70 degrees with the load line. Several investigators have shown that a journal centre moves normal to the load line until at some light load cavitation occurs and the more usual semi-circular path is resumed. Here it would appear, that due to unusual experimental conditions, we have a bearing which we know does not cavitate and has its line of centres almost normal to the load line. What is unusual is that the journal supports a static load of 3.35 and 6.7 tons f. in this position.

Reynolds predicts that the pressure in the oil film will reduce to half of its maximum value at the point of minimum film thickness. A prediction not supported by the experimental surveys. A similar variation from Reynolds film pressures has been reported by Carl at journal speeds of 1500 r.p.m. Carl considered that the difference was due to distortion of the bearing elements by the applied load. The present surveys confirm this opinion.

The measured film pressures are compared on Fig. 5.1 with those calculated from Ocvirk's narrow bearing theory for bearing with the same clearance and journal eccentricity. This comparison indicates that the magnitude of the calculated pressures is twice that of the measured pressures. Investigations by Motosh[25] have shown that replacement of the isoviscous term of the above calculations by a viscosity term dependent on the temperature and pressure of the oil reduces the maximum calculated pressure to within 10% of the maximum measured pressure.

The film pressure surveys of Fig 4.3a - 4.14b and 4.16 - 4.25 show typical pressure profiles for oil films supporting an alternating type of dynamic load. The surveys, completed in 1958, are similar

in form to those reported by Carl in 1962. They show a gradual generation of load bearing pressure in the convergent film of a journal bearing followed by a rapid fall in pressure to an area of sub-atmospheric pressure. No detailed information on the pressure conditions in this low pressure area has been available until now. Examination of a typical graph of the variation of the journal centre radial velocity with applied load recorded on the Second Testing Machine Fig 5.2, shows that during the period of decreasing load in a given direction the journal centre has a decreasing velocity with corresponding decrease in pressure generation by squeeze action. At the point of maximum eccentricity the load is entirely supported by pressure generated by Wedge action, (a circumstance substantiated in § 5.2). Further reduction of applied load reverses the direction of the journal centre velocity and the wedge action pressure peak leaks away in the expanding film and ideally reaches atmospheric pressure at zero load.

Due to the viscosity of the oil the generated film pressure requires a finite time to leak away. In the .0015.in. clearance bearing the rate of film pressure decay is less than the rate of change of applied load. This difference results in an out of balance pressure load which induces the pressure rise in the opposite half

of the bearing demonstrated at $\phi = 30$, 60, 90, 240, and 270 degrees on Fig 4.15.

At the instant of zero load the journal has considerable eccentricity and, on the reversal of applied load, experiences the rapid acceleration apparent from Fig 5.2. This velocity change has a twofold effect. It produces a considerable squeeze film pressure at one side of the bearing while at the other side oil will flow into the space behind the retreating journal surface. Even at the low load frequency of 5 cycles per second, the rate at which the journal retreats does not leave time for the surrounding oil to flow into a space 2 to 5×10^{-4} inches thick, and the oil already in the space is held in a state of tension as shown on Fig 5.3 - 5.14. Similar conditions exist upto the point of maximum load at $\phi = 0$, after which the area shown on Fig 5.3 - 5.14 is filled with a fluid at subatmospheric pressure.

Similar pressure contours plotted from the survey of Fig.4.2., show under Static conditions a rapid fall in pressure followed by a considerable area of either constant or slowly rising sub-atmospheric pressure, Fig 5.15. A visual examination of an oil film with corresponding pressure measurements reported by

Dowson[39], indicated that in such an area a number of large relatively stable air bubbles or cavities form in the oil. The pressure difference between the air in the cavities and the oil at the ends of the bearing holds the cavities in suspension within the oil film.

Hence the areas of constant, or slowly increasing, sub-atmospheric pressure shown on Fig 5.3 - 5.14 will be filled with cavitated oil. Due to the time factor the air in the cavity will not be concentrated in the large bubbles of the Constant Load case, but will be dispersed as tiny bubbles throughout the oil of the low pressure area. This type of air dispersion has been photographed by Cole and Hughes[40] on the unloaded side of a bearing subjected to rotating loads.

The upstream boundary of the cavity is not easily defined without visual observation of the oil film in the region of tensile stress. Some indication of its position can be gained from the reports of Dowson and McBroom[21] who observed a trough of sub-cavity pressure upstream from the boundary of the cavitated area. The oil film tensions shown in Fig 5.3 - 5.14 exist in such a trough, the problem left unsolved is whether the air comes out of solution along the line of absolute zero pressure or whether there is some earlier combination of tensile stress and rate of change of tensile

stress which releases the entrained air. Such a release of entrained air would be accompanied by an instantaneous rise in pressure to at least absolute zero. Both absolute zero pressure and tensile stresses of 2 lbs.f/in.^{2} were measured in the oil film, but survey points were not close enough to detect any instantaneous pressure rise as air was released. Fig 5.3 - 5.14, show clearly that as the tensile strength of the oil film is exceeded with changing journal position, the rupture of the oil film releases entrained air which sweeps the line of absolute zero pressure against the direction of rotation until tensile stresses cease to exist and the minimum cavity pressure rises above absolute zero.

The instant at which cavitation starts is not clearly defined in these surveys. At ϕ = 270 & 300° in both bearings the only suggestion of a low pressure plateau is near the point of maximum film tension. The pressure gradient between zero and atmospheric pressure are substantially the same on either side of the plateau indicating a trough of subcavity pressures without the following cavities. This raises the possibility, particularly in the .0015 in clearance bearing that no cavitation occurs until $\phi > 300^\circ$.

There is no doubt, however, that at $\phi = 0$ a large volume of cavitated oil occupies the unloaded arc of the bearing and that this condition exists until a change in direction of the applied load reduces the clearance space and the air of the cavity is reabsorbed in the oil film.

Measurement of the rate of solution of air in lubricating oil, reported by Hayward[41], indicates that 25% of the air is dissolved very rapidly on the application of pressure. The remainder of the air dissolves at a decreasing rate as the skin of oil surrounding each air bubble becomes saturated with dissolved air. The absorption process can be accelerated by increasing the pressure in the air oil mixture. This process can be followed in the pressure surveys of Fig 4.3a - 4.14b, where the depressions in the pressure film at $\phi = 90$ to 180° and $270 - 300^{\circ}$ are due to the presence of undissolved air. A proportion of the air in the cavity is swept out with the leakage oil and is clearly visible in the form of small bubbles suspended in the oil emerging from the bearing ends.

During these periods of low pressure oil can be drawn into the upper sections of the bearing from the supply of leakage oil

lying on the supper surface of the bearing housing. No such beneficial supply is available to the lower sections of the bearing. This results in the extended area of cavitation shown in the lower sections of Fig 5.3 - 5.8.

The question arises as to whether the stresses in the oil film reported above are some passing freak condition or a permanent feature of a Dynamically loaded bearing. Tensile stresses were measured in the oil film of both bearings throughout the range of dynamic loads examined. They were constant in magnitude and position every 0.2 seconds of the ten day period required for a 7 section survey. These facts place tensile stresses in the oil film in the category of a permanent feature of dynamically loaded bearings. The magnitude of such stresses provides negligible load carrying capacity at the load frequency examined.

5.2. Journal Eccentricity

The principal purpose in the investigation of Statically loaded bearing was to establish the validity of experimental techniques in a field where adequate experimental work was available for effective comparison. To this end the journal eccentricities

have been compared with those published by Clayton and Jakeman[42] and Ocvirk et al[43] for similar bearings.

Measurements made on the First Testing Machine do not compare favourably with those reported by the above investigators Fig 4.30 and 4.31. The grouping of eccentricity ratios into separate curves for given journal speeds reflects the effect of the variables in the Sommerfeld Number. Journal speed and oil viscosity are interdependent in a given bearing, and in the presentation of these curves it should be remembered that the speed of the journal was accurately measured while only an approximate value of the oil film temperature was available.

If the curve for a specific speed is chosen as a reference curve and the value of Sommerfeld Number for all other curves is modified by the ratio of its journal speed to that of the reference curve, the experimental points fall on a single curve.

As the policy of the author has been to avoid the application of correction factors to experimental results, it must be concluded that on the First Testing Machine insufficient experimental information was available to make a thorough evaluation of the journal paths measured under Dynamic Loads possible.

Journal eccentricity in a full length bearing shows close agreement with the short bearing work of Du Bois & Ocvirk [43] when measurements are made on the Second Testing Machine Fig 4.34. Similar measurements in a bearing with an L/D ratio of 2/3 do not display the same close agreement. The single curve indicated by Ocvirk is the Best line from a large number of tests on bearings in the range $1 \leqslant {}^{D}/D \leqslant \frac{1}{4}$ and speeds up to 5000 r.p.m. Each experimental curve in Fig 4.34, represents tests made in one bearing at speeds up to 1000 r.p.m., and both curves fall within the scatter of DuBois and Ocvirk's results.

The comparison of experimentally and theoretically determined Eccentricity Ratios shows on Fig 5.19, that, for bearings with $L/D \leqslant 1$, the predictions of Cameron and Wood[44] indicate thinner films, and those of Ocvirk thicker films, than have been experimentally determined. The upper curve of Fig 5.19 is representative of several independent investigations by, Cameron and Wood, Jakobsson and Floberg[45], and Sassenfeld and Walther[46]. The lower curve is evaluated from Ocvirks Short Bearing Approximation.

The above comparison of experimental results with published experimental and theoretical work indicates that the techniques

used on the Second Testing Machine place no restraint on the evaluation of journal paths measured under conditions of Dynamic Load.

The theoretical predictions of Burwell[9] and Hahn[10] indicate that a journal follows an elliptical path, when supporting sinusoidally alternating loads, except at the speed ratio $\sigma = 0.5$. At this ratio the journal path should be circular in form and if we neglect end leakage this circle should be coincident with the clearance circle giving zero load capacity. The major axis of the ellipse should lie, along the load line for $\sigma > 0.5$ and normal to the load line for $\sigma < 0.5$. At speed ratios $\sigma < 0.25$ the simple elliptical path of the journal becomes more complicated in form.

The journal centre paths for the full length bearing, Fig 4.37 - 4.39, agree with the theoretical points detailed above in that they are elliptical in form and at light loads the major axis of the ellipse rotates in the direction of journal rotation to a position where it makes an angle greater than 90° with the load line when $\sigma \ll 0.5$.(Fig. 5.17). At $\sigma = 0.33$ the path is more complicated than the simple ellipse associated with other speed ratios, Fig 4.37. At no time in any bearing was any critical condition detected at speed ratios at or near $\sigma = 0.5$.

Other experimenters have reported very small films at speed ratios in the range $.47 \leqslant \sigma \leqslant 0.5$, but a search for similar conditions proved fruitless in this testing machine. The influence of the change in journal speed necessary to effect a change in speed ratio may have been sufficient to make the critical condition illusive. A major alteration in the drive layout of both testing machines will be required before the load frequency becomes independent of the journal speed.

At Sommerfeld numbers $S_M < .1$ the journal paths are elliptical in form at all the speed ratios examined. There is no doubt that the film thickness is reduced at $\sigma = 0.5$ as on Fig 5.16, the journal centre shows the same maximum eccentricity at $\sigma = 0.5$ and $S_M = .08$ and at $\sigma = 1.0$ and $S_M = .05$. The only tendency to the circular paths of theoretical conditions is a distinct increase in the length of the minor axis of the ellipse at $\sigma = 0.5$.

The journal centre follows an elliptical path when operating in a half length bearing irrespective of the magnitude or speed ratio of the applied load, Fig 440 - 4.42. The major axis of these elliptical paths shows little inclination to swing away from the line of applied load, Fig 5.18. A comparison of the above journal paths

with those reported by Shawki and Freeman[22] Fig. 5.29 and those predicted by Hahn Fig 5.21 shows general agreement in the shape of the path, but total disagreement in the position of the major axis. The reason for this variation is due to the means of supplying fresh oil to the bearing. In cases where an oil supply hole is used (Shawki and Freeman) or the disturbance in the oil film due to the oil inlet is ignored, (Hahn), the journal path has its major axis tilted in the direction of journal rotation. When twin oil supply grooves are used, they cause a major oil film disturbance across the width of the bearing Fig 4.26, and hold the major axis of the elliptical path in line with the load line. This condition has been demonstrated by Carl[23] without comment, in a bearing with oil pockets.

An interesting feature of these journal paths arises from the journal position at specific points in the load cycle. The pressure surveys indicate that the maximum oil film pressure occurred at the instant of maximum applied load and yet at this instant, in the cases examined at $\sigma = 1$, the magnitude of the journal eccentricity is considerably less than the maximum value recorded in the cycle. This indicates the considerable load carrying capacity of the squeeze

film. A capacity underlined by the fact that when the journal path is an undistorted elliptical shape, the load applied to the journal in its position of maximum eccentricity is within 2% of the static load capacity of the bearing at the same eccentricity.

At zero load the journal centre was either coincident with or in the vicinity of the point of maximum eccentricity. As the former condition always occurred at one end of the path it must be assumed that the condition was due to a variable misalignment caused by the elasticity of the bearing mounting. There is no doubt that this combination of minimum load and near maximum eccentricity existed, as it was detected by the simultaneous recordings of applied load and journal displacement co-ordinates. Similar conditions are reported in a half length bearing by Carl, who found that the journal was at its minimum eccentricity at maximum load and passed through its maximum eccentricity in an undistorted elliptical path at zero load. The pressure surveys in the .0015 in. clearance bearing show clearly the conditions in the oil film when the journal is near its maximum eccentricity at zero applied load, Fig 4.15a & b. At $\phi = 90^{\circ}$ and 270°, both zero load conditions, a balancing pressure distribution is induced in the

opposing bearing arc by squeeze action. The absence of a clearly defined pressure film induced in the .003 in diametral clearance bearing at zero load, Fig 4.26a &b, does not infer that the pressures do not exist, but rather that the surveys have been made at load increments to large to detect the effect.

The large number of cycles required to repeat a given journal path (§ 4.2), raises the possibility of a recurrence of conditions reported by McBroom[21] in an investigation of Dynamic Loads. He observed that if an alternating load were applied to a bearing operating in an oil bath, a cavity quickly built up in the clearance space with a corresponding loss in load capacity. If the air trapped in the cavity was allowed to escape by temporarily stopping the journal the load bearing capacity was restored to the oil film until the cavity reformed.

It was observed during the prolonged cycling mentioned above (§ 4.2) that the normal flow of small bubbles suspended in the leakage oil was periodically augmented by groups of 3 or 4 larger bubbles about 1/8 inch diameter. In an attempt to relate the appearance of these groups of large bubbles with the cyclic period of the journal, a single high speed cine film was taken of the leakage oil.

This single film did not give conclusive evidence of a connection between these events but it did indicate a regular interval between escapes suggesting the build up and collapse of large cavities within the oil film.

The above discussion has dealt with the path a journal follows under a definite sequence of applied loads and has gone some way towards an explanation of how the bearing reacts to the applied load. In many applications the question is not how the bearing reacts to the load, but what is the magnitude of the safe working load? To this end, the summary curves of Fig. 4.43 - 4.45 show clearly the effect of load and speed ratio on the journal eccentricity when operating in various bearings. Comparison with Fig 4.34 shows the increased load capacity of the Dynamically Loaded bearing over the Statically loaded bearing for the speed ratio $\sigma = 1$.

To establish the validity of these curves comparison with the work of other experimenters is necessary. Four publications are currently available for comparison. The experiments of Simons[19, 20] and Middleton[27] use unit bearing loads smaller than the oil supply pressure and form no basis for comparison. Carl, and Shawki and Freeman, have investigated journal behaviour

under loads comparable to the current experiments, but only the latter present summary curves. These agree closely with the full length curves of Fig 4.43 at σ=1 and .25 as shown on Fig. 5.22 and 5.23.

It may seem surprising that this Non-Dimensional Load Parameter has been successful in comparing Dynamic Loads, as the Sommerfeld Number is based on Static Load conditions which have no squeeze film action. The study of the journal paths has shown that at the instant of maximum eccentricity the journal supports the load by wedge action only - The Static Load condition. The applied loads in the current experiment have a closely related variation with time, so that a similar proportion of the maximum load would be applied at each instant of maximum eccentricity. This accounts for the successful use of the Sommerfeld Number in the summary curves.

There is a danger in extending the use of these curves to conditions where the load does not vary sinusoidally with time. Further extensive investigations with alternative load forms will be required to establish the universality of the summary curves.

5.3 Bearing Friction

The coefficients of friction presented on Fig 4.46 are in close agreement with those published by Clayton and Jakeman but disagree with those published by Du Bois and Ocvirk Fig 5.24. The only variable not easily considered in these comparisons is the extent of cavitation in the oil film.

Cameron and Wood, and Sassenfeld and Walther assume that either the cavitated film behaves as an uncavitated film from the friction point of view, or that there is a complete film in the unloaded arc of the bearing. Jakobsson and Floberg calculate friction as the summation of components for the cavitated and uncavitated region. These theoretical treatises predict higher values of friction coefficient than has been measured experimentally in the 360° bearing Fig 5.25. This indicates that oil in a cavitated condition does not behave as oil in an uncavitated condition from the friction point of view and that the Jakobsson and Floberg estimation of friction in the vapour region is pessimistic or that the extent of the cavitation area is greater than they predicted.

The pressure surveys indicated that under Static Loads, 20% of the bearing surface was covered by large stable air bubbles and

this certainly accounts for the difference in the friction coefficients predicted by Sassenfeld and Walther, and Jakobsson and Floberg. One contributory factor to the 30% difference between Jakobsson and Floberg's predictions and the experimental measurements will be the affect of the variable temperature and pressure in the oil film on the friction produced by a given rate of shear.

The case of no friction in the unloaded arc is analogous to the calculations for 180° bearings. The experimental results show close agreement with the 180° case for Sommerfeld Number $< .15$ with diverging values at lighter loads. This indicates that the friction in the cavitated region is negligible and that as the static load increases the corresponding increase in cavitation reduces the friction force on the bearing.

The close agreement between measured and calculated friction for the half length bearing Fig 4.47, raises the question of the existance of a cavity in such a narrow bearing. No information as to the state of the oil film in the unloaded arc of the bearing is available at the time of writing.

The large difference in friction coefficients discussed above raises the possibility of faulty measuring technique. The author

is of the opinion that, as the friction torques are in agreement with those measured by Clayton and Jakeman and are lower in magnitude than those predicted theoretically, the techniques employed are valid. Had the measured friction values been significantly higher than the theoretical predictions some doubt as to the accuracy of the techniques would have been justified.

The observed pattern of friction variation under Dynamic Loads is compatable with the concept of a simple elliptical journal path. When the path becomes complicated, additional maximum values of friction occur within the period of the load cycle, Fig 4.55, 4.61, and 4.62. Where a complication in the journal path coincides with the point of maximum eccentricity a large friction force is recorded, Fig 4.55 - $\omega_p t = \frac{5\pi}{6}$ and Fig 4.62 - $\omega_p t = \frac{\pi}{3}$. Where the complication occurs remote from the point of maximum eccentricity or where the point of maximum eccentricity occurs remote from the complication, a smaller maximum value of friction force results.

Two exceptions to these rules occur in Fig 4.51 and 4.53. In both cases the journal follows a simple path and a possible explanation is that the additional friction maximum is due to

localised contact between the journal and the bush.

The friction variable curves indicate that, outside the zone of thin film lubrication, a full length bearing operates with a lower coefficient of friction than a half length bearing supporting the same unit bearing load. The zone of thin film lubrication which occurs in both bearings at Sommerfeld values $< .075$, infers that the peaks of the journal and bearing surfaces are in contact due to either the thinness of the oil film or some variable misalignment. The criticality of bearing and journal alignment in friction measurement is illustrated by the scatter of friction coefficients measured in the full length bearing. Measurements made before and after reassembling the full length bearing are presented in Fig 4.48 - 4.50. A single curve drawn through the values from each test series would approximate the best line shown on these figures.

The variations in friction force indicated in Fig 4.51 - 4.62 contradict the findings of Shawki & Freeman who reported that the friction force under similar conditions varied by only a few percent about a mean value. Shawki and Freeman used an assembly, with a solid drive connecting, a motor armature, flywheel, and test journal, which presumably had sufficient inertia at speeds up to 1500 r.p.m.

to absorb the true fluctuations in journal friction.

Comparison of the friction characteristics of the full length bearing indicates that when supporting Dynamic Load the bearing operates under thin film conditions at lighter loads than when supporting static loads.

5.4 Oil Flow

The oil film in a bearing can be split into separate areas for the estimation of oil flow. The convergent film, in which oil is above atmospheric pressure, will lose oil by end leakage and the divergent film in which subatmospheric pressures exist will draw oil into the bearing if advantageous conditions exist at the ends of the bush. The oil flow from the convergent film is definite and predictable and can be considered as the theoretical flow for the bearing. Variation of the measured flow from this value will indicate the adequacy of the oil supply to the bearing.

Theoretical calculations are based on the assumption that the bearing has a complete oil film at the point of maximum film thickness, a condition not substantiated by the pressure surveys of § 4.1. In recognition of the implication of these surveys the theoretical flow has been calculated as the difference in the oil

flow passing the oil inlet groove and the point of minimum film thickness as detailed in appendix A. Fig 4.63 - 4.65 show that the oil supply was inadequate for loads with Sommerfeld Numbers $<.2$. Whether this missing oil was in fact drawn from the leakage oil is not known. What is certain is that if conditions favoured the flow of oil into the low pressure region of the oil film, then under the static load test conditions that oil was available at the ends of the bearing.

The author has been unable to formulate a simple method of predicting oil flow under Dynamic Loads. The results of Fig 4.66 indicate that over a large range of applied loads the flow, is independent of Sommerfeld Number, and is less than the flow under an equivalent Static Load. This latter fact was reflected in the higher bearing temperatures measured under Dynamic Load conditions.

5.5 Comparison of Analytical and Experimental Results

Any given analysis in the range of finite bearing analyses currently available (Ref. 10-15) gives a clear qualitative indication of the behaviour of a journal bearing under any given polar load diagram. The investigation of journal bearings in large scale

experimental rigs indicates that the variable viscosity of the lubricant and the deflection of the bearing elements prevents good quantitative agreement between the measured and predicted behaviour of a journal bearing supporting Dynamic Loads in the normal working range of $P \geqslant 500$ p.s.i.

The computerised analysis of Lloyd et al[16] is the most comprehensive analysis currently available but no quantitative assessment of its results, based on a detailed comparison with the measurements from a large scale testing machine, has been available to date. An initial assessment has been made in the course of this research programme by supplying the load variations, shown in Fig 4.51 and 4.57 as applied to full length and half length bearings respectively, for analysis by Lloyd's programme. The resultant comparison is limited by the adaptability of the analysis to the particular problem set by any given bearing geometry. As presented the analysis handles bearings with any desired length to diameter ratio, provided it has some form of circumferential groove. The current axially grooved bearings are analysed as bearings with circumferential grooves at the extremities of a single land. The analysts' choice of uniform viscosity is that of the oil at outlet temperatures but, in fact, the solution of the

Reynold's Equation presented in this comparison is based on a viscosity equivalent to the maximum oil film temperature in the bearing; the author's choice (§ 4.2).

The measured and predicted journal centre paths for the full length bearing, Fig 5.26, show points of close agreement. The major axis of both paths lie in close proximity and the eccentricity of the journal at the instant of maximum Dynamic Load is substantially the same although the phase angles are different (points 4 and 12). The marked difference in the magnitude of the minimum eccentricity is due to the presence of axial grooves in the test bearing. The major disruption of the circumferential pressure profile in the vicinity of the groove rapidly reduces the oil film pressures in that region (Fig 4.15 and 4.26), so that the journal tends to travel in the direction of the applied load as the squeeze film pressures develop, points 0 - 4 and 8 - 12.

Circumferential grooves at the end of the analytical bearing must reduce the leakage rate from the load bearing pressure film as the ends of the bearing are 30 p.s.i. above atmospheric. The increase in the time required to disperse the squeeze film pressure, results in the analytical bearing running with a thicker film as the load reduces to zero.

Similar comments can be made regarding the half length bearing Fig 5.27, where as discussed in § 5.2 the major axis of the journal centre path is restrained by the axial grooves to a position close to the load line. The effect of the circumferential grooves in the analytical model does not have the same effect on the leakage rate from the half length bearing and the maximum eccentricities are similar in magnitude while the corresponding phase angles differ.

This analysis indicates the position and extent of the arc on the bearing centre-line with subatmospheric pressures which define analytically the disrupted film. The variations in the computed arc of oil film disruption are presented in Fig 5.32 along with similar variations of experimental arc length from Fig 5.9 - 5.14. The greater disrupted area predicted by the analytical study can be ascribed to the position of the grooves as the experimental bearing has a maximum arc of 180 degrees and not of 200 degrees as indicated. The analytical study does not recognise the existance of an air/oil mixture in the calculation of oil pressures and indicates the existance of a disrupted film over a shorter period of the load cycle than has been determined experimentally. In fact

the time required to dissolve the air in a bearing similar to the analytical model would be greater than that required by the experimental bearing as the circumferential grooves at the bearing ends prevent any escape of air from the Low Pressure region of the bearing.

The considerable differences between the computed journal friction and the measured bearing friction, indicated on Fig 5.33, are magnified by the author's selection of maximum film temperature as a basis of comparison. The shear forces in an oil film are proportional to the viscosity of the oil in that film, and the selection of an outlet or other mean temperature would be more suitable for friction calculations. The analytical curve presented on Fig 5.33 has been simplified by the removal of a large number of 'spikes' which are a peculiarity of the methods employed. The indications of zero friction force of which there are 5 per cycle are due to insufficient accuracy in the computer print out to cover a load phase increment of 0.333 degrees.

If the choice of maximum oil film temperature is accepted as a basis of oil viscosity, then these initial comparisons indicate that Lloyds' analysis is the first quantitatively accurate analysis to be

published for the determination of minimum film thickness. A basis for selecting a suitable viscosity for accurately predicting the variations of journal friction under Dynamic Loads has yet to be established.

COMPARISON OF THEORETICAL AND EXPERIMENTAL

PRESSURE DISTRIBUTIONS

STATIC LOAD: 6·7 TONF

DIAMETRAL CLEARANCE: ·003 INS.

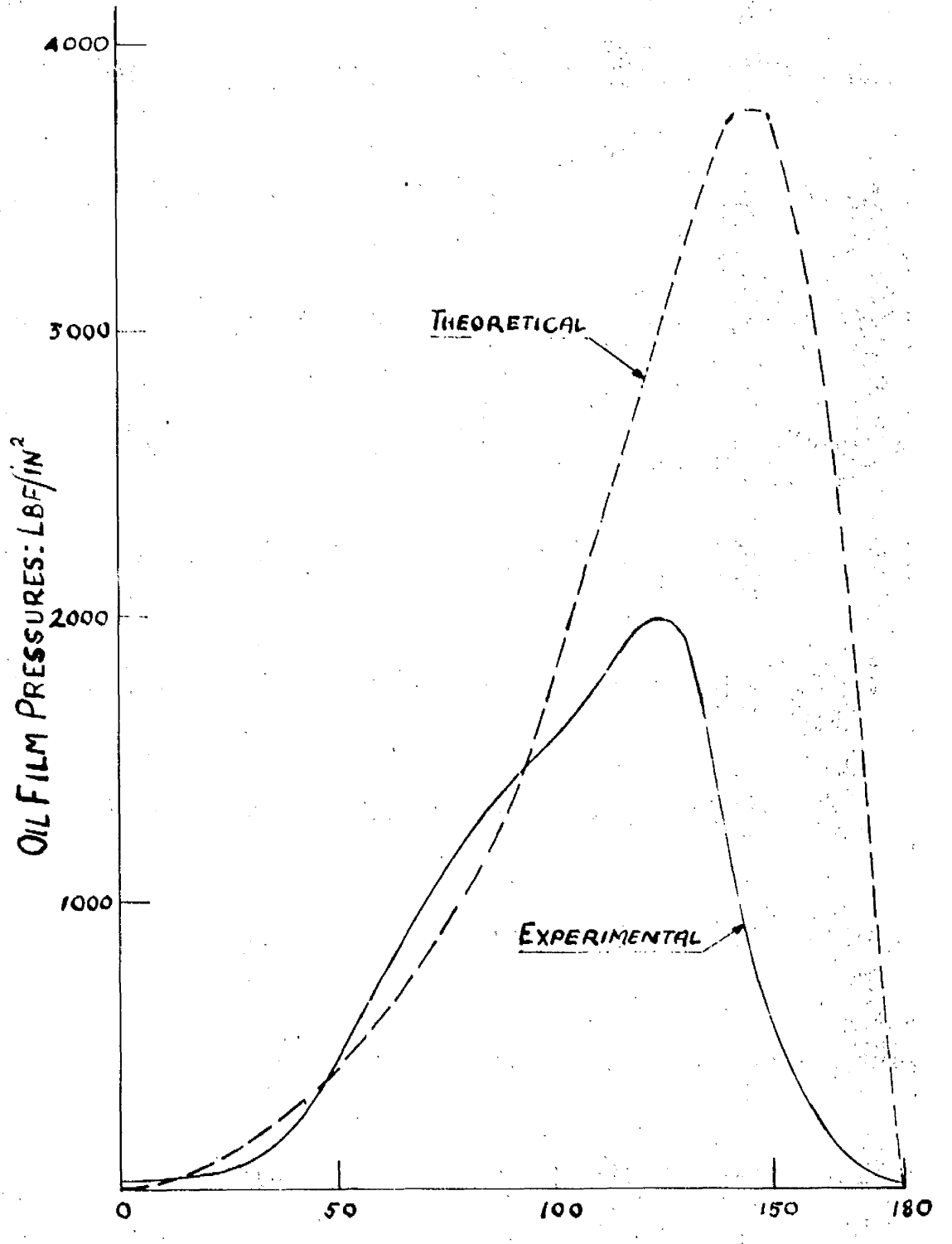

FIG: 5·1

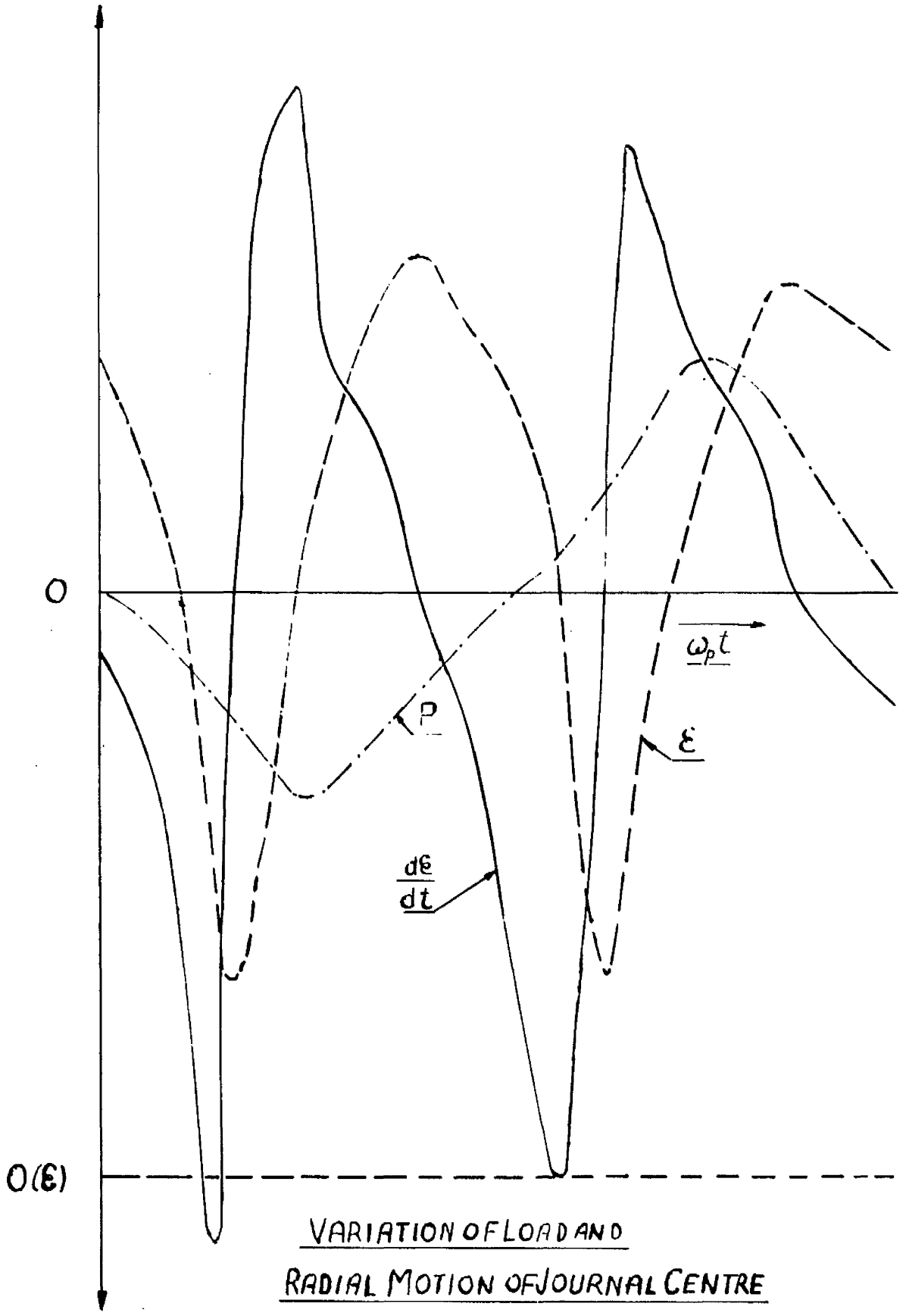

VARIATION OF LOAD AND
RADIAL MOTION OF JOURNAL CENTRE
WITH TIME

FIG: 5·2

EXPERIMENTAL RESULTS: 4 33 TONS f DYNAMIC LOAD $\phi = 270^\circ$

PRESSURE CONTOURS ON UNLOADED ARC OF BEARING : 3·0 DIA. × 3IN. LONG × ·0015 IN DIA. CL.

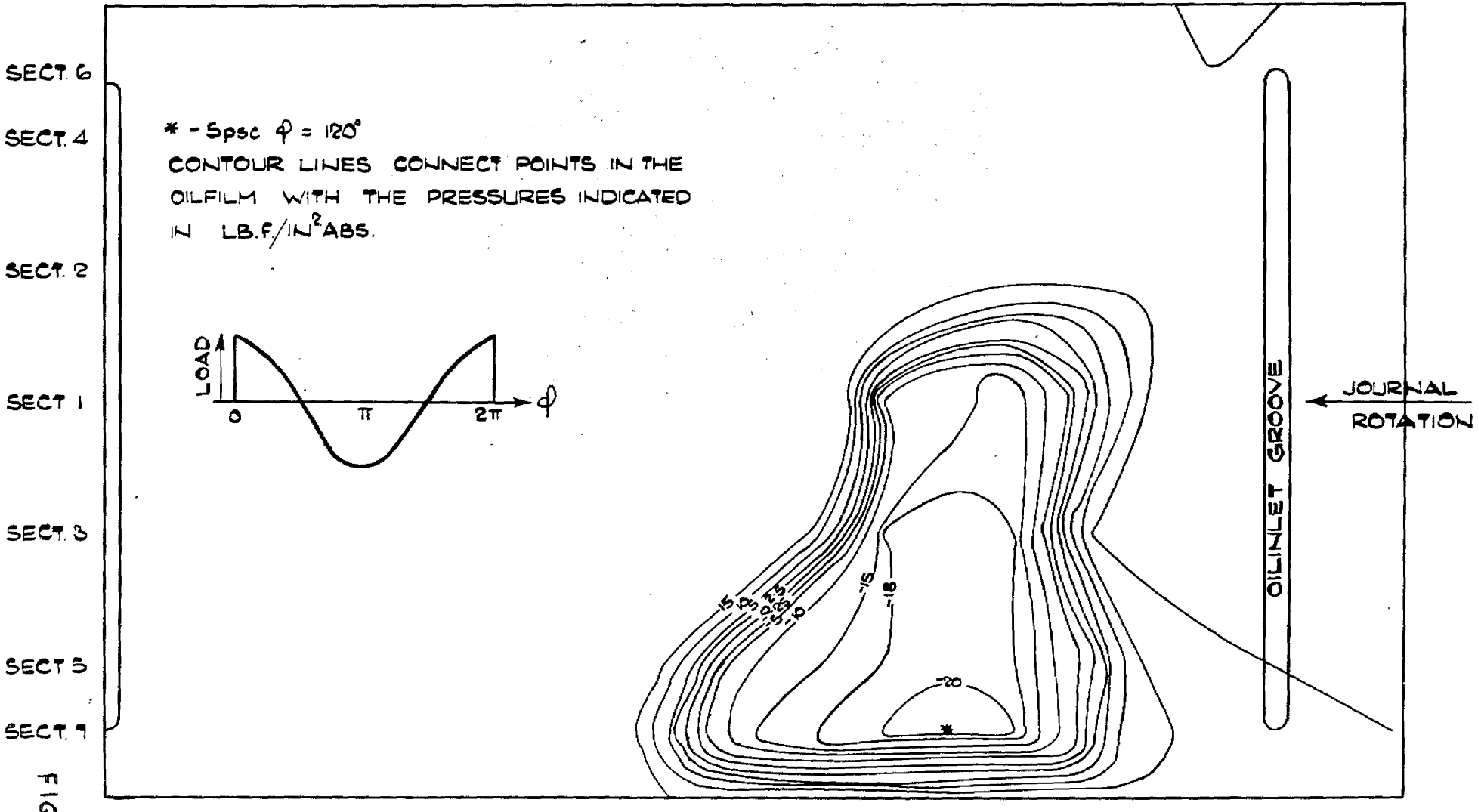

DEVELOPED BEARING SURFACE

FIG. 5·3

FIG. 5·3

EXPERIMENTAL RESULTS: 4·33 TONS f DYNAMIC LOAD ϕ = 300

PRESSURE CONTOURS ON UNLOADED ARC OF BEARING : 3·0 DIA. x 3INS LONG x ·0015 IN DIA. CL

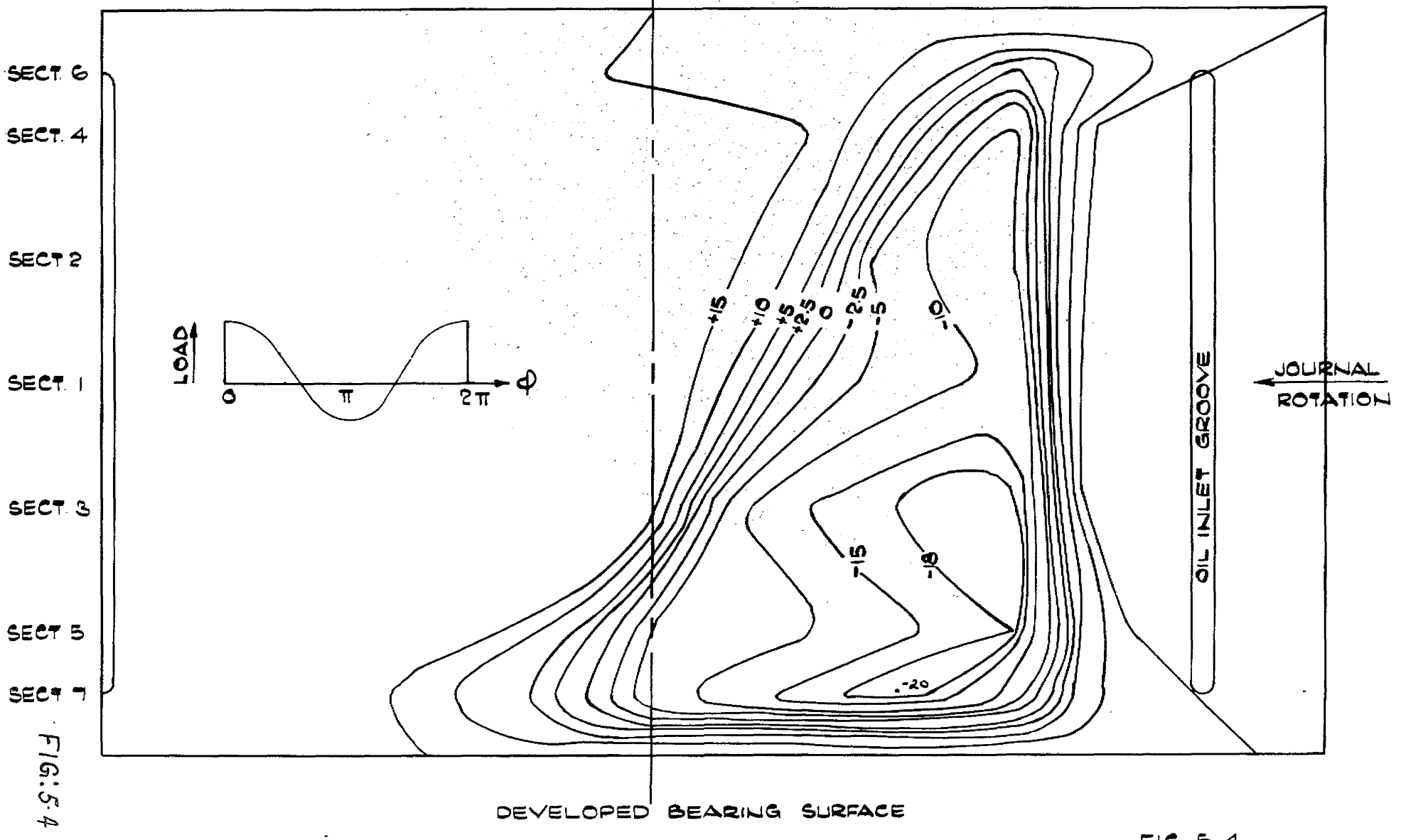

FIG 5·4

FIG 5·4

EXPERIMENTAL RESULTS : 4·33 TONS.f DYNAMIC LOAD ϕ= 330

PRESSURE CONTOURS ON UNLOADED ARC OF BEARING : 3·0 DIA. × 3IN. LONG × ·0015 IN DIA. CL

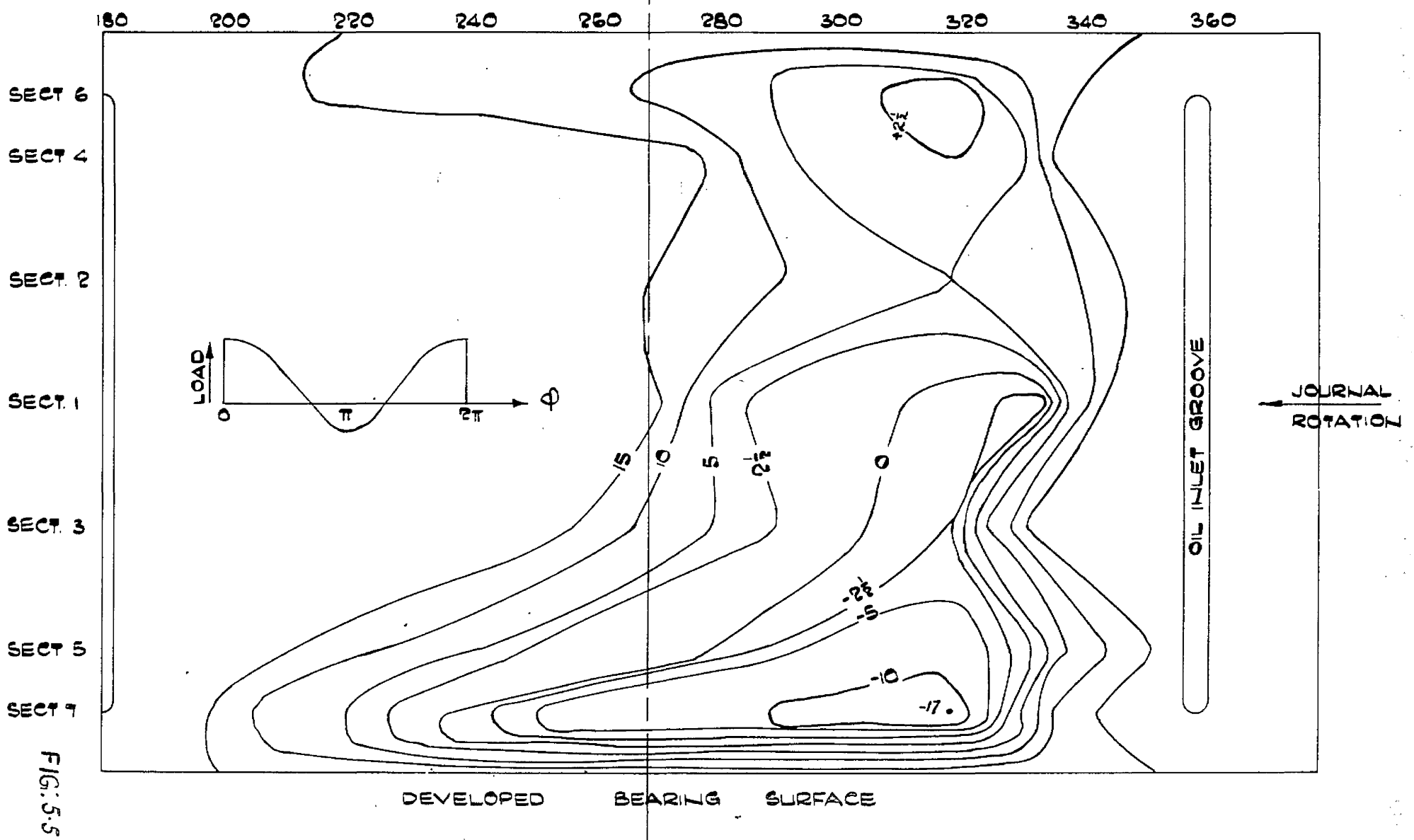

FIG. 5.5

FIG 5·5

EXPERIMENTAL RESULTS : 4·33 TONS f DYNAMIC LOAD $\phi = 20$

PRESSURE CONTOURS ON UNLOADED ARC OF BEARING : 3·0 DIA. × 3 INS. LONG × ·0015 DIA. CL.

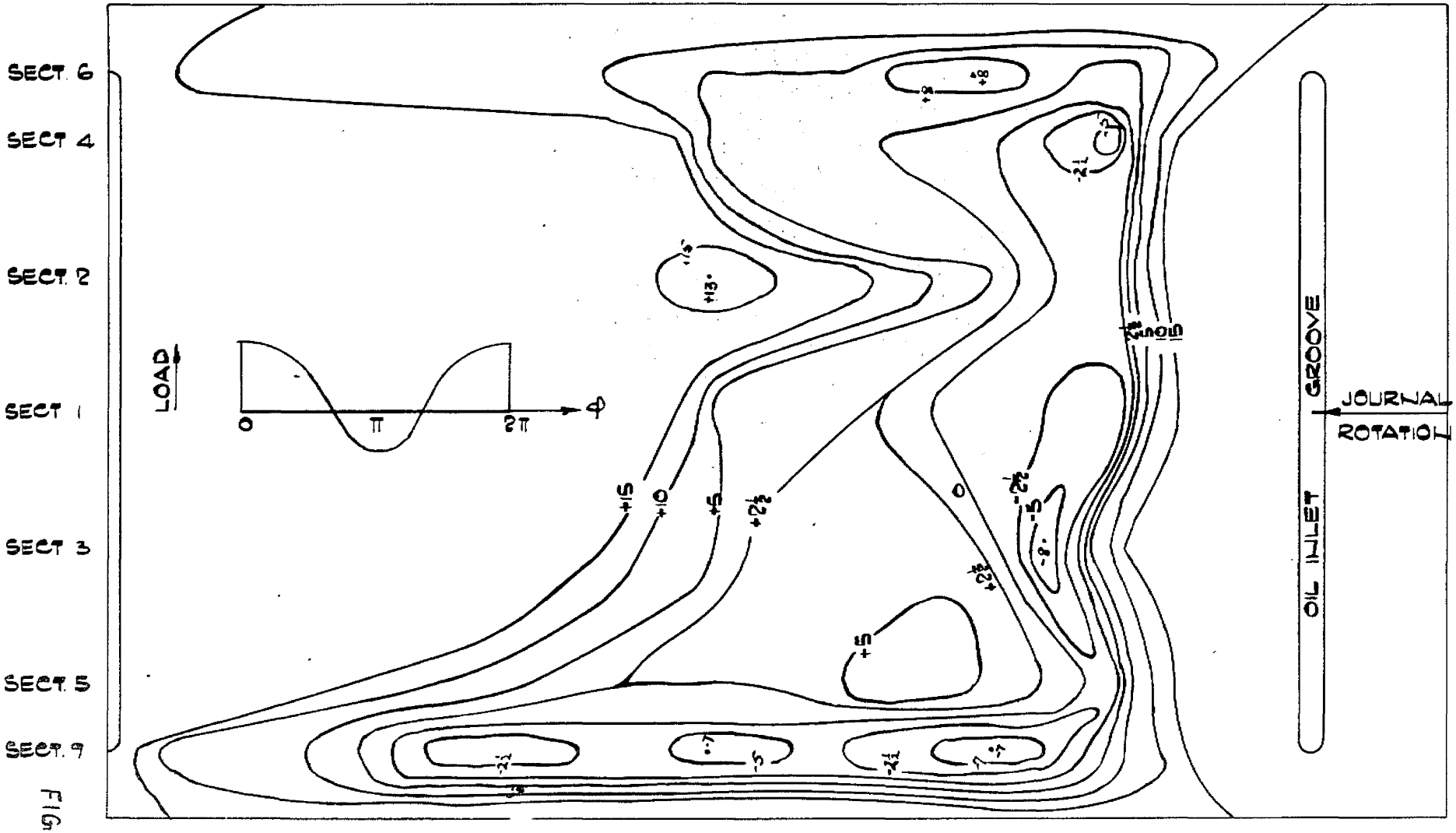

FIG. 5·6

FIG 5·6

EXPERIMENTAL RESULTS : 4·33 TONS f DYNAMIC LOAD $\varphi = 30$

PRESSURE CONTOURS ON UNLOADED ARC OF BEARING : 3·0 DIA x 3 INS. LONG x ·0015 IN. DIA. CL

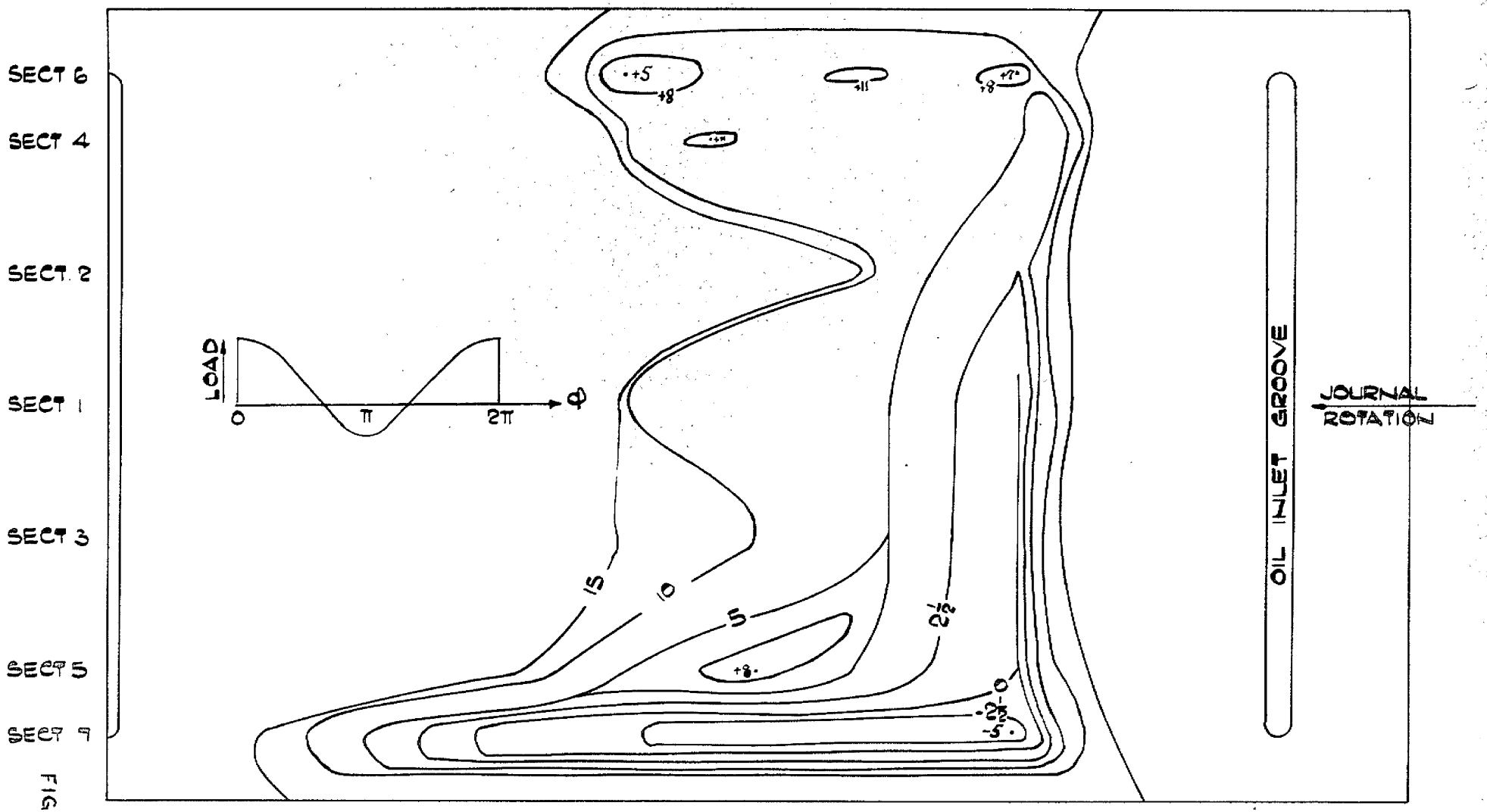

DEVELOPED BEARING SURFACE

FIG. 5·7

FIG. 5·7

4.33 lbf/in² $\varphi = 60°$

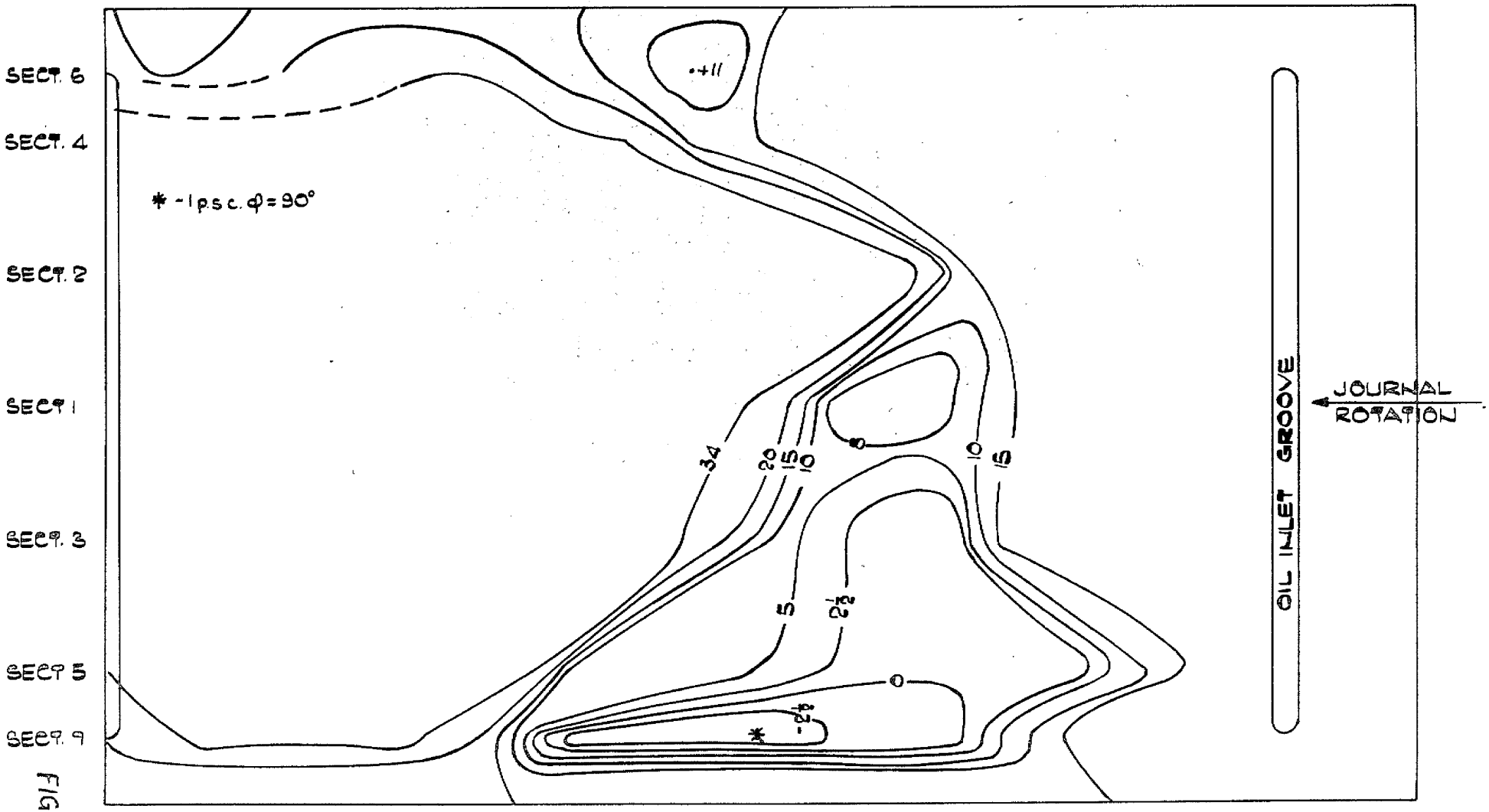

FIG. 5.8

FIG. 58

EXPERIMENTAL RESULTS: 6·25 TON.f DYNAMIC LOAD $\varphi = 270°$
PRESSURE CONTOURS ON UNLOADED ARC OF BEARING: 3·0 in. DIA. × 3·0 in. LONG × ·003 in. DIA. C.L.

CONTOUR LINES DRAWN THROUGH POINTS IN THE OIL FILM WITH THE PRESSURES INDICATED IN LB.f./IN^2 ABS.

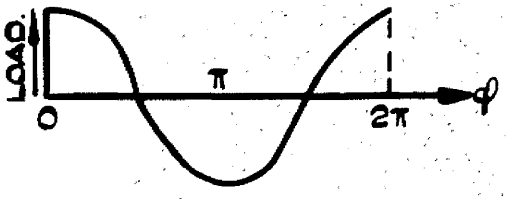

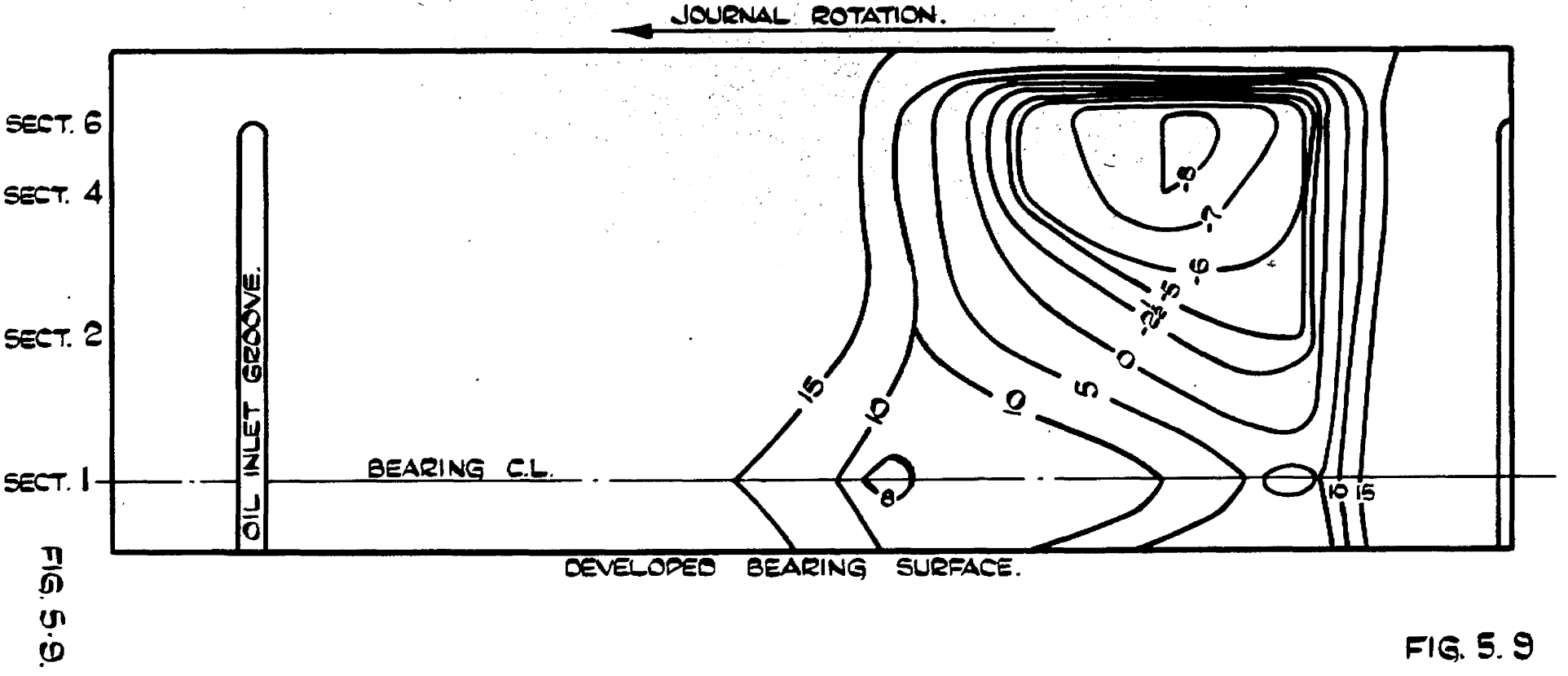

FIG. 5.9

FIG. 5.9

EXPERIMENTAL RESULTS : 6·25 TON.f. DYNAMIC LOAD φ = 300°
PRESSURE CONTOURS ON UNLOADED ARC OF BEARING : 3·0 in. DIA. × 3·0 in LONG × ·003 in. DIA. C.L.

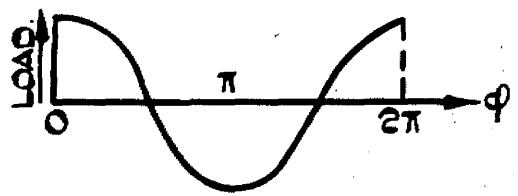

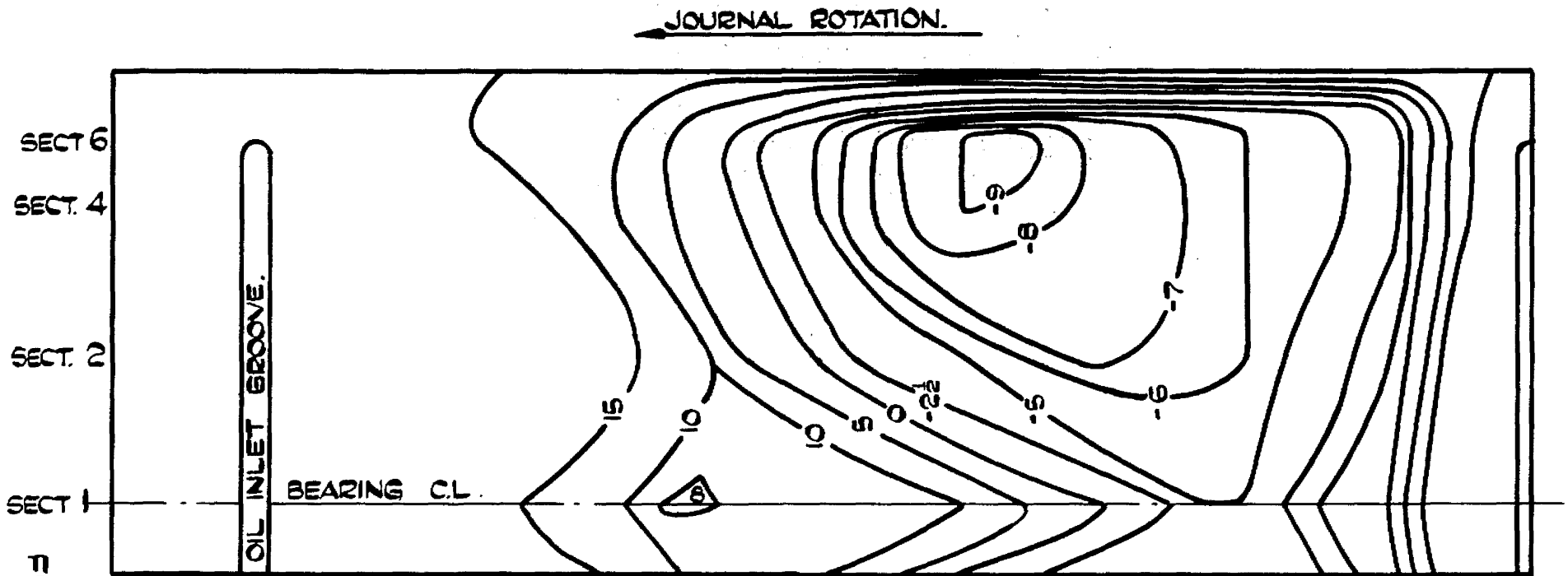

FIG. 5.10.

EXPERIMENTAL RESULTS : 6·25 TON. f. DYNAMIC LOAD $\varphi = 330°$
PRESSURE CONTOURS ON UNLOADED ARC OF BEARING : 3·0 in. DIA. × 3·0 in. LONG × ·003 in. DIA. C.L.

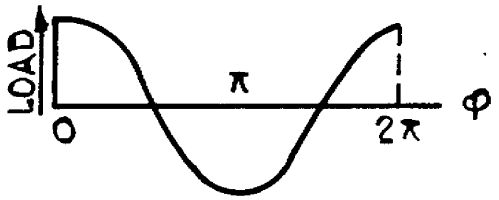

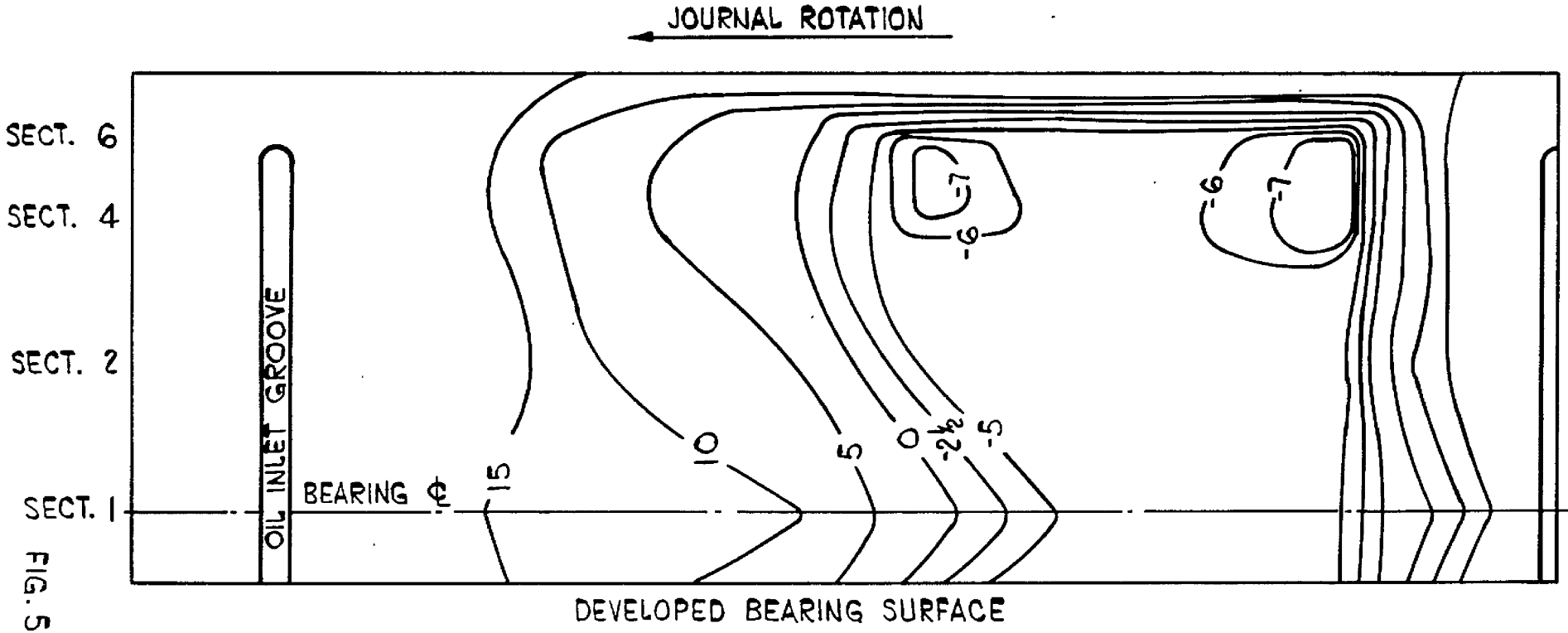

FIG. 5·11

FIG. 5·11

EXPERIMENTAL RESULTS : 6·25 TON.f. DYNAMIC LOAD $\varphi = 0^\circ$
PRESSURE CONTOURS ON UNLOADED ARC OF BEARING : 3·0 in. DIA. × 3·0 in. LONG × ·003 in. DIA. C.L.

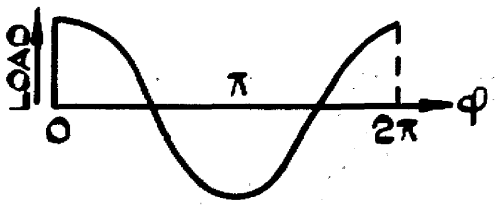

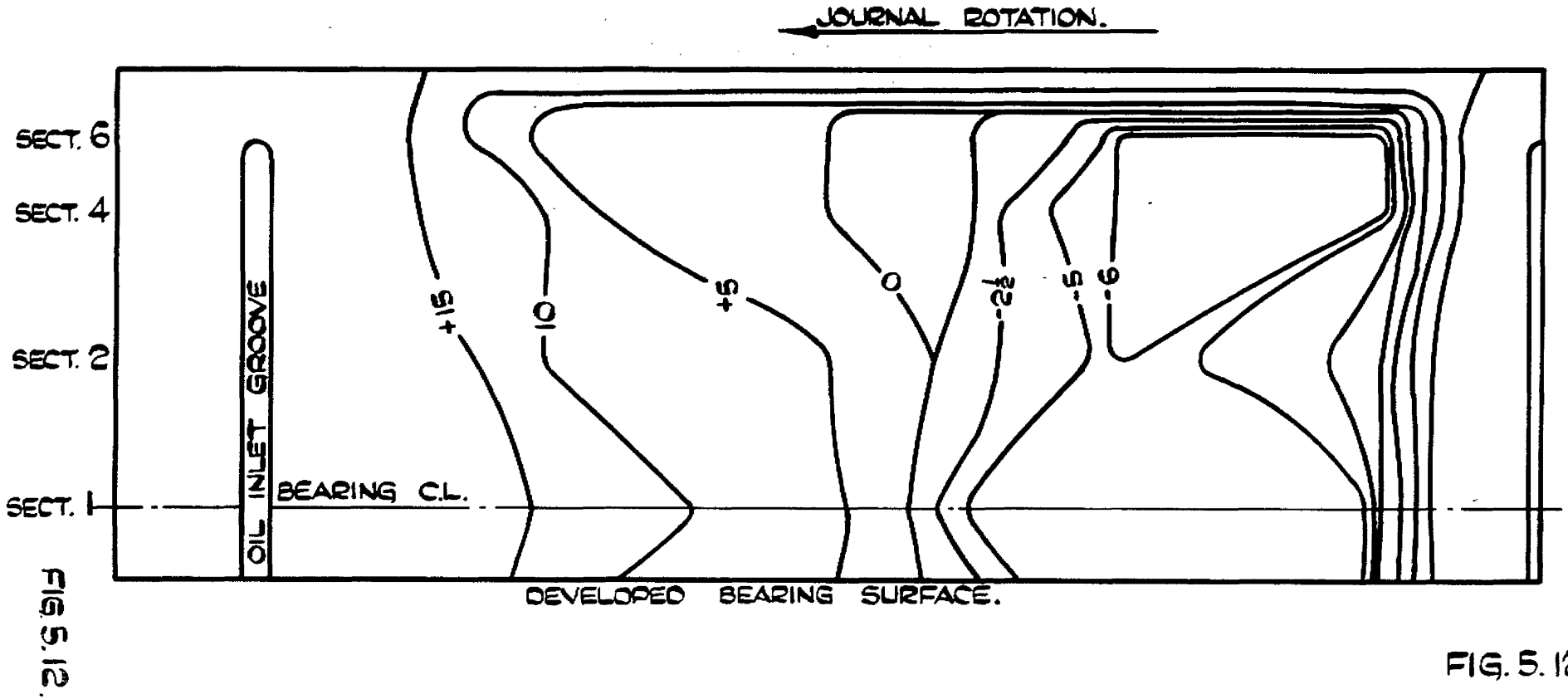

FIG. 5.12

FIG. 5.12

EXPERIMENTAL RESULTS: 6·25 TON.f. DYNAMIC LOAD $\varphi = 30°$
PRESSURE CONTOURS ON UNLOADED ARC OF BEARING: 3·0 in. DIA. × 3·0 in. LONG × ·003 in. DIA. C.L.

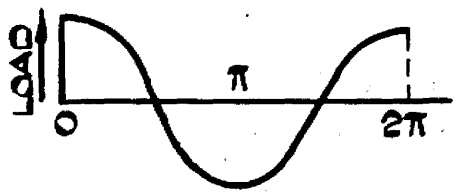

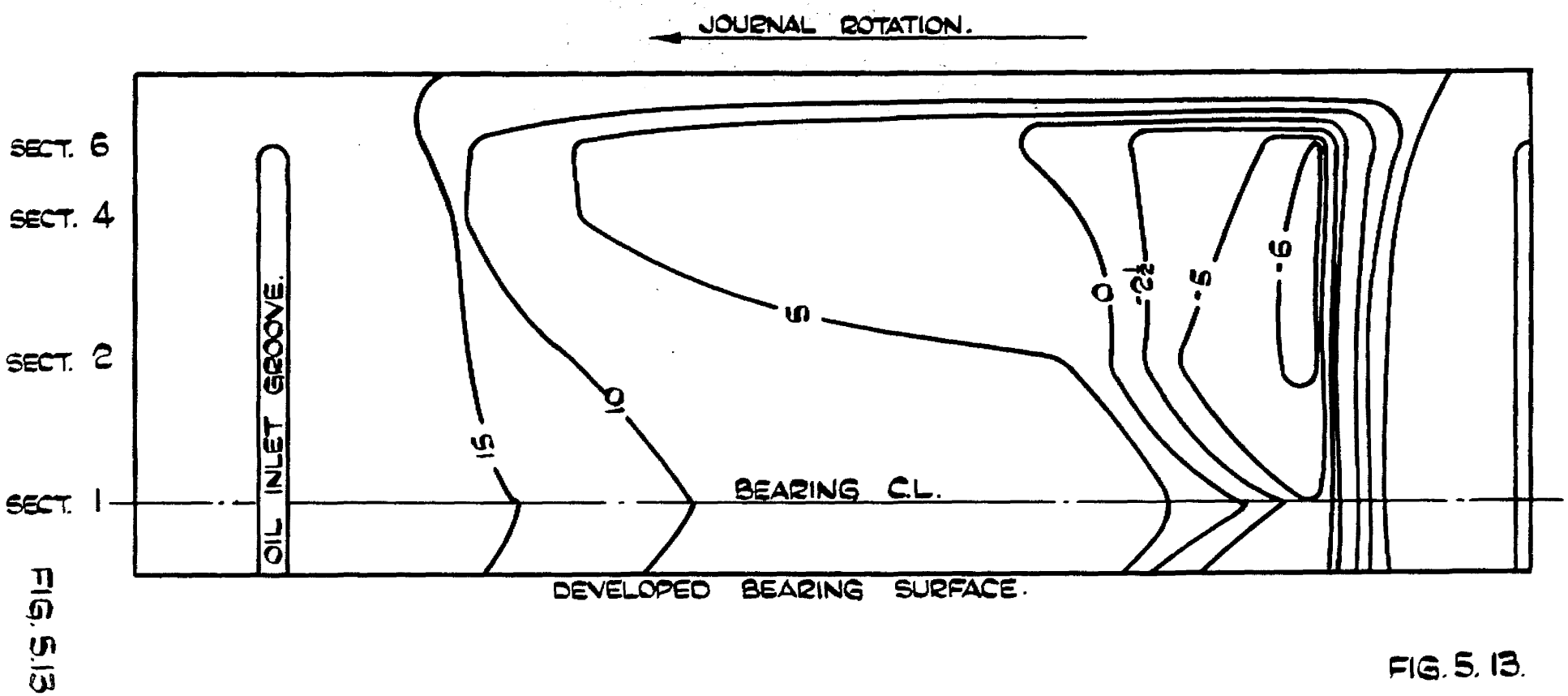

FIG. 5. 13.

EXPERIMENTAL RESULTS: 6·25 TON.f. DYNAMIC LOAD φ = 60°
PRESSURE CONTOURS ON UNLOADED ARC OF BEARING : 3·0 in. DIA. × 3·0 in. LONG × ·003 in. DIA. C.L.

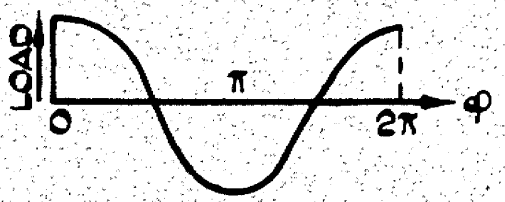

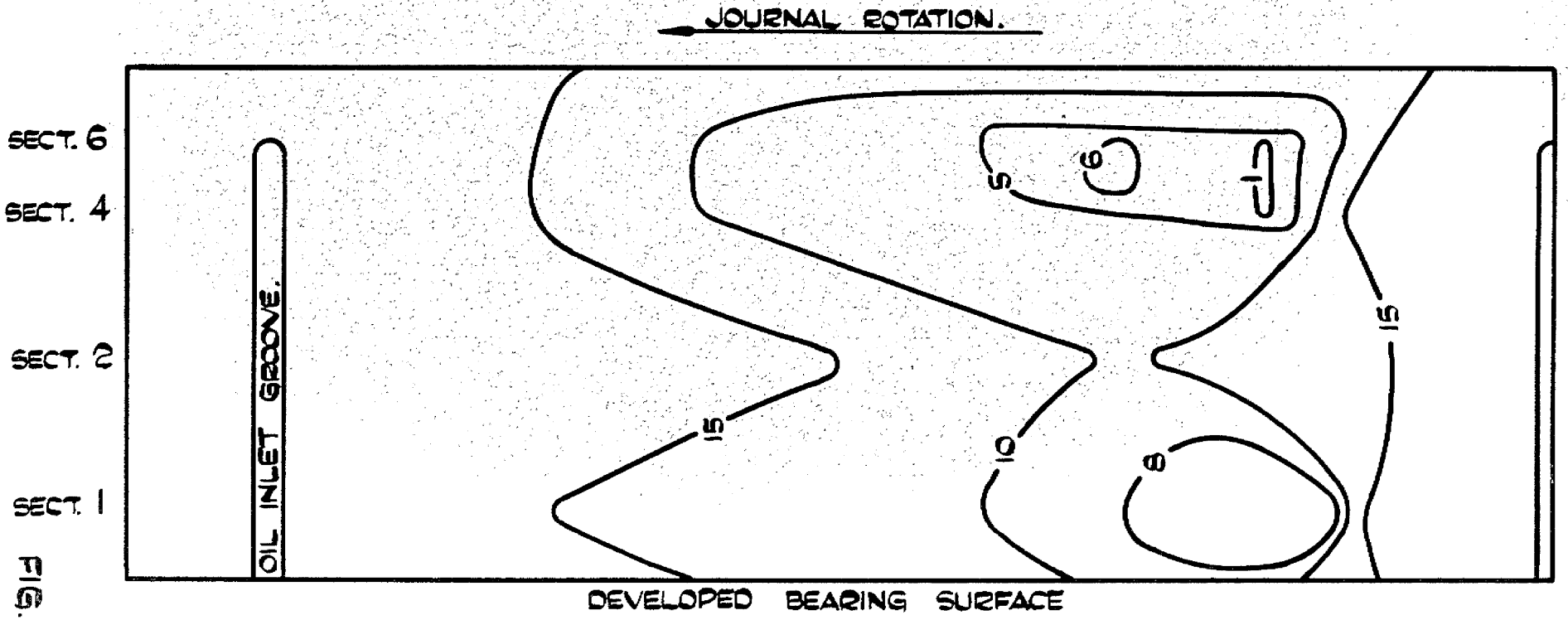

FIG. 5.14.

FIG. 5.14.

EXPERIMENTAL RESULTS
6·7 TONS f STATIC LOAD
PRESSURE CONTOURS ON UNLOADED ARC OF
BEARING: 3·01IN. DIA. × 3·00IN. LONG × ·003" DIA. CL.
CONTOUR LINES CONNECT POINTS IN THE OIL FILM WITH THE
PRESSURES INDICATED IN LB.f./IN.^{2} ABS.

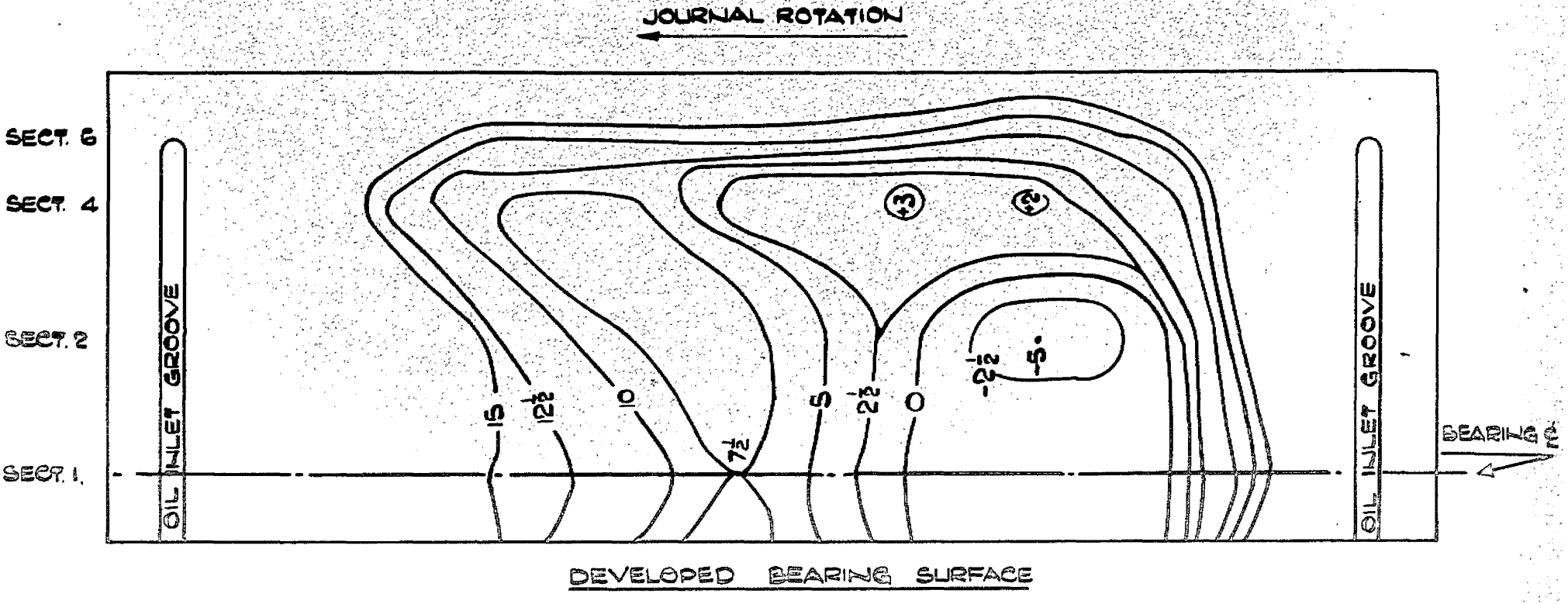

FIG. 5·15

FIG. 5·15

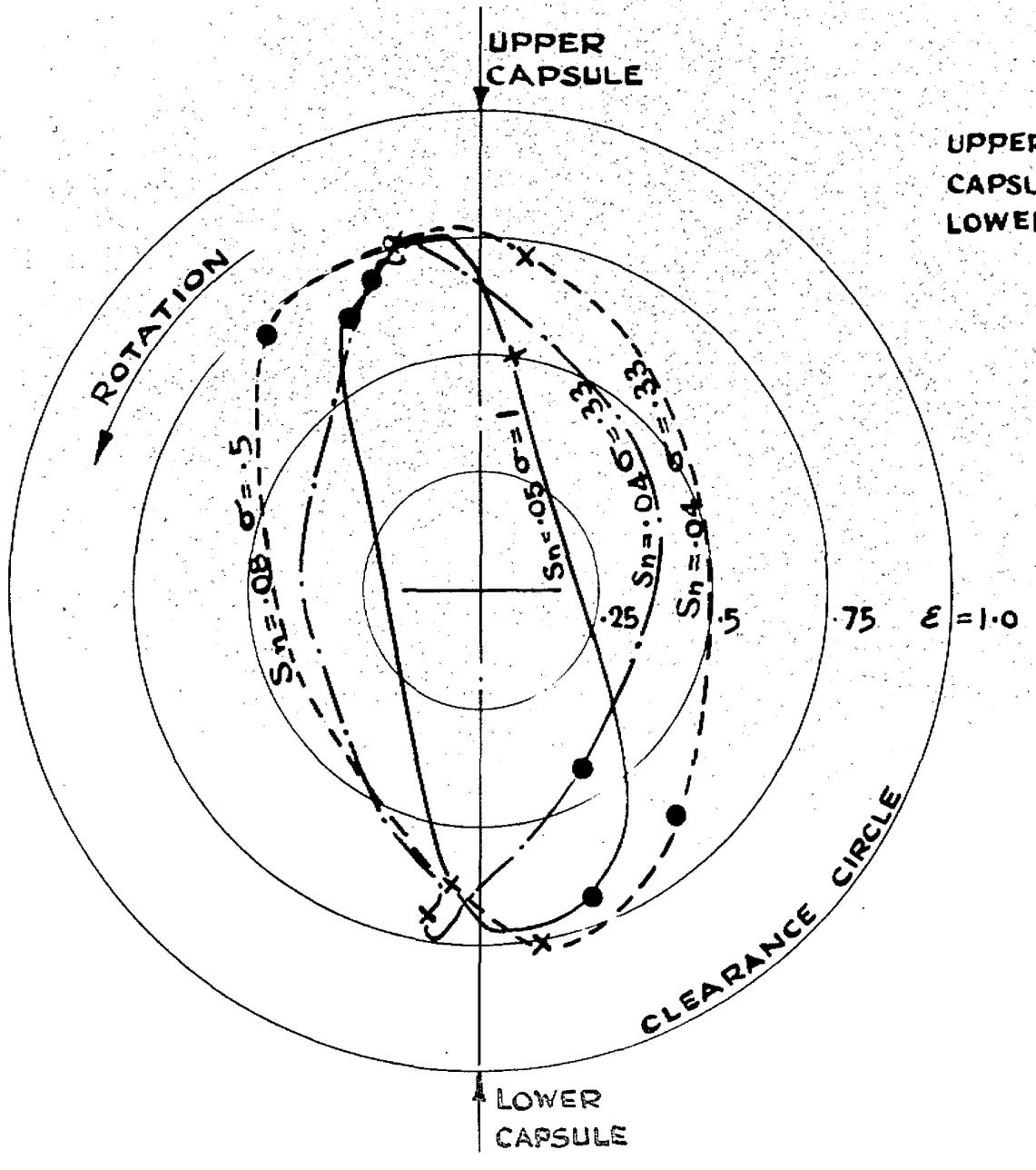

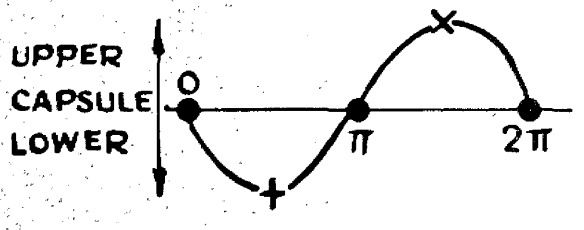

JOURNAL CENTRE PATHS

$\frac{L}{D}=1$ HEAVY LOADS

FIG. 5·16

FIG. 5·16

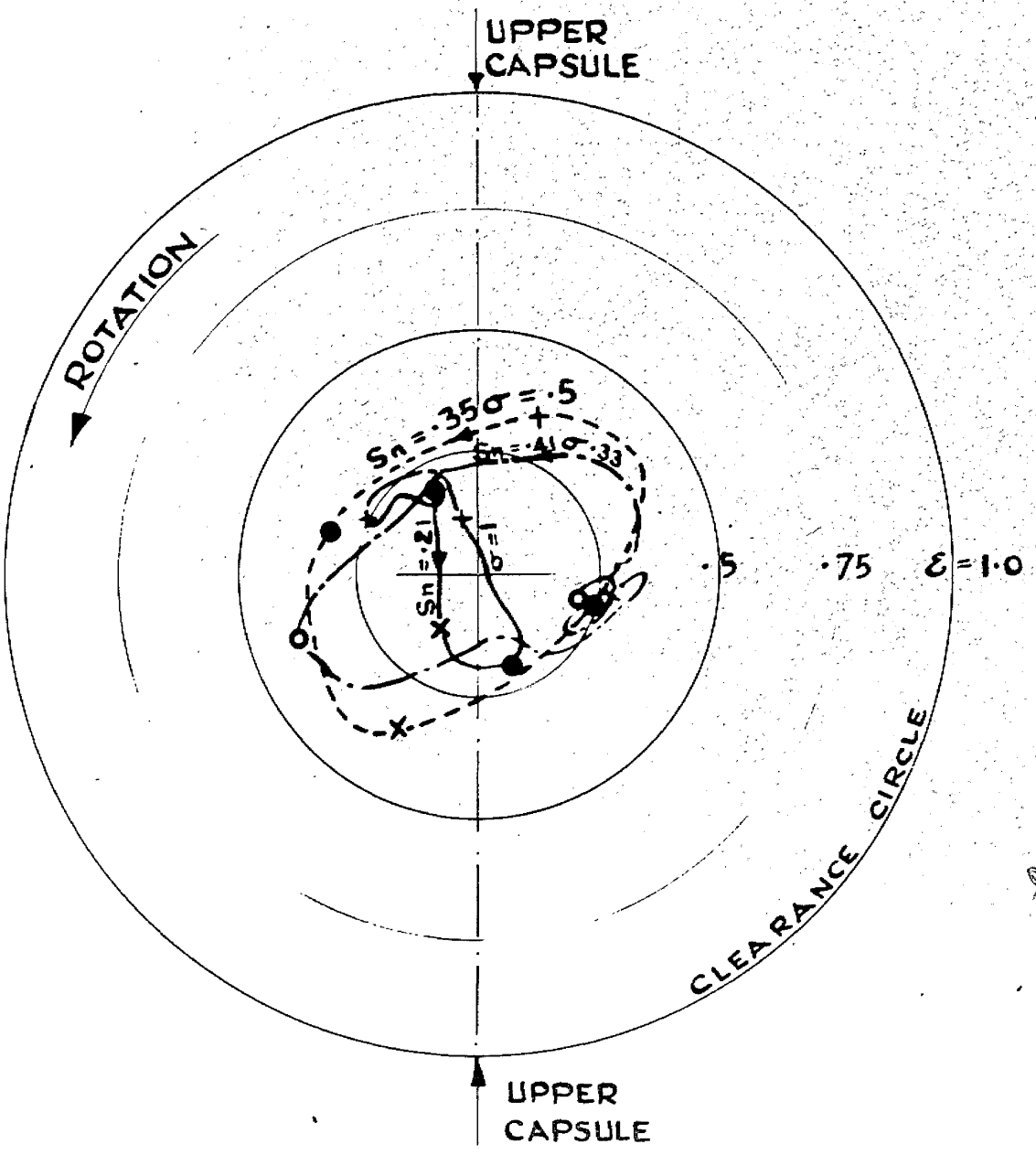

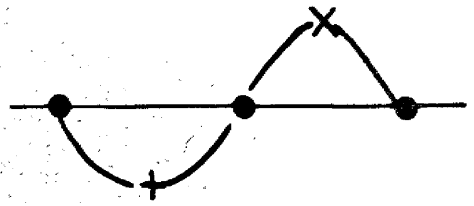

JOURNAL CENTRE PATHS
$\frac{L}{D} = 1$ LIGHT LOADS

FIG. 5·17

FIG. 5·17

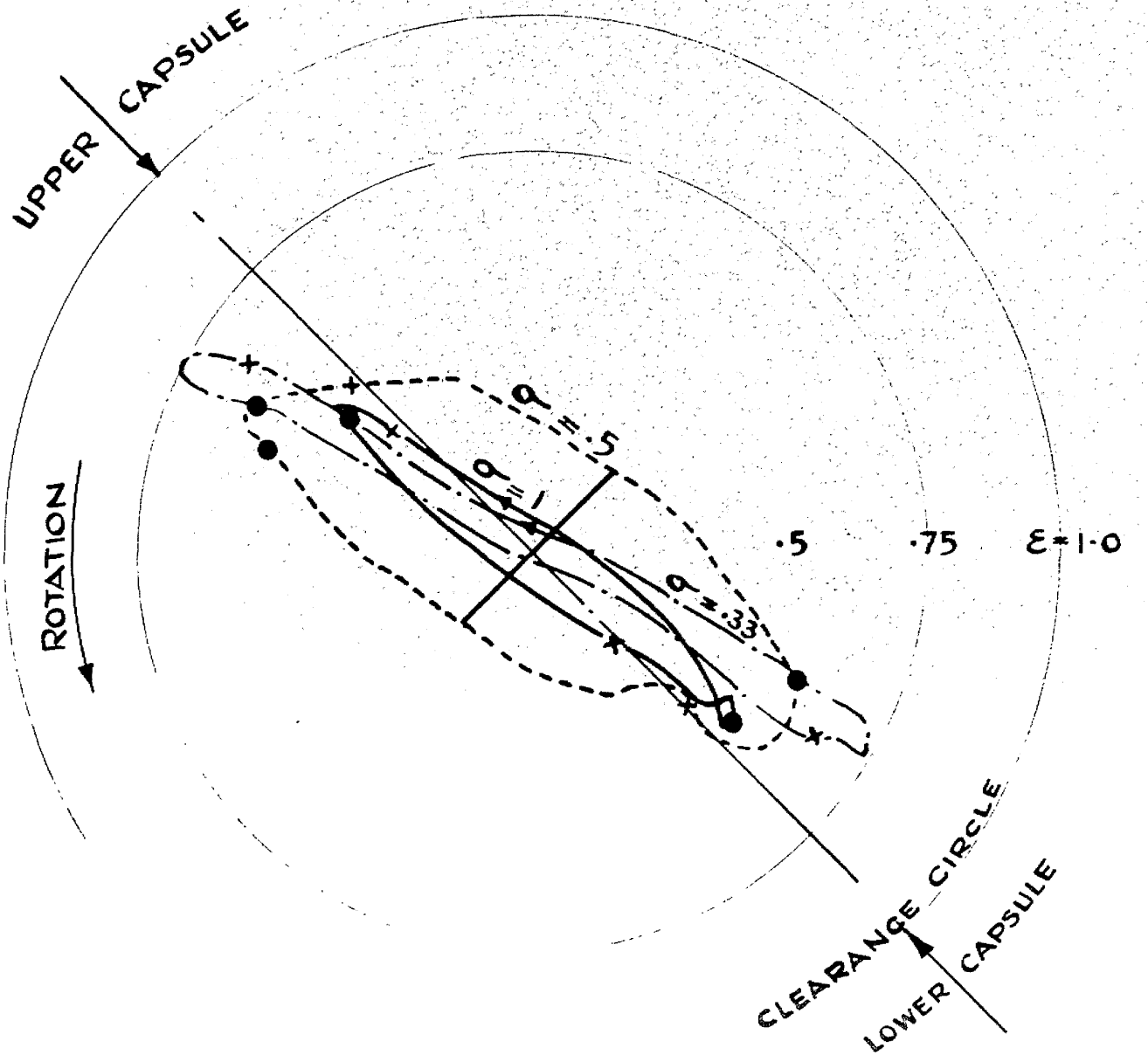

FIG. 5.18

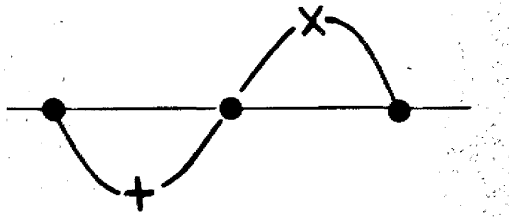

JOURNAL CENTRE PATHS
$\frac{L}{D}: \frac{1}{2}, S_n = \cdot 10$

FIG : 5·18

2ND TESTING MACHINE
STATIC LOADS

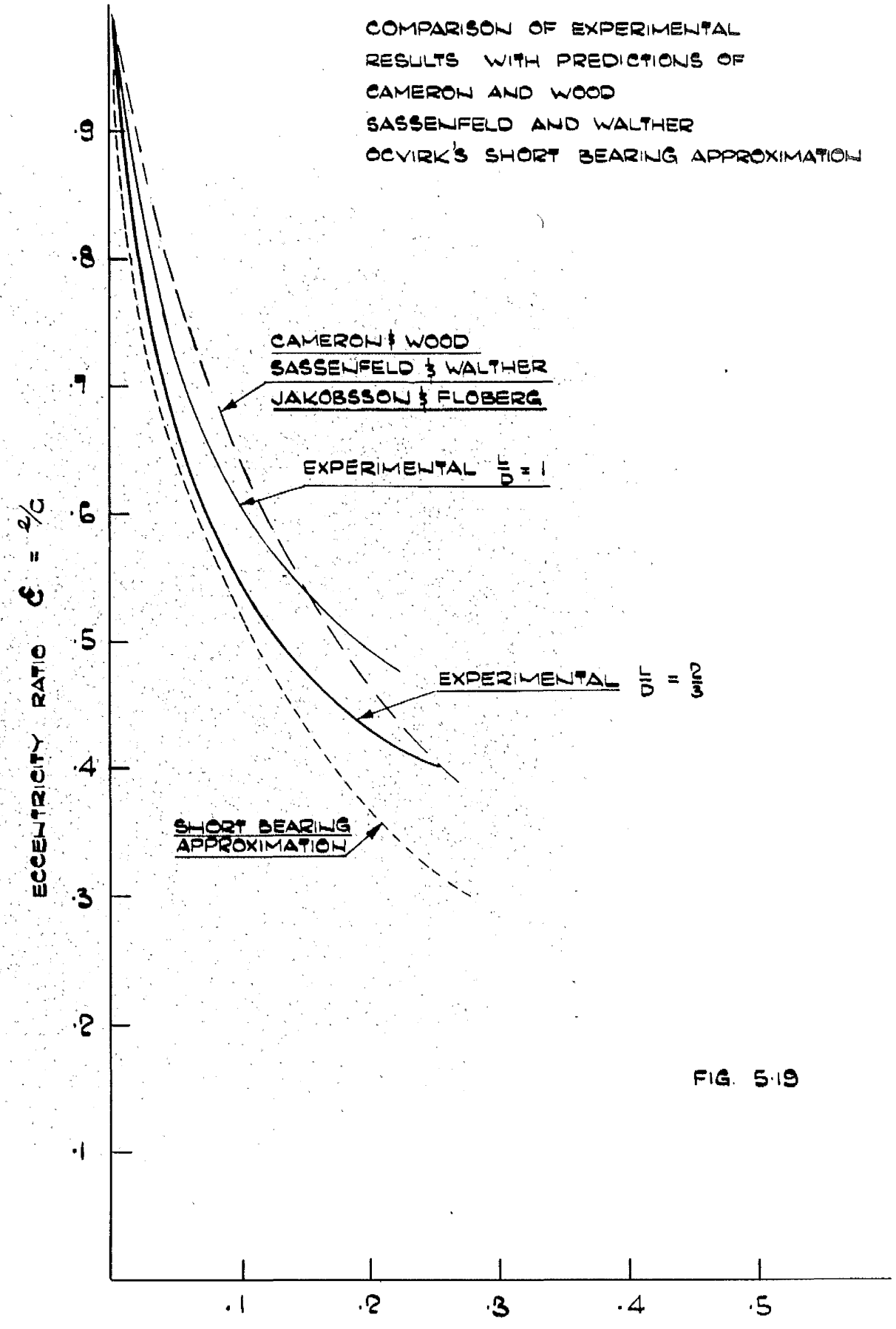

FIG. 5.19

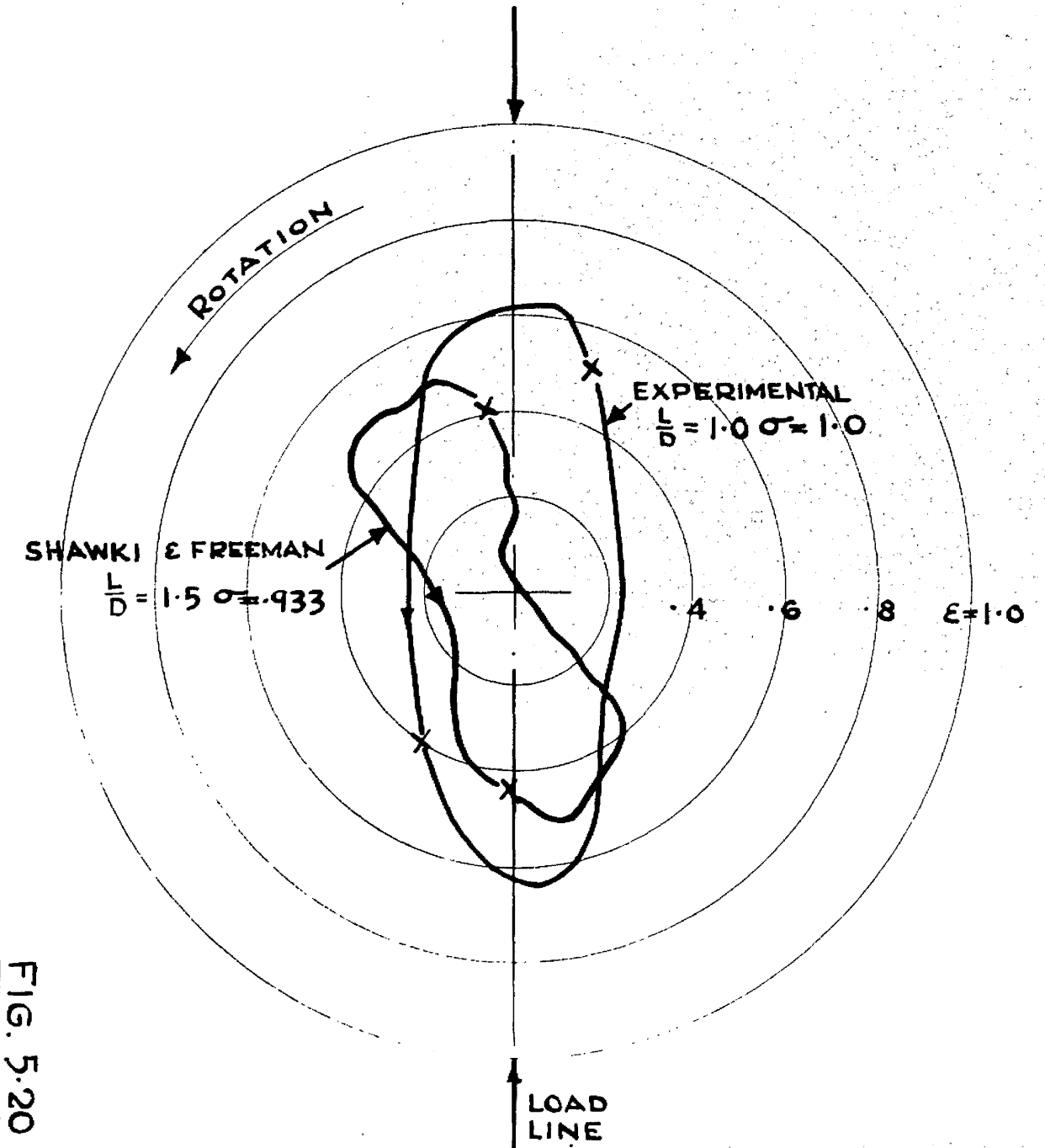

FIG. 5·20

JOURNAL PATHS: EXPERIMENTAL
$S_n \doteqdot 0{\cdot}1$

X : POSITION OF JOURNAL CENTRE AT INSTANT OF MAXIMUM APPLIED LOAD.

FIG. 5·20

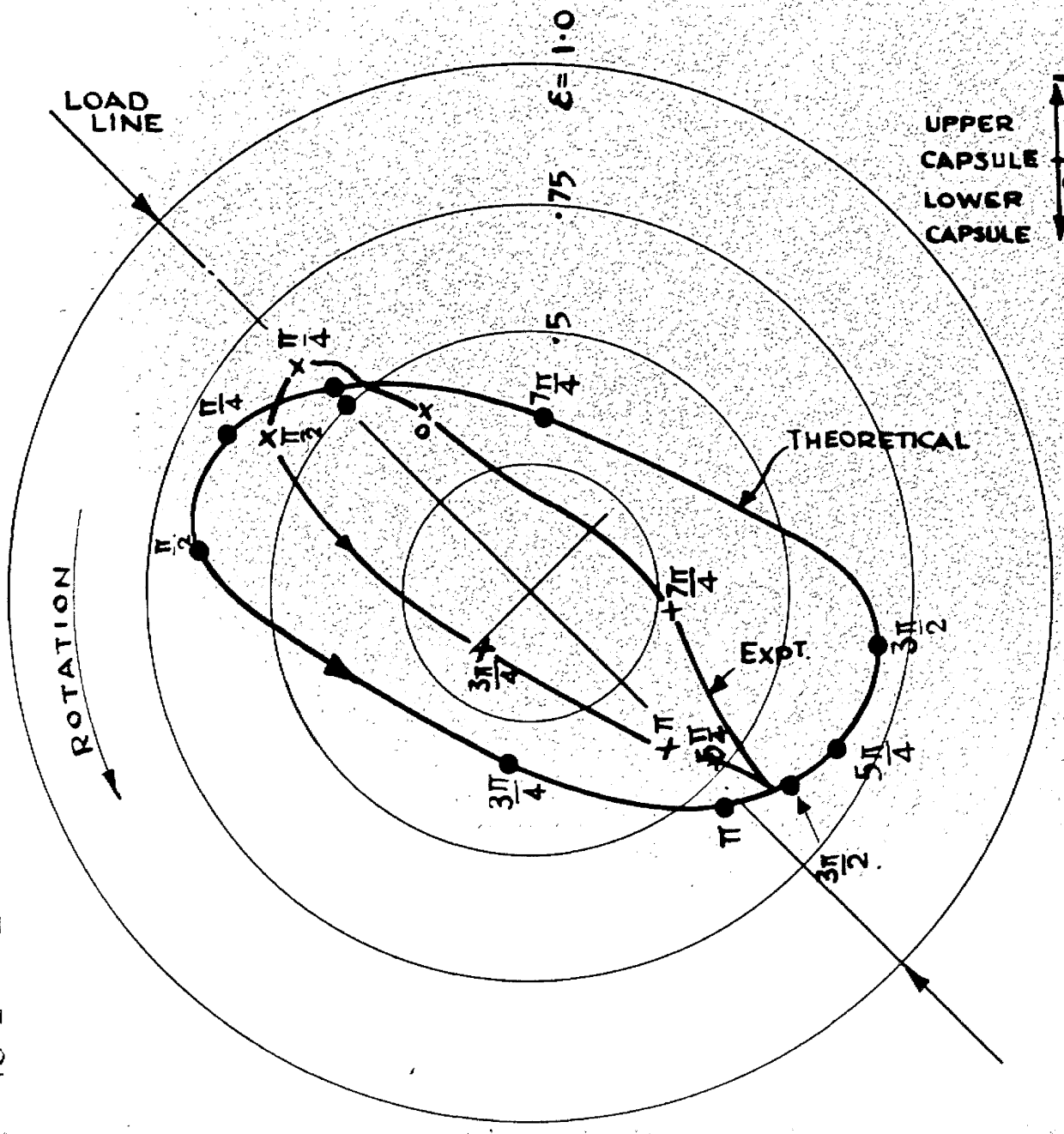

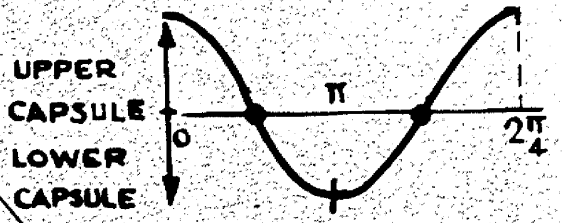

THEORETICAL PATH
HAHN : $\sigma = 1$ $L/D = 1/2$
EXPERIMENTAL : $\sigma =$, $L/D = \frac{1}{2}$

FIG. 5.21

FIG: 5·21

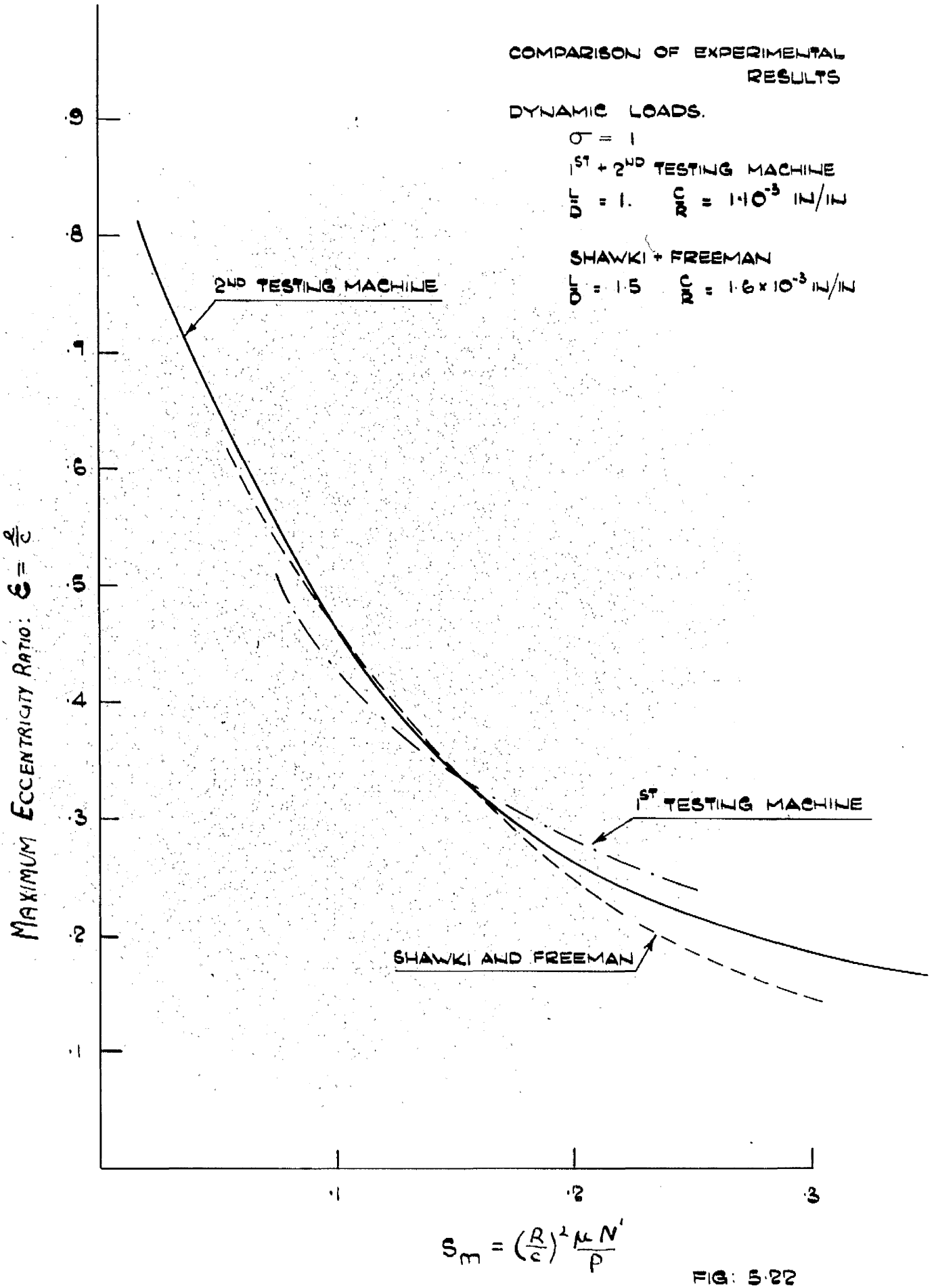
COMPARISON OF EXPERIMENTAL RESULTS
DYNAMIC LOADS.
σ = 1
1ST + 2ND TESTING MACHINE
L/D = 1. C/R = 1·10⁻³ IN/IN
SHAWKI + FREEMAN
L/D = 1·5 C/R = 1·6 × 10⁻³ IN/IN
2ND TESTING MACHINE
1ST TESTING MACHINE
SHAWKI AND FREEMAN
MAXIMUM ECCENTRICITY RATIO: ε = e/c
·9
·8
·7
·6
·5
·4
·3
·2
·1
·1
·2
·3
$S_m = \left(\frac{R}{c}\right)^2 \frac{\mu N'}{P}$

FIG: 5·22

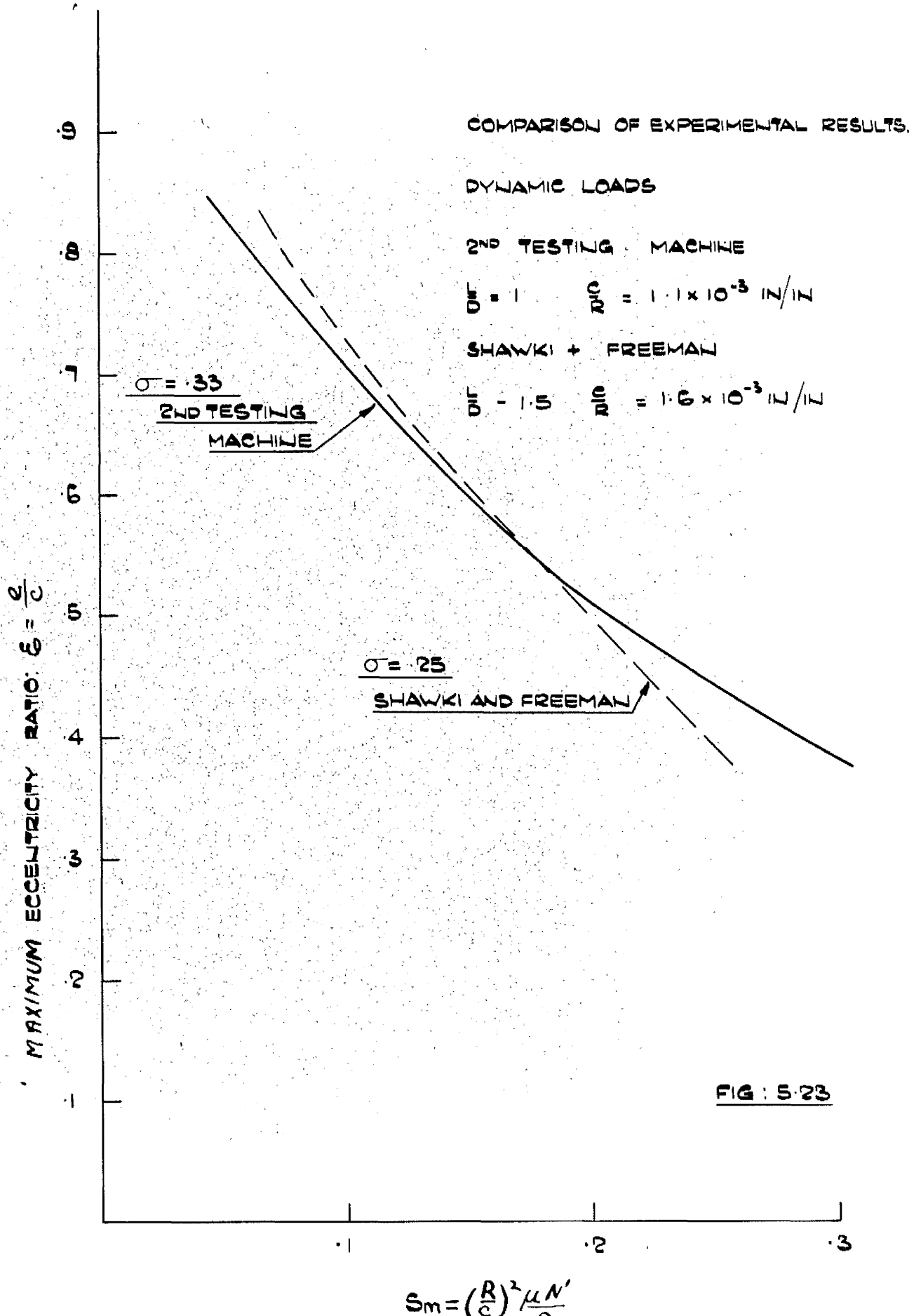
COMPARISON OF EXPERIMENTAL RESULTS.
DYNAMIC LOADS
2ND TESTING MACHINE
$\frac{L}{D} = 1$ $\frac{C}{R} = 1.1 \times 10^{-3}$ IN/IN
SHAWKI + FREEMAN
$\frac{L}{D} = 1.5$ $\frac{C}{R} = 1.6 \times 10^{-3}$ IN/IN
$\sigma = .33$
2ND TESTING MACHINE
$\sigma = .25$
SHAWKI AND FREEMAN
MAXIMUM ECCENTRICITY RATIO: $\xi = \frac{e}{c}$
.9
.8
.7
.6
.5
.4
.3
.2
.1
.1
.2
.3
$S_m = \left(\frac{R}{c}\right)^2 \frac{\mu N'}{p}$

FIG : 5·23

COMPARISON OF EXPERIMENTAL RESULTS WITH THOSE OF OTHER EXPERIMENTERS

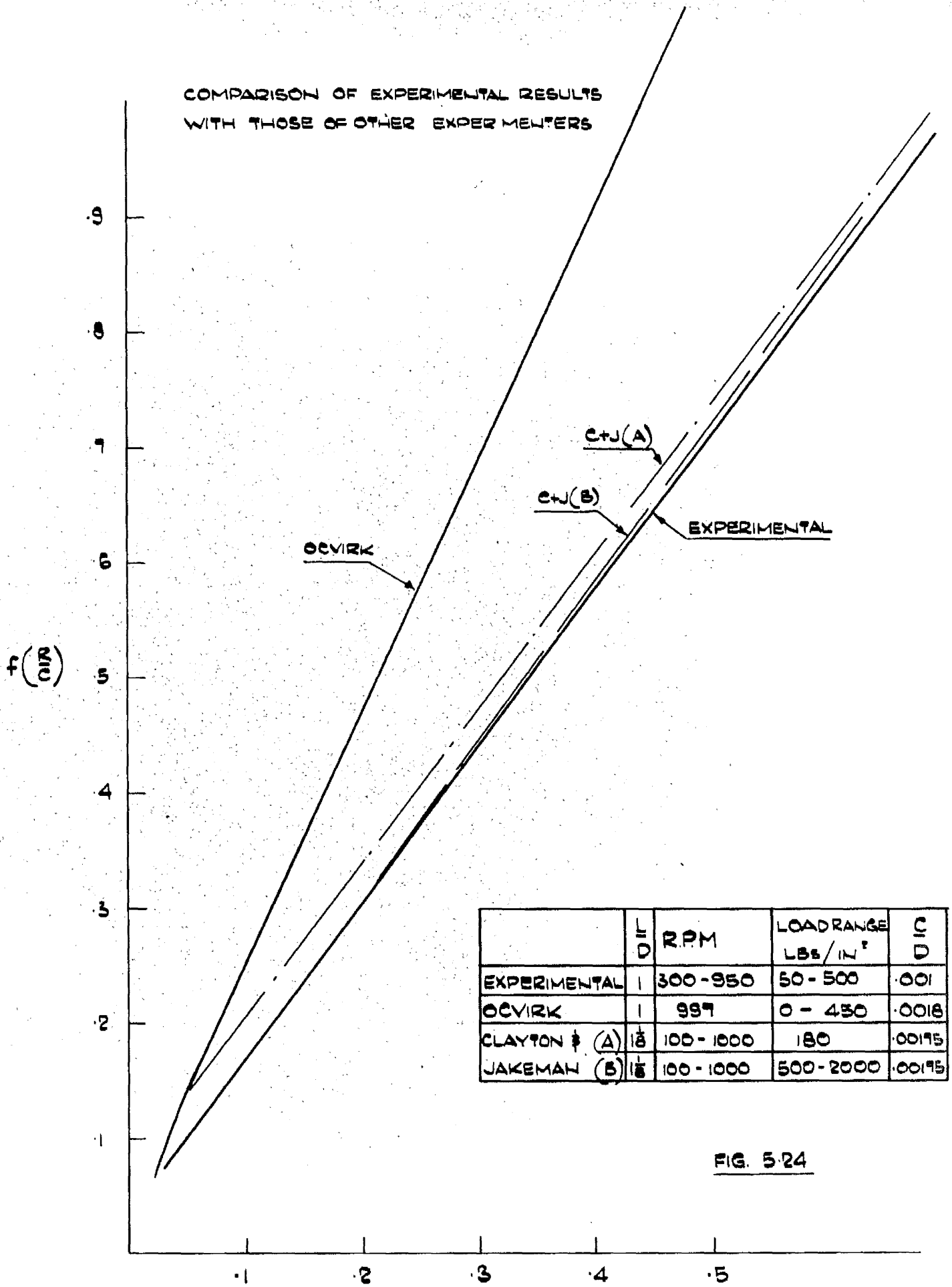

	L/D	R.P.M	LOAD RANGE LBS/IN²	C/D
EXPERIMENTAL	1	300-950	50-500	·001
OCVIRK	1	999	0-450	·0018
CLAYTON ⅛ (A)	1/8	100-1000	180	·00195
JAKEMAN (B)	1/8	100-1000	500-2000	·00195

FIG. 5·24

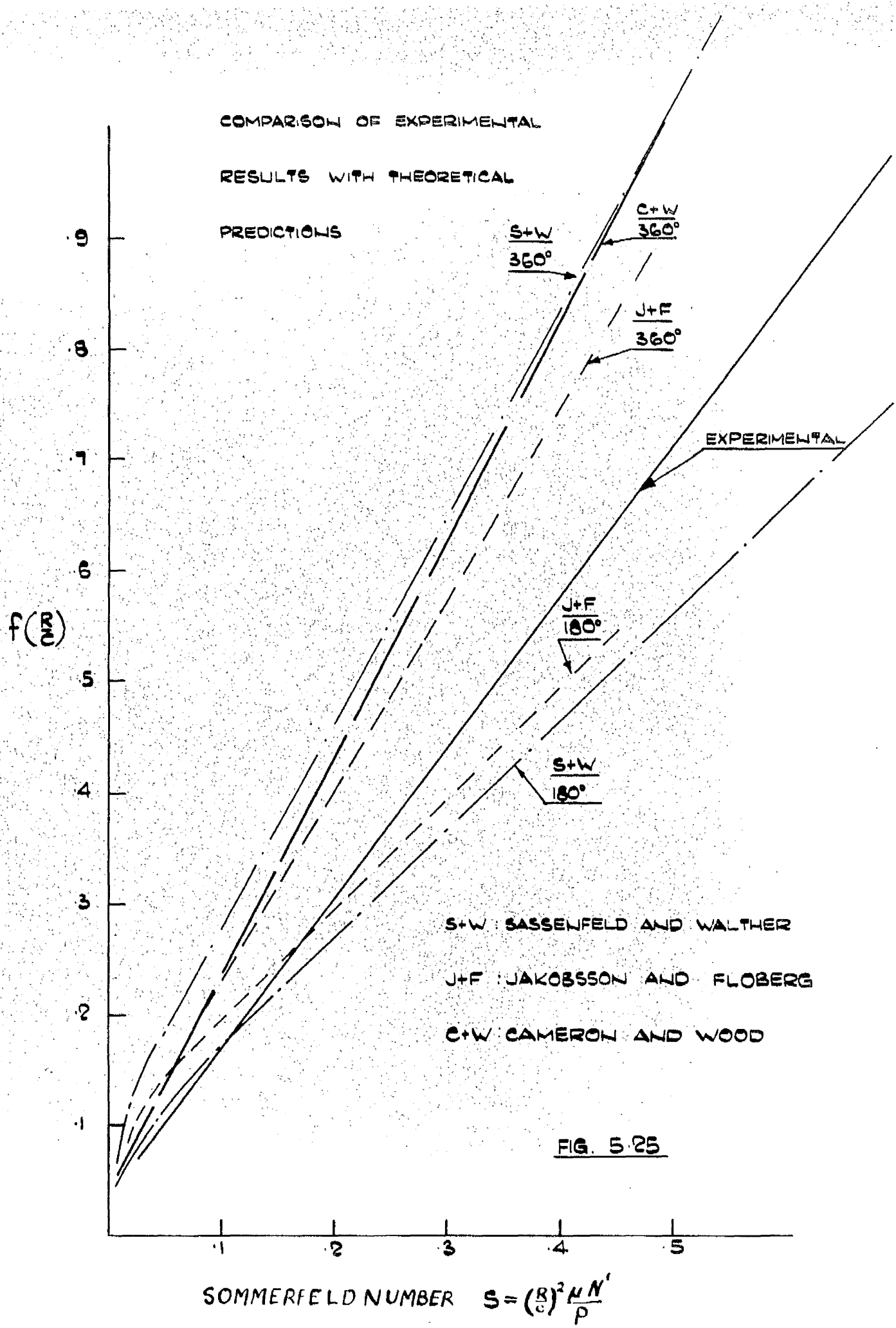
COMPARISON OF EXPERIMENTAL
RESULTS WITH THEORETICAL
PREDICTIONS
S+W
360°
C+W
360°
J+F
360°
EXPERIMENTAL
J+F
180°
S+W
180°
S+W : SASSENFELD AND WALTHER
J+F : JAKOBSSON AND FLOBERG
C+W CAMERON AND WOOD
f(R/C)
.9
.8
.7
.6
.5
.4
.3
.2
.1
.1
.2
.3
.4
.5
SOMMERFELD NUMBER S = (R/c)² μN'/p

FIG. 5·25

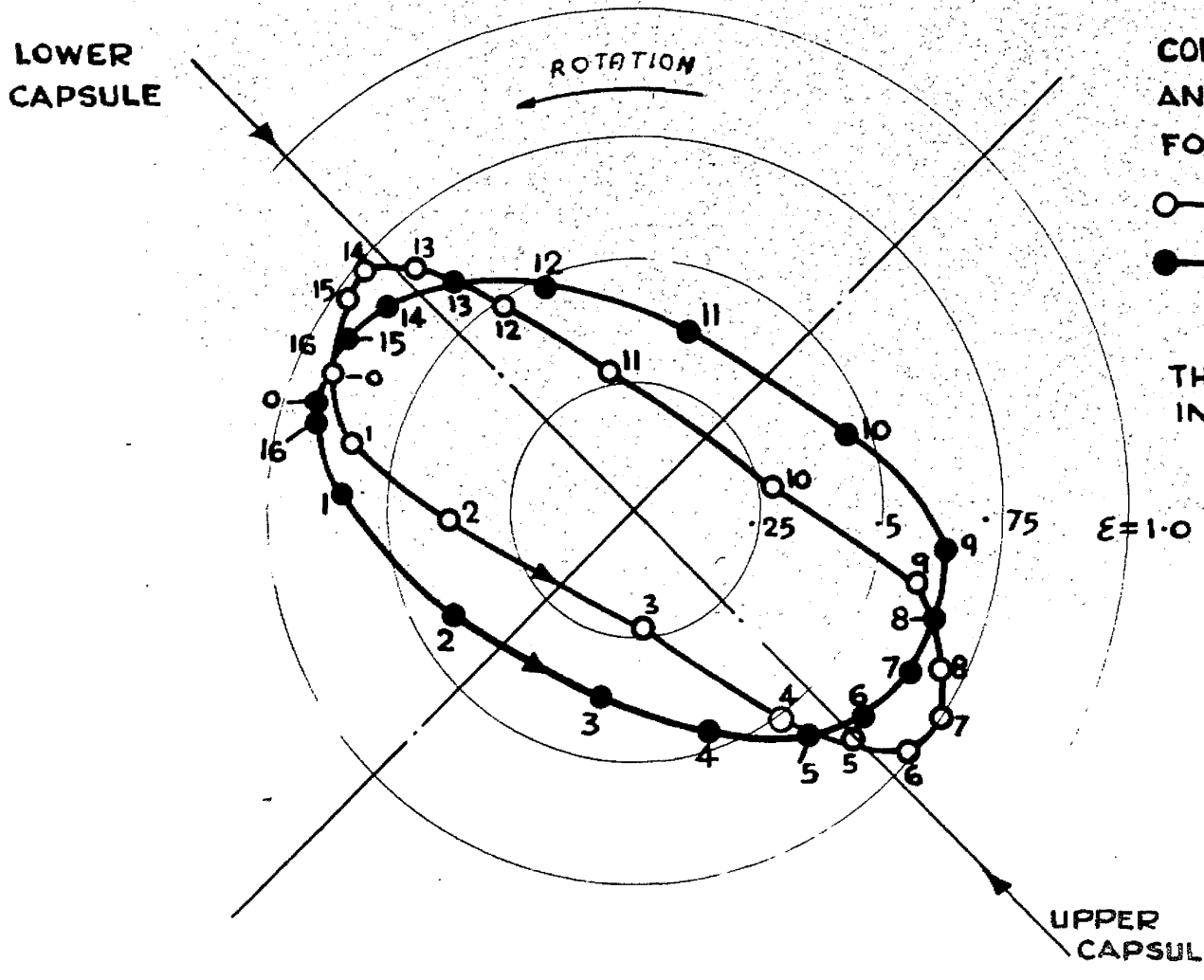

COMPARISON OF EXPERIMENTAL AND ANALYTICAL RESULTS FOR LOAD ON FIG: 4·51 $\frac{L}{D} = 1$

EXPERIMENTAL JOURNAL PATH

JOURNAL PATH PREDICTED BY ANALYSIS OF LLOYD ET.AL.

THE NUMBERS INDICATE LOAD PHASE INCREMENTS $\omega_p t = \pi/8$

FIG: 5·26

FIG: 5·26

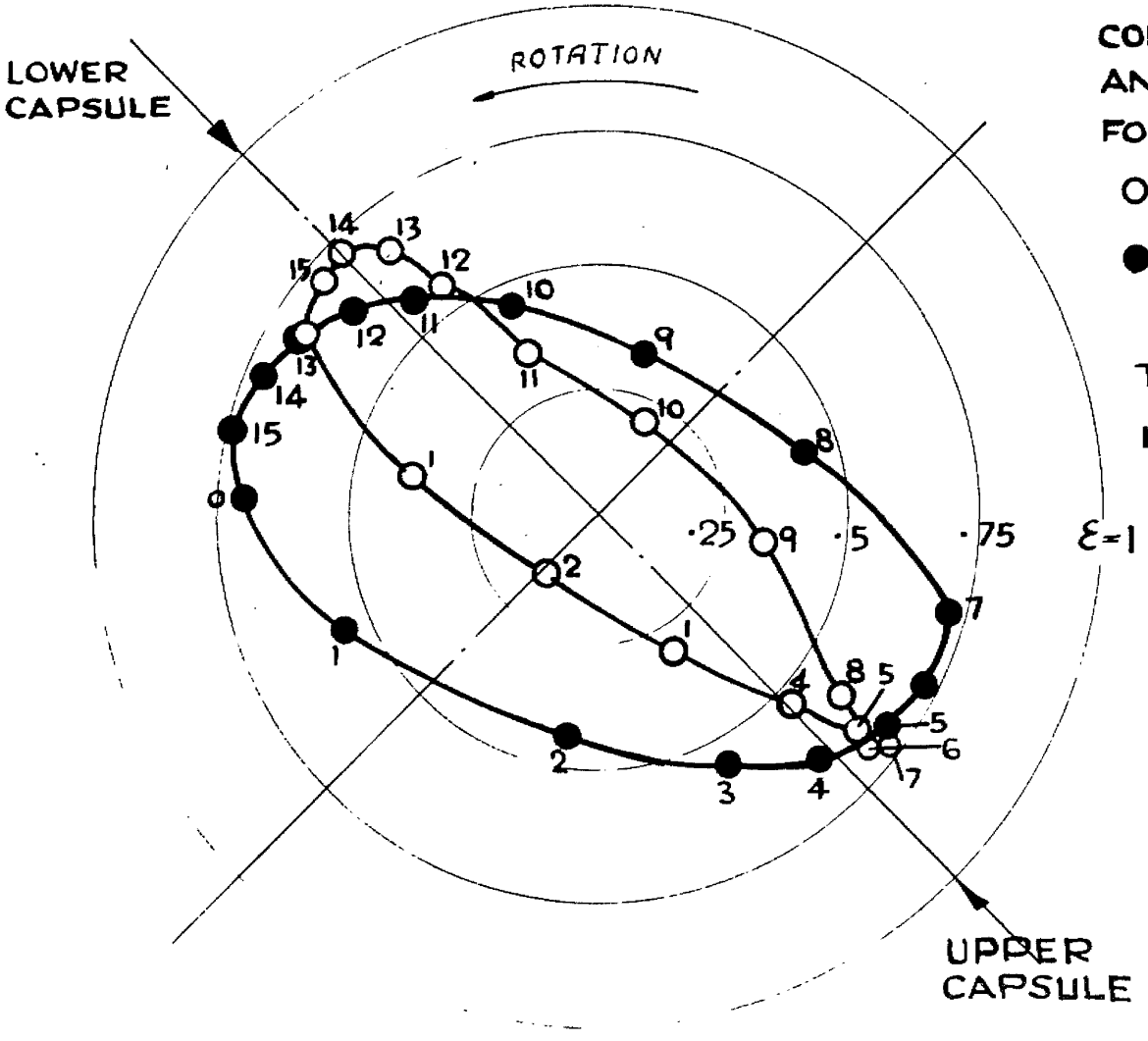

COMPARISON OF EXPERIMENTAL AND ANALYTICAL RESULTS FOR LOAD ON FIG: 4·57 $\frac{L}{D} = \frac{1}{2}$

EXPERIMENTAL JOURNAL PATH

JOURNAL PATH PREDICTED BY ANALYSIS OF LLOYD ET. AL.

THE NUMBERS INDICATE LOAD PHASE INCREMENTS $\omega_p t = \pi/8$

FIG: 5·27

FIG: 5·27

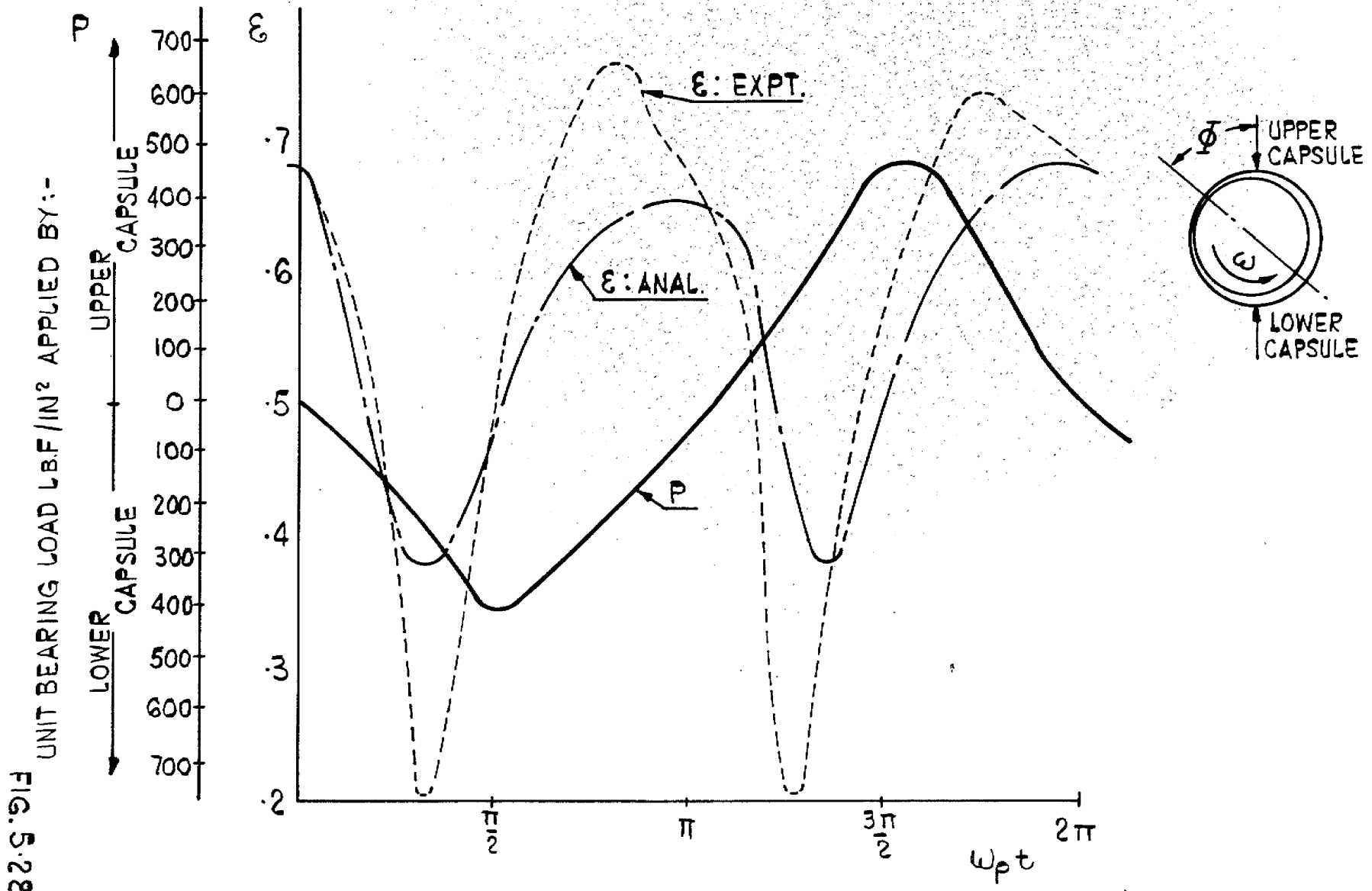

FIG. 5.28

COMPARISON OF EXPERIMENTAL RESULTS WITH ANALYSIS OF LLOYD, ET. AL. $\frac{L}{D}=1$ FIG. 5·28.

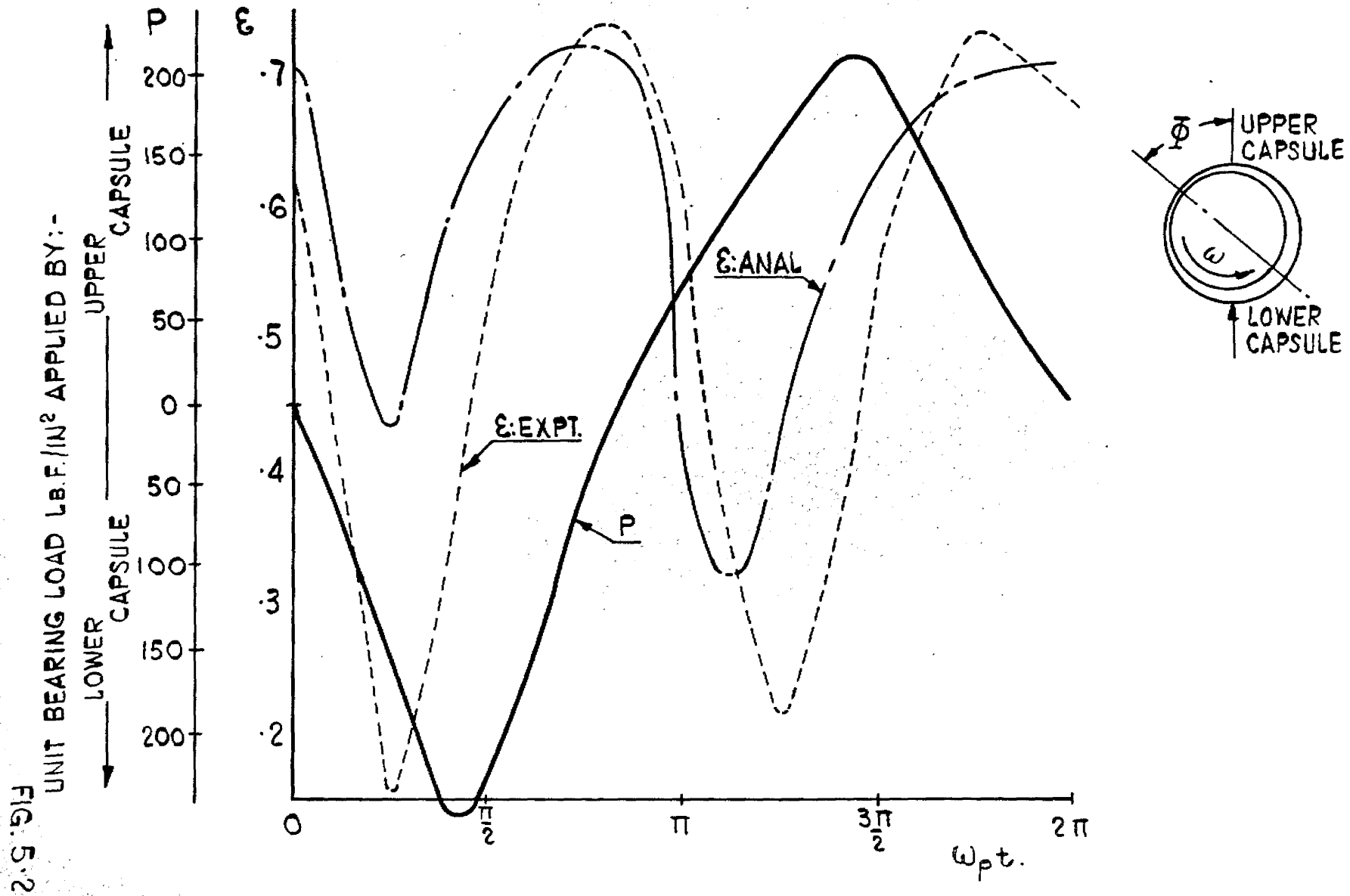

FIG. 5·29

COMPARISON OF EXPERIMENTAL RESULTS WITH ANALYSIS OF LLOYD ET AL. $\frac{L}{D} = \frac{1}{2}$ FIG.: 5·29

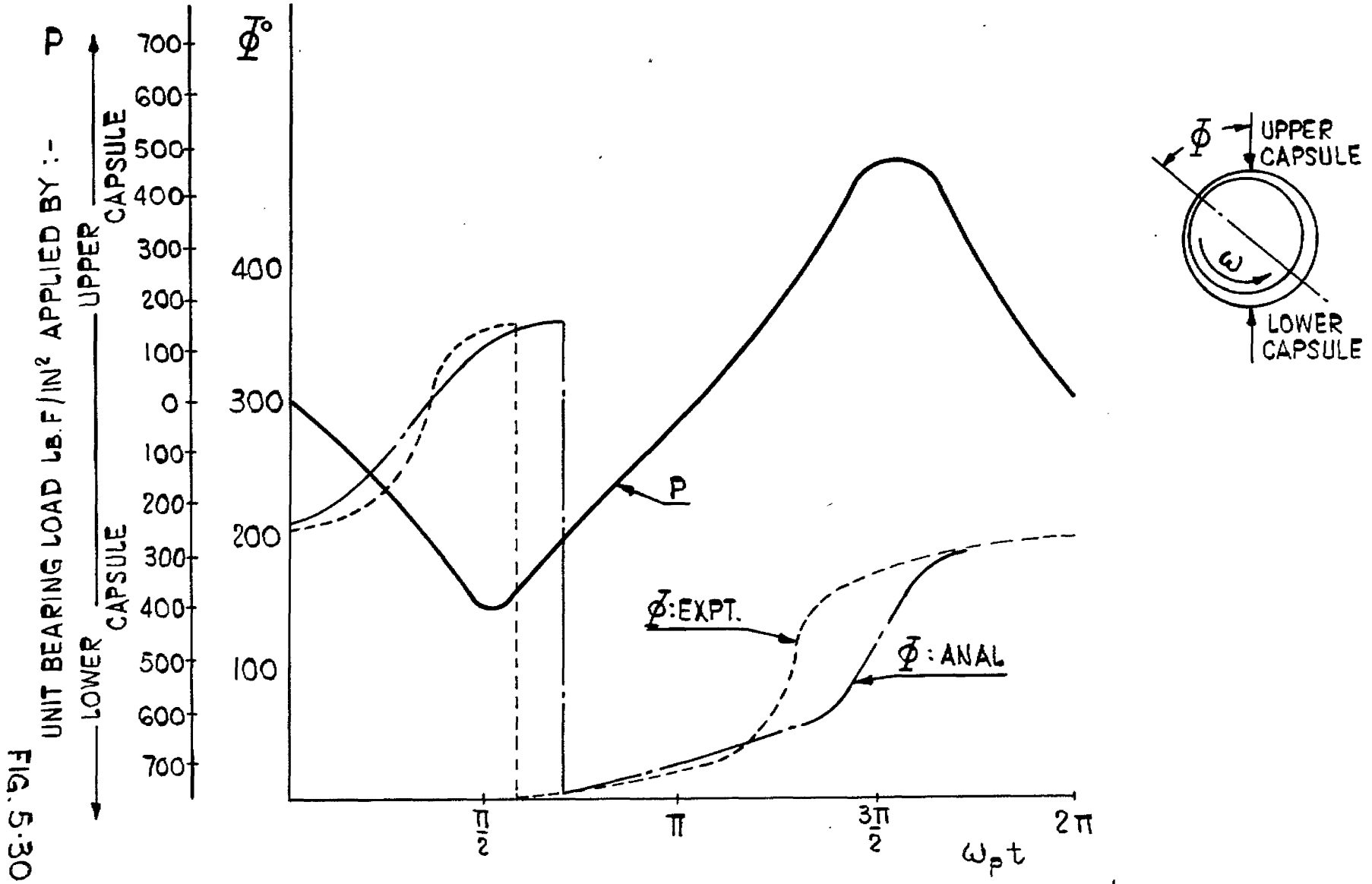

FIG. 5-30

COMPARISON OF EXPERIMENTAL RESULTS WITH ANALYSIS OF LLOYD ETAL. $\frac{L}{D}=1$ FIG. 5-30

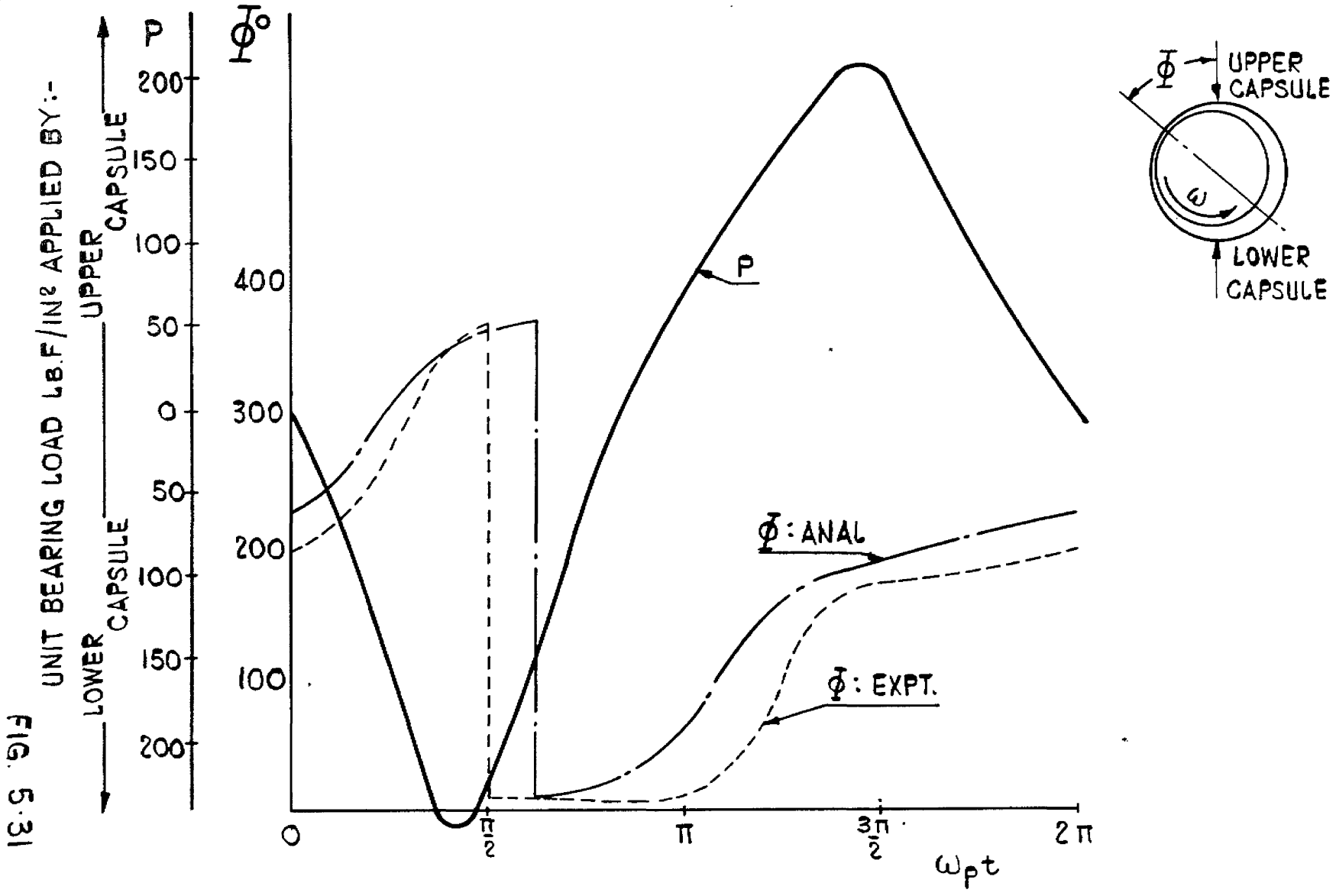

FIG. 5.31

COMPARISON OF EXPERIMENTAL RESULTS WITH ANALYSIS OF LLOYD ET AL $\frac{L}{D} = \frac{1}{2}$ FIG. 5·31

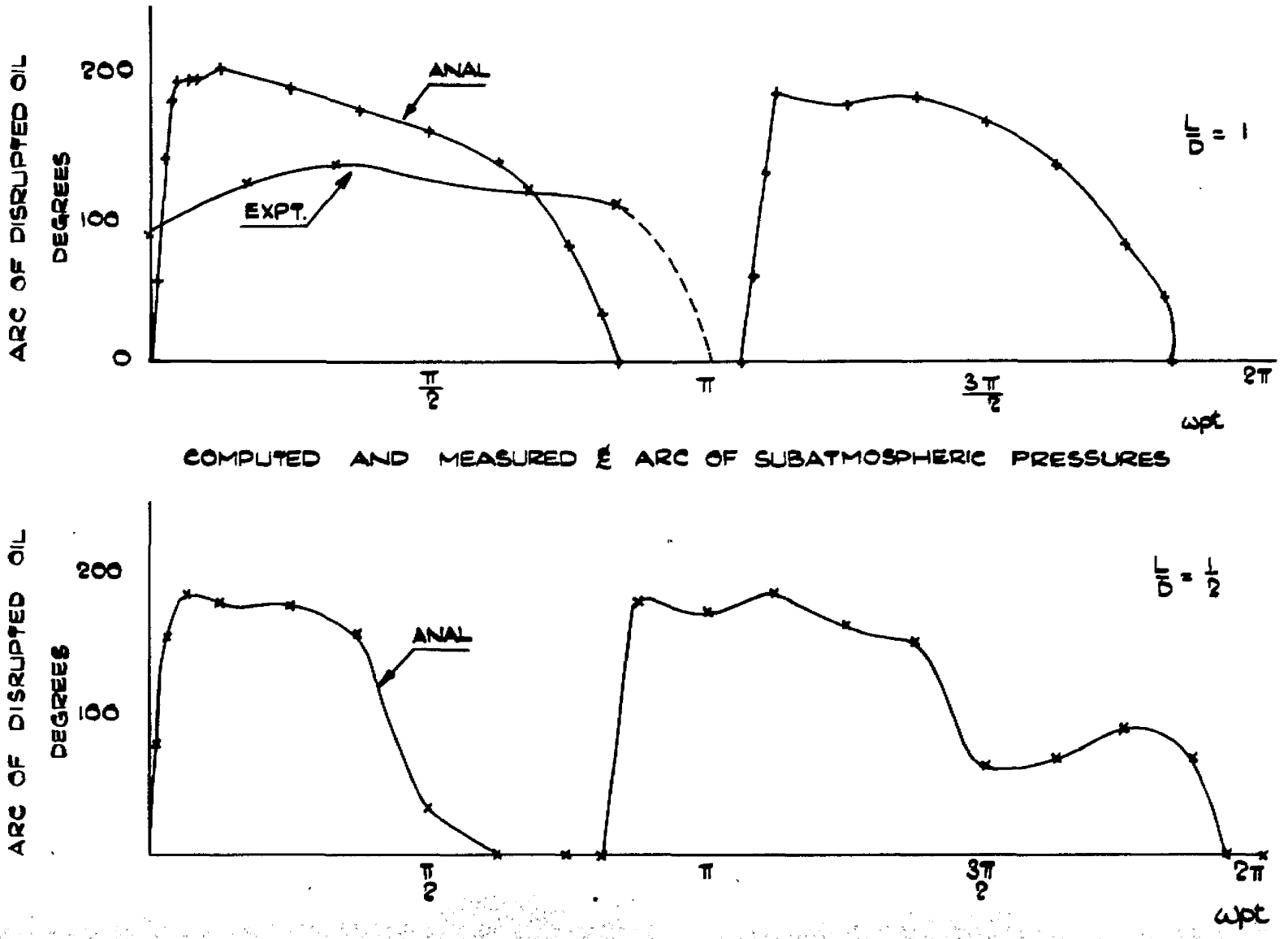

COMPUTED AND MEASURED ARC OF SUBATMOSPHERIC PRESSURES

FIG. 5.32

FIG. 5.32

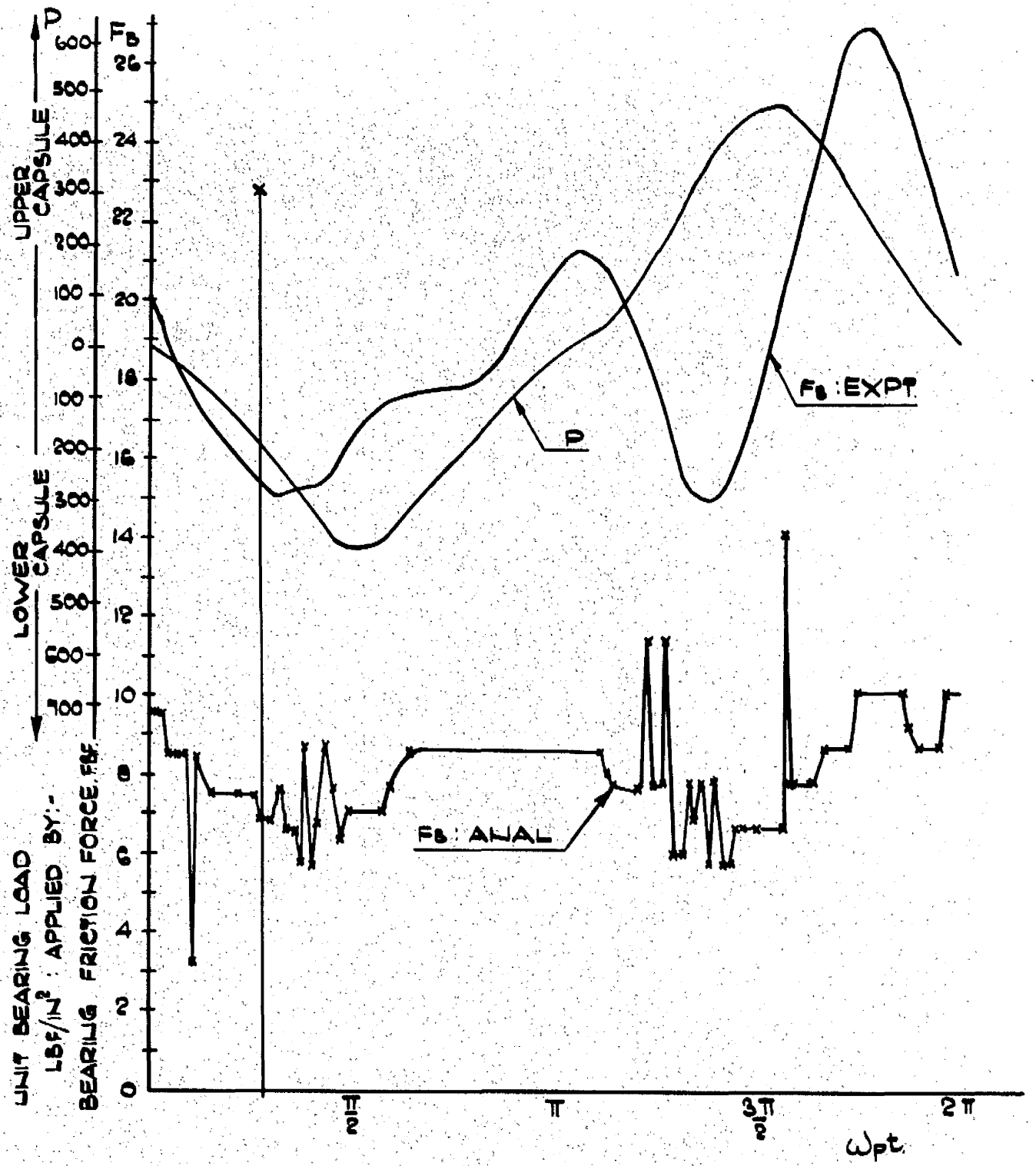

COMPARISON OF EXPERIMENTAL RESULTS WITH ANALYSIS OF LLOYD ETAL. $L/D = 1$

FIG.: 5·33

CHAPTER VI

6. Conclusions

The problems involved in the successful construction and operation of a large testing machine capable of producing Dynamic Loads comparable to those in current practice have been satisfactorily solved. The considerable effort involved in constructing the Second Testing Machine was justified by the quality of the results obtained.

Although the spring loaded balanced pressure piston proved to be a reliable instrument capable of measuring tensile stresses in the oil film, the time involved in completing a pressure survey by this means would be considered excessive by current standards.

The use of an externally pressurised bearing as a 'frictionless support' for a test bearing housing is, according to recent reports, unique in Dynamic Load applications. The sensitivity of the friction measurements, made possible by this construction, compensates for the considerable technical complications associated with such a bearing.

The initial concept of measuring journal displacement proved sound, and the refinement of the technique as applied to the Second

Testing Machine produced a sensitivity comparable to that of other experimenters. The co-ordinates of the journal centre position indicate the average film thickness in the bearing. No claim is made that the maximum journal eccentricity during a given load cycle gives the absolute minimum film thickness in the bearing as these measurements give no indication of the localised point to point contact suggested by the friction variable under Dynamic Loads.

Up to 20 per cent of the clearance space of a statically loaded axial grooved bearing is occupied by large stable air bubbles generated by the cavitation of the oil in the low pressure area of the bearing.

The unloaded arc of a Dynamically Loaded bearing is not an area of constant low pressure as has been previously reported, but consists of a trough of sub-absolute pressures in which the oil film sustains a tensile stress. When the oil film ruptures, air is released from sollution and cavitation is initiated. Tensile stresses exist in the oil film of the unloaded arc from the time the load direction reverses until the maximum load is reached. The subsequent period of decreasing load is associated with a general state of cavitation in the low pressure region of the bearing. The oil film

in a Dynamically Loaded bearing does not rotate with the journal but cavitates and reforms within a bearing arc bounded by the inlet grooves. Hence the air released by cavitation must be dissolved in the oil of the load bearing pressure film when the direction of the applied load reverses. The time required for this process is indicated by depression in the circumferential profile of the developing film pressures.

The major portion of the pressure in the load bearing pressure film is generated by squeeze film action, as the journal moves across the clearance space subsequent to the reversal of the direction of the applied load. At the instant of maximum eccentricity, when the squeeze film generation is zero, the Dynamically Loaded bearing supports approximately the same load as it would under Static Load conditions.

The principal difference between predicted and measured journal centre paths in bearings with two axial grooves is the that major axis of the elliptical path does not swing in the direction of rotation as the speed ratio falls below unity, but is held close to the line of the applied alternating load.

When Dynamic Loads have a variation which is approximately sinusoidal in form, the Sommerfeld Variable is a suitable

Non-Dimensional load number.

The Coefficient of Friction was considerably less than the value predicted by recent theoretical treatises, and no thin film conditions were detected within the range of Static Loads examined.

In both bearings investigated under Dynamic Loads, the variation of the bearing friction force was proportional to the magnitude of the applied load, and inversely proportional to the Speed Ratio. Thin film operation occurred within the range of Dynamic Loads examined, and the mean Coefficient of Friction was found to be greater than under an equivalent Static Load.

Estimation of oil flow in a Statically Loaded, axial grooved, bearing is more accurate if it is assumed that the complete oil film starts at the inlet groove.

Good quantitative agreement between measured journal eccentricities and those predicted by the computerised analysis of Lloyd et al., for a given Dynamic Load, vindicates the author's selection of an oil viscosity equivalent to the maximum bearing temperature for computational purposes.

REFERENCES

1. Reynolds, O. 'On the theory of lubrication and its application to Mr. B. Tower's experiments'. Phil. Trans. 1886, 177 (Pt. 1) 157

2. Sommerfeld, A. 'The Hydrodynamic Theory of Lubrication Friction'. Zeit. Math. Phys. 1904, 50, (Nos 1 & 2) 97 - 155.

3. Michell, A.G.M.: 'Progression Fluid - Film Lubrication'. Trans. A.S.M.E. 1929, 51, MSP-51-21, 153-163.

4. Cardullo, F.E.: 'Some Practical Deductions from Theory of Lubrication of Short Cylindrical Bearings'. Trans. A.S.M.E. 1930, 52, MSP-52-12, 143-153.

5. Ocvirk, F.W.: 'Short Bearing Approximation for Full Journal Bearings.' N.A.C.A. Tech. Note. 2808.

6. Swift, H.W.: 'Fluctuating Loads in Sleeve Bearings'. Journal Inst. Civil Eng. 1936-37, 5, 161.

7. Dick, J. 'Alternating Loads on Sleeve Bearings'. Phil. Mag. 1944, 35, 841.

8. Frankel, A. 'Calculation of the Performance Characteristics of Plain Bearings'. Eng. Digest (Am.) 1946, 3, 400.

9. Burwell, J.T.: 'The Calculated Performance of Dynamically Loaded Sleeve Bearings'. Trans. A.S.M.E. 1947, 69, A-231.

10. Hahn, H.W.: 'Dynamically Loaded Journal Bearings of Finite Length.' Proc. Conf. Lubrication and Wear, I.Mech.E. London, 1957. Paper 55, p.100.

11. Milne, A.A. 'Theoretical Studies of the Performance of Dynamically Loaded Journal Bearings. N.E.L. Report No. 70.

12. Horsnell, D. and McCallion, H. 'Prediction of Some Journal-Bearing Characteristics under Static and Dynamic Loading.' Proc. Lubrication and Wear Convention, I.Mech.E. 1963, paper 12, p.126.

13 Holland, J 'Beitrag zur Erfassung der Schmierverhaltnisse in Verbrennungs kraftmaschinen.'
V.D.I. Forsch. Hft 1959, 475.

14 Eberhard, A. and Lang, O. 'Zur Berechnung der Gleitlagerin im Verbrennungsmotor mittels elektronischem Digital rechner.'
M.T.Z. 1961, 22 (No. 7), 276.

15. Someya, T. 'Stabilitat einer in zylindrischen Gleitlagem laufenden, unwuchtfreien Welle'.
Dissertation, Technical University, Karlsruhe, 1962.

16. Lloyd, T., Horsnell, R., and McCallion, H., 'An Investigation into the Performance of Dynamically Loaded Journal Bearings: Theory'.
Proc. I. Mech. E. 1966 Vol 181 pt.3B, paper 6, p.1.

17. Hersey, M.D. and Snapp, R.B. 'A Short History of Bearing Testing Machines'.
Trans. A.S.M.E. 1957, 79, 1247.

18. Buske, A. and Rolli, W. 'Measurement of Oil-Film Pressures in Journal Bearings under Constant and Variable Loads'.
N.A.C.A. Tech. Memo. No. 1200. Translation from Jahrbuch 1937. Luftfahrtforschung p.67-68.

19. Simons, E.M. 'The Hydrodhynamic Lubrication of Cyclically Loaded Bearings'.
Trans. A.S.M.E. 1950, 72, 805.

20. Dayton, R.W. and Simons, E.M. 'Hydrodynamic Lubrication of Cyclically Loaded Bearings.'
N.A.C.A. T.N. 2544.

21. McBroom, H.L., 'Cavitation in Journal Bearings.'
Scientific Lubrication, April '53.

22. Shawki, G.S.A., and Freeman, P. 'Journal Bearing Performance under Sinusoidally Alternating and Fluctuating Loads'.
Proc. I. Mech. E. 1955, 169, 689.

23. Carl,T.E. 'An experimental investigation of a Cylindrical Journal Bearing under Constant and Sinusoidal Loading.'
Proc. I. Mech.E. 1964, 178, Part 3N, Paper 19, 100.

24. Radermacher, K. 'Experimental Investigation into Cylindrical Plain Bearings under Loads Varying in Magnitude and Direction.' Proc. I.Mech.E. 1964, 178, Part 3N, Paper 20, 120.

25 Motosh, N. 'Cylindrical Journal Bearings under Constant Load, The Influence of Temperature and Pressure on Viscosity.' Proc. I.Mech.E. 1964, 178, Part 3N, Paper 24, 148.

26. Cooke, W.L. 'Dynamic Displacements in a Diesel-Engine Main Bearing.' Proc. I.Mech.E. 1966, 180, Part 3K, paper 23.

27. Middleton. V., Dudley, B.R., and McCallion H. 'An Investigation into the Performance of Dynamically Loaded Journal Bearings: Experiment. Proc. I.Mech.E. 1966, 181, Part 3B, Paper 7.

28. Radermacher, K. and Hahn, H.W. 'Hydrodynamic Theory of Dynamically Loaded Bearings and its Application to Engine Bearing Design. Proc. I.Mech.E. 1966, 181, Part 3B, Paper 12.

29. Raimondi, A.A. and Boyd, J. 'An Analysis of Orifice and Capiliary Compensated Hydrostatic Journal Bearings.' A.S.M.E. - A.S.L.E. Conf. Oct. 1954. Paper No. 60-94451-8-P1.

30. Cunningham, S.E. 'A Design Procedure for a Six-Pool Non-Rotating Hydrostatic Bearing.' N.E.L. Internal Memo.

31. Becker, Green and Pearson. 'Properties and Uses of Thermistors.' Bell System Tech. Jour. 1947, 26. No.1, 170.

32. Howes, J.W. 'Characteristics and Applications of Thermally Sensitive Resistors or Thermistors.' Jour. Br.Inst.Radio Eng. 1953, 13 No 4, 223.

33. Muller, R.H. and Stolten, H.J. 'Use of Thermistor in Precise Measurement of Small Temperature Differences.' Anal. Chem. 1953, 25 No 7, 1103.

34. Bendersky, D. 'Thermocouples for Measuring Transient Temperatures.'
Trans. A.S.M.E. 1952, 74, A57.

35. Benedict, R.P. 'Thermistors v Thermocouples for Temperature Measurements.'
Elec. Mfg. 1954, 54 No 2, 120.

36. Rauch, W.G. 'Design and Construction of Needle Thermocouples.'
Metal Progress, 1954, 65 No. 3, 71.

37. McKee, S.A. and McKee, T.R. 'Friction of Journal Bearings as Influenced by Clearance and Length.'
Trans. A.S.M.E. 1929, 51, 149.

38. Leloup, L.
Rev. univ. Min., Ser. 9, 10 (1954) 258.

39. Dowson, D. 'Investigation of Cavitation in Lubricating Films Supporting Small Loads.'
Proc. Conf. Lub. and Wear. I.Mech.E. 1957.
Paper 49, p.93.

40. Cole, J.A. and Hughes, C.J. 'Visual Study of Film Extent in Dynamically Loaded Complete Journal Bearings'.
Proc. Conf. Lub. and Wear. I.Mech.E. 1957,
paper 87, p.147.

41. Hayward, A.T.J. 'Air Bubbles in Oil - Their Effect on Viscosity and Compressibility.'
D.S.I.R. N.E.L. Report No. 5. 1961.

42. Clayton, D. and Jakeman, C. 'The Measurement of Attitude and Eccentricity in Complete Clearance Bearings.'
Proc. I.Mech.E. 1936, 134, 437.

43. Du Bois, G.B. Ocvirk, F.W. and Wehe, R.L. 'Experimental Investigation of Eccentricity Ratio, Friction, and Oil Flow of Long and Short Journal Bearings with Load-Number Charts.'
N.A.C.A. T.N. 3491.

44. *Cameron, A. and Mrs W.L.Wood. 'The Full Journal Bearing.'*
Proc. I.Mech.E. 1949, 161, 59.

45. *Jakobsson, B. and Floberg, L. 'The Finite Journal Bearing Considering Vaporization.'*
Rep. No.3. Chalmers Inst. Goteborg, 1957.

46. *Sassenfeld, H. and Walther, A. 'Journal Bearing Calculations.'*
V.D.I. Forsch. 1954, 20, No. 441.

APPENDIX A

Theoretical Oil Flow Calculations

The pressure in the oil film at the inlet groove is low and may be assumed to have no effect on the film velocity. While the pressure at the point of closest approach is higher than at the inlet groove, it will be assumed for the purposes of this calculation that it has no significant effect on the film velocity. Thus the velocity gradient at both ends of the convergent film may be taken as linear.

Quantity of oil entering convergent film; Fig 4.63

$$= \left[e \sin\theta + (c^2 - e^2\cos^2\theta)^{\frac{1}{2}}\right] .L. \pi. DN.\tfrac{1}{2}$$

Quantity of oil entering divergent film.

$$= \left[c - e\right] L \pi D.N \tfrac{1}{2}$$

Nett flow from Convergent Film.

$$= \left[e \sin\theta + (c^2 - e^2 \cos^2\theta)^{\frac{1}{2}} - (c - e)\right] L \pi DN \tfrac{1}{2}$$

$$= \left[\varepsilon(1 + \sin\theta) + (1 - \varepsilon^2\cos^2\theta)^{\frac{1}{2}} - 1\right] cL \pi DN\tfrac{1}{2} \text{ where } \varepsilon = \frac{e}{c}$$

Oil Flow Number: $q_n = \dfrac{\text{Theoretical Flow}}{\text{Swept Volume}}$

$$= \frac{\left[\varepsilon (1 + \sin\theta) + (1 - \varepsilon^2\cos^2\theta)^{\frac{1}{2}} - 1\right]}{2}$$

As this is a function of the eccentricity ratio, it is convenient to compare it with another function of eccentricity ratio, The Sommerfeld Number,